2008-03-11

An RF System Design for an Ultra Wideband Indoor Positioning System

Hemish K. Parikh
Worcester Polytechnic Institute

An RF System Design for an Ultra Wideband Indoor Positioning System

By
Hemish K. Parikh

A Dissertation
Submitted to the Faculty of the

Worcester Polytechnic Institute

In partial fulfillment of the requirements for the
Degree of Doctor of Philosophy
in
Electrical and Computer Engineering

February 2008

Approved by:

Dr. William. R. Michalson, Thesis Advisor

Dr. Sergey Makarov, Committee Member

Dr. Reinhold Ludwig, Committee Member

Dr. James Matthews, Committee Member

Dr. Geoffrey Dawe, Committee Member

Dr. Fred Looft, Head of Department

Dedicated To

My Father, Kiran Parikh
My Mother, Anila Parikh
My Sister, Ripa Sanghvi
My Brother in Law, Hiren Sanghvi
My Lovely Nephews Youg and Haard
My Fiancée, Krupa Patel

ABSTRACT

One of the major drivers for developing indoor positioning and navigation systems is the vision to provide precise position information, of the fire fighters, during emergency situations. Three main elements of such an indoor positioning and navigation system design are the signal structure, the signal processing algorithm and the digital and RF prototype hardware. This thesis focuses on the design and development of RF prototype hardware. The signal structure being used in the precise positioning system discussed in this thesis is a Multicarrier-Ultra Wideband (MC-UWB) type signal structure.

Unavailability of RF modules suitable for MC-UWB based systems, led to design and development of custom RF transmitter and receiver modules which can be used for extensive field testing. The lack of RF design guidelines for multicarrier positioning systems that operate over fractional bandwidth ranging from 10% to 25% makes the RF design challenging as the RF components are stressed using multicarrier signal in a way not anticipated by the designers.

This thesis, first presents simulation based performance evaluation of impulse radio based and multicarrier based indoor positioning systems. This led to an important revelation that multicarrier based positioning system is preferred over impulse radio based positioning systems. Following this, ADS

simulations for a direct upconversion transmitter and a direct downconversion receiver, using multicarrier signal structure is presented. The thesis will then discuss the design and performance of the 24% fractional bandwidth RF prototype transmitter and receiver custom modules. This optimized 24% fractional bandwidth RF design, under controlled testing environment demonstrates positioning accuracy improvement by 2-4 times over the initial 11% fractional bandwidth non-optimized RF design. The thesis will then present the results of various indoor wireless tests using the optimized RF prototype modules which led to better understanding of the issues in a field deployable indoor positioning system.

ACKNOWLEDGEMENTS

First and foremost, I would like to thank my advisor, Prof. William R. Michalson for his support and guidance without which this work would not have been possible. He not only imparted tremendous technical knowledge but also put me on track every time I would loose direction and focus. I would like to sincerely thank Prof. Sergey Makarov, Prof. James Matthews, Prof. Reinhold Ludwig and Geoffrey Dawe for serving on my PhD thesis committee.

Many thanks to Prof. R. J. Duckworth, Prof. David Cyganski, Prof. John Orr, and Prof. Kaveh Pahlavan, all of whom have played a very important role in advising me in various stages of my PhD program. The PPL student team is truly responsible for making my learning interesting and fun and without Robert Boisse's help in populating all the PCBs, it would have taken me a few years longer to graduate.

Thanks to my close friends Anusha, Jitish, Pallavi, Shashank and Vishwanath, who helped me, stay longer in labs, by increasing my caffeine levels. A special thanks to my dear friend Abhijit for all his support and company.

Last but not the least, my parents, my sister, my brother-in-law, and my fiancée, have been the ones who influence me the most. It would not have been possible to complete this PhD thesis without their love, support, and beatings.

Table of Contents

List of Figures

List of Tables

Chapter 1 : Introduction

The Unsolved Problem

Accurately tracking individuals like fire fighters, in indoor locations is a very difficult technical problem – one which has not yet been completely solved. The operating environment involving a fire fighter search and rescue operation is very hostile in nature. It involves fire fighters going in to indoor structures that are filled with thick smoke, has low visibility, has very high temperatures, changing pressure levels, loud noise and obstructed corridors and exits. Severe RF signal attenuation, severe multipath and Non Line of Sight (NLOS) conditions are typical for such situations. Such applications cannot rely on any pre existing indoor wireless infrastructure, as they cannot guarantee

availability during a fire which makes indoor positioning system design and implementation a difficult problem to solve. The fire fighter user community agrees that an indoor positioning accuracy of better than 1m is ideal [1] but that 3m to 6m is acceptable, and may be a more practical goal. Indeed, this 3m (preferred) to 6m (acceptable) accuracy was later specified in as per the US Army Broad Agency Announcement (BAA). To the best of the author's knowledge, there is no realistic field deployable indoor positioning system prototype that can locate and track fire fighters inside a building with accuracies of 3m to 6m or better. Thus, the objective of the Precision Personnel Locator (PPL) project [2] being developed at WPI is to develop a realistic, field deployable, indoor positioning system that achieves 3m to 6m accuracy in a high multipath environment.

Figure 1.1 provides an overview of the envisioned indoor positioning system. Emergency vehicles and fire fighters carry RF based devices. Initially, the vehicles arriving at the scene go through a calibration phase during which an ad hoc network is established amongst the vehicles and the system is automatically configured. The fire fighters, transmit the RF signals which, when received at the emergency vehicles outside are used to calculate the relative positions of personnel in and around the building. The location of each fire fighter is sent to a command and control display which allows a scene commander to know the location and status of each firefighter. It is anticipated that such a

system will assist fire fighters and incident commanders in the field in real-time by providing vital information such as user location, user status and other telemetry to improve situation awareness and to assist in a rescue or other emergency operations.

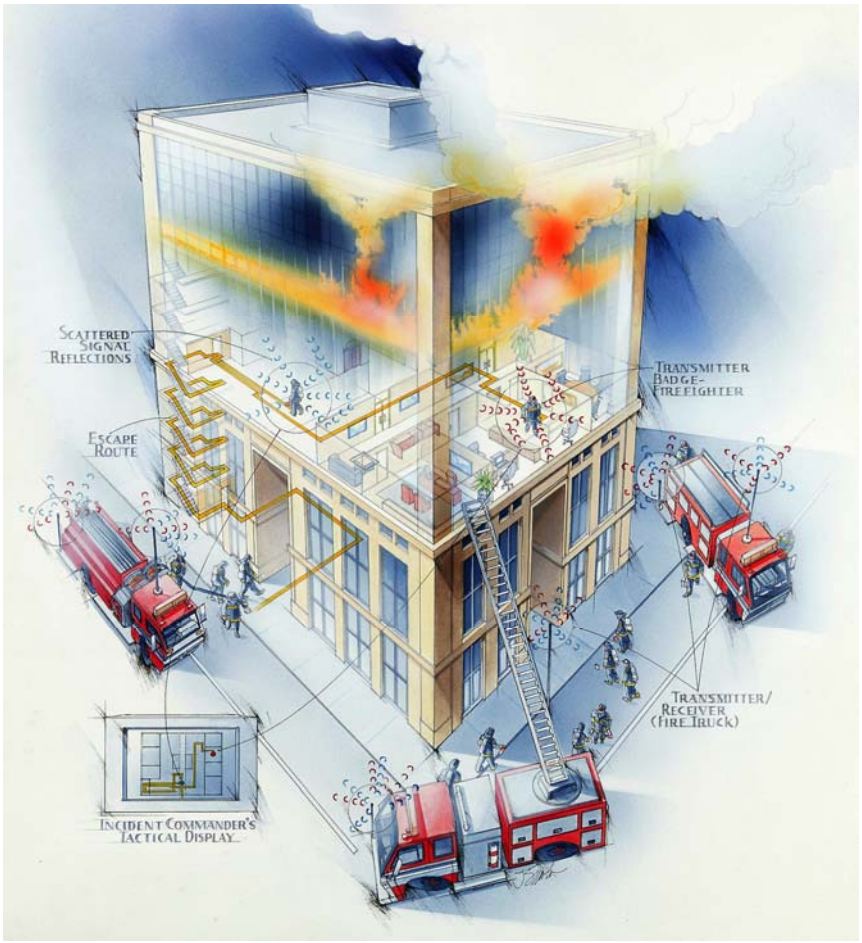

Figure 1.1 Concept drawing of integrated communication and navigation system being developed at WPI

Indoor Communication Systems vs. Indoor Positioning Systems

At first it may seem obvious to use existing communication systems such as GPS or WiFi for indoor positioning as well. Thus, before we discuss details of various existing indoor positioning systems, it is important to identify key differences between indoor communication systems and indoor positioning systems [3].

For a communication system, the Bit Error Rate (BER) and data rate are typically the most important system performance metrics. For a positioning system, the position accuracy is the most important system performance metric. For communications applications, total received power from all the multiple paths is important whereas for positioning applications the power level of only the shortest path received is important.

Multipath propagation is a commonly observed phenomenon indoors. Multipath is a result of reflection from objects around the antennas and results in two or more copies of the same signal being received at the receiving antenna. A Non Line of Sight (NLOS) condition occurs when there is no visual Line of Sight (LOS) between the transmitter and receiver antennas. Buildings, walls and furniture can cause NLOS conditions indoors which can result in a severe attenuation of the shortest path signal between the transmitter and receiver.

In such NLOS conditions, the presence of multipath is often what makes the communication system work indoors since the longer multipath signal paths may have less attenuation than the shorter, but more attenuated, direct path. Since navigation systems rely on measuring shortest paths, the reception of attenuated NLOS signals and signals with multipath delay could result in severe performance degradation.

Communication systems use diversity techniques to improve the system performance in the presence of multipath fading. Frequency diversity transmits the signal on multiple frequencies, the time diversity repeats the signal multiple times, and using multiple antennas provides space diversity. In NLOS and multipath conditions, these diversity techniques are very effective for a communication system.

Consider an example of a NLOS, multipath environment with spatial diversity where two receive antennas are used as shown in Figure 1.2. The transmitted power is spread due to multipath and let the path arriving at one antenna be weak (below minimum detection threshold), with a path delay of *d1* and the path arriving at the second antenna be strong (above minimum detection threshold), with a path delay of *d2*. The total (average) received power from both the antennas is high enough to correctly demodulate the transmitted information. Thus, the BER can actually be improved in a communication system by using multipath.

In the case of a navigation subjected to the above NLOS and multipath condition, these traditional diversity techniques do not provide significant improvements in position estimation [4].

Consider the same example of two antennas at the receiver as shown in Figure 1.2. Two paths arriving at two antennas will both be delayed in time by *d1* and *d2* and having two antennas does not help necessarily in improving the estimate for *d* which is the desired shortest path for positioning. When receiving a multipath signal, not only is the positioning accuracy not improved, but it will introduce a range error. Thus, two major sources of error for an indoor positioning system are multipath and NLOS conditions.

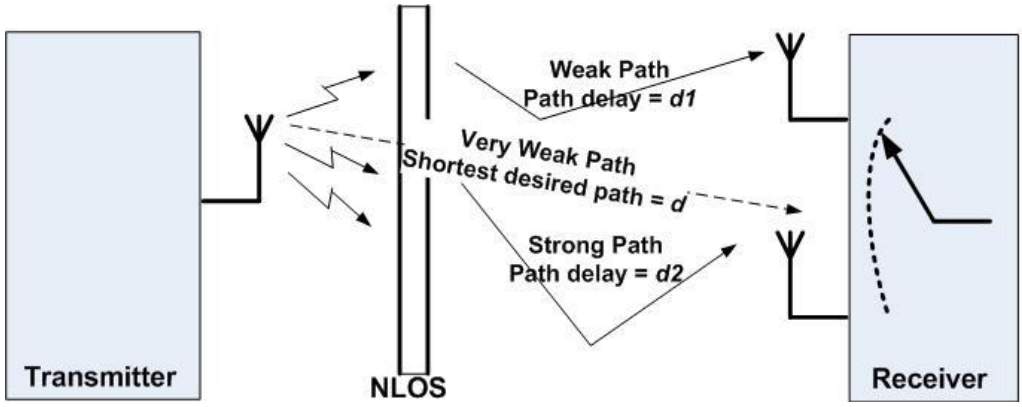

Figure 1.2 Example of Spatial Diversity

Indoor channel modeling [3, 4, and 5] becomes an important aspect for positioning systems as it provides tools to analyze the performance of a wireless system. As discussed in [3, 5] the main aim of indoor channel modeling for a communication system is to determine the relationship between distance and

total received power level and to calculate the multipath delay spread. The distance-power level relationship gives the system coverage area and the delay spread determines the data rate limitations. For a positioning system, indoor channel modeling can give us relative power level and time of arrival (TOA) information between the received multiple paths.

Currently, the existing indoor channel models [6] are designed for communication systems and they reflect the effects of channel behavior on the performance of the communication system where the multipath delay spread is what limits the performance. For positioning systems the existing indoor channel models don't adequately model the multipath channel for the estimation of Time Difference of Arrival (TDOA), Time of Arrival (TOA), Angle of Arrival (AOA) or Phase of Arrival (POA) based ranging techniques. If the existing indoor models are used for positioning applications, then the statistics of errors in distance estimation do not match with the experimental measurements [3-5].

Currently, there are no widely accepted channel models available that can be used for indoor positioning applications. The CWINS research lab at WPI [7], is actively working in developing indoor channel models and advanced signal processing algorithms like the super-resolution techniques [8] that are more suitable for indoor positioning systems.

State of the Art for Indoor Positioning Systems

In general there are two approaches to designing an indoor positioning system [5]. The first approach is to develop a new system, focused specifically on indoor positioning. The second approach is to use existing wireless networks and extend them to provide indoor positioning. The advantage of the first approach is that the signal and system design can be totally defined by the designer, at the expense of a time consuming design, development and deployment process. The advantage of the second approach is that it can avoid an expensive and time consuming design and deployment process but will be bound to operate within the technical specifications of the existing system. In this case the only optimization possible is in signal processing.

The goal for tracking fire fighters indoors is a positioning accuracy of 3m to 6m in extremely challenging multipath and NLOS indoor conditions. There are many non RF-based and RF-based positioning systems specific for indoor positioning [9-23] that are being developed at various research centers; each technology has its own advantages and disadvantages for indoor positioning. Figure 1.3 summarizes the technologies used in the Non RF-based and RF-based positioning systems that have been proposed in the literature [9-23].

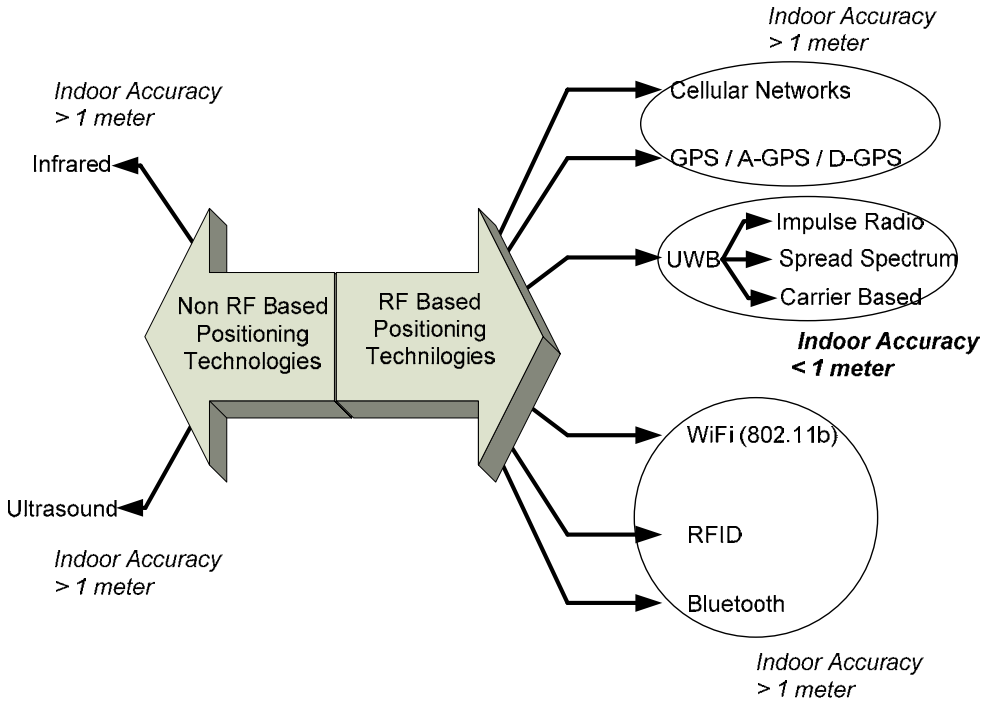

Figure 1.3 Non RF and RF Based Positioning Technologies

Non RF-based systems like the Infrared based Active Badge system and Ultrasound based Active Bat system have been proposed for indoor positioning [9, 10]. Cricket and Dolphin are other two systems proposed in literature [11, 12] that use a combination of both RF and ultrasound signals for positioning. Cricket and Dolphin take advantage of the difference in propagation speeds between RF (speed of light) and ultrasound (speed of sound) to calculate the time of arrival at the mobile node. These systems based on ultrasound introduce a source of error in the system since the speed of sound varies with varying temperatures and pressure. These non RF based systems require significant preinstalled infrastructure and are sensitive to the placement of the

sensors and motion of the mobile node, temperate and pressure changes [9-12]. These characteristics make them unsuitable for firefighting operations.

Two RF based technologies that could be used by fire fighters are cellular networks and GPS satellites. Cellular networks were developed with indoor and outdoor communication applications in mind and have to heavily rely on advanced signal processing algorithms as no major changes can be done in system implementation/deployment. Commercial cellular systems experience tremendous signal attenuation indoors and large-scale emergencies may lead to cellular network overload or may involve cellular base station damage, leaving the fire fighters without any means of communication, making cellular networks unsuitable.

The GPS was developed with outdoor positioning applications in mind with accuracy requirements of 10m to 30m. The GPS signal in an indoor environment is very weak and a stand alone GPS receiver cannot detect the satellites when indoors and hence cannot be used for indoor positioning. Indoor positioning solutions using Assisted GPS (A-GPS) have been proposed [24] to overcome this problem. Fundamentally A-GPS uses help from the cellular networks which broadcast the required information from the GPS satellites to the GPS receiver being assisted. This improves the GPS receiver sensitivity by approximately 10dB [24], which is good but not enough for achieving indoor positioning accuracies of under 6m. Implementing parallel correlation could

further provide an additional 20dB processing gain. The indoor positioning test result that uses A-GPS and 16000 correlators, inside a shopping mall are presented in [24] and the observed accuracies were around 17m which is still not good enough for the fire fighter application. Such high errors are observed because, fundamentally GPS-based positioning techniques not only suffer from poor signal strength indoors, but more importantly have low multipath immunity and an insufficient chipping rate to provide accurate indoor positioning. Indoor positioning techniques using GPS pesudolites or GPS repeaters have also been proposed [25] but such an implementation is not feasible as the positioning system cannot rely on a pre existing infrastructure such as a repeater which might not be available at the time of fire.

Other RF based indoor positioning systems in the literature that are independent of cellular networks and GPS satellites are based on 802.11b/Wi-Fi [14, 15, and 16], Bluetooth [17], RFID [18, 19]. These relatively narrowband systems also need preinstalled infrastructure – the presence of which cannot be relied upon for firefighting operations. Further, positioning accuracy is directly proportional to signal bandwidth and the narrowband systems are less suitable for indoor positioning in severe multipath environments as compared to wideband or ultra wideband systems [26, 27].

In 2002, the Federal Communication Commission (FCC) approved the use of frequency spectrum starting from 3.1GHz to 10GHz, for commercial

purposes [28]. As indoor positioning accuracy generally improves with increasing bandwidth, such systems can take advantage of the availability of ultra wideband (UWB) spectrum. Thus, the development of systems specifically for indoor positioning using UWB is gaining popularity as one can now design new signal and system architectures.

Two promising UWB based approaches for indoor positioning are Impulse Radio-UWB (IR-UWB) [22] and Carrier Based-UWB (CB-UWB) [23]. IR-UWB system occupies a large continuous frequency spectrum and transmits very short and low duty cycle pulses. The CB-UWB system is based on multicarrier techniques (OFDM/MC-UWB) which uses multiple modulated or unmodulated sinusoids that can be thought of as impulses in frequency domain. This MC-UWB signal structure is similar to the IEEE 802.15.3a standard, also referred to as multiband ultra wideband (MB-UWB). But since the IEEE 802.15a (MB-UWB) standard has been withdrawn in 2006 [29], no further comparison is made with the MC-UWB system discussed in this thesis.

Table 1.1 below shows a comparison of indoor positioning performance as published in the literature [14-19, 22, 23]. Our goal for an indoor positioning system is an accuracy requirement better than 6m (better than 3m is preferred). The cellular networks do not meet this requirement while GPS, WiFi, RFID and Bluetooth claim to achieve indoor positioning accuracy of better than six meters. The problem with Table 1.1 is that these accuracy estimates from the

literature are not based on severe multipath environments (workshop or warehouse) but are moderate multipath environments (home or office). Moreover these systems needed careful placement of the transmitters and receivers to make sure that multiple LOS paths were available, which is not a realistic system deployment for locating fire fighters inside a burning building.

Table 1.1 Comparison of RF Based Technologies for Positioning

Technology	**Claimed Accuracy**	**Signal Type**	**Positioning Technology**	**Bandwidth**
Cellular Network	5-10m	Single Carrier, DSSS	TOA, TDOA, RSSI, AOA, Fingerprinting	30 kHz - 1.25 MHz
A-GPS	2-5m	DSSS	TOA, TDOA	10 MHz
WiFi (802.11b)	2-3m	DSSS	RSSI, Fingerprinting	22 MHz
RFID	2-3m	Single Carrier	TOA, RSSI	60 kHz
Bluetooth	2-3m	FHSS	RSSI	1 MHz
IR-UWB	< 1m	Impulse Radio	TOA	20% fractional BW or 500MHz
CB-UWB	< 1m	OFDM/MC-UWB, FHSS,	TOA, TDOA, POA, AOA	20% fractional BW or 500MHz

The biggest challenge and cause for large errors in indoor positioning is the scenario when the signal strength of the desired shortest path is not the strongest path, referred to as Nondominant Direct Path (NDDP) or when the desired shortest path falls below the detection threshold of the receiver, referred to as Undetected Direct Path (UDP) [4]. The basic cellular networks,

GPS, WiFi, RFID and Bluetooth are not capable of coping with NDDP and UDP situations and will result in large errors, possibly of the order of few tens of meters. None of these systems have sufficient power, sufficient processing gain or resolution to achieve accuracy of better than six meters.

As mentioned earlier, bandwidth plays an important role in positioning accuracy [27] and as shown in Table 1.1, the UWB based systems, IR-UWB and MC-UWB in theory claim to achieve positioning accuracy of one meter or better. Note that in spite of these also being the best case results, the UWB systems, just because of their bandwidth, are better suited for indoor positioning compared to other systems shown in Table 1.1.

In theory, the short time domain pulse widths of IR-UWB systems provide a means for resolving multipath indoors. If the multiple paths arriving at different times can be separated then the shortest path, TOA or Two Way Ranging (TWR) can be more accurately estimated. Similarly the MC-UWB systems can implement frequency domain super-resolution algorithms over ultra wide bandwidths to better estimate the shortest path. For the NDDP and UDP conditions, the IR-UWB and MC-UWB designers can now design new optimized RF hardware that will make signal detection possible even when the shortest path is severely attenuated and very close to the noise floor, thus minimizing such errors.

Thesis Goals

As outlined in this Chapter, despite the variety of approaches that have been proposed for performing indoor positioning, the problem of accurately locating fire fighters inside a building has not been completely solved. Key differences between the characteristics of indoor positioning systems and communication systems were presented and the state of art on existing indoor positioning systems was reviewed.

The primary goal of this thesis is the development the RF hardware for a system that can overcome the challenges of the indoor positioning environment. Overcoming these challenges requires a "systems" approach to the design and development effort since, while certain approaches to performing indoor positioning are simply not viable in the operating environment associated with firefighting, others may, or may not be. Further, there are numerous issues which lie on the path between a system concept and a working implementation. It is a further goal of this thesis to illuminate some of these issues.

The first step in system design is to understand the phenomenology associated with the candidate technologies that appear most viable. To this end Chapter 2 compares Impulse Radio Ultra Wideband (IR-UWB) and Multicarrier Ultra Wideband (MC-UWB) systems which represent two promising techniques for implementing indoor positioning systems. This chapter provides an overview

of the signal structure, frequency spectrum, and transmitter and receiver structures for both of these techniques. This chapter then presents simulation results for indoor positioning using both IR-UWB and MC-UWB and concludes that the MC-UWB signal structure offers some significant advantages over the IR-UWB signal structure, a result which challenges some of the current literature. Based on the simulation results the author proposes the development of an MC-UWB based RF positioning system prototype.

Chapter 3 presents ADS simulation results for an initial RF prototype design and discusses the expected RF specifications for this prototype (referred to as the Phase 1 RF prototype). An important result obtained from ADS these simulations was that non modulated multicarrier signals are preferred over modulated multicarrier signals. Using the Phase 1 RF prototype consisting of extensive test and measurement equipment we were able to rapidly verify the functionality of the range estimation algorithms, validate the system architecture design and determine specifications for further optimizing the RF specifications for the system.

Chapter 4 presents the RF performance evaluation for short range wireless tests using a Phase 2 RF prototype consisting of evaluation boards. This led to better understanding of the multipath effect on the received frequency spectrum, better understanding of the required regions of operation for the RF

system, and provided insight to unforeseen issues like LO mismatch as well as internal and external interference.

Chapter 5 presents the design, development and specifications of completely custom RF transmitter and receiver PCB modules, which are referred to as the Phase 3 RF prototype. This chapter further discusses extensive indoor and outdoor wireless range estimation tests. The observed results were not consistent which indicated possibility of a fundamental flaw in the system. Upon further bench testing a non-intuitive system issue was discovered which was corrupting the multicarrier signal used by the range estimation algorithms. This chapter concludes by presenting two possible solutions to get around this fundamental flaw.

Chapter 6 discusses outdoor and indoor wireless range estimation tests after resolving the flaw discussed in the previous chapter. Consistent range estimation results were observed and the RF system was upgraded from a ranging system to a positioning system involving multiple receivers. The positioning results are discussed in this chapter which concludes by summarizing the limitations in the RF transmitter and receiver design.

Chapter 7 discusses the design, development, and specifications of the RF redesign referred to as Phase 4, which addresses the limitations discussed in previous chapter. This optimized Phase 4 RF system is a 24% fractional bandwidth, truly UWB, RF system.

Chapter 8 compares the performance improvement on positioning estimation due to optimized Phase 4 RF design over the non optimized Phase 3 RF design. Controlled tests demonstrated positioning accuracy improvements of 2-4 times over that of non optimized Phase 3 RF system. This chapter concludes by presenting more indoor positioning test results using this optimized 24% fractional bandwidth RF system.

Chapter 9 discusses the breakdown of Total System Error (TSE) based on extensive field tests. This chapter then identifies and quantifies a forgotten but important source of error due to building dielectric materials and concludes by summarizing the thesis contributions.

Summary of Thesis Contributions

To the best of author's knowledge, other than WPI's indoor positioning system [2], there exists no other indoor positioning system in the literature that uses a multicarrier signal structure to consistently achieve indoor positioning accuracies of 3m to 6m. Also the required RF architecture design for multicarrier based field deployable RF prototype cannot be found in the existing literature. Moreover, the performance characterization in terms of Total System Error (TSE) breakdown for multicarrier based positioning systems is not available in the existing literature. The thesis provides detailed insight to the above topics that were not previously available. In summary, the author's contributions are:

1) Presented simulation based performance evaluation of impulse radio based and multicarrier based indoor positioning systems. This led to an important revelation that multicarrier based positioning system is preferred over impulse radio based positioning systems. Thus the author proposes to develop a multicarrier based indoor positioning system prototype for further field testing and evaluation. A journal paper detailing these results has been provisionally accepted for publication in the ION Journal of Navigation [30].

2) Presented ADS based simulations for multicarrier based RF system which resulted in an important observation that non modulated multicarrier signals are preferred over modulated multicarrier signals when

designing multicarrier based indoor positioning systems. ADS multicarrier simulations showed orthogonal carriers results in good IMD behavior. This, simulation, in conjunction with experimental verification, provided justification for using narrowband techniques to design a wide band system. Also presented initial design parameters for RF prototype using which successful cable tests were performed which gave more confidence in the theory of using multicarrier signals for positioning. A conference paper detailing these initial design parameters and cable test results was published in ION GNSS 2004 [31].

3) Identified non-intuitive system issue that resulted from direct down conversion type receiver architecture when transmitting a Double Side Band (DSB) multicarrier signal. Thus the author identified that direct down conversion receiver architecture cannot be used when using multicarrier signal. The author then proposes to use Single Side Band (SSB) radio architecture when using multicarrier signal.

4) Designed first field deployable, 11% fractional bandwidth DSB radio architecture, following which designed an optimized 24% factional bandwidth SSB radio architecture. This optimized 24% fractional bandwidth RF design, under controlled testing environment demonstrates positioning accuracy improvement by 2-4 times over the initial 11% fractional bandwidth non-optimized RF design. Conference papers detailing the 11% and the 24% fractional bandwidth RF system designs, and wireless field test results using these

prototypes were published in ION NTM 2005, ION GNSS 2005 and ION AM 2007 [32, 33, 34].

5) Presented a realistic Total System Error (TSE) for multicarrier positioning systems, based on extensive indoor and outdoor wireless tests. This TSE lists the breakdown of the error sources providing more insight for further optimization. Identified and quantified an important error source from the TSE that results due to building dielectric materials, which to the best of author's knowledge has been forgotten and ignored by all other existing literature on positioning systems. Conference papers detailing these results have been accepted for publication in IEEE ICASSP 2008 [35] and ION NTM 2008 [36].

References

[1] “Wireless Personal Locator Requirements Assessment Focus Group Report”, *WPI Internal Report*, July 19-21 2004

[2] Worcester Polytechnic Institute, Electrical and Computer Engineering Dept., Official PPL Project Webpage, http://www.ece.wpi.edu/Research/PPL/

[3] K. Pahlavan, P. Krishnamurthy, J. Beneat, “Wideband Radio Propagation Modeling for Indoor Geolocation Applications ”, *IEEE Wireless Communications Magazine*, April 1998

[4] K. Pahlavan, F. Akgul, et.al “Indoor Geolocation in the Absence of Direct Path”, *IEEE Wireless Communications Magazine*, December 2006

[5] K. Pahlavan, X. Li, and J. Makela, "Indoor Geolocation Science and Technology", *IEEE Communications Magazine*, Vol. 40, No. 2, pp: 112-118, February 2002

[6] H. Hashemi, “The Indoor Radio Propagation Channel”, *IEEE Proc.* Vol. 81, Issue 7, Page(s):943 – 968, July 1993

[7] Worcester Polytechnic Institute, Electrical and Computer Engineering Dept., Official CWINS Webpage, http://www.cwins.wpi.edu/

[8] X. Li, K. Pahlavan, “Super-resolution TOA Estimation with Diversity for Indoor Geolocation”, *IEEE Transactions on Wireless Communications*, Vol. 1, No. 3, pp: 224-234, January 2004

[9] R. Want, A. Hopper, V. Falcao, and I. Gibbons, “The Active Badge location svstem”, *ACM, Transactions on Information Systems*, pp. 91-102, January 1992

[10] A. Harter, A. Hooper, P. Steggles, A. Ward, and P. Webster, “The Anatomy of a Context-aware Application”, *IEEE Proc. MOBICOM*, August 1999

[11] N. Priyantha, A. Miu, H. Balakrishnan, and S. Teller, “The Cricket Compass for Context-aware Mobile Applications”, *IEEE Proc. MOBICOM*, July 2001

[12] Y. Fukuju, M. Minami, H. Morikawa, and T. Aoyama, “DOLPHIN: An Autonomous Indoor Positioning System in Ubiquitous Computing Environment”, *IEEE Proc. Workshop on Software Technologies for Future Embedded Systems*, 2003

[13] G. Sun, J. Chen, W. Guo, and K. J. R. Liu, “Signal processing techniques in network-aided positioning”, *IEEE Signal Processing Magazine*, Vol. 22, no. 4, pp. 12–23, July 2005

[14] A. Harder, L. Song, and Y. Wang, “Towards an Indoor Location System Using RF Signal Strength in IEEE 802.11 Networks”, *IEEE Proc of International Conference on Information Technology: Coding and Computing*, 2005.

[15] P. Bahl and V. N. Padmanabhan, "RADAR: An Inbuilding RF-based User Location and Tracking System", *IEEE Proc. INFOCOM,* Tel-Aviv, Israel, March 2000

[16] A. Ali, L. A. Latiff, and N. Fisal, "GPS-free Indoor Location Tracking in Mobile Ad Hoc Network (MANET) Using RSSI", *IEEE Proc. Microwave Conf*erence, October 2004

[17] F. Forno, G. Malnati, and G. Portelli, "Design and Implementation of a Bluetooth Ad Hoc Network for Indoor Positioning", *IEEE Proc.*, Col. 152, No. 5, October 2005

[18] L. M. Ni, Y. Liu, Y. C. Lau, and A. P. Patil, "LANDMARC: Indoor Location Sensing Using Active RFID", *IEEE Proc. International Conference on Pervasive Computing and Communications*, 2003

[19] J. Hightower, R. Want, and G. Borriello, "SpotON: An Indoor 3D Location Sensing Technology Based on RF Signal Strength", UW CSE 00-02-02, University of Washington, Department of Computer Science and Engineering, Seattle, WA, February 2000, http://www.cs.washington.edu/homes/jeffro/pubs/hightower2000indoor/hightower2000indoor.pdf

[20] E. Saberinia, and A. H. Tewfik, "Single and Multi-Carrier UWB Communications", *IEEE Proc.* 2003

[21] I. C. Siwiak, P. Withington, S. Phelan, "Ultra-Wide Band Radio: The Emergence of an Important New Technology", *IEEE Proc. VTC,* Vol. 2.pp. 1169 -1172, spring 2001

[22] S. J. Ingram, D. Harmer, and M. Quinlan, "UltraWideBand Indoor Positioning Systems and their Use in Emergencies", *IEEE Proc.* 2004

[23] D. Cyganski, J. A. Orr and W. R. Michalson, "A Multi-Carrier Technique for Precision Geolocation for Indoor/Multipath Environments", *Institute of Navigation Proc. GPS/GNSS*, Portland, OR, September 9-12 2003

[24] F. V. Diggelen, "Indoor GPS theory & implementation", *IEEE Proc.* Position Location and Navigation Symposium, pp. 240 – 247, April 15-18 2002

[25] S. H. Im, G. I. Jee, and Y. B. Cho, "An Indoor Positioning System Using Time-Delayed GPS Repeater", *Institute of Navigation Proc. GPS/GNSS*, Fort Worth, TX, September 26-29 2006

[26] B. Alavi and K. Pahlavan, "Bandwidth Effect on Distance Error Modeling for Indoor Geolocation", *IEEE Proc.* 14th International Symposium on Personal Indoor and Mobile Radio Communications (PIMRC'03), Beijing, China, September 7-10 2003

[27] B. Alavi and K. Pahlavan, "Studying the Effect of Bandwidth on Performance of UWB Positioning Systems", *IEEE Proc.* Wireless Communications and Networking Conference (WCNC), Las Vegas, USA, April 3-6 2006

[28] http://www.fcc.gov/Bureaus/Engineering_Technology/News_Releases/2002/nret0203.html

[29] http://standards.ieee.org/board/nes/projects/802-15-3a.pdf

[30] **To Appear in ION Journal**: H. K. Parikh, W. R. Michalson, "Impulse Radio - UWB or Multicarrier Carrier - UWB for non GPS based Indoor Precise Positioning Systems", Journal, Institute of Navigation

[31] H. K. Parikh, W. R. Michalson and R. James Duckworth, "Performance Evaluation of the RF Receiver for Precision Positioning System", *Institute of Navigation, Proc. GPS/GNSS*, Long Beach, CA, September 2004

[32] R. James Duckworth, H. K. Parikh, W. R. Michalson, "Radio Design and Performance Analysis of Multi Carrier-Ultrawideband (MC-UWB) Positioning System", *Institute of Navigation Proc. NTM*, San Diego, CA, January 2005

[33] H. K. Parikh, W. R. Michalson and R. James Duckworth, "MC-UWB Positioning System – Field Tests, Results and Effect of Multipath", *Institute of Navigation Proc. GPS/GNSS*, Long Beach, CA, September 2005

[34] D. Cyganski, J. Duckworth, S. Makarov, W. Michalson, J. Orr, V. Amendolare, J. Coyne, H. Daempfling, S. Kulkarni, H. Parikh, B. Woodacre, "WPI Precision Personnel Locater System", *Institute of Navigation Proc. AM*, Cambridge, MA, April 2007

[35] **To Appear in IEEE Proc.**: H. K. Parikh, W. R. Michalson, "Error Mechanisms in RF-Based Indoor Positioning Systems", *IEEE Proc. International Conference on Acoustics, Speech and Signal Processing*, Las Vegas, CA, April 2008

[36] **To Appear in ION Proc.**: H. K. Parikh, W. R. Michalson, Provisional Title: "Performance Limiting Error Sources for RF-Based Indoor Positioning Systems", *Institute of Navigation Proc. NTM*, San Diego, CA, January 2008

Chapter 2 : Ultra Wideband Based Systems

Introduction

A goal in applications like tracking fire fighters indoors is to achieve a positioning accuracy of better than 1m in extremely challenging multipath and Non Line of Sight (NLOS) indoor conditions. Generally, indoor positioning accuracy improves with increasing bandwidth and/or increasing the ability to separate multipath reflections and extract the true Line of Sight (LOS) signal. Thus, development of systems for indoor positioning using Ultra Wideband (UWB) techniques is gaining popularity as one can design new signal and system architectures. Two promising UWB based approaches for

indoor positioning are Impulse Radio Ultra Wideband (IR-UWB) and Multicarrier Ultra Wideband (MC-UWB).

This chapter will discuss the essential details of the signal structure, transmitter structure, receiver structure, and receiver synchronization for both IR-UWB and MC-UWB systems. Following this, a comparison of the two system architectures is presented which provides more insight into practical system implementation issues in IR-UWB and MC-UWB systems. Simulation results are then presented to analyze the performance of IR-UWB and MC-UWB based positioning systems in the presence of multipath. These basic simulations indicate that an MC-UWB based positioning system may have advantages over an IR-UWB based system. Based on these simulations an MC-UWB based indoor positioning system prototype is implemented and used for extensive field tests. Ranging results using this prototype are then presented followed by our conclusions.

Impulse Radio Ultra Wideband (IR-UWB)

IR-UWB positioning systems measure the time of arrival of a short pulse to estimate the distance between the transmitter and the receiver. The positioning system initialization process involves estimating the first arrival path of the pulse after which the other path delays can be calculated with reference to this first path as the transmitter position changes. In principle, these narrow pulse widths allow the separation of the direct path from the multipath because their duration is short relative to the time of arrival of the multipath reflections.

Unlike narrowband radio systems, IR-UWB systems transmit carrier-free impulses. The IR-UWB signal is generated in the time domain after which pulse shaping and filtering is implemented to obtain a signal that has the desired frequency spectrum. The theoretical advantage of IR-UWB systems is their very good time domain resolution which is the pulse width of the signal. This pulse width is inversely proportional to the signal bandwidth and the wider the signal bandwidth, the narrower the pulse width. For example a signal using a 1nsec pulse width has a time domain resolution of 1nsec, meaning that pulses arriving 1nsec apart can theoretically be separated from each other. Many suitable pulse design options are available for IR-UWB systems, the most practical and feasible pulse shape being the bell-shaped Gaussian pulse and its derivatives as this family of pulses has the lowest side lobe energy due to the

smooth rise and fall of the time-domain signal. The equation below shows the time domain representation for a commonly used Gaussian monocycle pulse, where τ is pulse width.

$$g(t) = \frac{t}{\tau}\exp\left(\frac{t}{\tau}\right)^2 \tag{2.1}$$

This Gaussian monocycle pulse with a single zero crossing is the first derivative of a Gaussian pulse and its spectrum after spectral smoothing is shown in Figure 2.1. The pulse width τ, of this pulse is 1nsec.

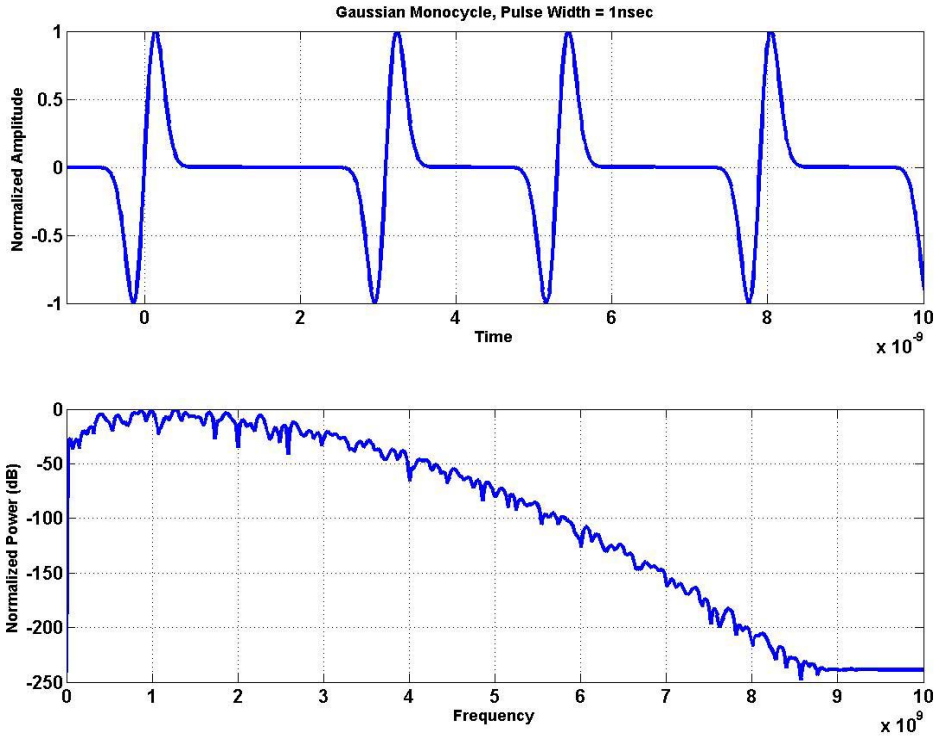

Figure 2.1 IR-UWB Gaussian Monocycle Pulse Train and its Frequency Spectrum

A UWB monocycle pulse has a center frequency, $f_o=1/\tau$. The -3dB bandwidth for a monocycle is approximately 116% of the center frequency [1]. Thus, for the UWB pulse shown in Figure 2.1, the half power bandwidth is approximately 1.16GHz, centered at 1GHz.

The IR-UWB receiver is only required to listen for a short time τ (pulse width), at the pulse repeat rate T_r. Thus, the effect of any external continuous interference is reduced and the Processing Gain (PG) in dB due to this low duty cycle is given by $PG_1 = 10log_{10}(T_r/\tau)$, which can be increased by reducing the pulse width or by increasing the pulse repeat rate. However, this increase in pulse rate to achieve more processing gain cannot be implemented in IR-UWB precise positioning systems as it will lead to a smearing of the pulses in the time domain, thus degrading the Time of Arrival (TOA) estimation. For highly dispersive indoor channel environments the worst case rms delay spread is approximately 25nsec [2], and thus the pulse repeat rate should be less than 40MHz (1/25nsec).

In addition to a pulse repeat rate, a pulse width also must be selected. For IR-UWB precise positioning systems, a narrow pulse width is desirable, as it determines the time domain resolution of the system. Reducing the pulse width, results in wider signal bandwidth and gives higher time domain

resolution at the cost of a higher noise floor and less signal to noise ratio, thus limiting the range of operation.

Thus, in an IR-UWB system design, the pulse width and the pulse repeat rate are chosen depending on the required time resolution and system performance. In navigation applications, as opposed to communications applications where high data rate is important, the pulse repeat rate requirements are not excessive since they tend to be related to the desired navigation update rate of the system. However, narrow pulse widths are critical to being able to achieve positioning accuracy of better than 1m.

Transmitter Structure for Impulse Radio Based Systems

Traditional IR-UWB systems generate carrier-free pulses that propagate in the radio channel. Such an approach is referred to as a baseband signaling approach where the transmitter signal occupies the available bandwidth of 3.1GHz to 10.6GHz (as per Federal Communications Commission - FCC, regulations in the United Sates). An example transmitter structure for IR-UWB [3] is shown in Figure 2.2 which consists of a low-level pulse generator followed by a bandpass filter and a transmit antenna.

Figure 2.2 IR-UWB Transmitter Structure

One practical way of implementing the impulse generator involves the use of a transmission line to generate tunable Gaussian monocycle pulses [4, 5]. It is also possible to generate the impulse digitally by adding two digital pulses that are delayed from each other [1]. Both techniques result in a Gaussian monocycle pulse.

Receiver Structure and Synchronization for IR-UWB

The most widely used IR-UWB receiver structure consists of a wideband analog correlator [6], which uses a multiplier followed by an integrator as shown in Figure 2.3. The received pulse is multiplied with the known Template Reference (TR) waveform as shown in Figure 2.3 and is the input to the integrator. The integrator output is then processed to extract range.

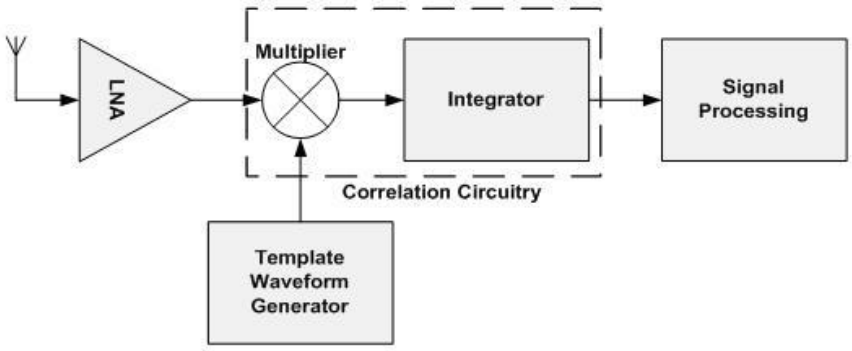

Figure 2.3 IR-UWB Receiver Structure

Positioning systems based on Time of Arrival (TOA) need the estimate of the first arrival path τ_0, from the transmitter. After estimating the TOA for this first path, other path delays τ_j can be calculated with reference to the first path. The received pulse consisting of L multipath components is;

$$P_R(t) = \sum_{j=0}^{L} \alpha_j p_T(t - \tau_j) \tag{2.2}$$

It is not practical to implement a peak detection correlation receiver structure using the ideal template PR(t) as the template reference since the unknown

multipath effects in the channel may severely distort the signal. Implementing the transmitted signal PT(t) as a reference template, is also not practical as this technique assumes that the correct correlation timing, or τ0 is known. Furthermore multiple peaks could appear at the correlator output due to multipath. To overcome these synchronization difficulties, a timing technique using dirty templates (TDT) is proposed in [7] to determine the time of first path arrival τ0. The TDT concept uses pairs of successive symbol-long UWB segments (each IR-UWB symbol is a pulse train) PR(t+kTs+τ) and PR(t+(k-1)Ts+τ), and one segment of this pair serves as a template to the other pair. Multiple such pairs are required at various candidate time shifts, $0 < \tau < Ts$. Integration is performed on the products of these pairs to obtain;

$$x_k(\tau) = \int_0^{T_s} r(t + kT_s + \tau) r(t + (k-1)T_s + \tau) dt \tag{2.3}$$

The crosscorrelation of successive symbol-long received segments reaches a unique maximum if and only if $\tau = \tau_0$. The TDT method does not require the receiver to store the transmit template. Once τ_0 for the initial location is determined, other path delays τ_j can be calculated with reference to τ_0 from the first path. But the challenges in implementing IR-UWB pulse detection even using the TDT technique are a need for fast rise and fall times for the received short pulses and a GHz wideband multiplier. Other challenges include the receiver's sensitivity to interference, signal cross talk and other parasitic effects.

Maintaining synchronization and correcting for clock drifts in an IR-UWB system is also challenging due to the short pulses. This topic is outside the scope of this thesis, but the interested reader can refer to [8] which propose an Orthogonal Sinusoidal Correlation Receiver (OSCR) for detecting and adjusting for clock drift.

Multicarrier Ultra Wideband (MC-UWB)

MC-WB positioning systems measure the phase of arrival of a multicarrier signal. The system initialization process involves estimating the phase differences between the subcarriers since the phase pattern of the received signal is unique for a fixed distance. Since each subcarrier in the multicarrier signal is generated based on the same reference clock, changes in the relative phases of the signal with respect to the initial phase pattern determines the change in distance.

In an MC-UWB system [2, 9, 10], many subcarriers that are orthogonal to each other are simultaneously transmitted. The MC-UWB signal structure no longer gives the time domain resolution of IR-UWB, but super resolution frequency estimation [10, 11, 12] algorithms can be effectively used for position estimation and tracking. Some advantages of the MC-UWB system are high spectral efficiency and good spectral flexibility.

High spectral efficiency comes from the fact that in spite of the multiple subcarriers spanning a wide range of frequencies, each subcarrier is an unmodulated sinusoid which occupies a near-zero bandwidth. Thus, the effective bandwidth occupied is very small compared to that occupied by an IR-UWB system.

Good spectral flexibility comes from the fact that it is not necessary to have subcarriers present at each of the possible subcarrier locations. Individual subcarriers can be nullified or placed at a frequency which allows it to co-exist with other systems occupying the same band. This feature allows the MC-UWB signal to accept interference from, and avoid interference to other systems. Like any other system, a MC-UWB based system also has its own disadvantages and complexities like a need for multiple oscillators, carrier synchronization, and carrier offset issues. The MC-UWB time domain signal is shown below and is the summation of M subcarriers:

$$s(t) = \sum_{m=0}^{M-1} Ae^{2\pi j(f_o + m\Delta f)t} \tag{2.4}$$

where, M is the total number of subcarriers with frequency spacing of Δf and these two parameters define the bandwidth of the MC-UWB. An example signal consisting of 20 subcarriers and its spectrum is shown in Figure 2.4. Signal frequency spacing Δf in the frequency domain is analogous to the pulse repeat rate T_r of an IR-UWB system. From a positioning system perspective, PG is achieved from higher M and wider subcarrier span, as it results in higher multipath resolution and improves multipath robustness.

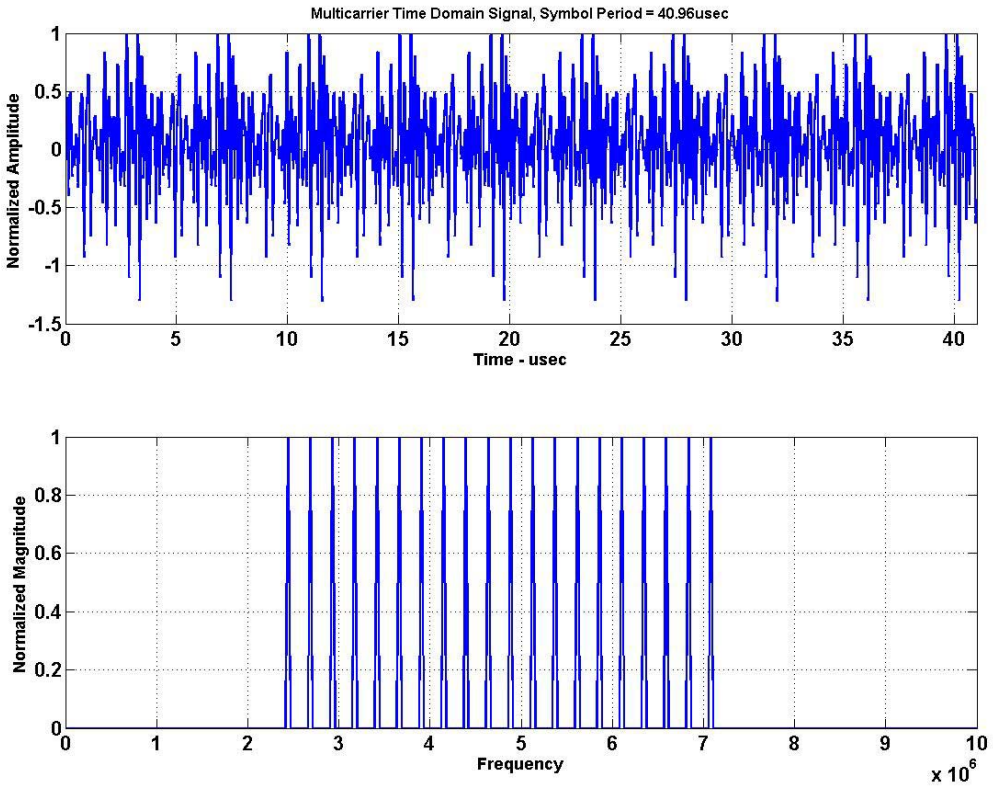

Figure 2.4 Multicarrier Time Domain Signal and its Frequency Spectrum

Transmitter Structure for MC-UWB

The transmitter structure for an example MC-UWB system [13] is shown in Figure 2.5. A signal consisting of multiple subcarriers is generated in software using an Inverse Discrete Fourier Transform (IDFT) operation, undergoes digital to analog conversion and is upconverted to occupy the desired spectrum. The analog front end of the transmitter consists of filters, mixers and amplifiers. One of the problems in such a MC-UWB transmitter architecture is the need for highly linear RF components due to the non-constant signal envelope as is shown in Figure 2.4. Higher linearity is desired as it implies higher dynamic range which directly determines the range of operation for the positioning system. Hence, the trade offs between amplifier efficiency, linearity and design of high dynamic range transmitters and receivers are important issues in MC-UWB based positioning system design.

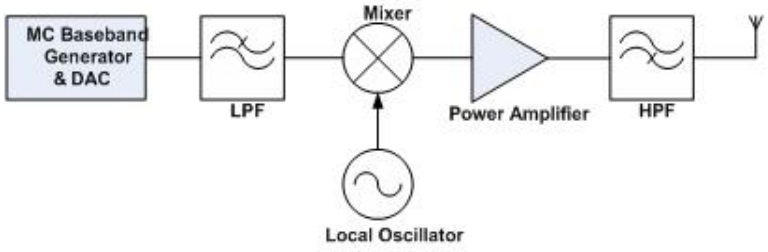

Figure 2.5 MC-UWB Transmitter Structure

Receiver Structure and Synchronization for MC-UWB

MC-UWB receiver structure shown in Figure 2.6 is a direct down conversion implementation. The sampled baseband signal is digitized and Discrete Fourier Transform (DFT) operation is implemented in the signal processing block shown in Figure 2.6 to extract the sinusoidal components. Any required signal processing can be performed on the baseband samples using this software radio based receiver structure.

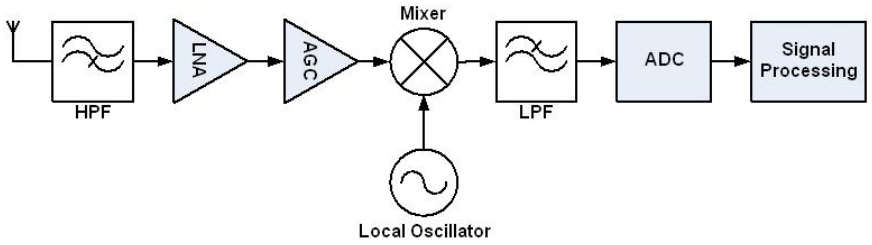

Figure 2.6 MC-UWB Receiver Structure

Similar to IR-UWB pulse detection, synchronization is needed at the receiver to detect the MC-UWB symbol. If the receiver knows some information about the received MC-UWB symbol, like a training sequence, then a delay and correlate technique [14] can be used to acquire symbol timing. Such a delay and correlate technique shown in Figure 2.7 takes advantage of a known training sequence. The two sliding windows used in the delay and correlate technique are C and P. The C window is the crosscorrelation between the received signal and its delayed version, where the delay D equals the time period of a known training sequence.

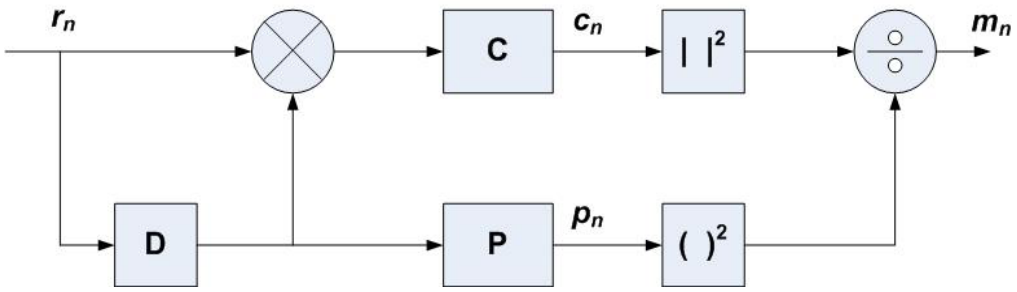

Figure 2.7 Delay and Correlate Symbol Detection

The threshold m_n is the ratio of c_n and p_n and are calculated as per the equations shown below.

$$c_n = \sum_{k=0}^{L-1} r_{n+k} r_{n+k+D}$$
$$p_n = \sum_{k=0}^{L-1} | r_{n+k+D} |^2 \qquad (2.5)$$
$$m_n = \frac{| c_n |^2}{(p_n)^2}$$

Thus when the symbol is received, the crosscorrelation output jumps to a maximum value, due to identical training symbols, indicating start of the symbol. For positioning applications using MC-UWB, phase of arrival information is used in range estimation and thus phase calibration at an initial known position is required. The phases of the subsequent symbols are then compared with this initial phase and the change of phase gives the distance estimate with reference to the initial position. Maintaining the synchronization and correcting for clock drifts in MC-UWB system is easier compared to IR-UWB system, as it can be done in digital domain. This topic is outside the scope of the thesis and interested

reader can refer to [13] which propose a frequency domain equalizer (ROTOR) to compensate for the phase rotation due to clock drifts.

Architecture Comparison

IR-UWB systems suffer from issues like pulse shaping, dispersion ringing effect, antenna and front-end co-design, high rate analog to digital converters, and precise time reference. Designing and optimizing the IR-UWB pulse generation circuitry to meet the desired pulse width, optimum bandwidth, and efficient transmit power requirements is difficult, as it is sensitive to parasitic capacitance and cross talk. The software based MC-UWB system makes signal generation, spectrum shaping, and receiver signal processing simple and repeatable. With the availability of high linearity RF components like automatic gain control amplifiers, mixers, and power amplifiers, the RF design and development is also comparatively more repeatable than IR-UWB systems as less tuning is required.

An IR-UWB system is a time domain based system. Figure 2.8 shows the IR-UWB time domain signal in absence of multipath (top) and in presence of multipath (bottom) for an example where three multipath signals are received at the receiver. As it can be seen, the pulses spread in time and the first pulse received need not be the strongest pulse received. In addition, the multipath reflections smear the received signal in time domain, making it difficult to separate reflections. These factors may lead to errors in an IR-UWB based positioning system.

MC-UWB system is a frequency domain based system. Figure 2.9 shows the MC-UWB frequency spectrum in absence of multipath (top) and in presence of multipath (bottom). As it can be seen, the frequency spectrum is no longer flat, thus causing the multicarrier phase distortion which could lead to errors in an MC-UWB based positioning system. Since not all carriers are required to resolve range, even though fading of some carriers occurs, it does not necessarily translate to range error in the system.

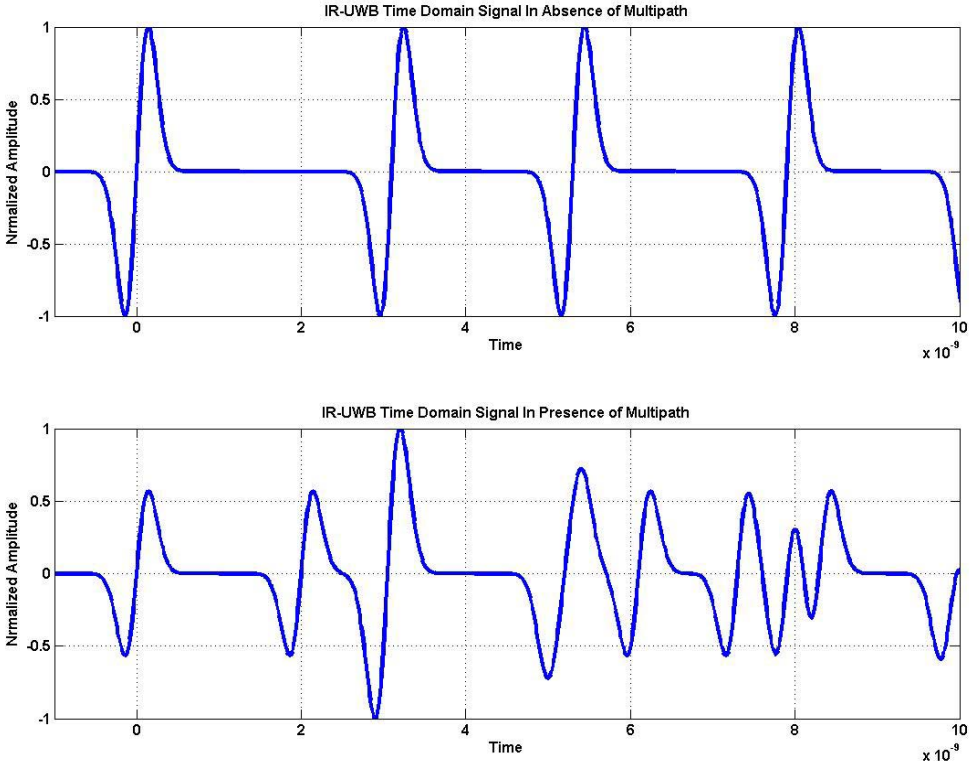

Figure 2.8 IR-UWB Signal in Absence and Presence of Multipath

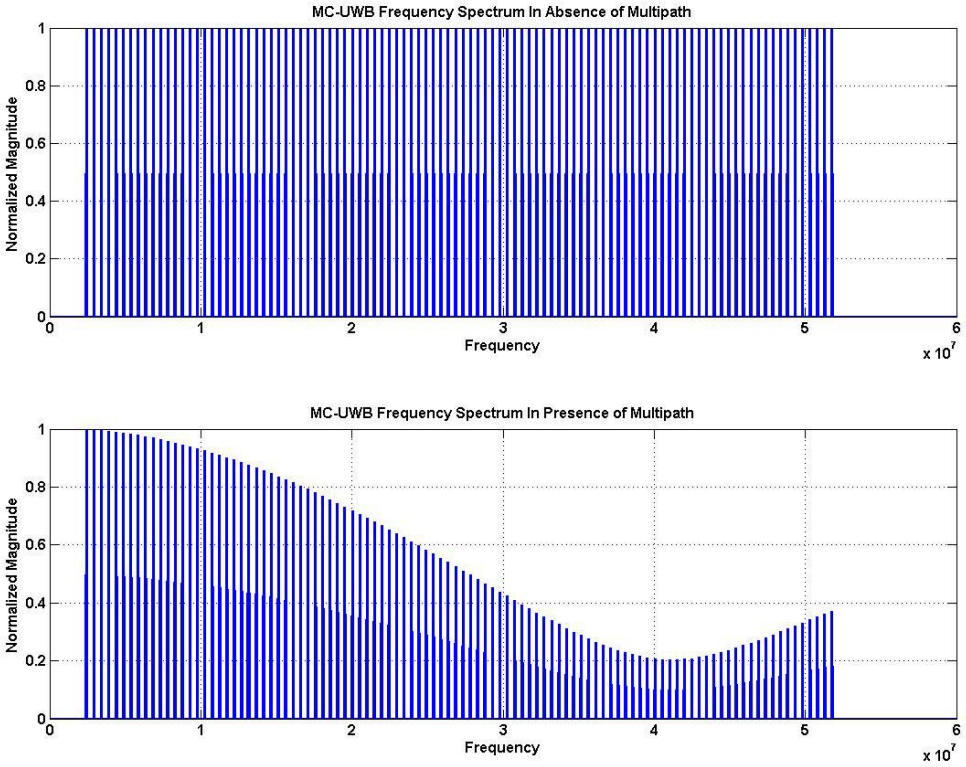

Figure 2.9 MC-UWB Signal in Absence and Presence of Multipath

Signal processing algorithms [10, 15] that optimize performance of IR-UWB and MC-UWB are needed to achieve precise positioning indoors. Table 2.1 shows the comparison of IR-UWB and MC-UWB radio architectures.

Table 2.1 Comparison between IR-UWB and MC-UWB

	IR-UWB	**MC-UWB**
Signal Generation	In time domain, very sensitive to parasitic capacitance, cross talk makes it difficult to control and fine tune the pulse width.	In frequency domain, is flexible as it is implemented in software.
RF Front End	Power amplifier and LNA are hard to design for narrow impulse signal type. Less RF components needed due to carrier free nature. Relaxed requirement on linearity of RF components.	Matching for RF devices is easier compared to IR-UWB. More RF components and circuitry are needed. Non constant envelope requires highly linear RF components.
Base band	High ADC requirements.	Less severe ADC requirements.
Antennas	Antenna and Front end co-design required as antenna distorts the pulse shape.	Antenna and the front end can be designed independently.

Positioning Using IR-UWB and MC-UWB / MC-WB

This section compares the simulated performance of multicarrier based and impulse radio based positioning systems. The impulse radio based positioning system from [15] is chosen because it was the most complete simulated IR-UWB implementations available in the literature. Thus, the positioning estimation results presented in [15] were chosen as a reference and the signal parameters for multicarrier based positioning system [10] were then chosen such that, they achieve positioning estimation results that are comparable to the chosen IR-UWB system. The simulated multicarrier based positioning system uses a multicarrier signal spanning a 50MHz wide band, centered at 440MHz. This MC-UWB configuration results in positioning accuracies comparable to those obtained by the reference IR-UWB system.

It should be noted that since this multicarrier signal has a fractional bandwidth of only 11.3% it actually does not satisfy the definition of a UWB system (the FCC defines UWB as 20% fractional bandwidth or 500MHz minimum bandwidth). Thus, henceforth this particular multicarrier configuration will be referred to as a multicarrier wideband system, MC-WB instead of MC-UWB. This 50MHz MC-WB system can be easily extended to a MC-UWB system (although this is not necessary in the current example).

In the MC-WB simulated system the signal processing algorithm uses eigenvalue decomposition methods based on a state space approach [11], to separate the direct path from the multipath reflections. Once the direct path is identified, the MC-WB positioning system observes the change of phase of the subcarriers to determine the distance between the transmitter and the receiver. The IR-UWB system is based on time of arrival estimation of a short pulse to determine the distance between the transmitter and the receiver.

The simulation parameters used for the two positioning systems being compared is summarized in Table 2.2. Both the simulated systems use 4 receivers to estimate the transmitter's position in three dimensions**.** The transmitter's final position estimate is obtained by averaging the estimates obtained over 1000 runs and a three path multipath model is used as the channel model for both systems. The IR-UWB signal has a pulse width of 400psec generated with 6GHz sampling rate. The MC-WB signal consists of 102 subcarriers, with 439.4kHz subcarrier spacing, which spans 50MHz centered at 440MHz and is generated at 200MHz sampling rate. Both of the simulated systems assume ideal synchronization to ensure a fair comparison.

The simulation result shown in Figure 2.10 compares the performance of the IR-UWB positioning system and the MC-WB positioning system. The IR-UWB results shown in Figure 2.10 are re-plotted from [15]. The errors in Figure 2.10 for IR-UWB and MC-WB systems are the RMS position

estimation errors for various SNR ratios. It can be seen in Figure 2.10 that the results are within 0.2m of each other. From the simulation results, it can also be observed that both IR-UWB and MC-WB techniques are capable of providing position estimation results that are accurate to within 1m. Hence the choice of which technique is better suited depends mainly on ease of practical design implementation.

To produce the results shown in Figure 2.10, the IR-UWB system needs 2.5GHz bandwidth and a sampling rate of 6GHz, while MC-WB system uses 50MHz bandwidth and a sampling rate of 200MHz, to achieve a similar level of accuracy. Moreover, unlike IR-UWB system, the MC-WB system can co-exist with other services as the unoccupied spectrum between the two subcarriers can be utilized by other services. In addition, the MC-WB system is spectrally efficient as compared to the IR-UWB system. Even if the MC-WB signal spans 50MHz, the actual spectral occupancy for total of 102 subcarriers is approximately only 51kHz (assuming 500Hz spectral occupancy for a single unmodulated subcarrier). This leads to an important conclusion that an MC-WB based positioning system implementation has a spectral footprint that makes it preferable over IR-UWB based positioning system.

Table 2.2 Simulation Parameters for IR-UWB and MC-WB System

	IR-UWB	**MC-WB**
Test Setup	1Tx-4Rx (3D Positioning)	1Tx-4Rx (3D Positioning)
Averaging over	1000 runs	1000 runs
Multipath Channel	3 Path Model	3 Path Model
Positioning Method	TOA	TOA
Algorithm	Non Linear Optimization based on Davidon-Fletcher Powell (DFP)	Eigen Value Decomposition based on State Space Approach
Sampling Rate	6GHz	200MHz
Bandwidth Span	Approx. 2.5GHz (400psec pulse width)	Approx. 50MHz (102 Subcarriers with 439.4kHz spacing)
Synchronization	Assumed Ideal	Assumed Ideal

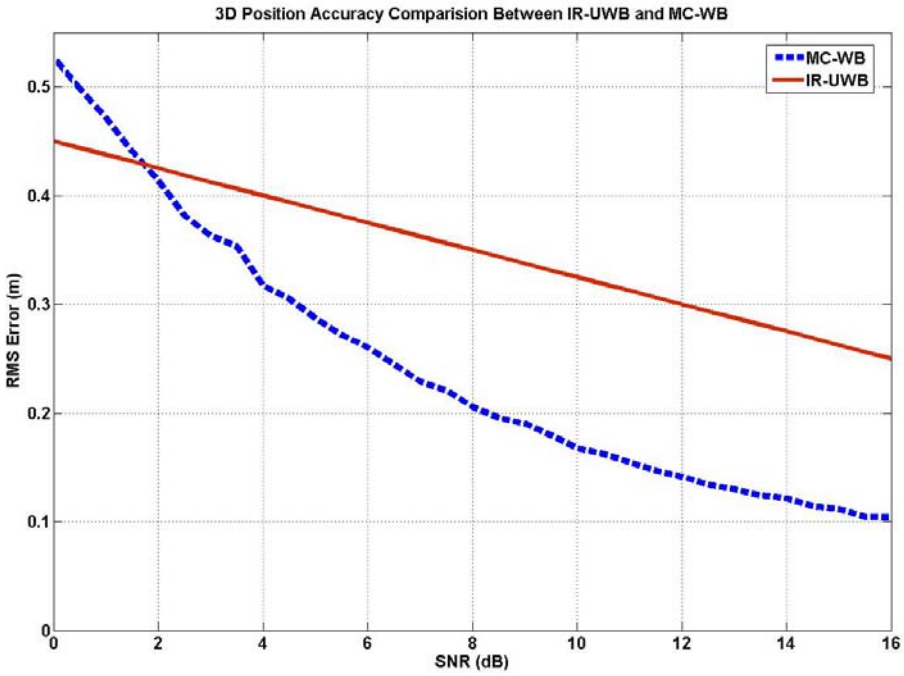

Figure 2.10 Position Estimates Using IR-UWB and MC-WB

Conclusion

UWB technology is an attractive means to achieve precise positioning indoors and various technical aspects of Impulse Radio based and multicarrier based UWB implementations were discussed. The concept of positioning using a MC-UWB system that is based on measuring the subcarrier phase differences was discussed and the positioning accuracy results were compared with an IR-UWB positioning system.

Using simulation it was shown that both MC-UWB and IR-UWB systems can perform equally well, and that both are capable of achieving accuracies under 1m. However, the less severe sampling rate requirement for MC-UWB, availability of frequency domain signal processing algorithms and ability to co-exist without interfering to other systems make the spectrally friendly MC-UWB system a more practical system for indoor precise positioning applications.

References

[1] I. Oppermann, "UWB: Theory and Applications", *Weily Publication*, ISBN: 0470869178, 2004

[2] A. Batra, J. Balakrishnan, G. R. Aiello, J. R. Foerster, A. Dabak, "Design of a Multiband OFDM System for Realistic UWB Channel Environments", *IEEE Transactions Microwave Theory and Techniques*, Vol. 52, September 2004

[3] R. J. Fontana, "Recent System Applications of Short-Pulse UWB Technology", *IEEE Transactions on Microwave Theory and Techniques,* Vol. 52, September 2004

[4] J. Han, C. Nguyen, "On the Development of a Compact Sub-Nanosecond Tunable Monocycle Pulse Transmitter for UWB Applications", *IEEE Transactions on Microwave Theory and Techniques*, Vol. 54, January 2006

[5] J. S. Lee, C. Nguyen, T. Scullion, "New Uniplaner Subnanosecond Monocycle Pulse Generator and Transformer for Time-Domain Microwave Applications", *IEEE Transactions on Microwave Theory and Techniques*, Vol. 49, June 2001

[6] H. Khorramabadi, P. R. Gray, "High Frequency CMOS Continuous-Time Filters", *IEEE Journal of Solid-State Circuits*, Vol. SC-19, NO. 6, December 1984

[7] L. Yang, G. B. Giannakis, "Ultra-Wideband Communications – An Idea Whose Time Has Come", *IEEE Signal Processing Magazine*, November 2004

[8] L. Ya-Lin, Y. Hua-Rui, F. Quan, X. Pei-Xia, "A Frequency Synchronization Method for IR-UWB System", *IEEE Proc., Wireless Communications, Networking and Mobile Computing,* September 21-25 2007

[9] S. Roy, J. R. Foerster, V. Srinivasa, D. G. Leeper, "Ultrawideband Radio Design: The Promise of High Speed, Short-Range Wireless Connectivity", *IEEE Proc.*, Vol. 92, No.2, February 2004

[10] D. Cyganski, J. A. Orr and W. R. Michalson, "A Multi-Carrier Technique for Precision Geolocation for Indoor/Multipath Environments", *Institute of Navigation Proc., GPS/GNSS*, Portland, OR, September 9-12 2003

[11] B. D. Rao, K. S. Arun, "Model Based Processing of Signals: A State Space Approach", *IEEE Proc.*, Vol. 80, no. 2, pp. 283-309, February 1992

[12] X. Li, K. Pahlavan, "Super-Resolution TOA Estimation with Diversity for Indoor Geolocation", *IEEE Transactions on Wireless Communications*, Vol. 3, no. 1, January 2004

[13] H. K. Parikh, W. R. Michalson and R. James Duckworth, “Performance Evaluation of the RF Receiver for Precision Positioning System”, *Institute of Navigation Proc., GPS/GNSS*, Long Beach, CA September 21-24 2004

[14] J. Heiskala, J. Terry, “OFDM Wireless LANs: A Theoretical and Practical Guide”, *SAMS* Publication, ISBN: 0672321572, 2001

[15] K. Yu, I. Oppermann, “Performance of UWB Position Estimation Based on Time-of-Arrival Measurements”, *IEEE Proc., Ultrawideband Systems and Technology*, May 18-21 2004

Chapter 3 : Initial System Design

Introduction

The type of signal structure used for the indoor positioning system plays a major role in the RF design, development and evaluation. Based on the analysis of Chapter 2, and previous success using the MC-UWB techniques in an audio test-bed [1] signal structure selected for WPI's PPL system is a multicarrier type signal. Although the previous simulation data illustrated potential advantages to an MC-UWB based positioning system, these simulations did not consider the impact of such a multicarrier signal on the RF design of the system. True verification of the system concept would require the development of a

test-bed which consisted of the RF and other systems needed to make a working indoor positioning prototype.

Traditional multicarrier systems use modulated sinusoids, which leads to severe IMD products and spurs in between the sinusoids, making the RF design and evaluation a difficult task. In our case the system does not provide a communications capability, and therefore it was decided to use unmodulated sinusoids. This decision is expected to not only reduce the problems associated with IMD products and spurs, but also has a major advantage that the signal will now occupy much less bandwidth.

An example of the unmodulated multicarrier signal frequency spectrum is shown in Figure 3.1. Such a signal structure contains multiple equally spaced unmodulated sinusoids, called subcarriers. The span of this multicarrier signal can be easily changed as the signal generation is performed in software.

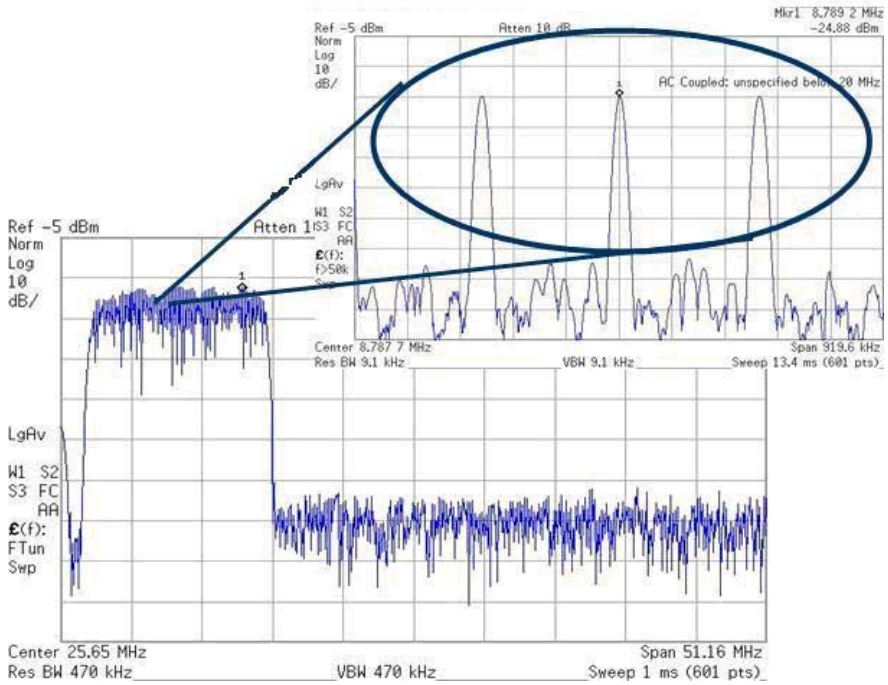

Figure 3.1 Example Unmodulated Multicarrier Signal Frequency Spectrum

In order to determine the behavior of unwanted IMD products and spurs, our initial RF system was simulated using ADS. These ADS simulations used two tone, multitone, orthogonal and non-orthogonal unmodulated sinusoids to excite the simulated RF chain. The simulation results are presented in this chapter. These results helped in developing a better understanding of the expected RF component behavior when unmodulated multicarrier signals are used to drive amplifiers, mixers and other RF components.

Multicarrier Effect on RF Design

The simulation model for a direct upconversion transmitter and a direct downconversion receiver RF chain using ADS is shown in Figure 3.2.

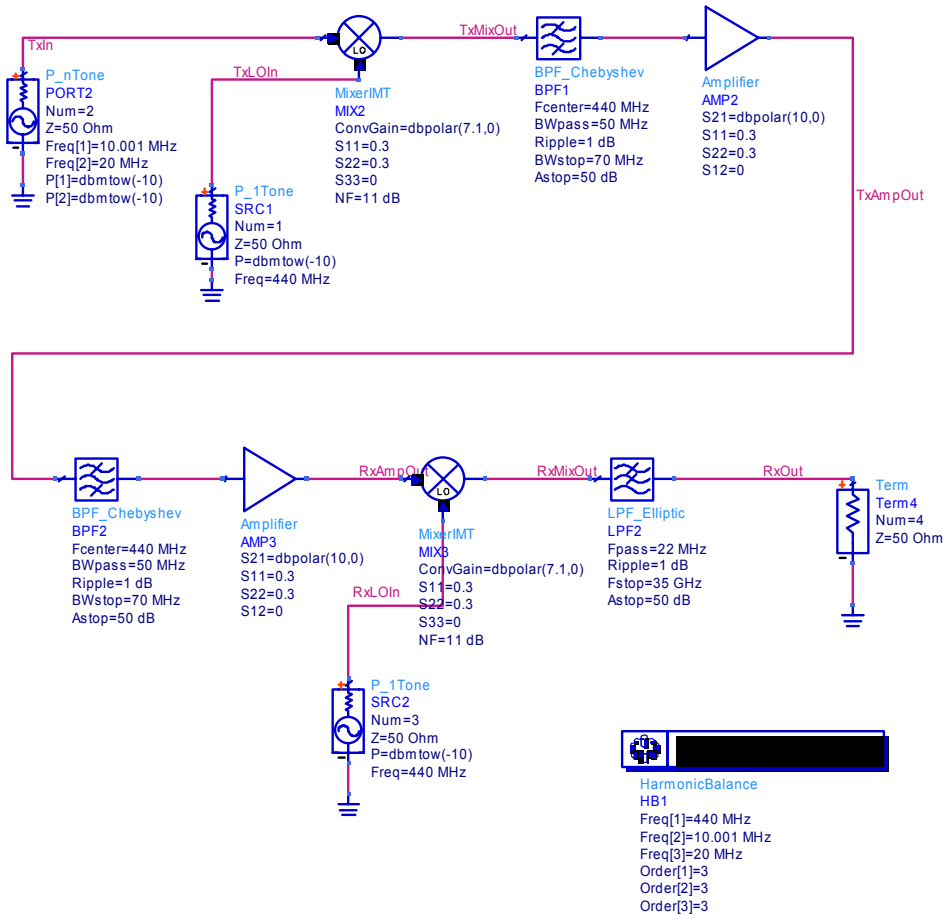

Figure 3.2 ADS RF Chain Simulation Setup

The two tone or multitone baseband signal is input to the mixer which has a conversion loss of 7.1dB and whose other input is a 440MHz local

oscillator. This is followed by a Band Pass Filter (BPF), with a 50MHz passband, the output of which is then the input to the RF amplifier of 10dB gain. As we want to analyze only the effect of two tone and multitone baseband inputs on the RF design, and not the effects of channel, the output of the transmitter is connected directly to the input of the receiver. The receiver RF chain similarly contains the BPF, amplifier, downconverting mixer followed by the Low Pass Filter (LPF). The Inter Modulation Table (IMT) was also provided for both the mixers to make the ADS simulations reflect more realistic results for the Inter Modulation Distortion (IMD) products and spurs.

The non-orthogonal two tone signal used consists of 11MHz and 19MHz unmodulated sinusoids, and the orthogonal two tone signal used consists of 10MHz and 20MHz unmodulated sinusoids. Similarly the non-orthogonal multitone signal (five tones) used consists of 3MHz, 7MHz, 11MHz, 16MHz, and 20MHz unmodulated sinusoids and the orthogonal multitone signal (five tones) used consists of 5MHz, 10MHz, 15MHz, 20MHz, and 25MHz unmodulated sinusoids. The baseband input and corresponding receiver LPF output for two tone and multitone, orthogonal and non-orthogonal signals are shown in Figure 3.3 to Figure 3.6.

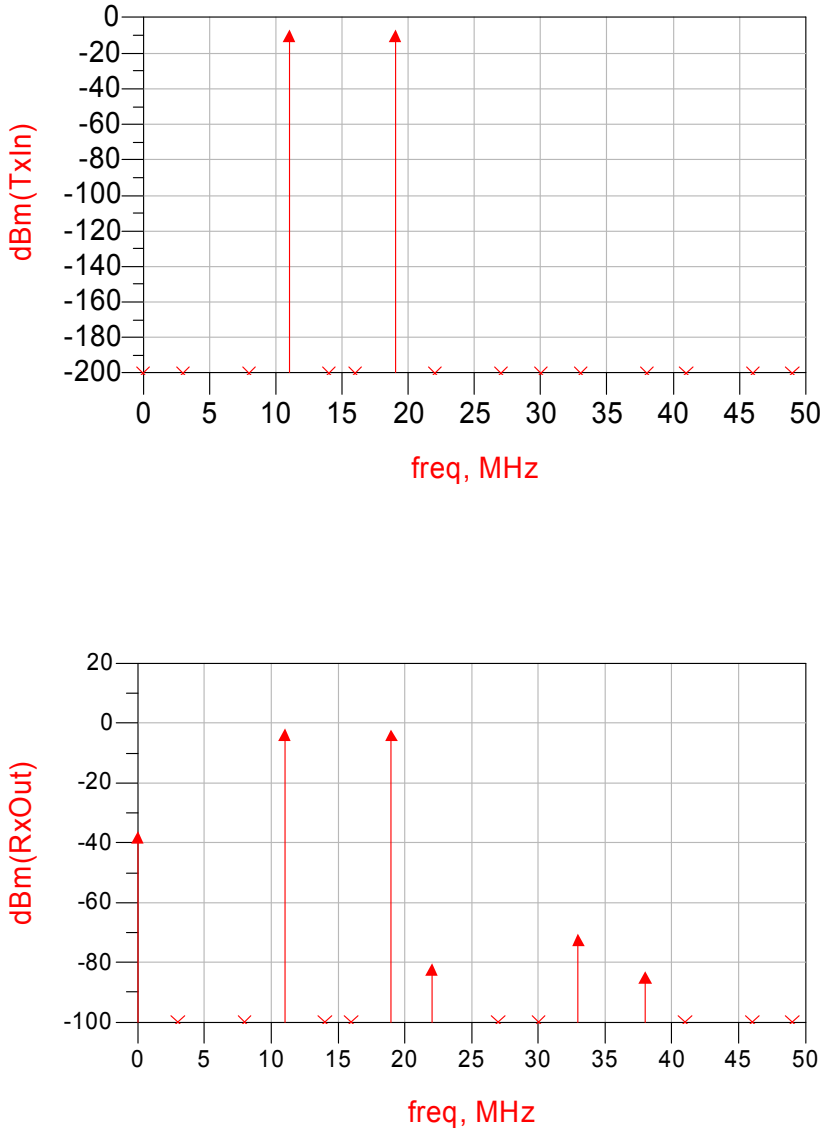

Figure 3.3 Two Tone Non-Orthogonal Input (Top) and LPF Output (Bottom)

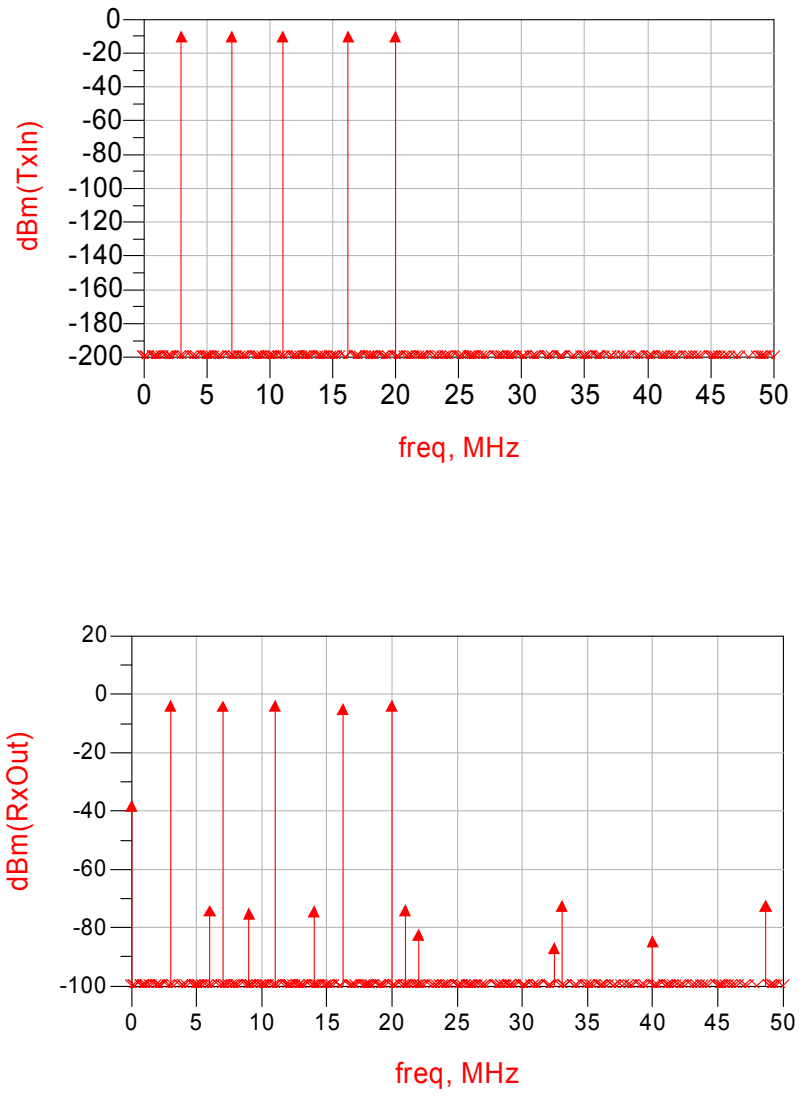

Figure 3.4 Multitone Non-Orthogonal Input (Top) and LPF Output (Bottom)

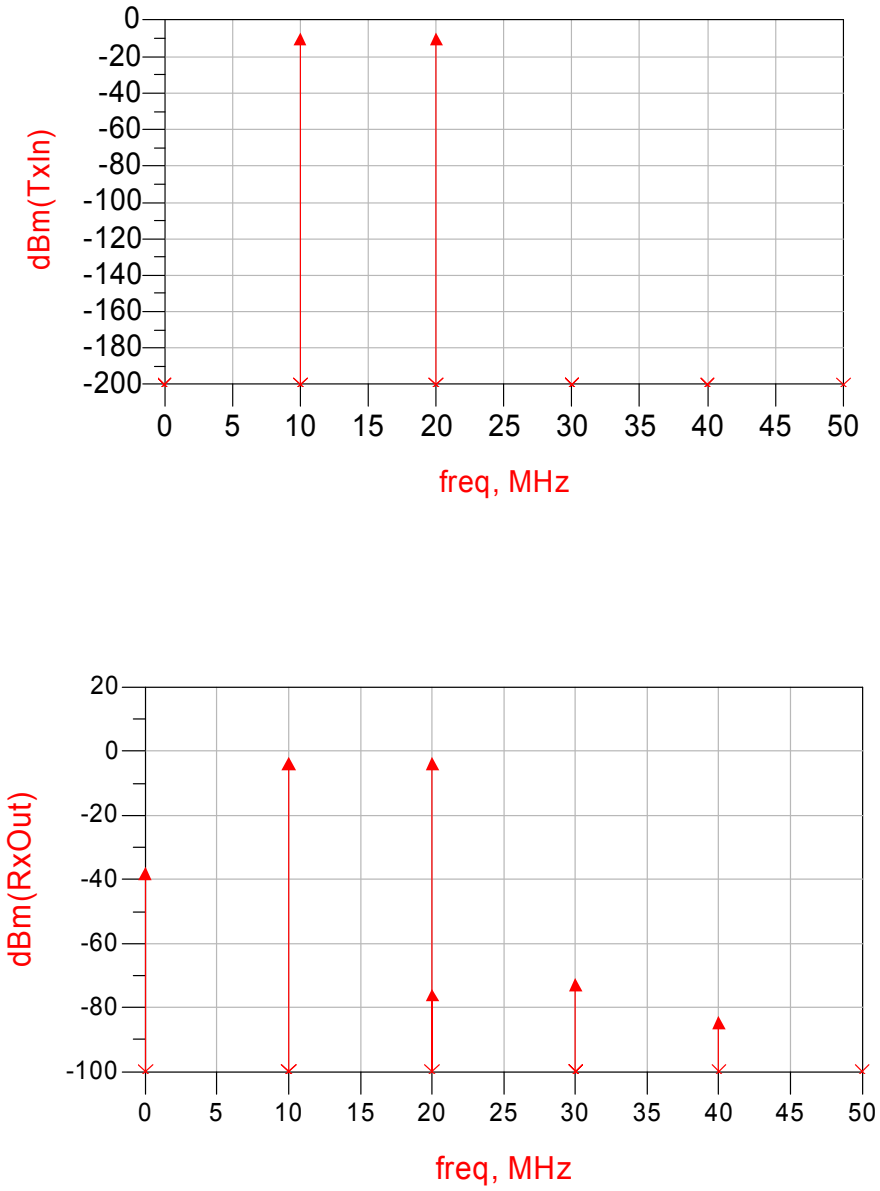

Figure 3.5 Two Tone Orthogonal Input (Top) and LPF Output (Bottom)

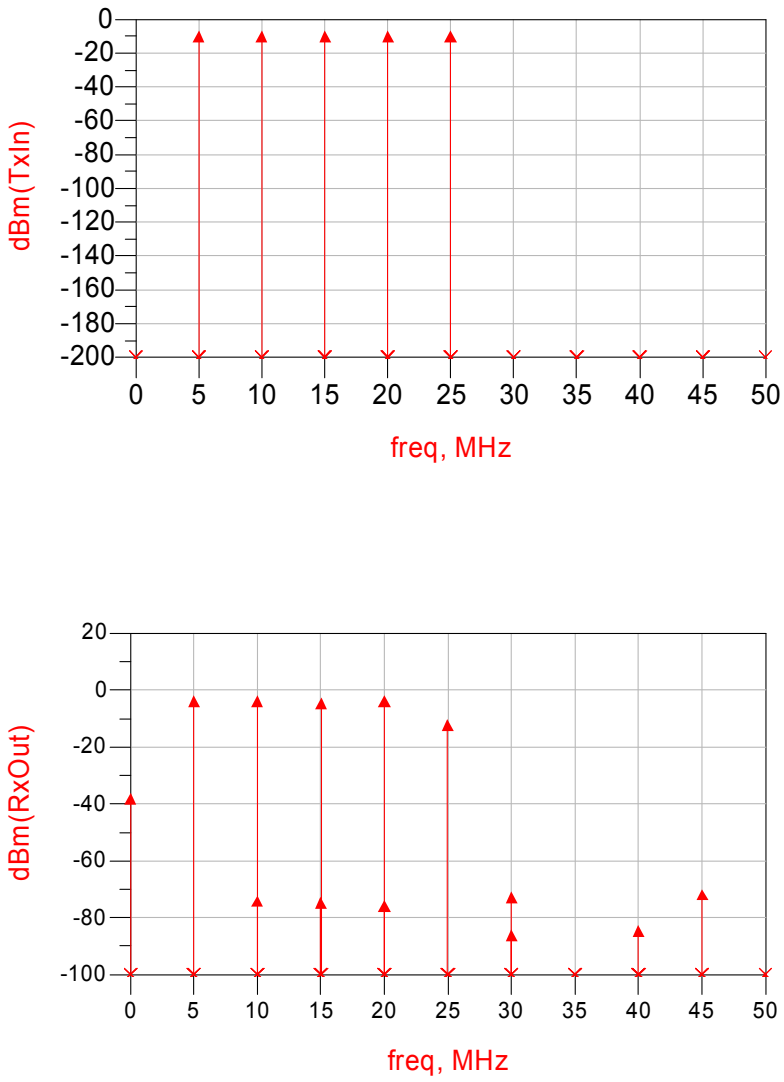

Figure 3.6 Multitone Orthogonal Input (Top) and LPF Output (Bottom)

The output of the non-orthogonal two tone test shown in Figure 3.3, shows the IMD products at approximately -75dBm. The output of non-orthogonal multitone test shown in Figure 3.4 shows two effects. First, using multiple non-orthogonal signals increases the magnitude of some of the IMD products and hence not desired as it will affect the Spurious Free Dynamic Range (SFDR) of the system. Second, the IMD products are spread erratically across the occupied bandwidth, potentially leading to problems maintaining reasonable spurious emission components. This leads to a conclusion that non-orthogonal signals are not suitable to be used in the anticipated MC-UWB positioning system.

Simulation results using orthogonal signals are shown in Figure 3.5 and Figure 3.6. It can be seen that in this case the IMD products fall on top of the required sinusoids. While this may cause a change in phase for that sub carrier, the change is constant and can therefore be eliminated through calibration. Thus using orthogonal signals improves the Spurious Free Dynamic Range (SFDR) of the system.

Also notice that the IMD levels for the two tone and multitone tests using orthogonal signals are similar, at approximately -75dBm. Thus another major advantage of using orthogonal signals is that one can use two tone tests, instead of using multitone tests to further characterize the RF prototype system. This will greatly simplify the RF prototype development and evaluation.

Thus, based on the above ADS simulations, three important system design aspects for a MC-UWB based positioning system are proposed:

1) Unmodulated multicarrier signals should be implemented as they occupy less bandwidth and reduce the IMD products and undesired spurs.
2) Orthogonal signals should be used as they further help improve the system SFDR.
3) Two tone tests can be used for RF evaluation when the signal used is unmodulated orthogonal multicarrier signal.

After completing the ADS simulations, the next important step was to develop a test-bed which is referred to as the Phase 1 RF prototype design. The next section discusses the specifications for this initial Phase 1 RF prototype design. The goals for developing such a RF prototype are to validate the above ADS simulation results and verify the MC-UWB based positioning algorithms.

Phase 1 Initial Design Parameters

In our application, the baseband multicarrier signal is upconverted to a suitable RF frequency and transmitted. This brings us to the issue of selecting a suitable RF frequency for transmission. Using the VHF band (30MHz to 300MHz) means large dimensions for antennas, which is undesirable as it is not portable and wearable. The UHF band, from 300MHz to 3GHz, allows the use of physically smaller antennas, but it is expected that the effect of multipath reflections will increase with increasing frequency.

At frequencies in the range of 1GHz to 3GHz metal objects as small as 0.075m to 0.025m (1/4 wavelength) are reflectors, making GHz band frequencies undesirable. With 800 to 950MHz being allocated for cellular services, the 400MHz to 800MHz band seems like a band where bandwidth may be available, antenna sizes are reasonable and the number of multipath reflectors may be tolerable.

Most of this band, however, is occupied with TV broadcast stations, which demands a design strategy that allows us to share the spectrum with unused TV spectrum. This can be easily achieved due to the spectrally friendly nature of the multicarrier signal since the signal spectrum can be modified by nulling any subcarriers that overlap with TV spectrum in use.

For the purpose of rapid prototyping of Phase 1, the 30MHz band centered at 440MHz is used as it is an approved band for radiolocation and amateur radio. This band is readily available for use and will have minimal interference from other existing services. Thus, the Phase 1 RF prototype design will be such that it can initially use a maximum of 30MHz bandwidth centered at 440MHz and is ample bandwidth for initial tests. Although 30MHz bandwidth is available, it is desired to use minimum possible bandwidth to achieve indoor positioning accuracy of less than 6m. In addition to determining the acceptable minimum bandwidth, the following RF receiver system parameters also need to be considered while designing a RF receiver front end:

- Receiver Sensitivity (*RxSens*)
- Receiver Spurious Free Dynamic Range (*SFDR*)
- Input 3rd Order Intercept Point (*IIP3*)
- Noise Figure (*NF*)
- Gain (*G*)

Based on our findings from ADS simulations, two tone tests will be used to characterize the above system parameters. The *IIP3* of the system is a function of the total power and thus instead of considering the power level per subcarrier we will consider the total power of all subcarriers and then apply the two tone tests for further evaluation. As shown in earlier ADS simulations, the use of an unmodulated orthogonal signal allows us to do the two tone test for a multicarrier

system as long as the power is scaled from per subcarrier to total power of all subcarriers.

For example, if the maximum receiver signal input is -60dBm/SC, then the total power for all 100 subcarriers, will be -40dBm. This is equivalent to using a single carrier of power level -40dBm and then applying two tone tests to determine the system *IIP3*. This makes the *IIP3* evaluation more accurate and consistent as all the RF component datasheets have single carrier *IIP3* specifications and hence the RF component evaluation results can be compared with the datasheet values with more confidence. Henceforth, *IIP3* will always refer to single carrier equivalent *IIP3* which will also be used for the *SFDR* calculations to keep the RF system parameters consistent with each other.

The relations and tradeoffs between these receiver system parameters are shown in Figure 3.7. The signal level diagram shown in Figure 3.7 shows that the minimum required received signal level, called the receiver sensitivity (*RxSens*), is dependent on the thermal noise floor (-174*dBm/Hz*), system noise figure (*NF*), the minimum required SNR ($SNR_{\min}$), and the system bandwidth (*BW*). Thus, the receiver sensitivity is defined as shown below and it is desired to have this receiver sensitivity level as low as possible as it reflects the ability of the system to detect weak signals.

$$RxSens = -174\,dBm + NF + SNR_{\min} + 10\log BW \tag{3.1}$$

The system dynamic range is defined as shown below, which is dependent on the *IIP3* and the *RxSens*.

$$SFDR = \frac{2}{3}(IIP3 - RxSens) \tag{3.2}$$

where, *IIP3* is the point where the desired carrier and the inter modulation products (IMD) of a two tone test are of equal power level. Thus to maximize the dynamic range it is desired to have a low *RxSens* and high *IIP3*.

It is challenging to design an RF system that optimizes these relations. For example the bandwidth of the signal directly affects the receiver sensitivity as higher signal bandwidth degrades the receiver sensitivity. Better sensitivity is achieved by reducing the signal bandwidth, but higher signal bandwidth is desirable to achieve better positioning accuracy in multipath environments. Thus, in all aspects, the design should maintain a balance between realistic RF system parameters and their effect on positioning accuracy. The lack of any guidelines and specifications for multicarrier based indoor positioning systems make design and development of the RF prototype even more challenging.

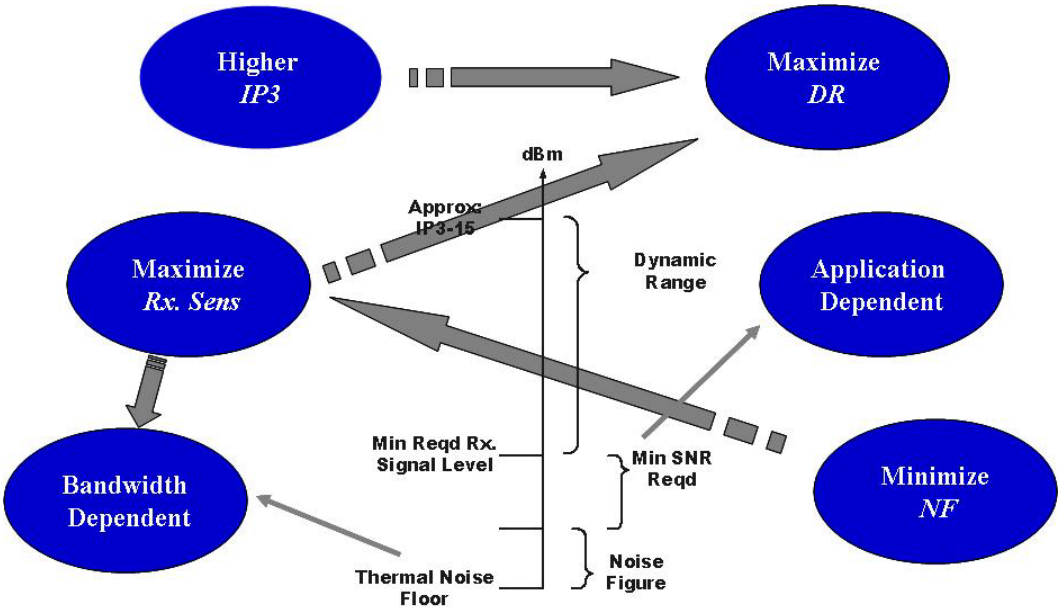

Figure 3.7 RF System Parameters Relationships

Determining Initial Design Parameters

The theoretical RF performance evaluation for a multicarrier receiver is presented in [2] where the position estimation variance, σ_r was determined to be;

$$\sigma_r = \frac{1}{8}\frac{c\sqrt{6N_o}\sqrt{5h^2 + 2w^2}}{\pi\sqrt{P_s TBh}} \tag{3.3}$$

where, h and w depend on the receiver geometry, B is the signal bandwidth, P_s is the received power, T is the time duration of one multicarrier symbol, and N_o is the received signal noise power spectral density. The equation [1] for the ratio of signal power to receiver noise can be expressed as;

$$\frac{P_s}{N_o} = \frac{6c^2(5h^2 + 2w^2)}{8^2\pi^2\sigma_r^2 TBh} \tag{3.4}$$

The relation between receiver noise figure NF and noise power spectral density N_o is;

$$NF = 10\log\left(\frac{N_o}{4k_b T_a}\right) \tag{3.5}$$

where, NF is the receiver noise figure, T_a is the ambient temperature in degrees Kelvin and k_b is Boltzmann's constant. The position estimation variance σ_r, derived in [1], is for a particular geometry shown in Figure 3.8, defined by h and w wherein six receivers are used, three placed in the z=0 (ground level) plane in a

triangle comprising the origin and two points w meters offset in x and y directions from origin. The remaining three receivers are each *h* meters above the first set. Since, we do not have a set of firm specifications, using this example receiver geometry and simulating the above equations gives us intuition about the anticipated system performance and helps us derive initial desired receiver system parameters.

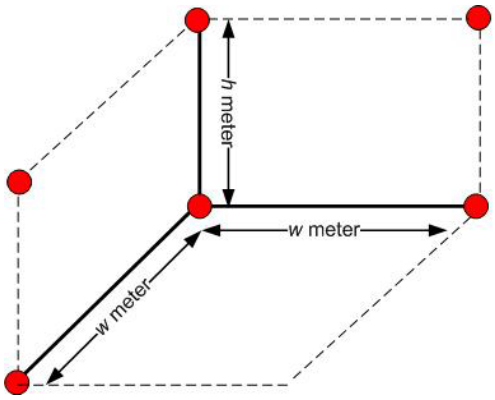

Figure 3.8 Receiver Geometry for Six Receivers

Figure 3.9 shows the effect on the position location variance as the signal bandwidth changes for receivers with different noise figures. We can see that for a 5MHz signal bandwidth, the 1m position location variance can theoretically be achieved with a receiver designed for a noise figure of 5.5dB. This, combined with the availability of spectrum in the 440MHz Amateur Band, led us to consider an initial design which would support a 6MHz-12MHz wide signal, centered at 440MHz. For the initial prototype, we chose a system bandwidth of 6.1MHz.

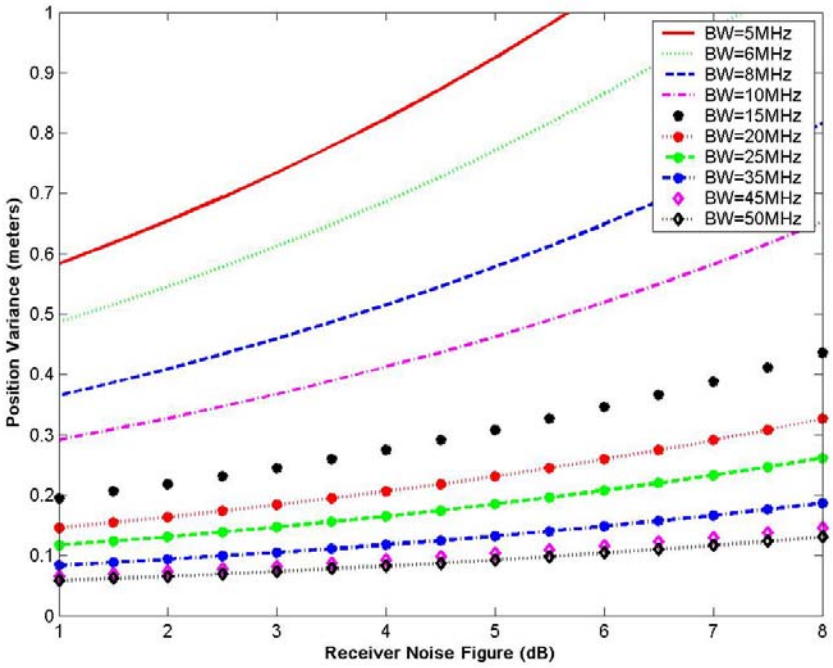

Figure 3.9: Position Variance as Signal BW and Receiver Noise Figure changes

The selection of a 6.1 MHz bandwidth was primarily motivated by the fact that this bandwidth would require minimal changes to be made in the signal processing software used in an earlier audio band prototype of the positioning system [1]. The signal used in this audio band demonstration was generated by repeated D/A conversion of a discrete signal with 8192 samples transmitted at 44.1kHz to produce a 5.38Hz periodic wave. This audio transmitted signal had 101 subcarriers. Keeping the number of subcarriers the

same, and increasing the transmitter sampling rate to 50MHz, generates a baseband signal of 6.1MHz.

Since lower noise figure is always better, the target noise figure for the receiver to be designed was set to 4.5dB. This provided a bit of design margin, while still being a realistic target. Figure 3.10 shows the effect on position variance as the received power and the signal bandwidth varies for a receiver with a target noise figure of 4.5dB. We see that for a bandwidth of 6.1MHz the received power required is greater than -82dBm to achieve a theoretical position accuracy variance of less than 1m. This means that the receiver sensitivity should be lower than -82dBm.

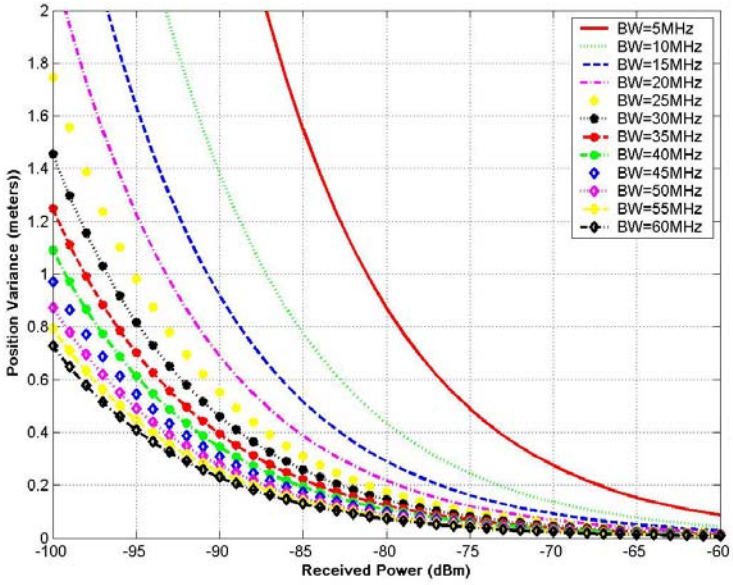

Figure 3.10: Position Variance as Signal BW and Received Power changes

Figure 3.11 shows how sensitive the position variance is to the receiver noise figure for a signal bandwidth of 6.1MHz. Depending on the noise figure achieved in the receiver PCB, Figure 3.11 shows what the required received power levels are, such that the theoretical location variance stays under 1m. To achieve the target receiver noise figure of 4.5dB, a Low Noise Amplifier with a high gain of approximately 20dB and a noise figure of less than 2dB is desirable. A VGA with a gain variation range of approximately 15dB is desirable. Thus, the initial target receiver gain is set to approximately 30dB considering the mixer conversion loss, filter insertion loss and connector insertion loss in the RF chain.

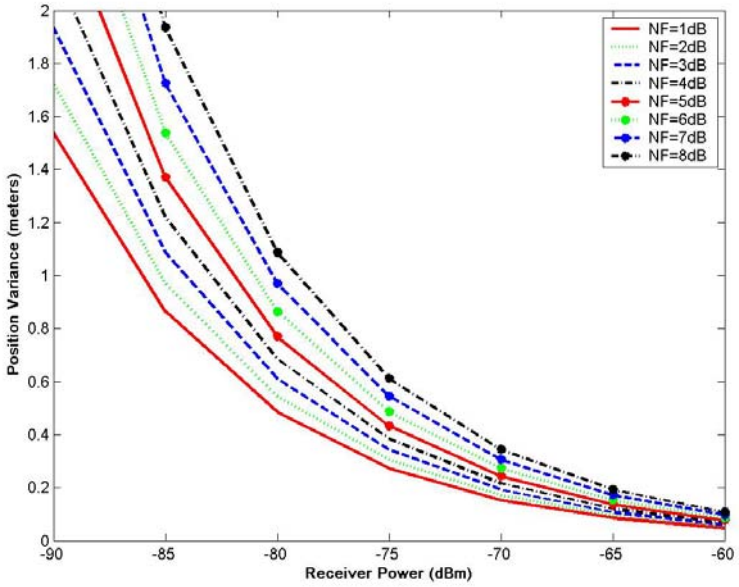

Figure 3.11: Position Variance as Received Power and Receiver Noise Figure Changes

Figure 3.12 shows the minimum required SNR for various theoretical accuracy targets using a receiver having a gain of 30dB and noise figure of 4.5dB. We see that increasing the signal bandwidth improves the location variance but at the same time makes the system design more difficult and complex. The best case location variance of 0.1meter requires the minimum required SNR for signal bandwidth of 6.1MHz to be about 10dB. Thus, the receiver will be designed with the minimum required SNR set at 10dB. The tradeoff between accuracy, bandwidth and received power is such that accuracy can be maintained for lower received power levels by increasing signal bandwidth.

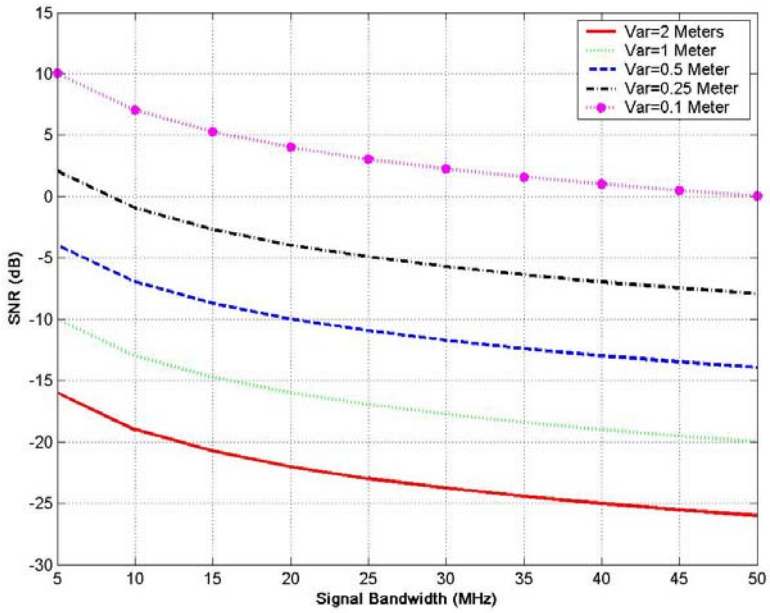

Figure 3.12: Minimum SNR for Various Position Location Variances

Receiver sensitivity plays an important role in making a potential Undetected Direct Path (UDP) signal detectable and in determining the range of the system. Degradation in receiver sensitivity reduces the possibility of extracting weak direct path signals from the noise and hence increases the positioning error. Given the receiver noise figure (4.5dB), the signal bandwidth (6.1MHz) and the minimum required SNR (10dB) the target receiver sensitivity is calculated using equation shown below:

$$\begin{aligned} RxSens &= -174\,dBm + NF + SNR_{\min} + 10\log BW \\ RxSens &= -174\,dBm + 4.5 + 10 + 10\log(6.1MHz) \\ RxSens &= -91.6dBm \end{aligned} \tag{3.6}$$

The receiver *IIP3* plays an important role in suppressing the intermodulation products and a higher intercept point implies a receiver with better dynamic range. The *SFDR* can then be calculated using equation;

$$SFDR = \frac{2}{3}(IIP3 - RxSens) \tag{3.7}$$

Setting the initial transmitter power to -30dBm/SC (dBm/SubCarrier), the received signal will be approximately -60dBm/SC (-40dBm total power for 101 subcarriers). Thus, the initial target *IIP3* specification is set to -10dBm to make sure that the receiver is never in the non-linear operating region. Using the above equation we can then calculate the target *SFDR* as 54.4dB.

Figure 3.13 shows how the bandwidth affects spurious free dynamic range (*SFDR*) and receiver sensitivity (*RxSens*). Smaller signal bandwidths result in lower (better) receiver sensitivity and higher dynamic range, however these improvements come at the cost of deteriorating location estimate accuracy. Thus, an important tradeoff must be made to operate the system using a particular signal bandwidth that also achieves the location accuracy goal.

One possibility is to keep the signal bandwidth variable and adaptive depending upon the wireless channel and the environment. Thus, an important objective for the Phase 1 RF prototype design is to allow the design to be sufficiently flexible that it will allow using signals occupying bandwidths wider than the 6-12MHz which will be used for initial tests. Therefore, the initial RF prototype will be designed to allow signals up to 50MHz which provides significant flexibility in bandwidth while testing the system, but does not seriously impact the ability to build a realizable system. Providing this flexibility facilitates a "software radio" design approach which allows changing system parameter without requiring changes in the RF hardware.

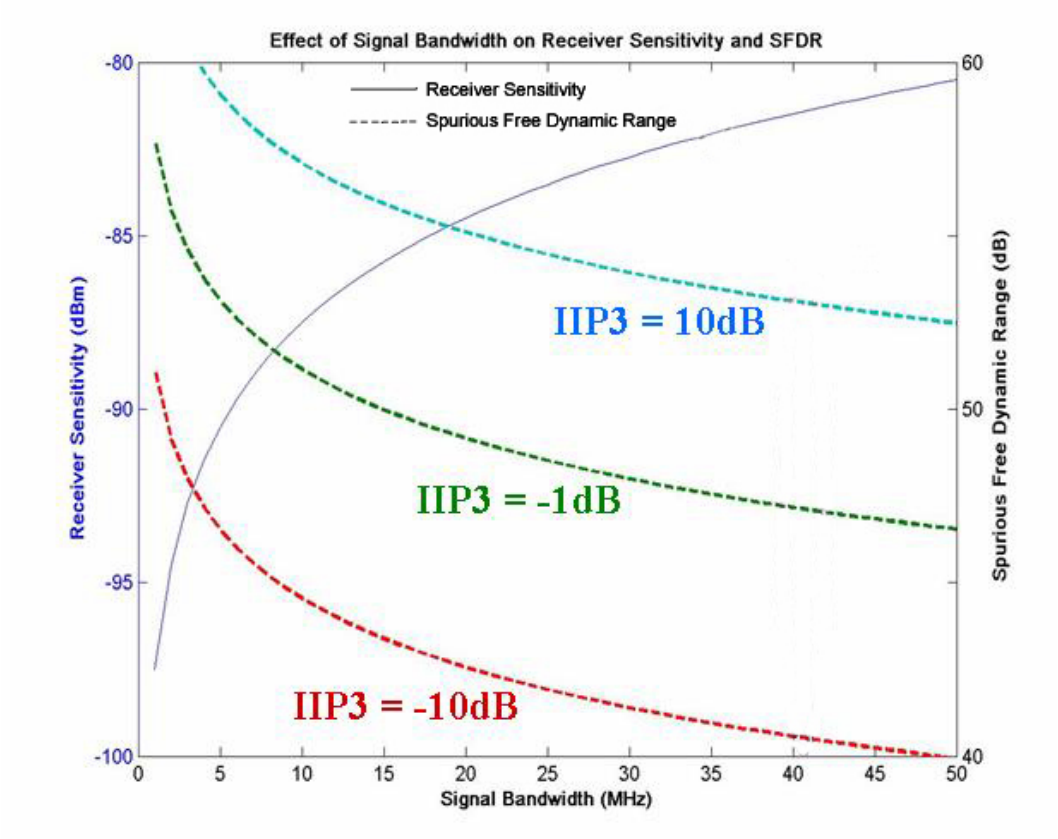

Figure 3.13: Effect of varying the Signal BW on Sensitivity and SFDR

In summary, based on the above computations, the Phase 1 initial target RF receiver design specifications, translated to single carrier equivalent are:

1) **Receiver Sensitivity** : -91.6dBm
2) **SFDR** : 54.4dB
3) **IIP3** : -10dBm
4) **NF** : 4.5dB
5) **Gain** : 30dB
6) **Min SNR Required** : 10dB
7) **BW** : 6.1MHz
8) **Carrier frequency** : 440MHz

Phase 1 Prototype Implementation

From the computations performed in the previous section, we now have a notion of the required signal bandwidth, and the RF receiver system parameters. However, we still did not have any experience regarding the performance of a practical RF system and do not know how susceptible the ranging algorithms will be to real-world effects like noise, interference, drift. We did realize that we could initially use a Vector Signal Generator (VSG) as a transmitter. This allowed us to generate a highly stable signal of known purity at a reasonable power level. So, within limits, the VSG could be used as a transmitter but the receiver specifications were still unknown. Thus, the Phase 1 prototype specifications act as a set of starting specifications to help better understand and study the RF behavior for a multicarrier system.

The setup of the Phase 1 prototype test-bed is shown in Figure 3.14. The transmitter consists of a laptop executing a MATLAB script to generate an equally spaced multicarrier signal. This multicarrier signal is then loaded into a VSG to modulate a 440MHz RF carrier internally to provide an RF output power of -30dBm/SubCarrier (-30dBm/SC). This upconverted signal is then available at the instrument's RF output port which can be connected to an antenna or, with appropriate attenuation, can be connected to the receiver input.

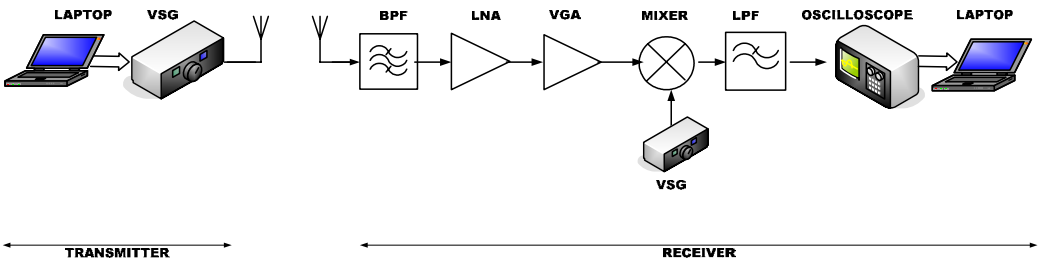

Figure 3.14 Phase 1 Prototype Bench Test-bed

The initial goal for the receiver was to keep it very simple. As shown in Figure 3.14 a direct down conversion architecture was chosen for this initial system to bring the multicarrier signal to baseband where it can be sampled. This minimizes RF-related problems like cross-talk and RF leakage creeping into the system as the number of local oscillators and mixers is minimized. Since the system operates over a varying distance, a variable gain control amplifier is also implemented to ensure that the ADC can be driven to a reasonable level.

For this initial prototype, it was also desirable to speed the design process by using pre-existing RF evaluation boards. It was hoped that this approach would allow rapid prototyping and better understanding of how these RF components perform. Thus, the initial receiver RF front end was implemented using evaluation boards consisting of RF amplifiers, a mixer and commercial filters.

As shown in Figure 3.14 an external signal generator was used to provide the mixer with the required local oscillator (LO) signal. The downconverted output of the receiver is fed to the oscilloscope's input channel

where it is sampled, stored and then transferred to a laptop where the range estimation algorithms are housed.

RF Receiver Component Selection

This section discusses the detailed specifications and characteristics of the RF receiver building blocks used and will present an evaluation of the receiver system parameters achieved in practice.

The implemented RF receiver front end shown in Figure 3.14 consists of an antenna, RF amplifiers, a signal generator for generating the local oscillator (LO) signal, a mixer and filters. The component selection discussed next was a critical step in designing a receiver to achieve the target specifications outlined above.

The portable receiver antenna used in the Phase 1 prototype was a unity gain commercially available rubber duck antenna with a wide bandwidth from 400MHz to 512MHz. The RF bandpass filter (BPF) used is a custom made seven-section tubular filter with a sharp roll off. The computations performed using a theoretical model of the positioning system indicated that a multicarrier signal of 6.1MHz bandwidth could result in position variance of better than 1m. However, since this model had not been verified in a real channel, it was decided to design a 50MHz bandwidth RF system so that wider bandwidth multicarrier signals could be used if they were needed.

The seven-section filter provides the necessary roll off to protect the RF front end from external interference. The BPF chosen has a low insertion

loss of 1.6dB and a passband of 50MHz centered at 440MHz. 40dB of attenuation occurs at 380MHz on the lower side and at 500MHz on the upper side. The low noise amplifier (LNA) follows the BPF. The selection of the LNA is very crucial as the noise figure of the LNA sets the noise figure of the receiver.

There are two configurations possible for the LNA at the receiver front end. In the first case, the LNA is the first receiver input block, followed by the BPF. This gives a better receiver cumulative noise figure but leaves the LNA unprotected from out-of-band interfering signals. In the second case, the BPF is the first block and then the LNA follows. In this case the cumulative noise figure is higher than the first case but the LNA is protected from unwanted interfering signals.

The test setup for the receiver uses this second configuration since, by careful component selection, it is in theory possible to achieve the target noise figure of 4.5dB using this second configuration, it seemed prudent to protect the receiver from interfering signals. The LNA chosen has a high gain of 22.5dB, a low noise figure of 1.6dB, and a high *IIP3* of 5.5dBm. The Variable Gain Amplifier (VGA) is used following the LNA, which is the input to the down converting mixer. The amplifier stages boost the signal energy and bring it to the appropriate level before mixing with the LO signal.

The VGA has a gain variation range of -10dB to 25dB, and is set to approximately 15dB gain under normal test conditions. The VGA also has a

high input intercept point of 15.5dBm. A high performance active mixer is used as a direct downconverter. An external signal generator was used to provide the mixer with the required LO level. A nine-section, custom made Chebychev LC LPF follows the mixer. This LC filter is designed with a very sharp cut off and a very low insertion loss of 0.4dB. The filter has a cutoff frequency of 50MHz and 50dB attenuation occurs at 65MHz. The nine-section filter provides the necessary roll off to protect the ADC from the IMD products generated at the mixer output. Table 3.1 shows the measured gain values, noise figure and the 3rd order input intercept point for the RF front end receiver building blocks.

Table 3.1 Receiver Building Block Specifications

	BPF	**LNA**	**VGA**	**Mixer**	**LPF**
Vendor	Lorch Microwave	RFMD	Analog Devices	Analog Devices	Eagle
Part #	7BD-440/50-S	RF2361	AD8370	AD8343	CBL-510-MF
Gain (dB)	-1.6	22.5	15.5	-5.5	-0.4
***NF* (dB)**	1.6	1.6	7.2	12.5	0.4
IIP3 (dBm)	∞	5.5	15.5	22	∞

Using the values from the above table, the cascaded noise figure (*NF*) and the cascaded third order input intercept point (IIP_3) of the receiver is

calculated using equations shown below, where *IP* corresponds to input intercept point of the individual RF components transferred at system input. Other than the *NF* values in Table 3.1, all other values are the measured values obtained from evaluation boards. For the *NF* the maximum *NF* value specified in the component datasheet is used in calculating cascaded *NF* using the formula shown below.

$$NF = NF_{BPF} + \frac{NF_{LNA} - 1}{G_{BPF}} + ...$$
$$IIP_3 = 10 \log \left(\frac{1}{IP_{BPF}} + \frac{1}{IP_{LNA}} + ... + \frac{1}{IP_{LPF}} \right)^{-1} \quad (3.8)$$

Figure 3.15 shows the Phase 1 receiver front end designed using evaluation boards. The rubber duck antenna is followed by BPF, LNA, VGA, Mixer and LPF. The receiver architecture in Figure 3.15 also shows a PLL evaluation board provided for future use, but for purposes of tests discussed in this chapter a signal generator as shown in Figure 3.14 is used to provide the required LO.

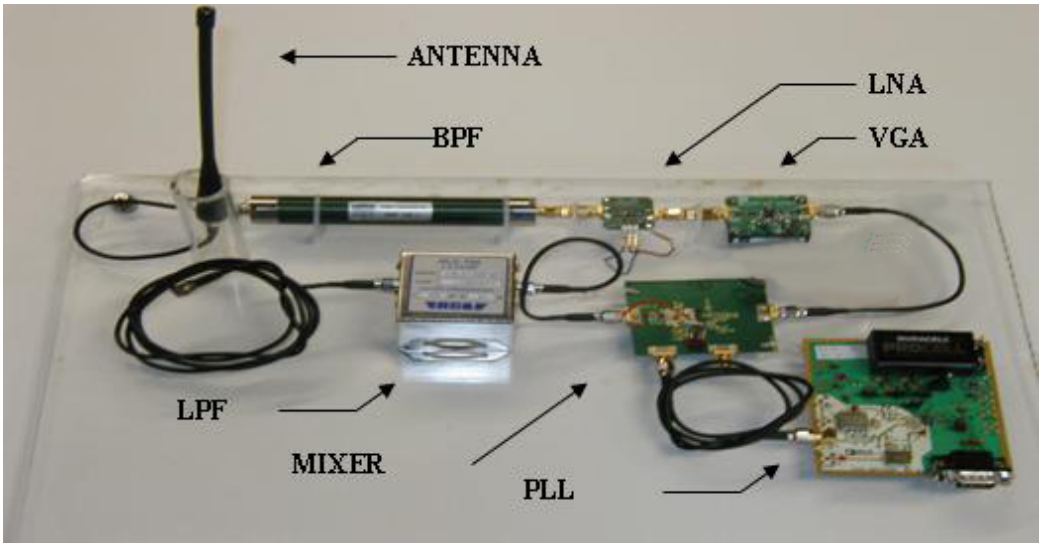

Figure 3.15: Designed Phase 1 Receiver Front End

Table 3.2 compares the original target RF receiver system parameters, the expected values after component selection and the achieved RF receiver system parameters for the designed Phase 1 RF receiver prototype. The achieved receiver gain was 30dB and the achieved *IIP3* was -17dBm. The original target *IIP3* based on calculations was -10dBm and in the process of component selection and balancing the other receiver system parameters, the *IIP3* was compromised from -10dBm to -15dBm. The achieved *IIP3* for the designed prototype shown in Figure 3.15 was -17dBm. The achieved receiver sensitivity was -90dBm and receiver spurious free dynamic range was 48dB. The cascaded system *NF* calculated using *NF* values from Table 3.1 was 3.3dB. The noise due to various cables and connectors between the evaluation boards as it can be seen

from Figure 3.15 is approximated to 3dB which is added to the cascaded *NF* of 3.3dB to give an *NF* estimate of 6.3dB.

Table 3.2 RF Receiver System Parameters

System Parameter	Original Target after simulations	Expected after component selection	Achieved
System G (dB)	30	30.5	30
System *NF* (dB)	4.5	3.3	6.3
System IIP3 (dBm)	-10	-15	-17
Rx. Sensitivity (dBm)	-91.6	-92.8	-90
Rx. SFDR (dB)	54.4	51.4	48

The zoomed in spectrum view at the phase 1 receiver output is shown in Figure 3.16. As it can be seen from Figure 3.16 the IMD levels observed at the output of the RF receiver are in agreement with the levels predicted in ADS simulations and are below -75dBm.

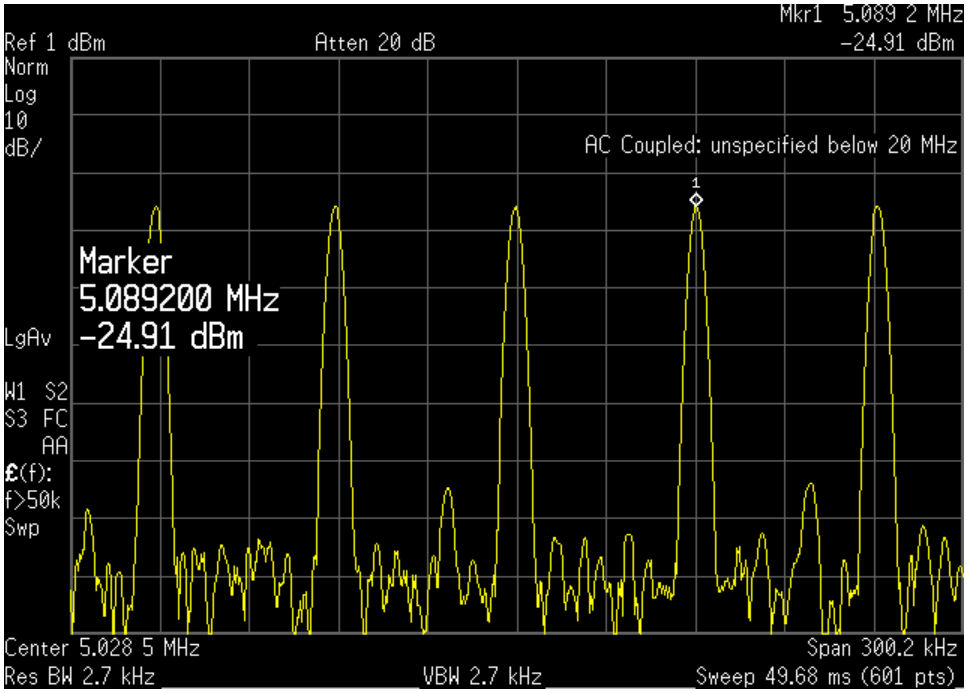

Figure 3.16 Phase 1 Zoomed In Receiver Output Spectrum

Now that the ADS simulations have been verified and the RF design methodology using two tone has been verified, it is desired to verify the multicarrier based positioning algorithms using this RF prototype, which is discussed in the next section.

Ranging Using Phase 1 Prototype

The Phase 1 test setup shown in Figure 3.14 was successfully implemented as a proof of concept demonstration for ranging using RF signals. Figure 3.17 shows the single transmitter receiver bench test setup for the Phase 1 prototype (the picture does not show the laptops at the transmitter and receiver). The transmitter consists of a laptop and the VSG and the RF front end receiver design consists of various RF building blocks, cascaded together. The output of the receiver LPF is digitized and is loaded to a general purpose laptop for further analysis and TDOA estimation

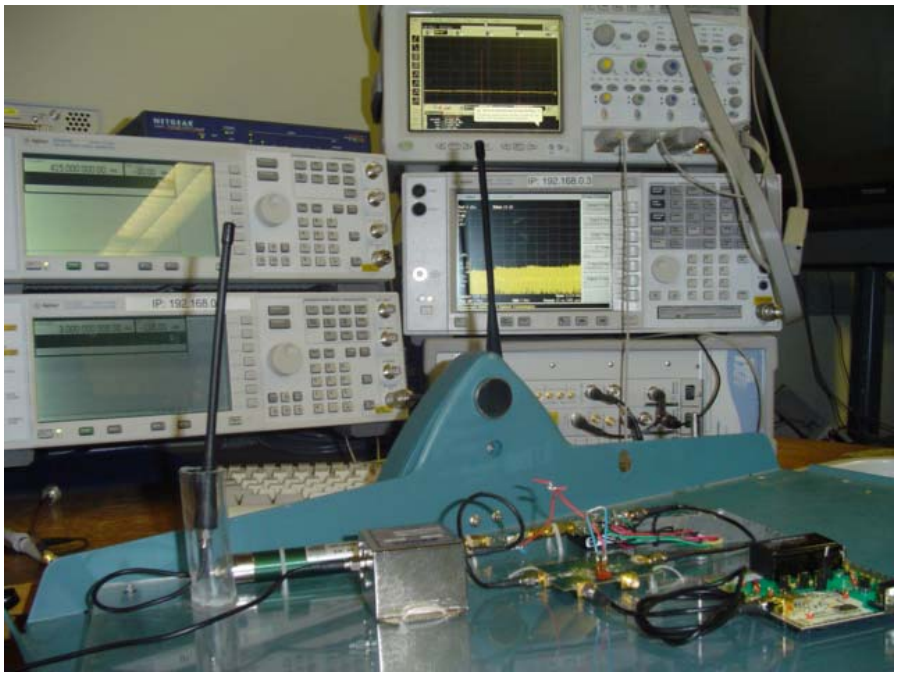

Figure 3.17 Phase 1 Bench Test Setup (Supporting PCs Not Shown)

The goal of the bench tests is to validate and verify that the basic range estimation using 6.1MHz wide multicarrier signal structure is possible using the multicarrier range estimation algorithms. It was necessary to do these initial tests in the absence of multipath, over a known distance. To accomplish this, the transmitter output was connected directly to the receiver RF front end using a cable of known length (and some attenuators, to make sure that the receiver does not go in to saturation) thus keeping the test setup multipath free.

Since the algorithms were TDOA based, it was necessary to process the multicarrier signal received at two receivers which would then provide a TDOA estimate between the received signals at both receivers. One way to fake the second receiver without adding hardware complexity was to slightly modify the RF test setup as shown in Figure 3.18. As shown in the figure, the RF receiver input is cabled to the transmitter output. The RF receiver baseband output is then split using a power splitter to provide two outputs to which two cables of different known lengths were connected. These two signals provided to the signal processing algorithms are not affected by multipath, NLOS, or synchronization issues and are used to estimate TDOA between the two signals.

Figure 3.18 shows the test setup used to estimate TDOA using a signal generated by a VSG and received using the initial prototype receiver hardware. Success in TDOA estimation using these signals would verify and

validate both our signal processing algorithms and our baseline RF design. From this point we can slowly move towards more realistic tests, as will be discussed in future chapters.

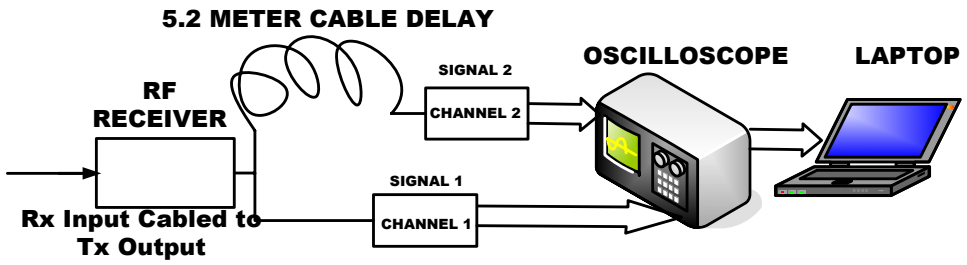

Figure 3.18: TDOA Estimation Setup

As shown in Figure 3.18, the signal at the output of the receiver is directly connected to channel 1 of the oscilloscope, which is referred to as SIGNAL 1. SIGNAL 2 is then obtained by inserting a 5.2 meter cable between the receiver output and the Channel 2 input which acts as a delay line. The two signals at the inputs to the oscilloscope are then sampled at the same time at sampling rate of 50MHz and are downloaded to a portable laptop for TDOA estimation between the two signals.

The results from this simple test are as shown Table 3.3. The wave propagation in the cables used in the setup shown above is approximately 80.2% that of free space wave propagation of $3x10^8$m/sec. Thus the wave propagation in the cable is 4.15nsec/m, which means that the true TDOA is 21.59nsec. The estimated TDOA is 21.71nsec/m thus resulting in 0.12nsec error which is equivalent to 0.03m (0.1ft).

Table 3.3 TDOA Estimation Results

Cable Length	5.2m
Cable Delay	4.15nsec/m
True TDOA	21.59nsec
Estimated TDOA	21.71nsec
TDOA estimate error	0.12nsec
Accuracy	0.03m

Thus the above results verified and validated the basic range estimation algorithms and the initial receiver prototype, therefore further prototyping is justified. The next step is to develop a transmitter prototype made of evaluation boards similar to the receiver prototype and to perform basic short range wireless tests. The upgrade to such a test setup is referred to as the Phase 2 RF prototype design which is discussed in the next chapter.

Lessons Learnt

The Concept Works: The ADS simulations presented in this chapter provided insights into few key aspects of RF design. It is desired to use unmodulated, orthogonal sinusoids for the MC-UWB positioning system. Also, using such a signal structure, simplifies the RF evaluation as now two tone tests can be used to characterize the RF system, even though it consists of multiple carriers. The IMD performance of the phase 1 RF prototype was in agreement with the ADS simulations thus confirming that the RF design methodology is correct.

Obviously not much can be read regarding the TDOA estimation accuracy obtained in this test, as it was a wired test, without multipath. But the TDOA wired test results shown in Table 3.3 are consistent with the theoretical results presented in Figure 3.10 and Figure 3.11, which adds more confidence in the RF evaluation methodology. Thus the test setup in Figure 3.17 proves that the basic concept of multicarrier based positioning system using TDOA works and that the software developed by the algorithms team could be integrated with the developed RF based platform. This provides a first step towards moving away from simulations and towards building a field deployable RF prototype and hence is very important.

Component Selection: The component selection plays a very critical role in RF design. For example, the VGA chip that was originally picked (VGA-024 from WJ Communications) was after careful evaluation, found unsuitable. Figure 3.19 shows the *IIP3* and *NF* characteristics of VGA-024 for various ranges of gain value over which the VGA can operate. Figure 3.19 shows that at low gain values the VGA-024 chip has a very high *IIP3*, which is good, but at the same time the *NF* is also very high, resulting in higher cascaded receiver *NF*, which is not desirable. For high gain values the VGA-024 chip has a low *NF*, but has also has a low *IIP3*, thus lowering the cascaded *IIP3*, which is not desirable.

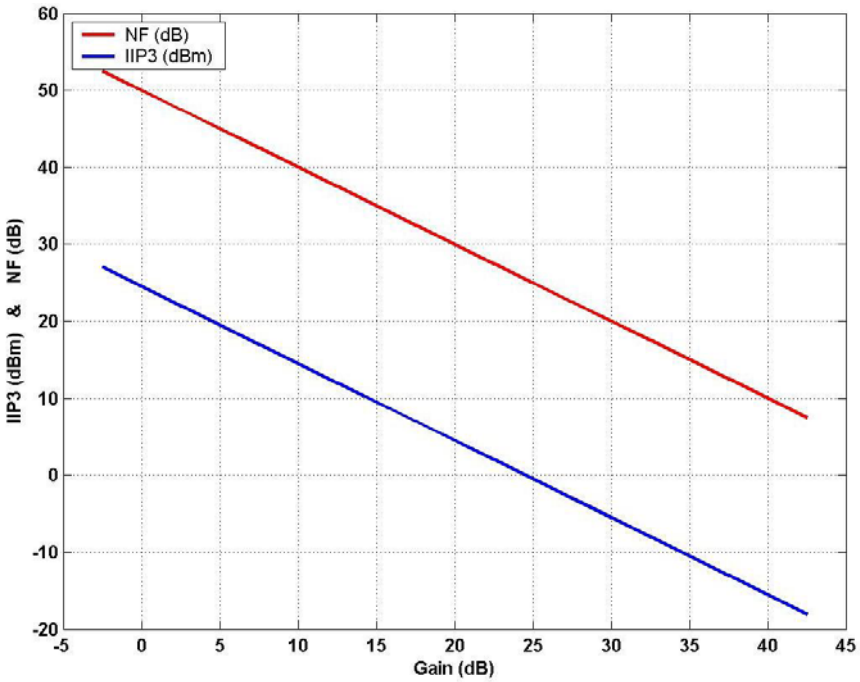

Figure 3.19 VGA Gain vs. IIP3 & *NF* Characteristics

Figure 3.20 shows the dynamic range of the VGA which stays constant for various possible gain settings and is about 25dB.

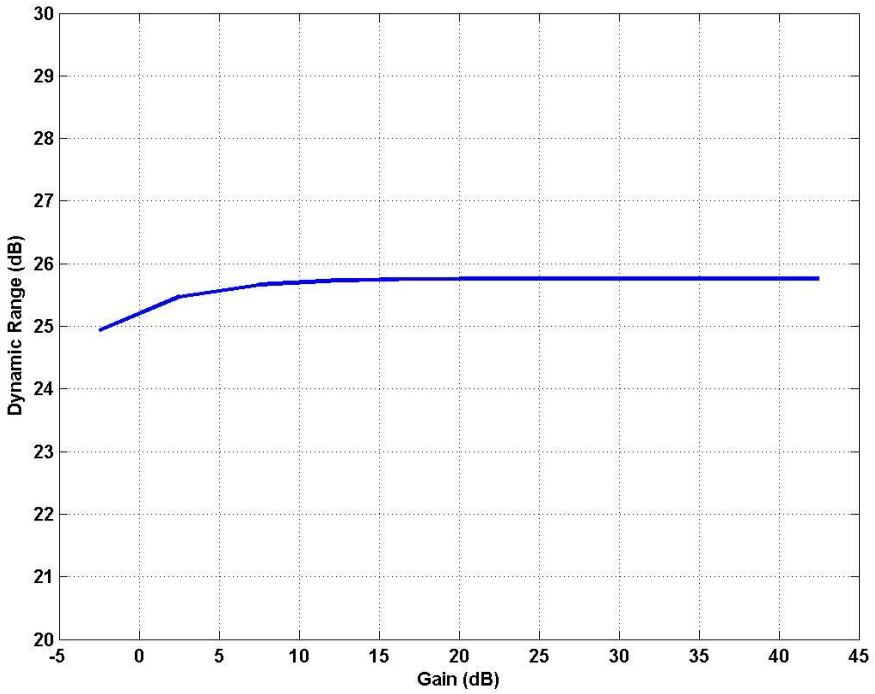

Figure 3.20 Dynamic Range of the VGA

The poor dynamic range and high *NF* made the VGA-024 unsuitable to use for the RF front end design. It was eventually replaced by VGA AD8370 from Analog Devices.

Correct Use of the Test and Measurement Equipment: At the receiver end one needs to make sure that the oscilloscope is sampling at the same rate as the VSG to ensure signal integrity and make sure that the subcarriers are in the correct FFT locations. It is very important that the oscilloscope that is used is a multi-channel oscilloscope that can sample at the same time or else it will result

in a TDOA estimation error equal to the difference in the sampling time between the two channels. The interpolation option on the oscilloscope, which could be enabled by default, needs to be disabled as it is equivalent to changing the sampling rate at the receiver which now will be different than that used by the transmitter resulting in loss of signal integrity.

The non-linearity of the VSG needs to be taken into account while doing multicarrier signal generation and tests. One cannot use the same signal generator for a two tone test as this will result in prominent IMD products from the signal generator itself which will look like they are being generated by the RF receiver. One needs to use two different signal generators to generate the two tones and add them externally using a power combiner to get a cleaner two tone signal as an input to the receiver.

The multicarrier signal is generated in laptop and is loaded in the VSG. Care must be taken that the signal loaded is normalized appropriately and is occupying about 70% of the full scale range of the VSG to avoid signal clipping which will lead to distortion and eventually result in range/TDOA estimation error. Even though the VSG is specified to output a maximum of +20dBm total output power of the multicarrier signal, operating at full output power results in much higher IMD at the VSG output port which will result in phase corruption of the multicarrier signal. Hence the VSG output is set to approximately -10dBm total output power (-30dBm/SC for 101 subcarriers) to

keep the internally generated IMD as low as possible. Figure 3.21 shows an example of VSG internally generated IMD. The left plot shows the multicarrier output at the VSG of -32dBm/SC and the IMD products can be seen on the side of the spectrum. The right plot shows the VSG output for power level of -13dBm/SC, which results in IMD that are comparatively much higher and will now have greater phase distortion effect on the multiple subcarriers.

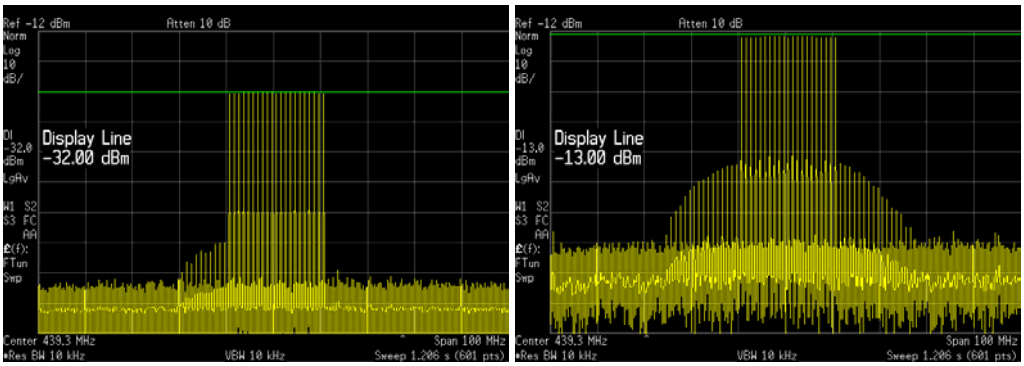

Figure 3.21 IMD for VSG Generated Multicarrier Signal

Conclusions

This chapter discussed the ADS simulations leading to a better understanding of key aspects related to the RF system design. Based on these simulations the author proposes using unmodulated orthogonal multicarrier signals which allows the RF evaluation to be performed using two tone assumptions, thus greatly simplifying the RF system design and evaluation.

Initial specifications for the multicarrier carrier based prototype were also presented along with a family of curves that can be used by a designer as reference to pick initial RF receiver design specifications depending on the application. Based on these initial specifications, the first RF based prototype was developed whose IMD performance was in agreement with that predicted in ADS simulations.

Simple ranging cable test was performed in multipath free environment. The successful ranging test results provided more confidence in the theory of using multicarrier signals for positioning, thus motivating further prototyping.

References

[1] D. Cyganski, J. A. Orr and W. R. Michalson, "A Multi-Carrier Technique for Precision Geolocation for Indoor/Multipath Environments", *Institute of Navigation Proc. GPS/GNSS*, Portland, OR, September 9-12 2003

[2] D. Cyganski, J.A. Orr and W. R. Michalson, "Performance of a Precision Indoor Positioning System Using Multi Carrier Approach", *Institute of Navigation Proc. NTM*, San Diego, CA, January 26-28 2004

Chapter 4 : RF Evaluation Using a Multicarrier Signal

Introduction

The success of the cable-based ranging tests discussed in Chapter 3, motivated further system development. The Phase 1 prototype involved using test and measurement equipment to quickly prove the concept of positioning using multicarrier signals. It is now required to further develop the system by replacing the test equipment with RF components consisting of evaluation PCBs.

The main motivation for developing such an RF system consisting of evaluation PCBs was to better understand the RF-related system issues and potential problems in a practical RF system. The ultimate goal of the RF Design is to preserve as much spectral purity of the multicarrier signal at the receiver output as possible as this will result in better range/position estimation. Thus, the focus of the tests discussed in this chapter is not on range/position estimation, but rather is focused on RF-related issues that would potentially impact range/position estimation.

This chapter will first discuss the design of an RF transmitter which uses evaluation PCBs similar to RF receiver discussed in Chapter 3. Using this rapid prototype, a series of wired and wireless tests using multicarrier signals are presented. The motivation of the wired test is to identify and resolve any potential RF issues which arise due to the characteristics of the RF components being used. The motivation of the wireless test is to observe the actual effects of multipath, noise, and interference due to wireless channel. Both the wired and wireless RF evaluation tests resulted in identifying RF issues which were resolved to improve the spectral purity of the multicarrier signal input to the ADC, which is used by ranging/positioning algorithms.

Phase 2 Prototype Design

For practical system implementation reasons, it was required to eliminate the VSG and laptop for multicarrier signal generation and the oscilloscope for receiver sampling. Thus an RF transmitter front end was designed using evaluation PCBs similar to the RF receiver front end design discussed in Chapter 3.

It was also required to replace the oscilloscope by a digital back end design consisting of ADC and an FPGA. Such a prototype system, free of test equipment, is illustrated in Figure 4.1 and is referred to as the Phase 2 prototype. For greater flexibility in system testing, the transmitter and receiver LO can be provided by using independent PLL PCBs or by using a synchronized LO from a common signal generator source.

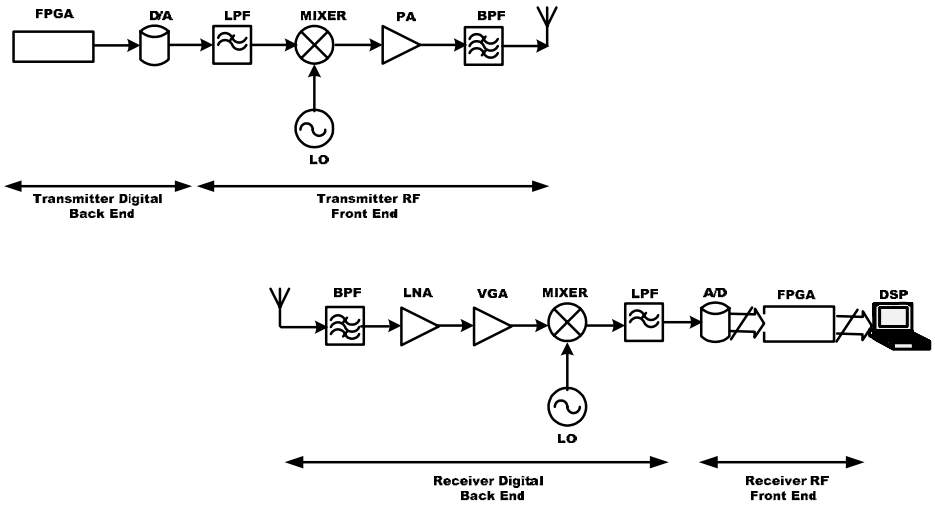

Figure 4.1 Phase 2 Prototype Test Setup

The RF front end transmitter architecture shown in Figure 4.2 consists of filters, a mixer, a PLL-based LO/signal generator running at 440MHz and a final power amplifier. The mixer, PLL, BPF, LPF and antenna used in the transmitter front end are the same as those used in the receiver front end. This component reuse greatly helps in quickly prototyping the transmitter, as the chip performance and input and output tuning components are already known. The power amplifier chosen is highly linear and is capable of generating up to 33dBm output power and has a gain of 33dB. The frequency range of operation for the power amplifier is 400MHz to 500MHz.

The Phase 2 RF transmitter front end prototype provides maximum of -20dBm/SC output power when the baseband input (DAC output) is approximately -45dBm/SC. The RF front end portion of receiver structure for the Phase 2 is same as that used in Phase 1 but the digital back end replaces the oscilloscope with an ADC and an FPGA. The complete Phase 2 receiver structure is as shown in Figure 4.3.

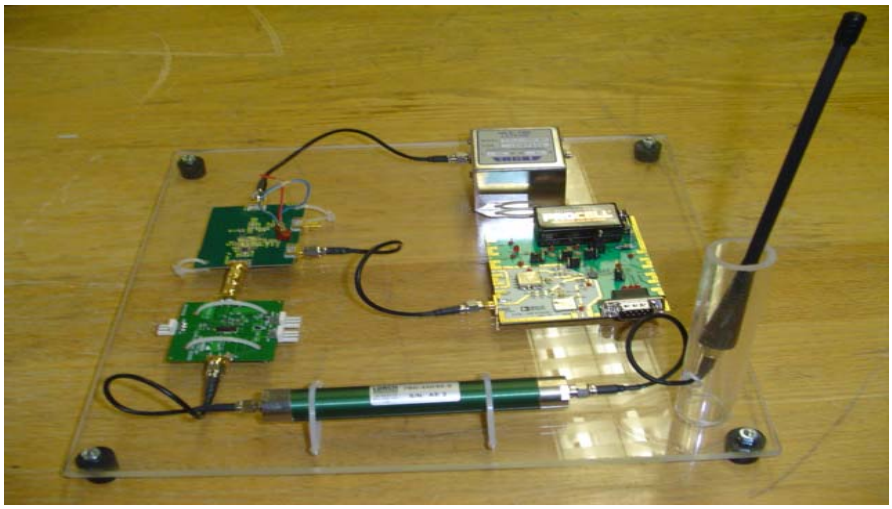

Figure 4.2 Phase 2 Transmitter RF Front End

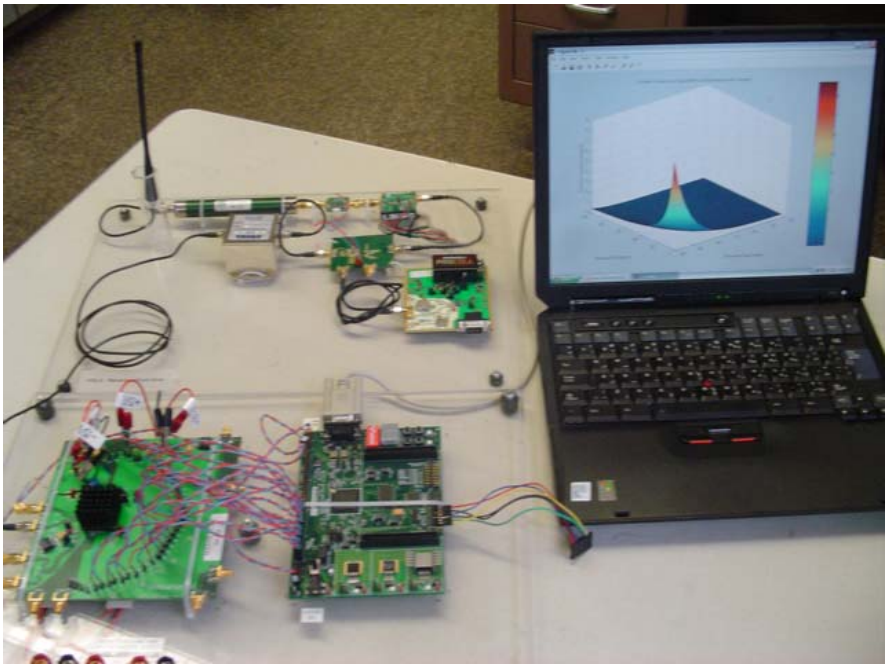

Figure 4.3 Phase 2 Receiver Front End and Digital Back End

Wired RF Evaluation Using Multicarrier Signal

This section discusses the basic wired RF evaluation tests performed using the Phase 2 prototype. The objective was to identify and resolve potential RF issues and improve the overall spectral purity of the multicarrier signal in the RF chain. The test setup for the wired RF evaluation is as shown in Figure 4.4.

In this test it was desired to keep the test setup as simple possible, and to minimize variables, and thus the transmitter and receiver LO are synchronized and are generated from a common signal generator running at 440MHz. The transmitter and receiver sampling clocks are also synchronized and are generated from another signal generator running at 200MHz. The implication of non-synchronous LOs is discussed later in this chapter and the implication of non-synchronous sampling clocks is outside the scope of this thesis.

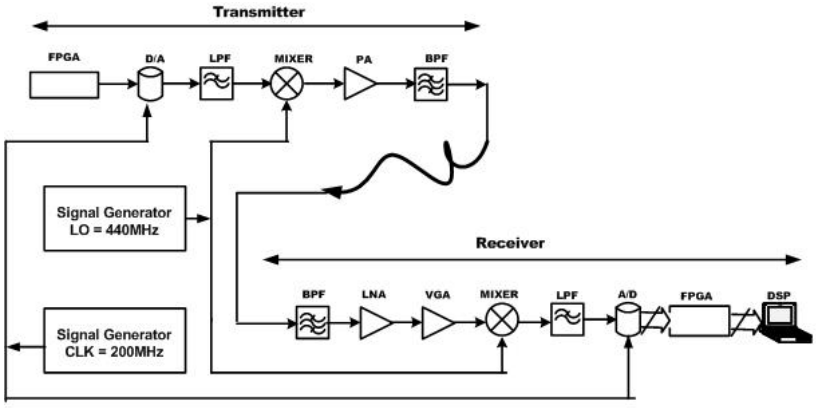

Figure 4.4 Wired RF Evaluation Test Setup

While performing the wired RF evaluation test it was observed that the RF component performance significantly changes from the data sheets depending on the number of subcarriers being used in the system. This simple but non-intuitive fact observed during initial tests is due to the fact that the datasheet specifications hold true for single carrier systems and not for multicarrier signal inputs.

When using a multicarrier signal, the system parameters and specifications will be degraded depending on number of subcarriers used. For example, the poor multicarrier output of the DAC shown in Figure 4.5 was obtained even though the DAC was operating within its datasheet specifications. As can be seen from the figure, spurious power levels as high as 42.99dBc degrade the spectral purity, which is contrary to the performance one would expect after reading the datasheet.

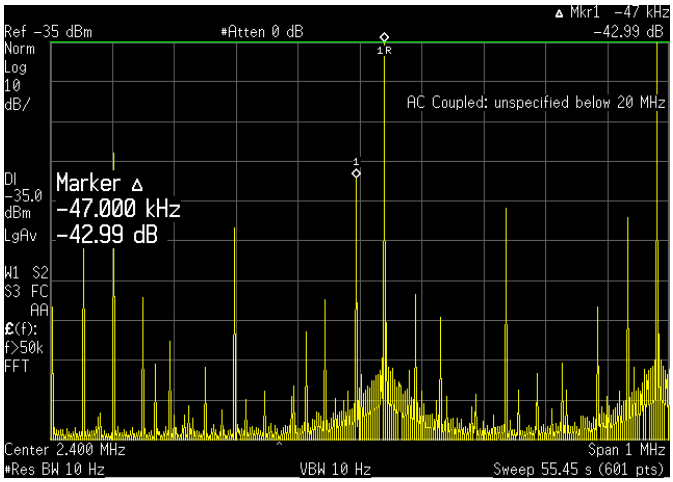

Figure 4.5 Poor Multicarrier DAC Output

The multicarrier output of the same DAC operating after decreasing the operating current and slew rate is shown in Figure 4.6. As can be seen in the figure, the spurious power levels are very close to the noise floor, resulting in much better spectral purity. Thus an important observation made is that while designing a multicarrier based system, it is important to derate the component specifications.

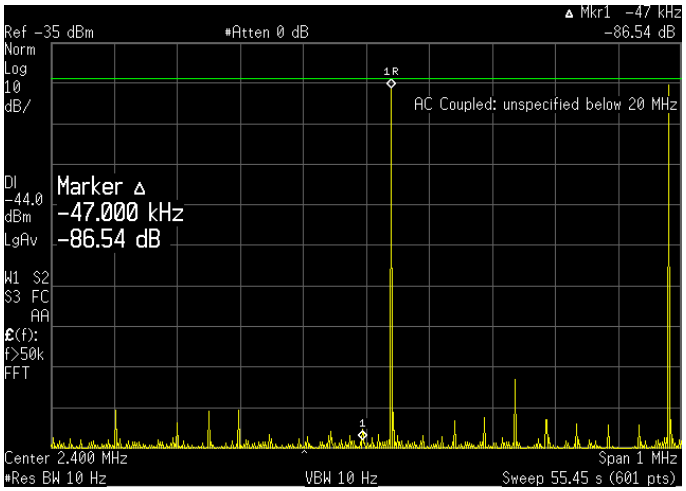

Figure 4.6 DAC Output after Reducing Current and Slew Rate

Let the signal input to the transmitter RF front end be a multicarrier baseband signal spanning from DC-25MHz and observe the spectrum at the transmitter and the receiver output. The transmitter LO is set at 440MHz, therefore the transmitter RF output is a double side band (DSB) multicarrier signal spanning from 415MHz to 465MHz with the lower side band (LSB) spanning 415MHz to 440MHz and the upper side band (USB) spanning 440MHz to 465MHz. This 50MHz wideband multicarrier signal at the output of the transmitter is shown in Figure 4.7. This output is connected to the receiver RF

front end input using a cable with appropriate attenuation such that the power level at its input is around -55dBm/SC.

The downconverted receiver output is shown in Figure 4.8. In Figure 4.8 it is clear that there is a severe roll off of approximately 30dB, at frequencies from DC-3MHz. After further investigation it was found that the mixer characteristics at these frequencies make it difficult to provide good matching at these low frequencies which results in power loss at frequencies from DC-3MHz.

From a ranging/positioning perspective this implies loss of SNR seen by the signal processing algorithms which will degrade the ranging/positioning accuracy. Thus, to avoid this SNR degradation it is desired to shift the entire multicarrier baseband spectrum approximately 3MHz away from DC into a region where there is less attenuation.

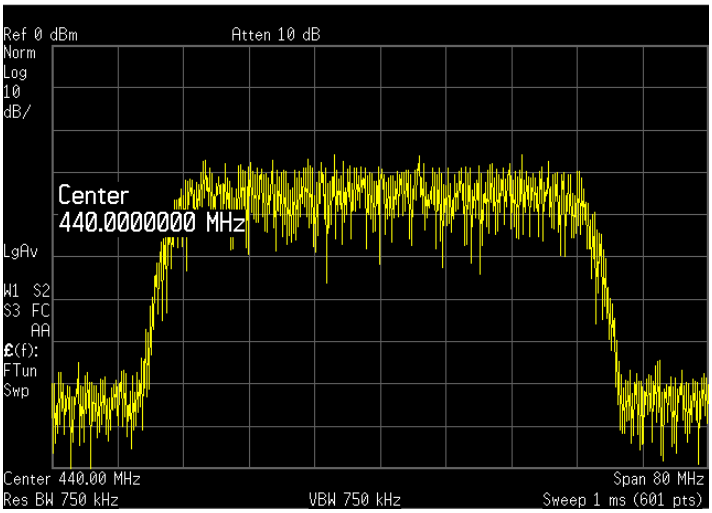

Figure 4.7 Transmitter Output DSB for Baseband Span of 25MHz

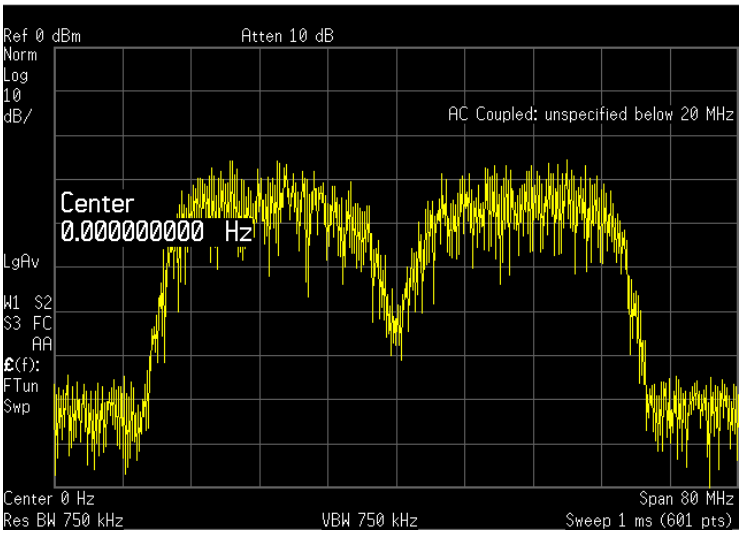

Figure 4.8 Receiver RF Front End Output for Baseband Span of 25MHz

From the initial system design parameters and initial ranging tests presented in Chapter 3, it was observed that a bandwidth of 6.1MHz might be good enough to achieve 3-6m accuracy. Since the near DC frequencies must not contain subcarriers due to power loss observed above, a 6.1MHz baseband signal consisting of 101 subcarriers was generated to span from 2.4MHz to 8.5MHz.

Thus the wired test is repeated for this 6.1MHz baseband signal to observe the spectrum at the transmitter and receiver output. The upconverted spectrum at the transmitter output is a DSB spectrum as shown in Figure 4.9 which spans about 17MHz centered at 440MHz. As shown in Figure 4.9, the USB occupies 442.4MHz to 448.5MHz and the LSB occupies 431.5MHz to 437.6MHz. This DSB signal is cabled to the receiver input after appropriate attenuation, making sure not to saturate the receiver RF front end.

The receiver RF front end output spectrum centered at DC after direct downconversion is shown in Figure 4.10. The roll off seen in Figure 4.10 is due to the receiver mixer characteristics which do not have a flat magnitude response at low frequencies, but the response was greatly improved by shifting the spectrum 2.4MHz away from the DC.

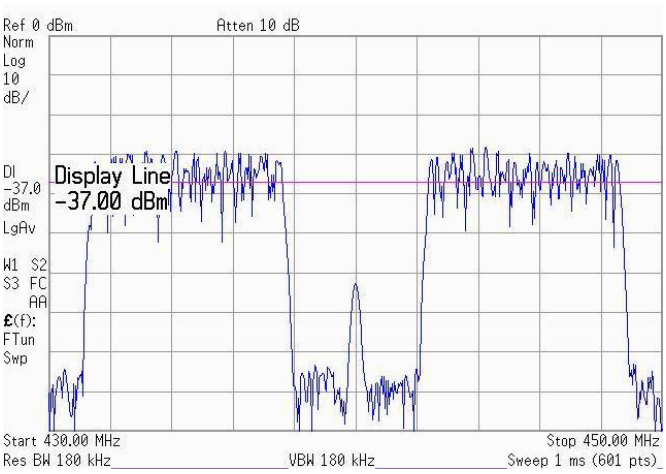

Figure 4.9 Transmitter Output DSB for Baseband Span of 6.1MHz

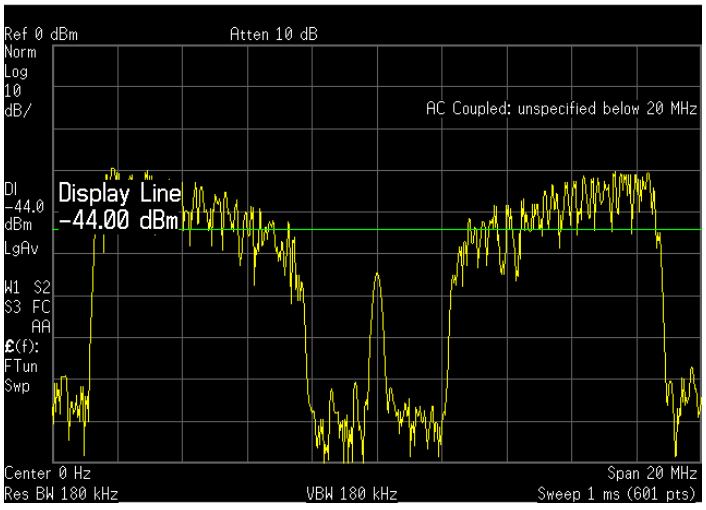

Figure 4.10 Receiver RF Front End Output for Baseband Span of 6.1MHz

The above wired RF evaluation tests led to identifying and resolving two RF issues. The first issue was related to the properties of the multicarrier signal, which required derating the RF components to improve spectral purity. The second issue was the roll off observed in the spectrum near DC that required shifting the baseband signal spectrum 2.4MHz away from DC. Both these solutions resulted in better overall spectral purity of the multicarrier signal at the receiver RF front end output as shown in Figure 4.11.

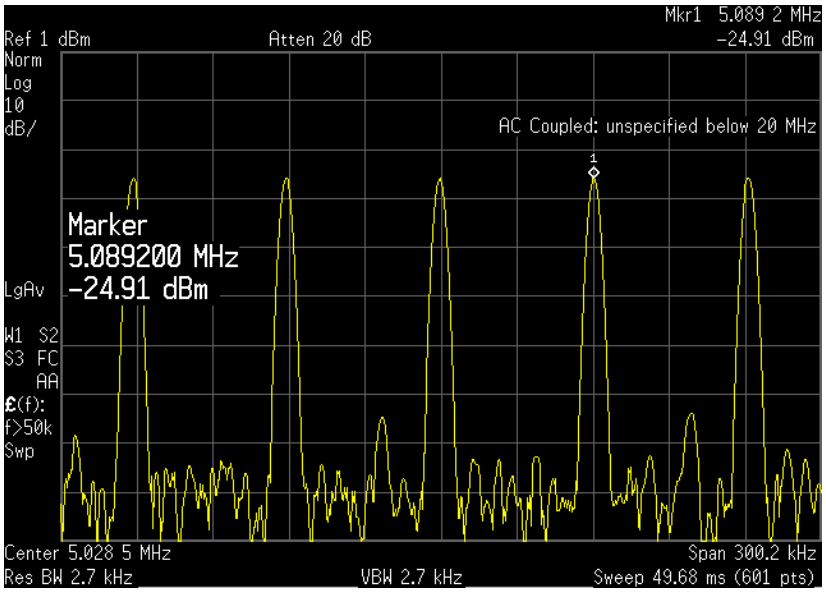

Figure 4.11 Zoomed In Receiver RF Front End Output

Wireless RF Evaluation Using Multicarrier Signal

The next step was to perform an indoor short range LOS wireless RF evaluation test to evaluate and observe the effects of multipath, noise, and interference in a wireless environment. The goal again is to further improve the overall spectral purity of the RF chain. The test setup for wireless RF evaluation is shown in Figure 4.12.

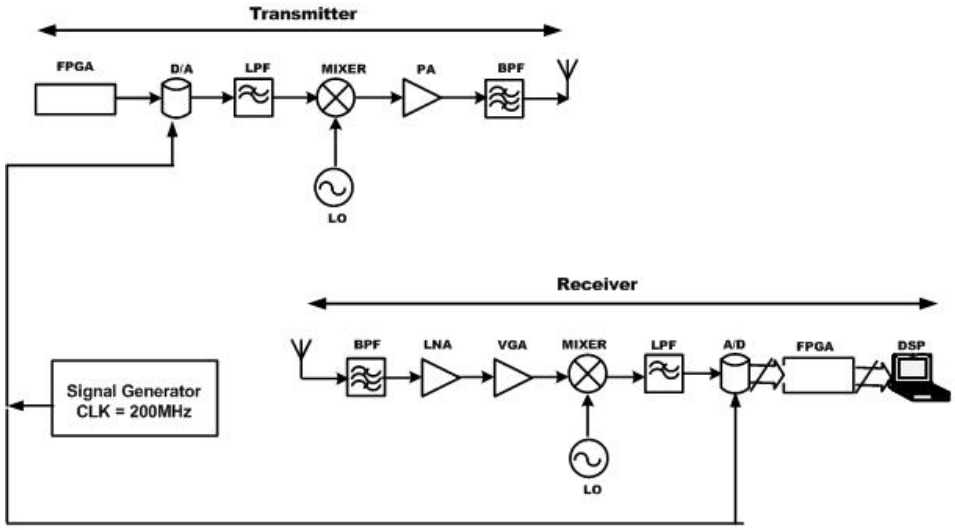

Figure 4.12 Wireless RF Evaluation Test Setup

In this wireless RF test the 440MHz LO at the transmitter and receiver are generated from their own independent PLL evaluation boards, but the sampling clocks were synchronized using a common signal generator. The transmitter power level into the antenna is normally -20dBm/SC. In this test the receiver was kept at a distance of approximately 10 meters away from the

transmitter. A rubber duck antenna is used at the transmitter and the receiver and the test was setup indoors in a wireless environment with multipath and a Line of Sight (LOS) path between the transmitter and the receiver. The observed spectrum from DC-100MHz at the output of the receiver RF front end was severely distorted and is shown in Figure 4.13.

Due to the indoor environment, it is expected that the multicarrier signal spanning from 2.4MHz to 8.5MHz will be effected by multipath. The multicarrier signal processing algorithms should be able to resolve these multiple received paths [1].

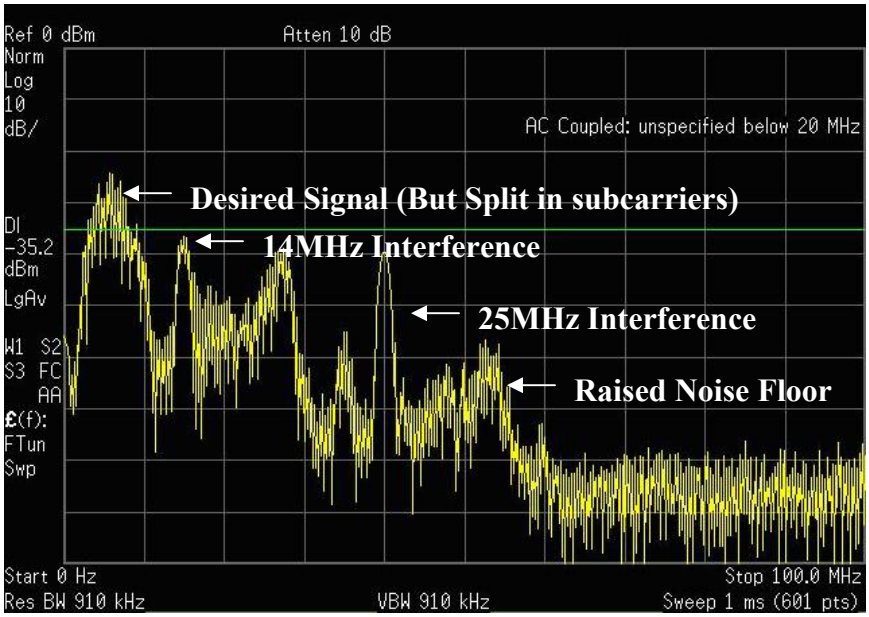

Figure 4.13 Receiver Output Spectrum for Wireless RF Evaluation Test

However, when analyzing the collected data, it was observed that in addition to the expected effects of multipath, we also observed three other

undesirable system behaviors in the frequency band greater than 8.5MHz which are of greater concern from an RF design perspective. The three observed undesirable effects that are discussed in following sections are:

- Raised noise floor, resulting in spectral purity degradation
- Interfering signals at 14MHz and 25MHz, resulting in desensitizing the receiver, and
- Split in the subcarriers, causing the subcarriers to shift from the required frequency, zoomed in picture of which is shown in a subsequent figure.

Raised Noise Floor: Effect of VGA Operating Modes

Note that the noise floor observed in Figure 4.13 is significantly raised. Further investigation showed that the noise source was the VGA chip being used in the receiver RF front end. The VGA being used can be operated in two different gain modes, high gain mode and a low gain mode. The gain of the receiver VGA is controlled using a serial 8 bit gain control word. The value of this control word is based on the received signal strength, allowing receiver gain can be increased or decreased. The maximum total receiver gain when the VGA is operating in high gain mode is approximately 45dB and when the VGA is operating in low gain mode it is approximately 35dB.

The VGA chip noise floor characteristics for the high gain mode (left plot) and the low gain modes (right plot) are shown in Figure 4.14. Note that the noise floor level for high gain mode is raised (noise floor = -50dBm) as compared to that in the low gain mode (noise floor = -70dBm). In this wireless RF evaluation test, the receiver is operated in high gain mode and hence we see the raised noise floor in Figure 4.13, which results in degrading the SNR. Hence it is preferable to operate in the low gain mode to improve the received signal SNR.

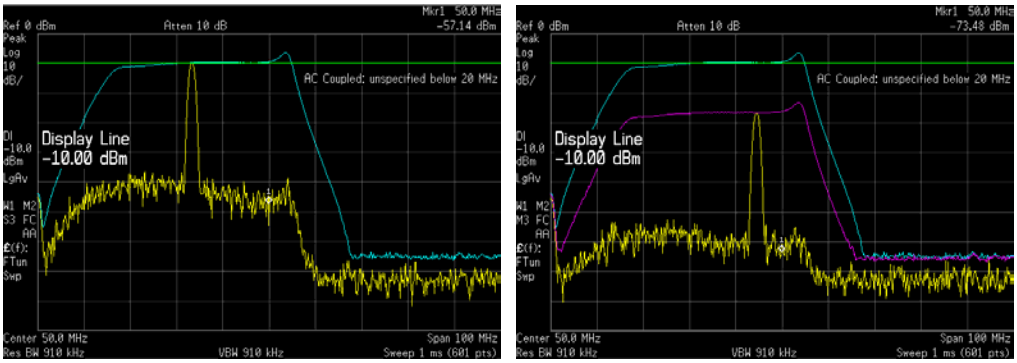

Figure 4.14 Noise Floor for VGA Operating in High Gain Mode (left plot) and Low Gain (right plot) Mode

Interference: External and Internal Sources

Note that in Figure 4.13, in addition to receiving the multipath affected multicarrier signal, a few other undesirable signals, one at approximately 14MHz, a second at approximately 25MHz and the third at 40MHz are also seen at the downconverted output of the receiver. The signals around 14MHz and 25MHz are due to the fact that the antenna picks up 454MHz and 465MHz signals used by other external land mobile radio services which happen to fall in the BPF and LPF passbands. This indicates that even if there is provision for receiving 50MHz wide signals, the BPF and LPF should be designed to receive only the desired multicarrier signal and filter out as much external interference as possible. These external interfering signals degrade the linearity of the amplifiers and mixers of the receiver RF chain.

A first look at the 40MHz signal looks like it could be an alias of external signals at 400MHz or 480MHz. However, both of these frequencies lie outside the BPF passband and therefore should not appear at the downconverted receiver output. Moreover, a survey of the spectrum using a wideband receiving antenna could not pick up any signal from external services operating at 400MHz or 480MHz, leading to the conclusion that the 40MHz undesirable signal is not due to external interference alias of 400MHz or 480MHz. After further investigation, it was found that this 40MHz undesirable signal was due to internal

interference from the ADC sampling clock running at 200MHz. The ADC clock harmonic of 400MHz is radiated and picked up by the receiver RF chain after the BPF. This discovery led to reducing ADC sampling clock radiation by using appropriate shielding.

Subcarrier Split: Effect of Local Oscillator Mismatch

At first look at the received frequency spectrum in Figure 4.13, it appears that the received multicarrier signal spanning from 2.4MHz to 8.5MHz is just affected by frequency selective fading. While this is an expected consequence of multipath in the environment, a closer look at the signal reveals a discontinuity, or split, in each subcarrier as shown in Figure 4.15.

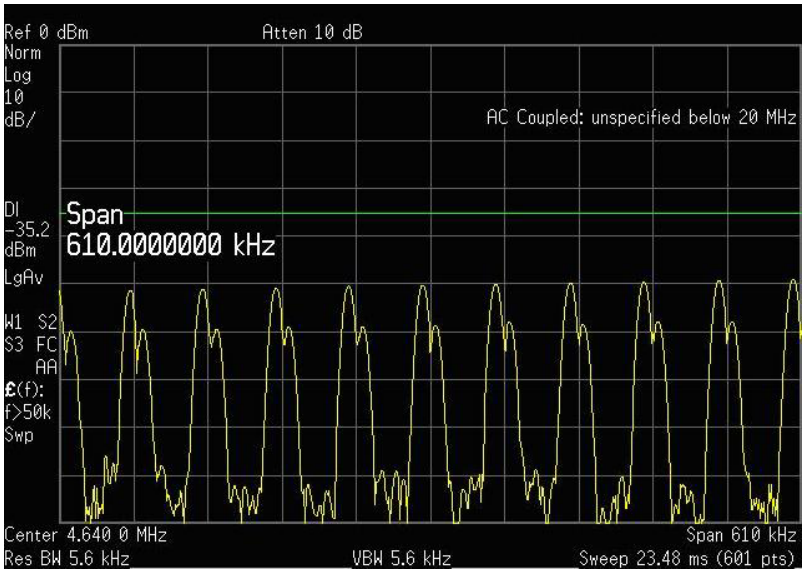

Figure 4.15 Effect of Transmitter - Receiver LO Frequency Mismatch

This subcarrier splitting is a result of the transmitter and receiver LO frequencies not being identical. In this case the subcarriers are no longer upconverted and downconverted at the required frequency and are therefore offset by a few kHz which is proportional to the transmitter receiver LO frequency mismatch.

The signal processing algorithms do not search for subcarrier peaks but rather, assume that the peak lies at the ideal subcarrier frequency locations, ignoring power present at other frequencies. Thus, the offset in the multicarrier signal causes degradation in the SNR as now the subcarriers are not at their ideal frequency locations. Moreover this offset also leads to Inter Carrier Interference from adjacent carriers as they are not sampled at the zero crossings of adjacent subcarriers.

For systems which continuously transmit multicarrier symbols, algorithms can be implemented in time domain to estimate the carrier frequency offset [2]. Let the transmitted signal be s_n, then the complex transmitted signal is;

$$y_n = s_n e^{j2\pi f_{TX} nT_s} \tag{4.1}$$

where, f_{TX} is the transmitter carrier frequency, T_s is the multicarrier symbol period. The receiver downconverts the signal with a carrier frequency f_{RX} and the received complex baseband signal r_n is given by;

$$\begin{aligned} r_n &= s_n e^{j2\pi f_{TX} nT_s} e^{-j2\pi f_{TX} nT_s} \\ &= s_n e^{j2\pi (f_{TX} - f_{RX}) nT_s} \\ &= s_n e^{j2\pi \Delta f nT_s} \end{aligned} \tag{4.2}$$

where, Δf is the carrier frequency offset between the transmitter and receiver local oscillator frequencies. Thus, given two repeated symbols, the local oscillator frequency offset estimator is;

$$z = \sum_{n=0}^{L-1} r_n r_{n+1}^*$$
$$= \sum_{n=0}^{L-1} s_n e^{j2\pi\Delta f n T_s} \left(s_{n+1} e^{j2\pi\Delta f (n+1) T_s} \right)^* \tag{4.3}$$

$$z = \sum_{n=0}^{L-1} s_n s_{n+1}^* e^{j2\pi\Delta f n T_s} e^{-j2\pi\Delta f (n+1) T_s}$$
$$= e^{-j2\pi\Delta f T_s} \sum_{n=0}^{L-1} \left| s_n \right|^2 \tag{4.4}$$

$$\hat{\Delta f} = \frac{-\angle z}{2\pi T_s} \tag{4.5}$$

Every subcarrier experiences a phase shift that is proportional to the carrier frequency offset *Δf*, which can be estimated as shown by the above equation.

To identify the need for implementing such a local oscillator frequency offset correction algorithm, an experiment was performed using the Phase 2 prototype hardware. The goal of this experiment was to analyze the effect of transmitter receiver LO frequency mismatch on range estimation in order to determine what level of mismatch would be acceptable in a fielded system. This test used a signal generator for the receiver and transmitter LO instead of the PLL evaluation boards and the transmitter output was connected to the receiver input using a fixed length cable using appropriate attenuation. The transmitter LO was kept fixed at 440MHz and the receiver LO was then offset from 0Hz to

50kHz in increments of 1kHz and the receiver downconverted signal was sampled and stored for each increment.

This sampled data was then post processed using algorithms developed by the algorithms team to provide a range estimation error plotted on the right y axis of Figure 4.16. It can be seen from Figure 4.16 that an LO frequency mismatch of less than 10kHz is desirable to ensure that the range error due to LO frequency mismatch is almost zero. This requires the PLL crystal oscillator accuracy to be 20ppm or better, which at 440MHz LO will result in its frequency offset of less than 10kHz. The crystal oscillator accuracy in the PLL boards used in the RF front end is 2.5ppm which results in a frequency offset between the transmitter and the receiver LO of less than 10kHz. Therefore, the split seen in Figure 4.15 will not cause degradation in the positioning accuracy and there is no need to implement local oscillator frequency offset correction algorithms or to track the ideal subcarrier frequencies in software.

The fact that the specification on required crystal accuracy and its effect on positioning accuracy was not known until these initial wireless RF evaluation tests were performed makes this an important result which serves as a guideline for other multicarrier positioning system designers.

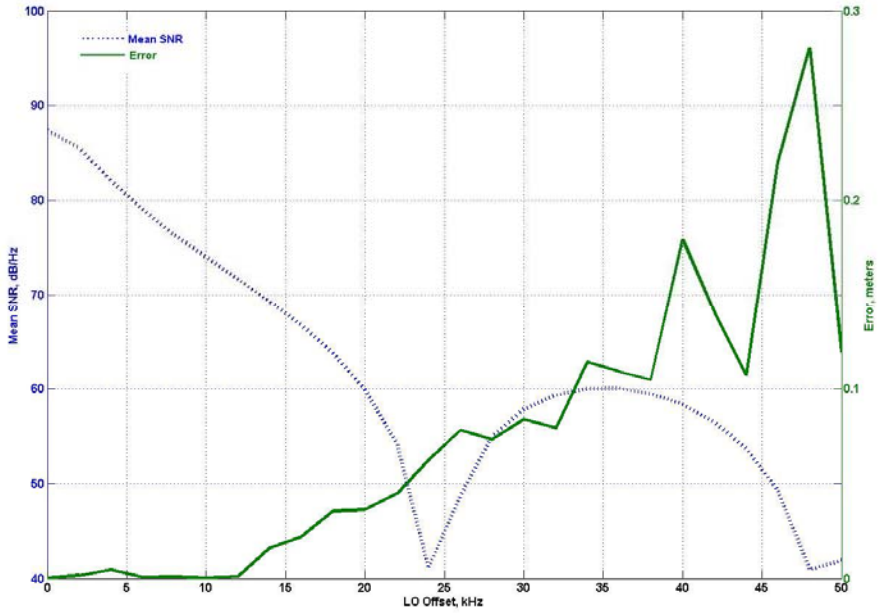

Figure 4.16 Effect of LO Frequency Mismatch on Range Estimation

Effect of Sampling Clock Mismatch

Similar to the local oscillator offset, there also exists sampling clock offset between the transmitter and the receiver. Detailed analysis on the effect of a frequency mismatch between sample clocks on the transmitting and receiving ends for a multicarrier precise positioning system is presented in [3]. Small initial offsets between the receiver sample clock frequency, f_R, and the transmitter sample clock frequency, $f_T=f_R+\alpha f_R$, from its initial value will result in a simple scaling of TDOA estimates by the frequency skew factor α, where $|\alpha|<<1$. Figure 4.17, shows the effect of the sampling frequency offset on the subcarriers, where n is the subcarrier number from 1 to M, and Δf is the original subcarrier spacing.

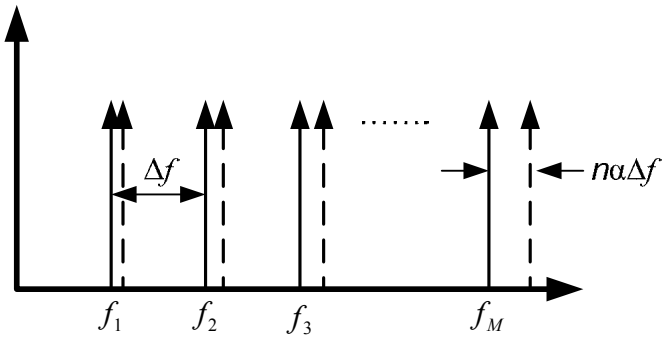

Figure 4.17 Effect of Sampling Frequency Offset

This error becomes very significant in two situations: first when the sampling frequency of the transmitter has drifted since the system was calibrated, and

second when the periodic sampling routine is not synchronized, across all receivers, to within a close tolerance. In a realistic system, both of the above conditions will be true, which will impose constraints on the system implementation to maintain the goal of sub-meter accuracy. The two receivers could start sampling the signal at two different times and if the sampling window offset between two receivers is greater than Δt this sampling window offset, combined with the sampling clock drift, causes severe position estimation degradation as discussed in detail in [3].

Lessons Learnt

Multicarrier Effect: An important observation made during the RF evaluation tests is that when using multicarrier signals, the RF component performance significantly changes from the data sheets and needs to be accounted for depending on the number of carriers being used in the system. Derating the component specifications is important for multicarrier based systems.

Gain Modes: For the VGA chip, operating the receiver VGA in high gain modes is not desirable as this significantly raises the noise floor, thus degrading the multicarrier SNR. Therefore, it is preferred to operate the VGA in its low gain mode.

External Interference: The LPF and BPF of the RF transmitter and receiver front end are usable for multicarrier signals spanning 50MHz. However, if the multicarrier signal span is going to be much less than 50MHz, then this capability starts to degrade the system performance due to external interference resulting in RF front end overload. Hence the BPF and LPF cutoffs need to be changed to less than 50MHz if the span of multicarrier signal is much less than 50MHz.

Internal Interference: Radiation due to the ADC sampling clock gets picked up by the receiver RF front end and could cause the mixer and the amplifiers to operate in their non linear region. This internal interference from

our own system need to be eliminated and proper shielding of the crystal at the ADC is required.

LO and Sampling Clock Mismatch: The transmitter and the receiver LO mismatch affects the range estimation and a 2.5ppm accuracy crystal oscillator is preferred in the PLL implementation, which for a 440MHz LO will result in frequency offset between the transmitter and the receiver LO to be less than 10kHz. As compared to the local oscillator offset more stringent timing and synchronization is required for the sampling clock as is discussed in detail in [3].

Conclusion

A first wireless RF evaluation test over short range was performed which led to useful observations in the system behavior while transmitting over air and the proper regions of operation for the RF electronics was also better understood. Important issues like internal interference, LO mismatch, VGA behavior and external interference were identified and resolved. In general it is important to evaluate the components using multicarrier signals, as derating the components is required when designing a multicarrier based system.

The two aspects that need to be considered are local oscillator and sampling clock offsets between the transmitter and receiver. The details of effect of local oscillator offset on range estimation were discussed in this chapter and it was concluded that it is not a major source of error and can be easily controlled by using inexpensive crystal oscillator. The sampling window offset between two receivers in addition to the sampling clock offset could result in large range errors and is a more serious error source compared to local oscillator offset, this error can be eliminated by co-locating the ADC boards and running them using a common sample clock.

The next chapter discusses the prototype designs for a transmitter and receiver which eliminate the evaluation boards and replace then with custom RF PCB designs. Custom RF PCB designs are more suitable for extensive field

testing and will bring the system closer to our desire to have a portable, field deployable RF based positioning system.

References

[1] D. Cyganski, J. A. Orr and W. R. Michalson, "A Multi-Carrier Technique for Precision Geolocation for Indoor/Multipath Environments", *Institute of Navigation Proc. GPS/GNSS*, Portland, OR, September 9-12 2003

[2] J. Heiskala, J. Terry, "OFDM Wireless LANs: A Theoretical and Practical Guide", *SAMS* Publication, ISBN: 0672321572

[3] J. Coyne, R. J. Duckworth, W. R. Michalson, H. K. Parikh, "2-D Radio Navigation Between MC-UWB", *Royal Institute of Navigation Proc.*, RIN, UK, October 2005

Chapter 5 : Ranging Using a Multicarrier Signal

Introduction

This chapter first discusses the design of our custom made RF transmitter and receiver PCBs which are referred to as the Phase 3 RF prototypes. This 440MHz prototype provided a foundation for the extensive indoor and outdoor wireless ranging tests which are discussed next. The focus of the tests discussed in this chapter is on ranging, which is an essential element of positioning, as accurate ranging translates into accurate positioning.

The first test discussed in this chapter is a wired ranging test using synchronized sampling clocks and local oscillators between a single transmitter

and a single receiver. The success of this wired ranging test led to extensive wireless ranging tests, also using synchronized sampling clocks and local oscillators.

These wireless tests and the analysis of collected data, led to the discovery of an unexpected source of error which will be discussed in this chapter. This error resulted as a consequence of the overlap of the two sidebands at the direct downconversion receiver output which resulted in degraded ranging accuracy. This error appears to be unique to multicarrier based positioning systems and this chapter concludes by proposing a simple solution which led to a substantial improvement in ranging accuracy.

RF Receiver Custom PCB

This section will discuss the RF receiver custom PCB design. The receiver front end consists of a Band Pass Filter (BPF), Low Noise Amplifier (LNA), Variable Gain Control (VGA), Downconverting mixer, PLL for mixer LO and a Low Pass Filter (LPF) as shown in Figure 5.1.

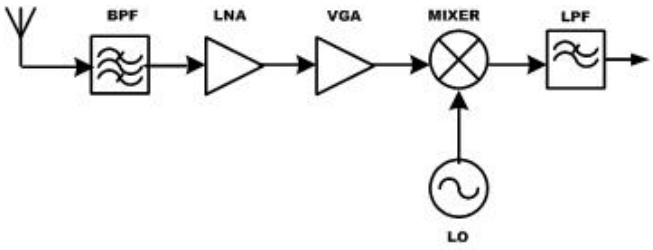

Figure 5.1 Receiver RF Front End

From the cable tests discussed in the previous chapters, it was concluded that the BPF 3dB bandwidth should be less than 50MHz if the multicarrier signal being used does not span the entire 50MHz range. Since the current plan was to use less bandwidth, it was decided to design this custom PCB to receive signals spanning up to 25MHz, centered at 440MHz. The BPF used a triple tuned helical BPF with 3dB bandwidth of 25MHz centered at 440MHz. The helical BPF was tuned for the required passband and the frequency response of the BPF from 400MHz to 500MHz is as shown in Figure 5.2. The PCB was designed with a provision to bypass the on-board helical filter and use an external filter. This would allow the RF system to be adapted to receive signals spanning up to 50MHz.

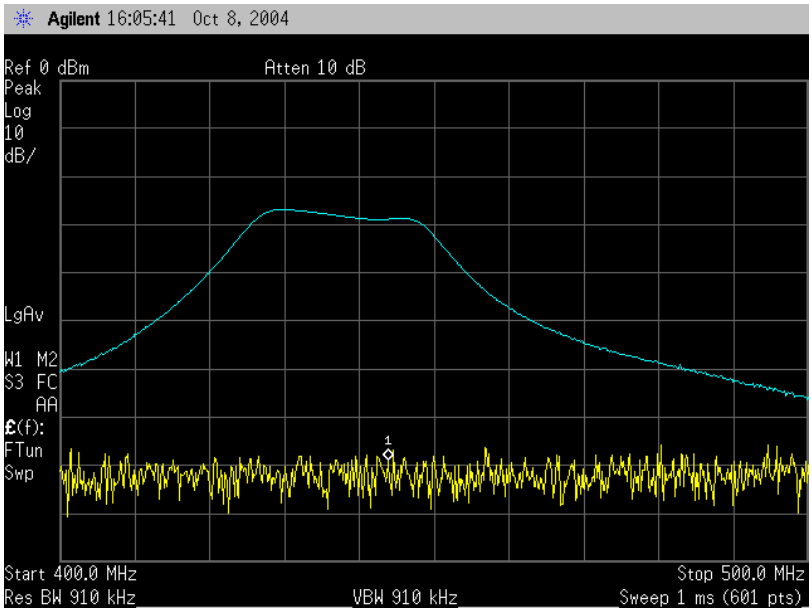

Figure 5.2 Helical BPF Frequency Response

The LNA, VGA and the mixer chip used in the custom RF receiver PCB are the same as those used in the Phase 1 prototype system. The LNA which follows the BPF has a gain of 22.5dB and a low noise figure of 1.6dB. The wideband VGA that follows the LNA has a gain variation range from -11dB to 34dB and can be digitally controlled through a serial 8 bit gain control word. A high performance active mixer is used as a direct downconverter.

The required local oscillator signal to drive the mixers is approximately -10dBm. An external RF PLL PCB provides the required 440MHz mixer LO which is the same evaluation PCB that was used in the Phase 2 prototype. The crystal oscillator used in the PLL synthesizer is a 10 MHz TCXO and has frequency stability over temperature of 2.5ppm. The VCO used in the

PLL circuit has a frequency range of 415MHz to 475MHz and a tuning sensitivity of 10MHz/V.

A 7-section LC LPF with very low insertion loss of 0.3dB follows the mixer and then drives the ADC. The LPF used provides a very flexible design as the same package is available for 3dB cutoff frequencies of 6MHz, 15MHz, 30MHz and 60MHz. The approximate LPF frequency response for a 3dB cutoff frequency of 15MHz was measured using a high frequency probe on the spectrum analyzer and is shown in Figure 5.3. The designed RF receiver front end custom PCB which is a 3.5"x4" size board is shown in Figure 5.4.

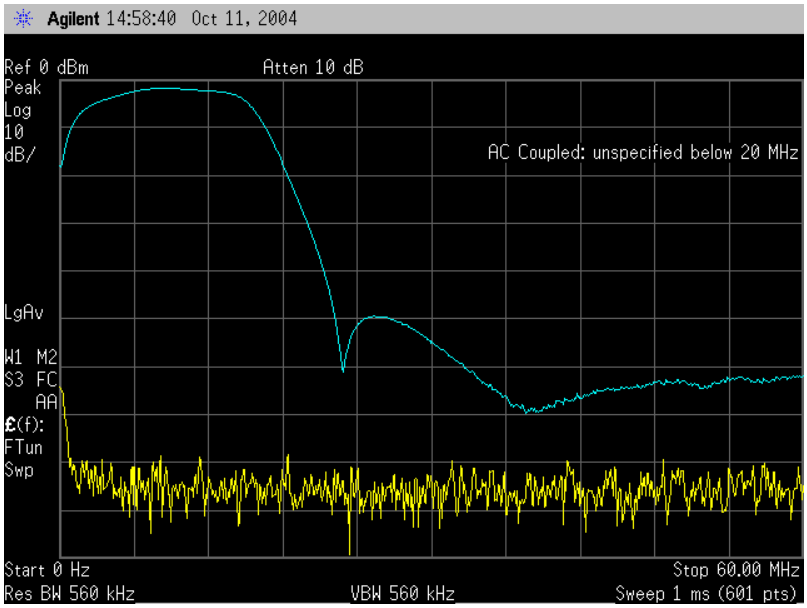

Figure 5.3 LC Low Pass Filter Frequency Response

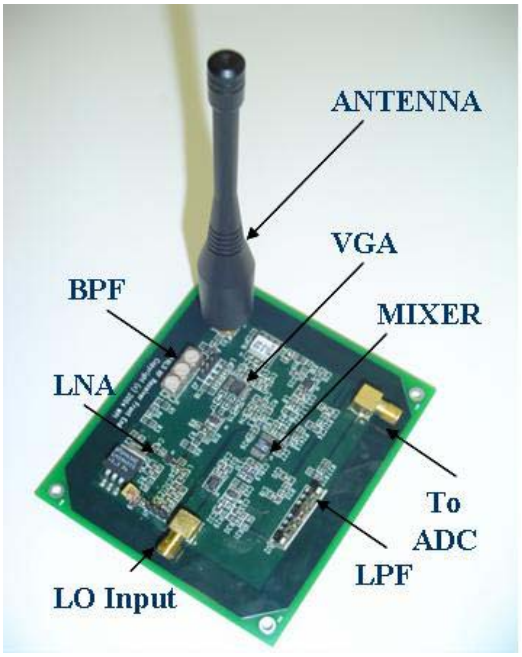

Figure 5.4 Designed Receiver RF Front End PCB

Table 3.1 shows the measured gain values, noise figure and the 3rd order input intercept (*IIP3*) point for the stage in the RF receiver front end.

Table 5.1 Receiver Building Block Specifications

	BPF	**LNA**	**VGA**	**Mixer**	**LPF**
Vendor	TOKO	RFMD	Analog Devices	Analog Devices	Coilcraft
Part #	5HT44020	RF2361	AD8370	AD8343	P7LP156
Gain (dB)	-3	22.5	15.5	-5.5	-0.3
***NF* (dB)**	3	1.6	7.2	12.5	0.3
IIP3 (dBm)	∞	5.5	15.5	22	∞

The receiver RF front end PCB shown in Figure 5.4 was tested and Table 5.2 shows the achieved system parameters for the Phase 3 RF receiver. The achieved receiver gain was 27dB, the system *NF* was 5.1dB and the achieved *IIP3* was -17dBm. The achieved receiver sensitivity was -85dBm and receiver spurious free dynamic range was 44.8dB.

Table 5.2 RF Front End System Parameters

System Parameter	**Achieved**
System G (dB)	27
System *NF* (dB)	5.1
System *IIP3* (dBm)	-17
Rx. Sensitivity (dBm)	-85
Rx. SFDR (dB)	44.8

RF Transmitter Custom PCB

Similar to the RF receiver custom PCB, a custom RF transmitter PCB was also designed. As shown in Figure 5.5, the transmitter RF front end consists of an LPF, upconverting mixer, PLL for mixer LO, Power Amplifier and a BPF.

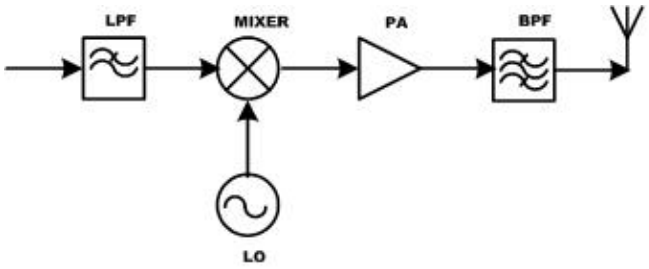

Figure 5.5 Transmitter RF Front End

The LPF used is the same 7-section LC LPF used in the receiver RF front end. These LPF's have the advantage of flexible cutoff frequency, low insertion loss and high power handling. The active mixer used for upconvertion is also the same as that used in the receiver RF front end. This mixer has advantages of having wide bandwidth on all of its ports and low intermodulation distortion. The power amplifier chip used is the same as that tested and evaluated in the Phase 2 prototype. The required local oscillator signal to drive the mixers is approximately -10dBm. An external RF PLL PCB similar to that used in the receiver generates the required 440MHz mixer LO. The BPF used is a triple tuned helical BPF (25MHz bandwidth centered at 440MHz), identical to the one

used in the receiver PCB. Similarly, the transmitter has provisions for an external 50MHz BPF if bandwidth needs to be upgraded to 50MHz. The designed RF transmitter front end custom PCB which is also a 3.5"x4" size board is shown in Figure 5.6.

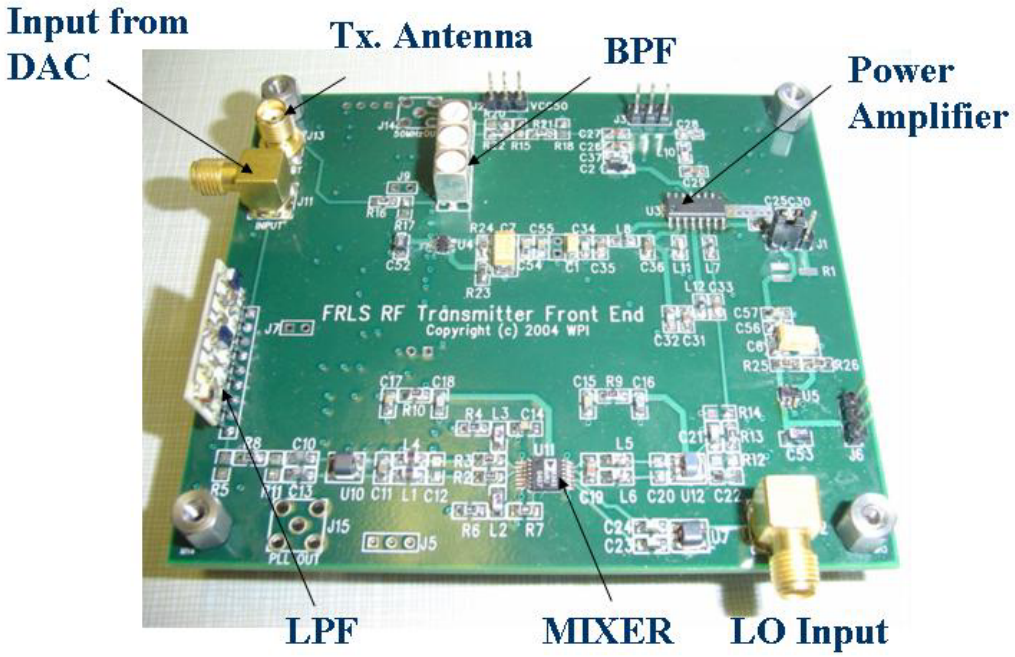

Figure 5.6 Designed Transmitter RF Front End PCB

Wired Range Estimation Using Custom RF PCBs

The designed RF transmitter and receiver custom PCBs can now be used for range estimation tests. The receiver stack, consisting of the RF front end and the digital back end, is shown in Figure 5.7. A similar transmitter stack was built making it possible now to perform extensive field testing.

Before using these new RF PCBs for wireless ranging tests, it was first necessary to confirm that they do not exhibit any unexpected behavior and hence cable ranging tests are performed first. This wired test setup and its results are discussed in this section.

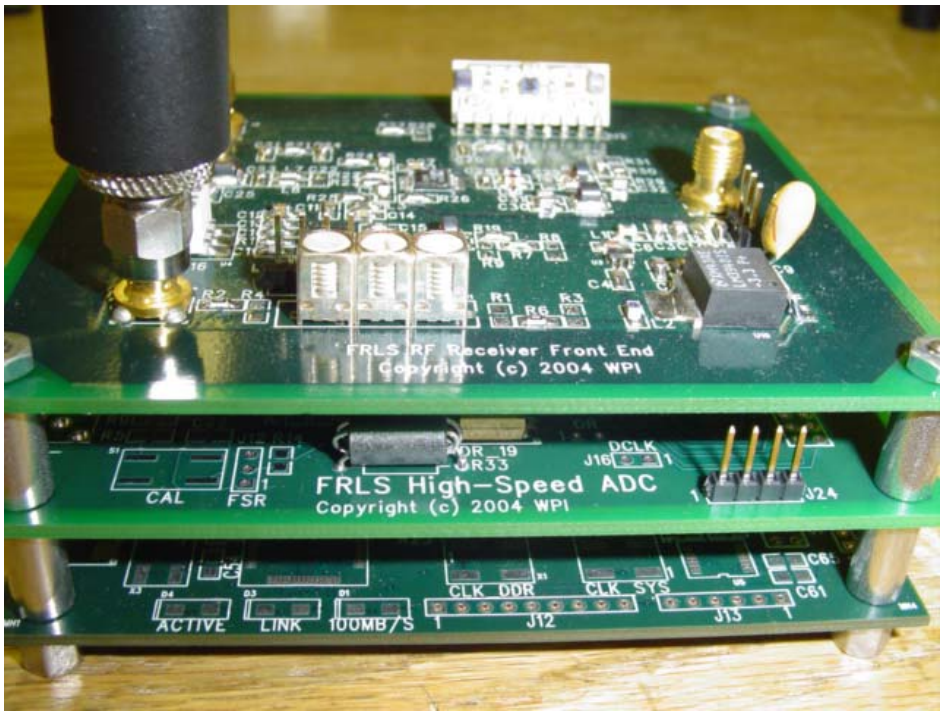

Figure 5.7 Custom Receiver Stack Design

Since positioning accuracy improves with increasing bandwidth, it was decided to increase the signal bandwidth from 6.1MHz to 12MHz and reduce the number of subcarriers from 101 to 51. Increasing the bandwidth is expected to lead to improved range estimation accuracy, while reducing the number of subcarriers results in reducing the DAC slew rate requirements and thus improving the transmitted signal spectral purity.

Figure 5.8 shows a part of the baseband multicarrier-wideband (MC-WB) signal. The 51 unmodulated subcarriers span 12.2MHz starting from 2.4MHz to 14.6MHz. The frequency spacing between subcarriers is set to 244kHz which is approximately equal to about 20 Narrowband FM channels. This means that there is a significant amount of unoccupied spectrum between any two subcarriers of the MC-WB signal that can be utilized by other services. Although the subcarriers are spread over 12.2MHz, the actual spectrum occupied is only approximately 25kHz (51x500Hz), assuming that the 99% power bandwidth for an unmodulated sinusoid is 500Hz. The frequency spacing and the number of subcarriers can be easily modified to avoid interference to or from other external services using the same spectrum. The characteristics of the generated MC-WB signal currently being used are listed in Table 5.3.

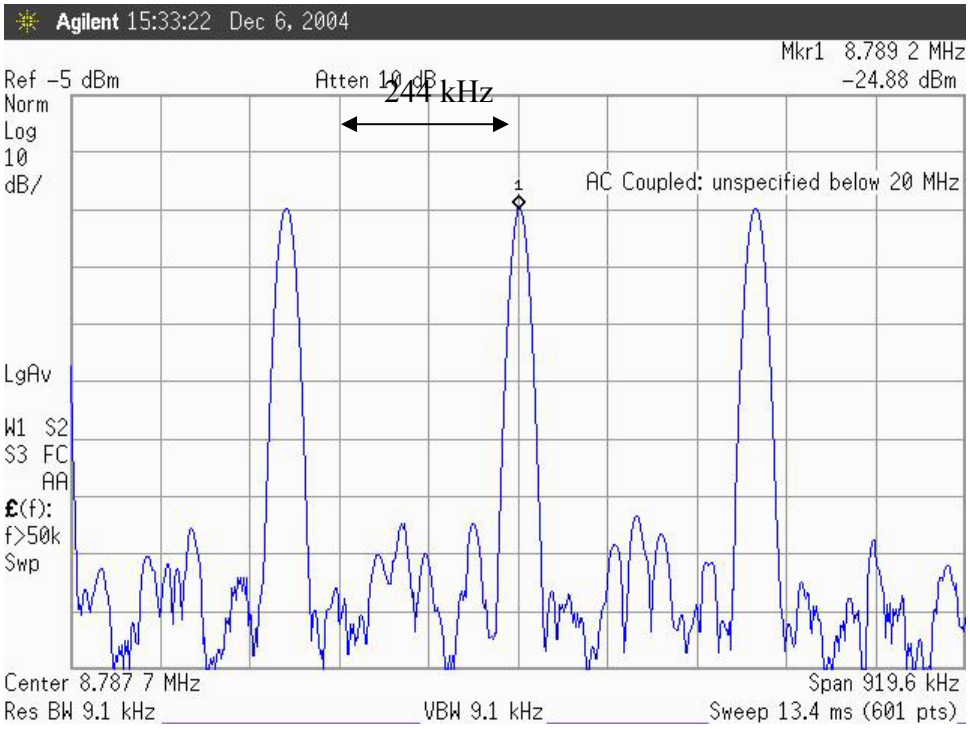

Figure 5.8 Subcarriers of Generated Multicarrier signal

Table 5.3 MC-WB Signal Characteristics

Number of Subcarriers	51 Subcarriers
Subcarrier Spacing	244kHz
First Subcarrier at	2.44MHz
Last Subcarrier at	14.64MHz
Spanned Signal BW	12.2MHz
OFDM signal period	40.96usec

Figure 5.9 shows the block diagram for the wired ranging test setup. The DAC and the ADC, both use a sampling clock signal generated from a common signal generator. The LOs for both the transmitter and receiver RF

PCBs are also generated from a common signal generator, thus eliminating any errors due to sampling clock or LO offsets between the transmitter and receiver.

The multicarrier signal output of the DAC drives the transmitter RF front end PCB, where the MC-WB signal is upconverted, amplified and filtered. This output of the transmitter is attenuated to a level of approximately -55dBm using external resistive attenuators and is connected to the input of the receiver RF front end PCB using a cable. The downconverted MC-WB signal is then digitized and transferred to a PC for range estimation. The initial range estimation test setup is:

- Setup: Single Transmitter – Single Receiver
- Antenna: Not used, transmitter output cabled to receiver input
- Transmitter: DSB Transmission
- Receiver: Direct Down Conversion Receiver (DCR)
- Baseband MC-WB Signal Span: 12MHz
- Tx-Rx Sampling Clock: Synchronized
- Sampling Clock: 200MHz
- Tx-Rx Carrier Frequency: Synchronized
- Carrier Frequency: 440MHz

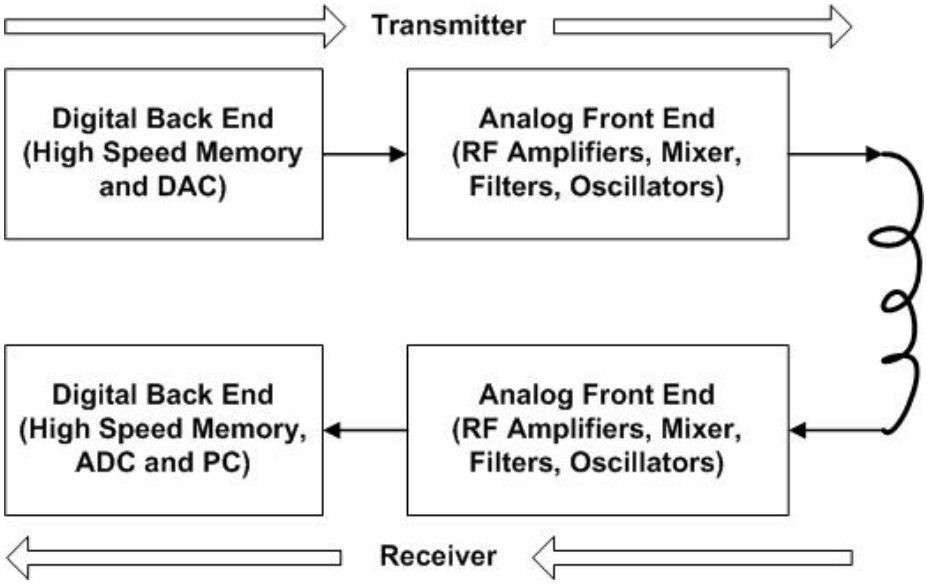

Figure 5.9: MC-WB Based Range Estimation Test Setup

The transmitted DSB signal is as shown in Figure 5.10. The output of the transmitter is connected to the input of the receiver using RF cables of various lengths l_i, thus artificially introducing delays in the received signal for longer cables. The electrical length of the cable l_i is the true range between the transmitter and the receiver and the results of the range estimation should be close to this electrical length of the cable. Five cables of various lengths were used; making it look to the receiver like the transmitter is being moved farther away.

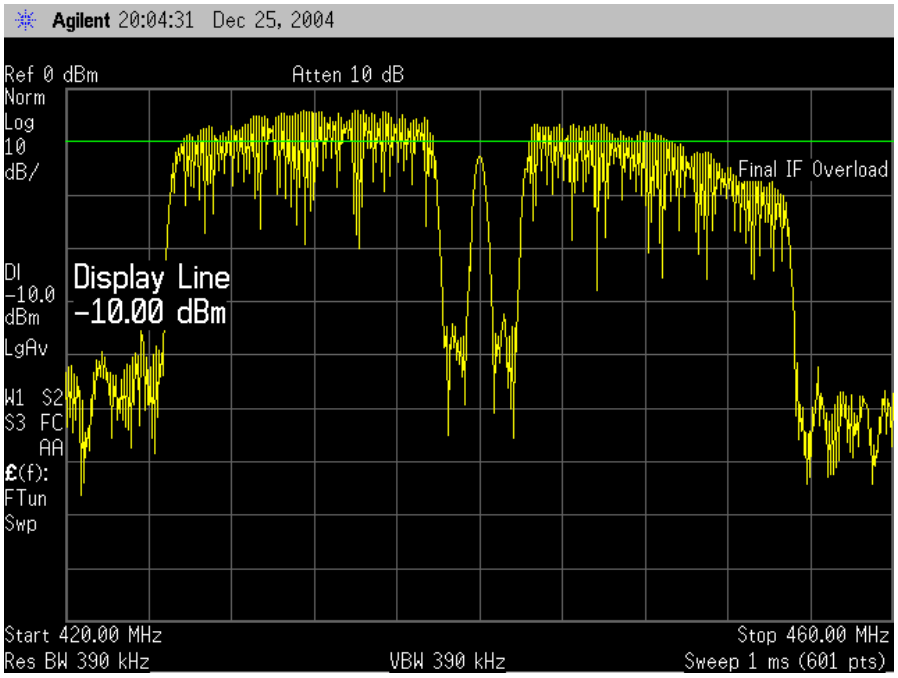

Figure 5.10 Transmitted 12MHz MC-WB DSB Signal

The results of the range estimation are shown in Figure 5.11. At each increase in cable length, five measurement data sets were collected. The results of each measurement correspond to the sets of five points close to each other as seen in Figure 5.11. Five different cable lengths were used, and hence a total of 25 data sets were sampled and range estimations were performed for each one of them.

We can see that the range estimates look like the expected staircase, where the jump in the step is the difference in the successive cable lengths. Note that the cables used were calibrated first as the physical length of

the cable is shorter than its calibrated electrical length. The average range estimation errors are shown in Table 5.4.

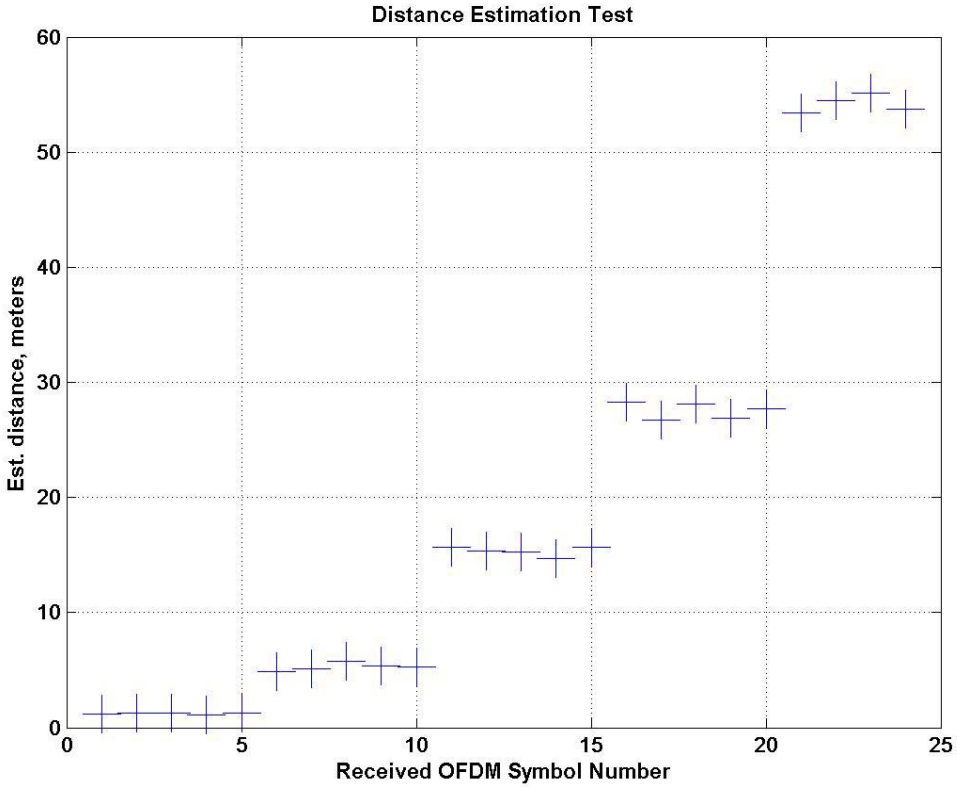

Figure 5.11: Range Estimates for MC-WB Based System

Table 5.4: Range Estimates

l_i	Calibrated Electrical Cable Length (m)	Estimated Range (m)	Error (m)
i = 1	1.2	1.5	0.3
i = 2	4.2	5	0.8
i = 3	17	16	1
i = 4	27.8	27	0.8
i = 5	51.5	53	1.5

The average range estimation errors shown in last column of Table 5.4 are within 1 meter when the cable length is less than 30 meters. For cable lengths greater than 30 meters, the average range estimation error increases due to decreased signal to noise ratio. Thus, using the custom designed RF PCBs and algorithms; it is possible to consistently estimate the range between the transmitter and receiver in controlled, multipath free, environment. This provided verification that the algorithm and the Phase 3 RF PCBs work as expected. The next step is to perform similar ranging tests in a wireless environment.

Wireless Ranging Test Setup in AK108

After successful wired ranging tests, wireless ranging tests were performed using the same set up shown in Figure 5.9. The only difference is that now the rubber duck monopole antennas are used at the transmitter and receiver instead of a cable being connected between them. The receiver and transmitter stacks were placed indoors in a small 10x10m classroom in Atwater Kent - AK108 and the test setup [1] is shown in Figure 5.12.

Figure 5.12 Indoor AK108 Ranging Test Setup

To keep the testing process simple, a 50m cable was connected from the transmitter RF output to the monopole antenna. Now only the transmitter antenna needs to be moved relative to the receiver and not the complete transmitter stack. The transmitter antenna was initially at a distance of

1.8m from the receiver antenna where a set of measurements was made to form a calibration point. The transmitter was then moved from 1.8m to 2.4m in increments of 0.15m, and the received signal at each location was sampled and stored. Five symbols were captured at each transmitter antenna position starting at a distance of 1.8m and moving to a distance of 2.4m. Thus, the first five range estimates shown in Figure 5.13 correspond to the range estimates at a true distance of 1.8m and the last five estimates correspond to the range estimates at a true distance of 2.4m.

Comparing Figure 5.13 with Figure 5.11, it is clear that there is something wrong that is causing large errors in the range estimation, some as high as 90m. With the sampling clocks and the local oscillators being generated from the same source, there are no synchronization errors, which indicate that either multipath or some other system issue could be causing the errors.

Figure 5.14 shows the spectrum of the received signal at 1.8m and 2.4m. Note that the frequency spectrum looks severely multipath effected for LOS short range condition. This spectrum does not look correct as one would expect the frequency selective fading characteristics to be relatively smooth as a consequence of phase cancellations. In contrast, the observed spectrum shows a periodic dip at approximately every 3MHz. Since the room dimensions are small compared to the wavelength at 3MHz (approximately 100m), it is unlikely that

multipath could be causing such an error. The problem had to be in the system configuration.

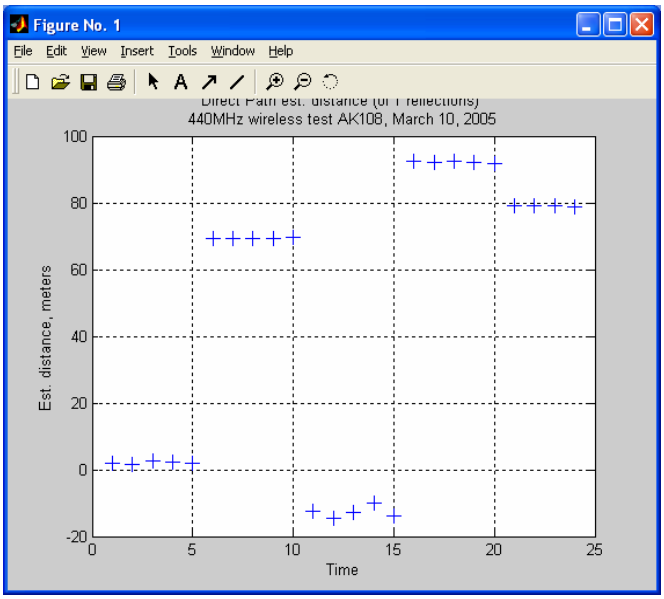

Figure 5.13 Indoor AK108 Ranging Test Results

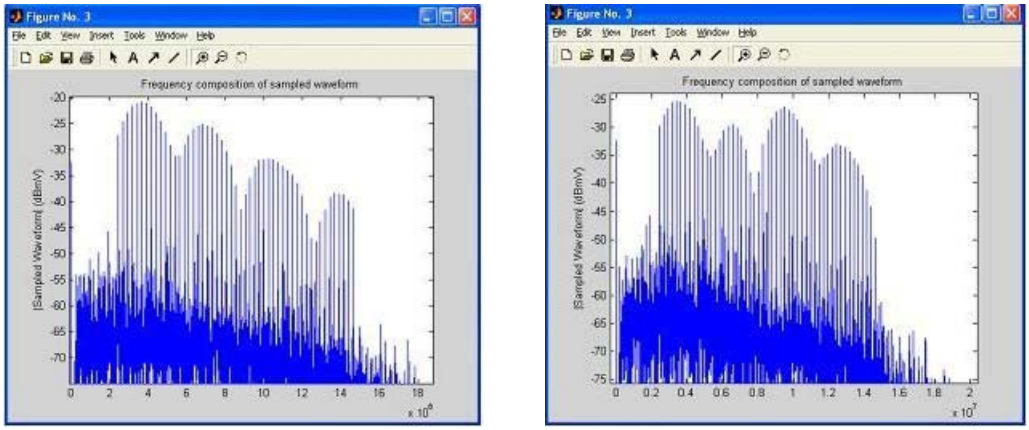

(a) (b)

Figure 5.14 (a) Sampled waveform amplitude (dBmV) v. Frequency (Hz x 10^6), shows Received Frequency Spectrum at 1.8m, (b) Sampled waveform amplitude (dBmV) v. Frequency (Hz x 10^7), shows Received Frequency Spectrum at 2.4m

The only component in the test that had a length related to the 3MHz period seen in Figure 5.14 was the 50m cable between the transmitter output and the antenna. This cable was removed and the antenna was mounted directly at the transmitter RF output. The received spectrum at 1.8m after removing this 50m cable is shown in Figure 5.15(a). The received spectrum when the transmitter output was cabled directly to the receiver, eliminating the antennas and the 50m cable is also shown in Figure 5.15(b). Note that the dips in the frequency spectrum have now been eliminated and the received spectrum over the air is similar to the cabled spectrum with some smooth frequency selective fading as expected. Thus the dips in the frequency spectrum were due reflections caused internally in the 50m cable due to mismatch between the cable and the antenna. These reflections were corrupting the phase information of the received signal and were causing large errors of up to 90m.

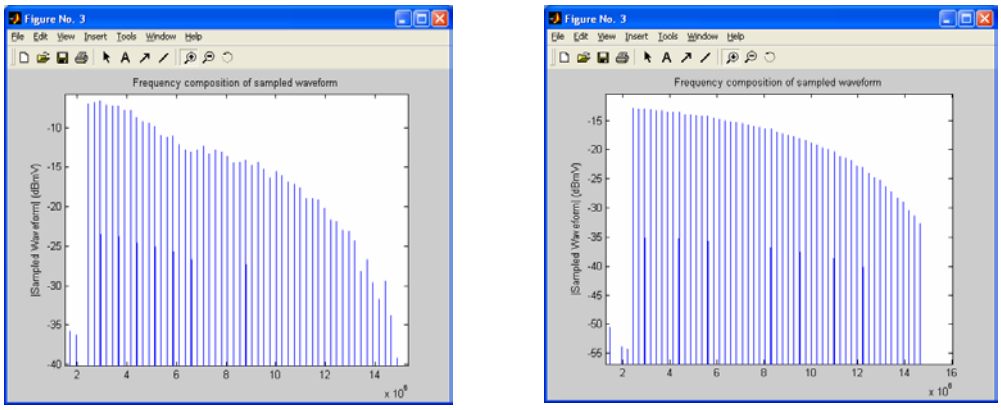

(a) (b)

Figure 5.15 Sampled waveform amplitude (dBmV) v. Frequency (Hz x 10^6) (a) Received Frequency Spectrum, After Eliminating 50m cable, over the air, (b) and when cabled

Another wireless test was performed [2, 3] after eliminating the 50m cable. This time the transmitter PCB stack was moved from a 1m starting distance from the receiver, up to 5m in increments of 1m, keeping the rest of the setup and the testing location the same (AK-108). As in the previous wireless test, five symbols were captured at each distance and the computed range estimates for each symbol are shown in Figure 5.16.

For each symbol, the most likely range estimate is marked as '1', for that symbol. The algorithm also calculates less likely solutions to provide an indication of the relative strengths of solutions in a multipath environment. In Figure 5.16 the marker '2' corresponds to the second most likely solution which was plotted to aid in system debugging. From the range estimates marked '1', it can be seen that errors on the order of 90m are eliminated, but that the ranging errors for most cases are between 5m and 10m. This is greater than our desired range estimation accuracy of better than 3m.

Figure 5.17 shows the received frequency spectrum at transmitter locations 1m (left plot) and 5m (right plot) away from the receiver. This test was performed in AK-108 which is approximately 10mx10m classroom with many metal chairs and desks. The multipath in the room due to its small size could be strong enough that the receiving antenna is receiving strong multipath signals in addition to the direct path which could be causing the errors shown in Figure 5.16.

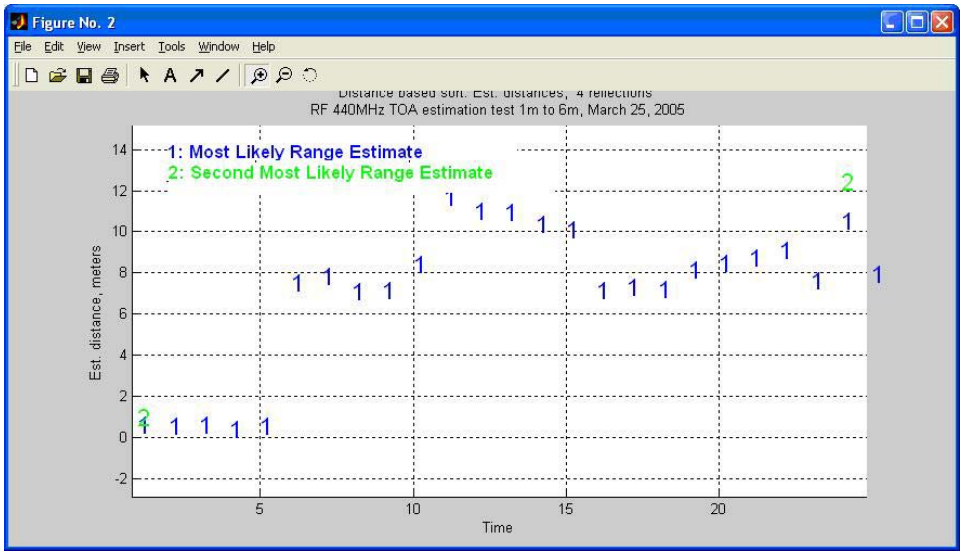

Figure 5.16 Indoor AK-108 Ranging Test Results After Eliminating 50m Transmitter Antenna Cable

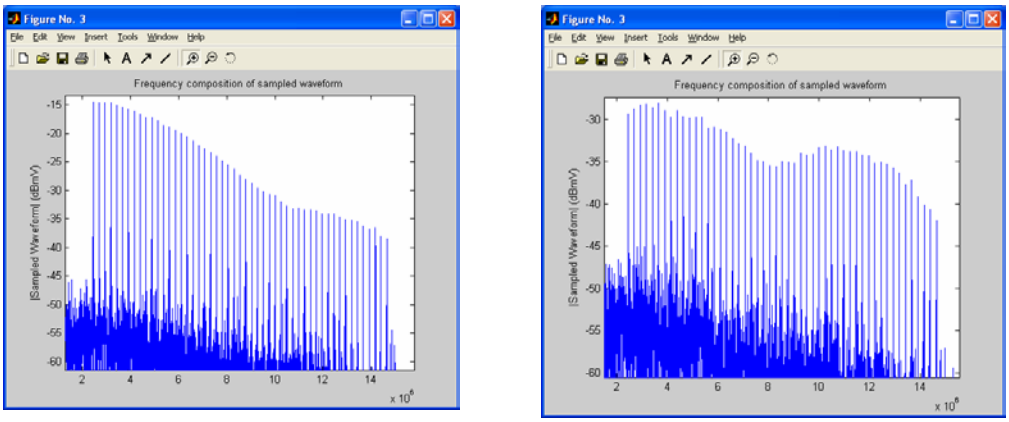

(a) (b)

Figure 5.17 Sampled waveform amplitude (dBmV) v. Frequency (Hz x 10^6) (a) Shows Received Frequency Spectrum at 1m, (b) and at 5m, after Eliminating 50m Transmitter Antenna Cable

Ranging Test Setup in AK 3rd Floor

Based on these initial tests, it was thought that the small room of about 10mx10m could result in the receiving antenna seeing multipath reflections which were stronger than the direct path signal. Therefore, the next tests were performed in a larger indoor area, hoping that the multipath effect would be reduced. Thus, the 3rd floor corridor in the Atwater Kent building at WPI was selected as the venue for performing additional tests [4].

The only system hardware change made between this test and the previously test in AK108 was that the omnidirectional monopole rubber duck antennas at the transmitter and the receiver were replaced by directional dipole antennas. As shown in Figure 5.18, the receiver was kept fixed in one end of the corridor and the transmitter was mounted on a wooden table which was moved along the corridor. It was also decided to use horizontally polarized dipoles to minimize the effect of multipath reflections due to the dense vertical metal structures in the corridor (the walls contain metal studs spaced approximately 41cm apart). The initial distance between the transmitter and receiving antennas was set to 4m. The transmitter was then moved from 4m to 10m, 14m, 18m, and then to 22m. As in the previous tests five symbols were saved for range estimation at each of the five transmitter locations.

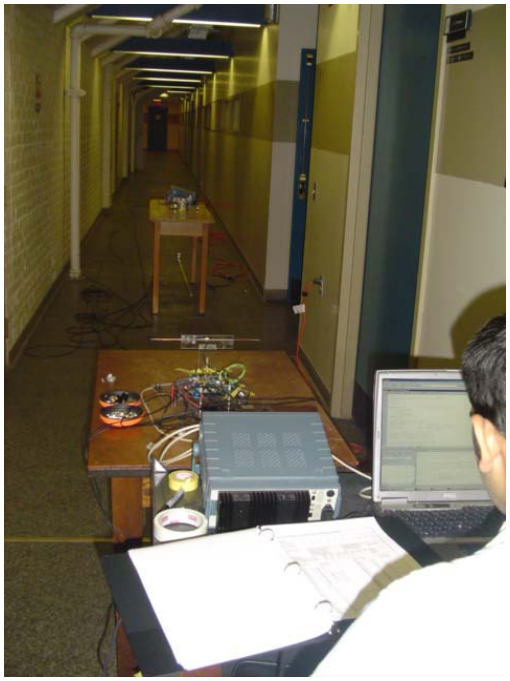

Figure 5.18 Indoor AK 3rd Floor Ranging Test Setup

As before, Marker '1' in Figure 5.19 shows the most likely range estimation results at these locations. Note that the first set of five range estimates at 4m has zero error as this is the initial known starting reference point and used as the calibration point for the range estimation algorithms. The other range estimates are then calculated using the signal received at 4m as a reference phase measurement.

The results shown in Figure 5.19 reveal that the range estimation tends to follow the change in the transmitter position, but that the estimation errors are always greater than 3m. For the 10m and 14m locations, the range estimate variance is within 2m, but the range estimation errors are always greater than 3m. The worst range estimation error of approximately 10m is seen when the transmitter is 18m from the receiver. Note that at 18m and 22m, the range estimate variance increases to approximately 5m.

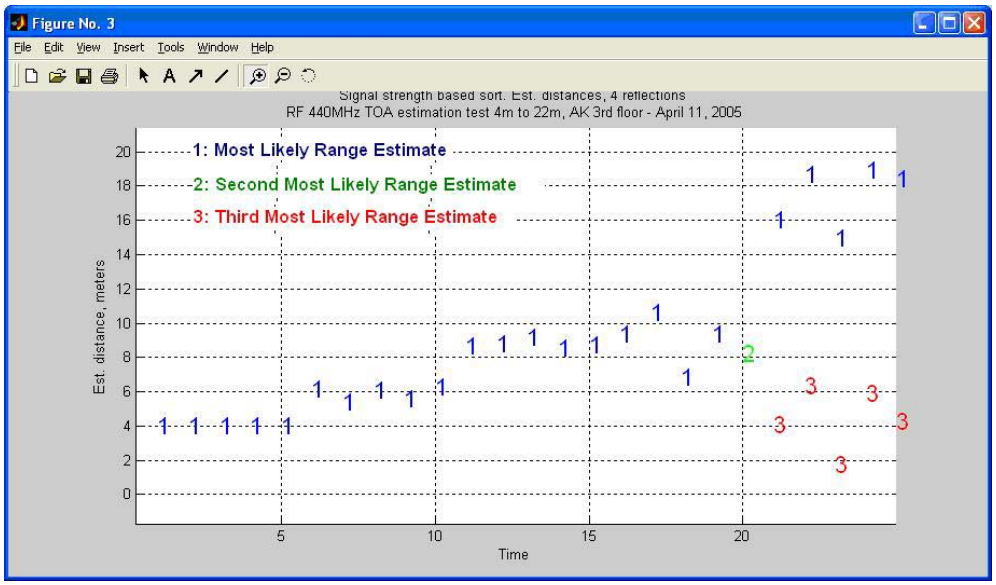

Figure 5.19 Indoor AK 3rd Floor Ranging Test Results

Figure 5.20 shows the received frequency spectrum at 18m (left plot) and at 22m (right plot). Note that the later half of the frequency spectrum at 18m is severely affected by multipath fading which could be corrupting the subcarrier phase information and causing observed errors of the order of 10m. In addition to the

effects of multipath, the SNR degradation at 18m and 22m could be causing the range estimation variance of 5m.

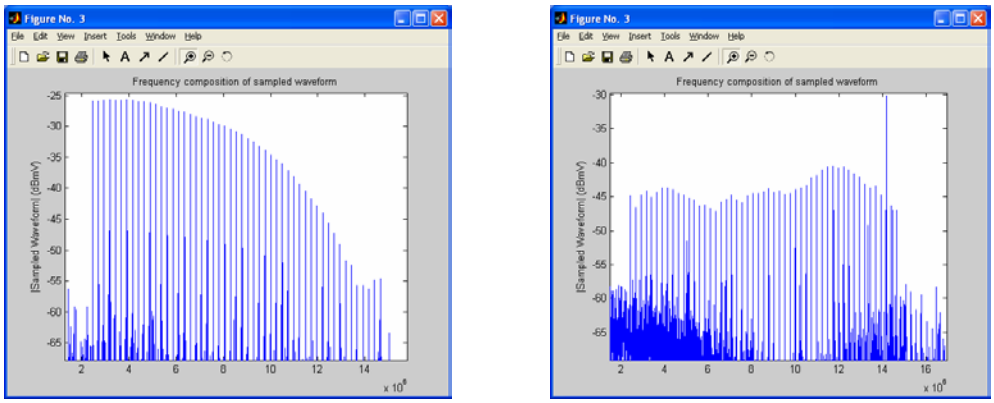

(a) (b)

Figure 5.20 Sampled waveform amplitude (dBmV) v. Frequency (Hz x 10^6) (a) Shows Received Frequency Spectrum at 18m, (b) and at 22m

At this point in the testing, the algorithms team thought that while the multicarrier signal structure provides frequency diversity, adding spatial diversity at the receiver might help improve the range estimates by adding angle of arrival information to the system. It was also hypothesized that multiple received signals could be average over time in order to obtain some processing gain which would improve the SNR. Thus, the next test discusses the range estimation results after implementing spatial diversity and symbol averaging at the receiver.

Ranging Test Setup in AK 3rd Floor with Spatial Diversity and Averaging

The basic system setup, and transmitter and receiver positions are exactly the same as that discussed in the previous test. The two additions in this test [5, 6] are spatial diversity and symbol averaging at the receiver. To support spatial diversity, a wooden antenna base was used such that the receiving dipole antenna could be mounted at nine different positions in a 3x3 grid as shown in Figure 5.21 (left plot). In previous tests only five symbols were captured at the receiver and range estimates due to all five symbols were plotted. In this test 256 symbols were captured at each transmitter position and then averaged. The range estimation is then performed on this single averaged symbol and the test is repeated for all nine antenna positions at each transmitter location (4m, 10m, 14m, 18m, and 22m).

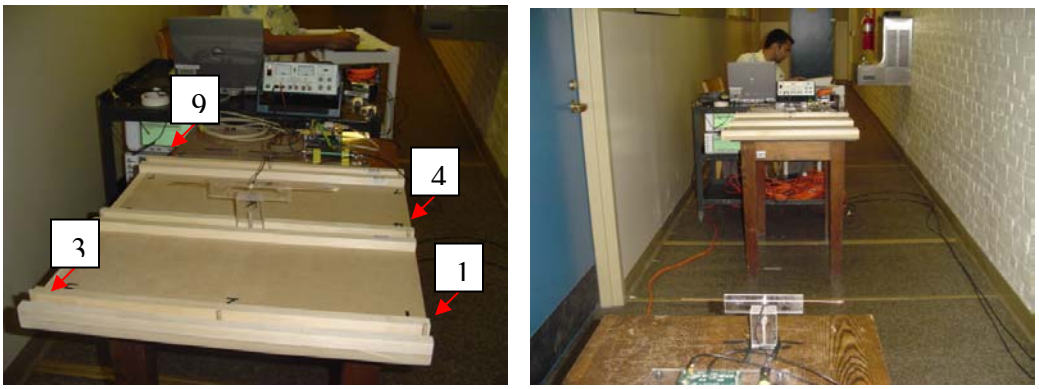

Figure 5.21 Indoor AK 3rd Floor Ranging Test Setup Using Spatial Diversity

The range estimation results for all 9 antenna positions are shown in Figure 5.22. Notice that for each transmitter location at least one of the nine antenna positions results in range estimate that is within 3m of the true transmitter position. Also, notice that the range estimate variance for any fixed transmitter position due to all 9 antenna positions is always greater than 5m. The transmitter at the 22m location results in the worst range estimation variance of approximately 20m. It is clear that the results are not as desired.

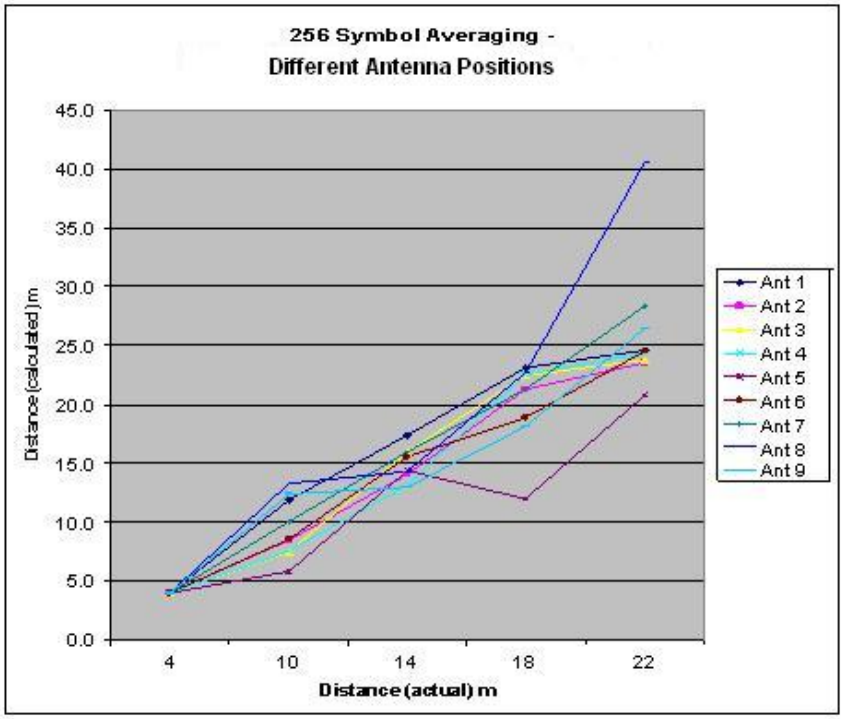

Figure 5.22 Indoor AK 3rd Floor Ranging Result for 9 Antenna Positions with Averaging of 256 Symbols Test 1

Ranging Test Setup in AK 3rd Floor Using Multicarrier Signal Spanning 24MHz

Note that the tests discussed in the previous section were performed using a multicarrier signal spanning approximately 12MHz. As shown in the theoretical calculations in Chapter 2, the indoor ranging accuracy is expected to improve with increased multicarrier span. Thus, the multicarrier span was increased from 12MHz to 24MHz and the baseband input to the transmitter RF front end was modified to generate a multicarrier signal spanning between 2.4 and 26.4MHz.

The required BPF and LPF modifications were made in the RF transmitter and receiver hardware. The LPF was changed from a 15MHz 3dB cutoff to one with a 30MHz 3dB cutoff. The onboard helical BPF was removed and the external tubular BPF used in the phase 2 prototype setup discussed in Chapter 4 was added in the RF transmitter and receiver PCBs. The rest of the test setup [7] remained exactly the same as in previous test, including the spatial diversity and the averaging.

The received, downconverted, signal spanning 24MHz is shown in Figure 5.23. Two tests were performed and the results at transmitter locations (4m, 10m, 14m, 18m and 22m) for all 9 antenna positions are shown in Figure 5.24. From these results it is clear that increasing the subcarrier span to

24MHz did not result in any improvement in range estimation and that the results are not as desired.

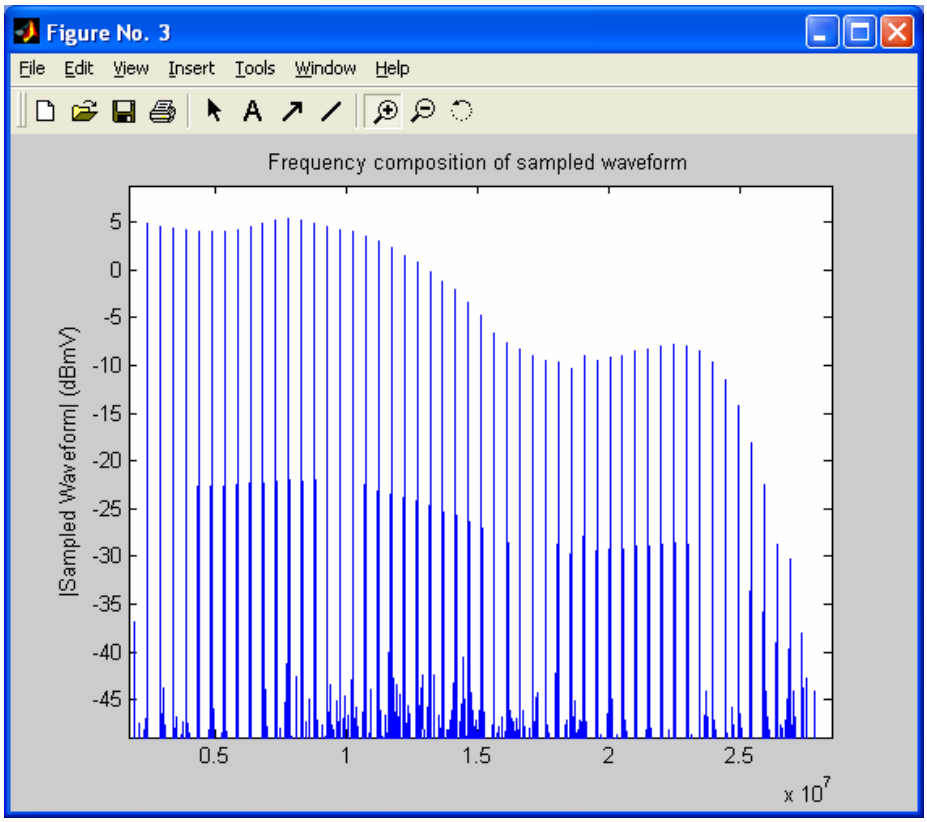

Figure 5.23 Sampled waveform amplitude (dBmV) v. Frequency (Hz x 10^7), Shows Received Frequency Spectrum Spanning 24MHz

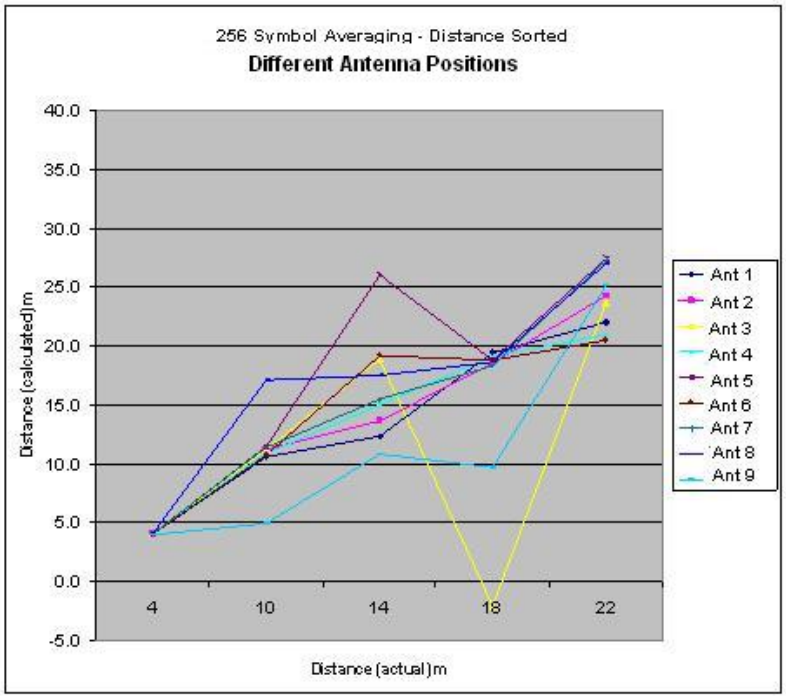

Figure 5.24 Indoor AK 3rd Floor Ranging Result for 24MHz Signal Test 1

None of the upgrades implemented (increasing bandwidth, adding spatial diversity and increasing SNR using signal averaging) in the above tests resulted in range estimate accuracy improvements. It is well known that multipath is the biggest source of error for indoor positioning systems. In addition, unavailability of suitable multipath models for indoor positioning makes it difficult to characterize the effects of multipath on positioning accuracy.

While it would be easy to attribute the errors observed in the above tests to multipath, theory suggests that even in the presence of multipath the ranging accuracy should improve when the bandwidth is doubled from 12MHz to 24MHz. This improvement, however, was not observed. This indicated that

some systemic issues may be causing the observed errors. Performing a similar ranging test outdoors in an open field where the multipath effects are negligible, or at least comparatively less severe, could provide some insight to the system behavior. These outdoor tests are discussed in the next section.

Ranging Test Setup for Outdoor Field

The basic hardware setup for an outdoor wireless test discussed in this section [8] is the same as that used for the indoor wireless tests discussed in previous sections. For this test, the receiver and transmitter stacks were placed outdoors in the WPI's grass field as shown in Figure 5.25 and the multicarrier signal spanning 12MHz is used, which can be increased to 24MHz if required.

Figure 5.25 Outdoor Ranging Test Setup

The receiver was kept fixed and the transmitter was moved starting from 4m away from receiver down to 6m and then up to 38m in increments of 4m each, giving a total of 10 transmitter locations. Spatial diversity and symbol averaging was implemented at the receiver and the MC-WB signal spans 12MHz. The multipath free received spectrum (right plot) is shown in Figure 5.26 and one can notice the difference in the spectrum compared to the multipath affected received spectrum (left plot) from previous indoor tests.

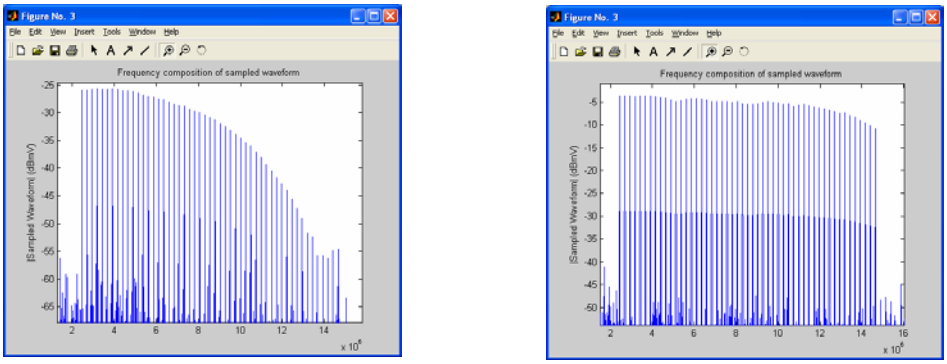

(a) (b)

Figure 5.26 Sampled waveform amplitude (dBmV) v. Frequency (Hz x 10^6)
(a) Shows Received Frequency Spectrum at 18m - Indoors
(b) and at 26m - Outdoors

Similar to the indoor test results discussed earlier, range estimation results for outdoor tests at each of the 10 transmitter locations for all 9 antenna positions are shown in Figure 5.27. The Ant n in the legend refers to test result for n^{th} antenna position. It is clear from these results that even in a relatively benign multipath environment, the range estimates are inconsistent. The transmitter and receiver sampling clocks and the LO frequency synchronization are ideal, and this indicates that there is some fundamental flaw in the system which thwarts accurate position determination even in a low multipath environment. This fundamental flaw is discussed in the next section.

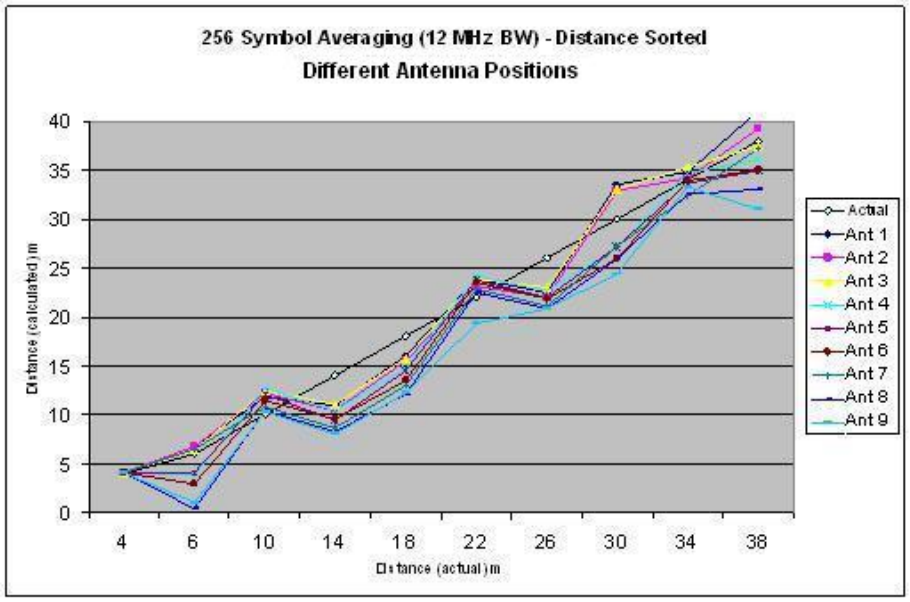

Figure 5.27 Outdoor Ranging Results Test 1

Issues with Direct Downconversion Receiver Architecture

The precise positioning system is based on phase difference of the received subcarriers. Any non-uniform phase distortion between the subcarriers, in the end-to-end system will result in errors in the range estimation similar to those seen in the indoor and outdoor wireless tests discussed earlier. Consider a multicarrier signal *s(t)* consisting of *M* subcarriers as shown below,

$$s(t) = \sum_{m=1}^{M} A e^{2\pi(f_0 + m\Delta f)(t-\tau)} \tag{5.1}$$

where, Δf is the frequency spacing between the two subcarriers, f_0 is the carrier frequency and $\tau = d/c$ is the time delay in the signal that traveled distance d. Let the phase change of the m^{th} and $(m-1)^{th}$ subcarrier received at distance d is,

$$\phi_m = 2\pi(f_0 + m\Delta f)\tau \tag{5.2}$$

$$\phi_{m-1} = 2\pi(f_0 + (m-1)\Delta f)\tau \tag{5.3}$$

Thus the phase difference between the two subcarriers is,

$$\Delta\phi = \phi_m - \phi_{m-1} = 2\pi[(f_0 + m\Delta f) - (f_0 + (m-1)\Delta f)]\tau \tag{5.4}$$

$$\Delta\phi = 2\pi\Delta f\tau \tag{5.5}$$

$$\tau = \Delta\phi/(2\pi\Delta f) \tag{5.6}$$

Since $\tau = d/c$, the above equation can be written as shown below, where the phase difference, $\Delta\phi$, is now in degrees.

$$d = c\Delta\phi(\pi/180)/(2\pi\Delta f) \tag{5.7}$$

Thus, if there is any phase difference error $\Delta\phi$ between the two subcarriers that are separated by Δf, then this results in a theoretical distance estimation error d as per the above equation. Similarly, the total theoretical range estimation error across the multicarrier signal span can be calculated from the above equation, where $\Delta\phi$ is the average phase difference error, and Δf is now the multicarrier span. Figure 5.28 shows the range estimation error due to average phase difference errors for various multicarrier spans.

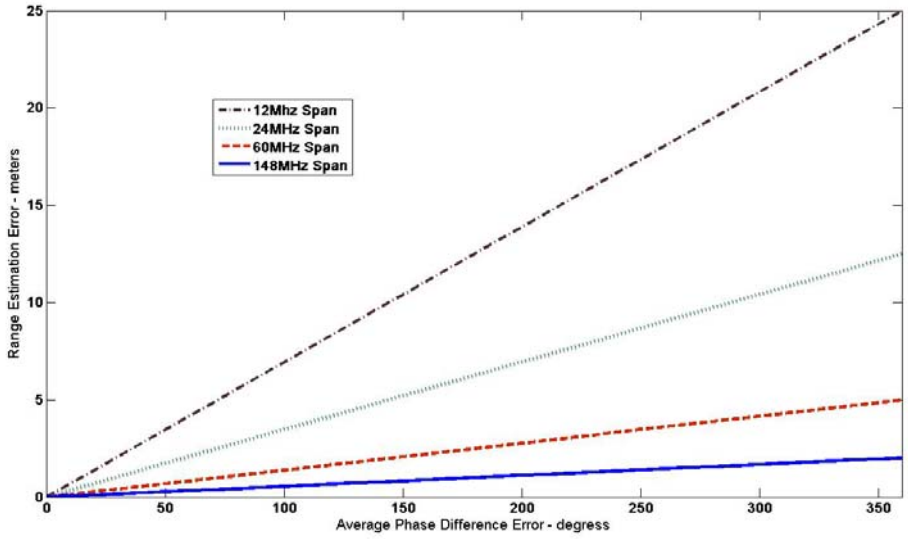

Figure 5.28 Average Phase Different Error vs. Range Estimation Error

As shown in Figure 5.28, wider multicarrier span results in lower range estimation error. For example, a 30 degree average phase difference error results in 1m

range error for a multicarrier signal spanning 24MHz as compared to 0.42m error for a multicarrier signal spanning 60MHz.

Non-coherent detection techniques, where the local oscillators at the receiver and the transmitter are not phase synchronous but are only frequency synchronous, could lead to amplitude and phase distortion if not demodulated correctly. A more detailed analysis of two cases of DSB demodulation is shown in Figure 5.29, which shows their end-to-end implementation with expected magnitude and phase difference responses.

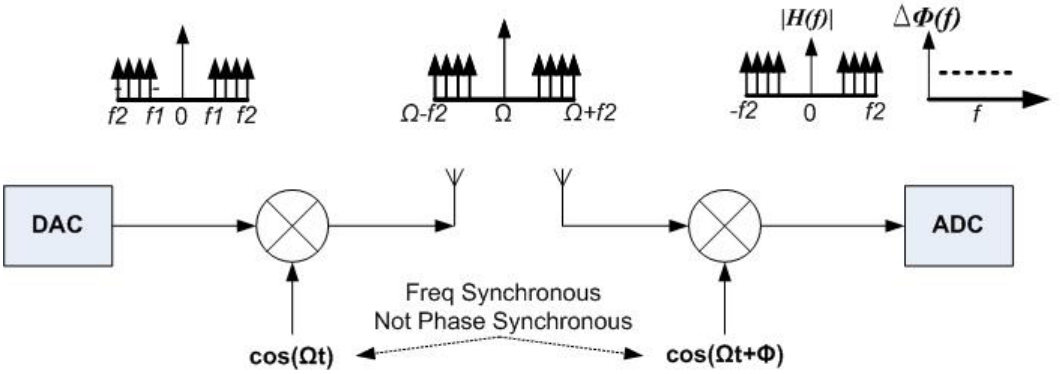

(a) Semi-Ideal DSB, Frequency Synchronous but Not Phase Synchronous

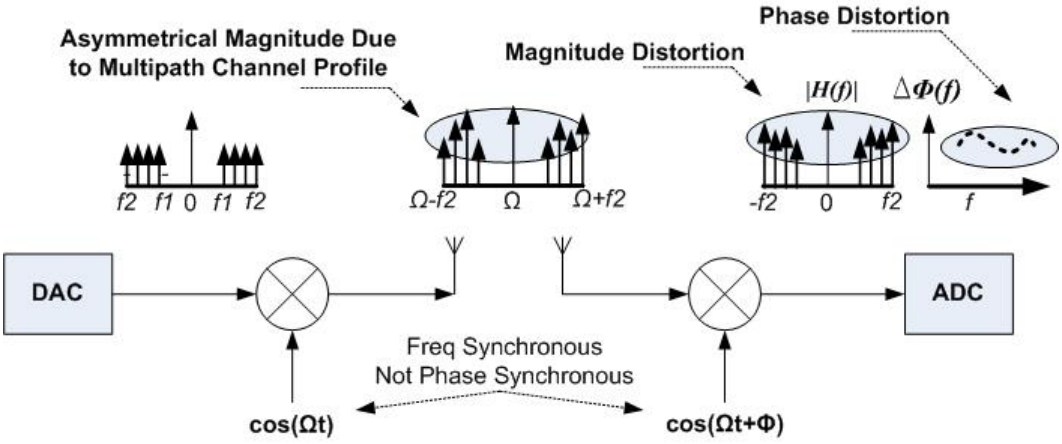

(b) Practical DSB, Frequency Synchronous but Not Phase Synchronous

Figure 5.29 Various DSB Demodulation Conditions and Expected Amplitude and Phase Response

Figure 5.29(a) shows a semi-ideal DSB system, which is frequency synchronous, but not phase synchronous. This situation results in a constant phase offset for all subcarriers, but the phase difference between the subcarriers will only be a function of distance between the transmitter and receiver as derived

below. Consider a simple example of the baseband signal, $s_{bb,}$ consisting of only two pure cosine components at frequencies w_1 and $w_2=2w_1$;

$$s_{bb}(t) = \cos(w_1 t) + \cos(w_2 t) \tag{5.8}$$

The transmitted DSB signal after upconversion, using local oscillator frequency Ω, is written as;

$$s_{tx}(t) = [\cos(w_1 t) + \cos(2w_1 t)]\cos(\Omega t) \tag{5.9}$$

The received signal is the delayed version of the transmitted signal, where the delay τ depends on the distance between the transmitter and the receiver and is written as:

$$s_{rx}(t) = [\cos(w_1 (t-\tau)) + \cos(2w_1 (t-\tau))]\cos(\Omega(t-\tau)) \tag{5.10}$$

Let the receiver local oscillator be frequency synchronous with the transmitter but not phase synchronous and the demodulated received signal is;

$$s_{rx}(t) = [\cos(w_1 (t-\tau)) + \cos(2w_1 (t-\tau))]\cos(\Omega(t-\tau))\cos(\Omega t + \phi)) \tag{5.11}$$

The above demodulated signal after low pass filtering is:

$$s_{rx}(t) = \cos(\phi)\left[\cos(w_1 t) + \cos(2w_1 t)\right] \tag{5.12}$$

From the above equation we see a constant phase offset $\cos(\phi)$ on all the subcarriers, due to non synchronous local oscillator phase, which does not cause any distortion in the phase difference between the subcarriers.

Figure 5.29(b), shows a practical DSB system, which considers the effects of a variable multipath channel profile at different distances. Such a

system results in variable magnitude distortion and variable phase distortion of the received subcarriers at different distances. Consider a simple case of magnitude distortion for a DSB signal as shown in Figure 5.30. Figure 5.30(a) shows the phasor representation for subcarriers k and $k+1$ at a distance d and Figure 5.30(b) shows the same at distance $d+\Delta$.

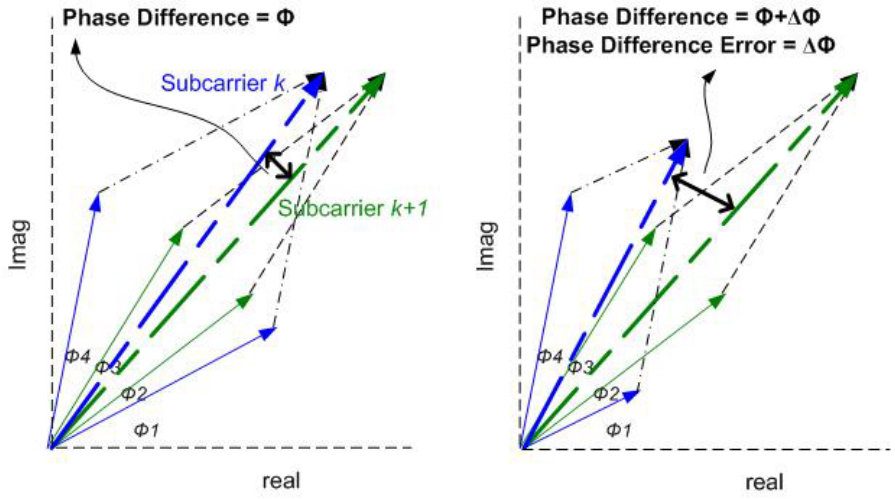

Figure 5.30 Phase Difference Error Due to Varying Multipath Channel Profile

Figure 5.30 shows that in case of asymmetrical magnitude response, there is a phase difference error term, $\Delta\Phi$, which depends on the level of asymmetry due to channel effects and the hardware response. The direct downconversion of a multicarrier DSB signal exacerbates this phase difference error, which leads to errors in range estimation. A simple technique to circumvent this problem is discussed in the next section.

Need for Near-Zero Down Conversion Architecture

The phase distortion in direct downconversion architecture arises from the asymmetry in the two sidebands caused by a varying multipath channel. This leads to errors in the phase differences between the subcarriers of the demodulated DSB multicarrier signal, which further leads to errors in range estimation, as the algorithm is based on a phase comparison between subcarriers.

A very simple, but non intuitive, solution is to implement a near-zero downconversion architecture, which ensures that the two asymmetric sidebands do not overlap [9, 10, 11]. Thus, as shown in Figure 5.31, the receiver local oscillator can be offset appropriately by Θ, to ensure that the two asymmetric sidebands do not overlap.

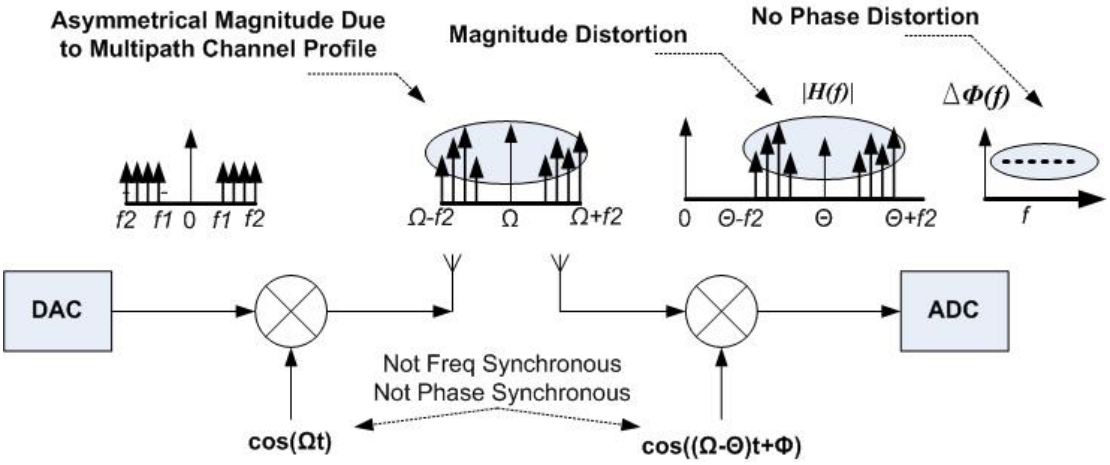

Figure 5.31 Non Zero Downconversion of Received DSB Signal

Mathematically, the difference between near-zero downconversion and direct downconversion can be derived as follows.

Let the baseband signal s_{bb} consist of only two pure cosine components at frequencies w_1 and $w_2=2w_1$;

$$s_{bb}(t) = \cos(w_1 t) + \cos(w_2 t) \tag{5.13}$$

The transmitted DSB signal, after upconversion using local oscillator frequency Ωc, is written as;

$$\begin{aligned} s_{tx}(t) &= [\cos(w_1 t) + \cos(2w_1 t)]\cos(\Omega t) \\ &= \frac{1}{2}[\cos((\Omega + w_1)t) + \cos((\Omega - w_1)t) + \cos((\Omega + 2w_1)t) + \cos((\Omega - 2w_1)t)] \end{aligned} \tag{5.14}$$

The output of the direct downconversion receiver can be derived as

$$\begin{aligned} s_{rx}(t) &= \frac{1}{2}[\cos((\Omega + w_1)t) + \cos((\Omega - w_1)t) + \cos((\Omega + 2w_1)t) + \cos((\Omega - 2w_1)t)]\cos(\Omega t + \phi) \\ &= \frac{1}{4}[\cos(2\Omega t + w_1 t + \phi) + \cos(w_1 t - \phi) + \cos(2\Omega t - w_1 t + \phi) + \cos(-w_1 t - \phi) \\ &\quad + \cos(2\Omega t + 2w_1 t + \phi) + \cos(2w_1 t - \phi) + \cos(2\Omega t - 2w_1 t + \phi) + \cos(-2w_1 t - \phi)] \end{aligned} \tag{5.15}$$

The lowpass equivalent of the above signal can be written as

$$s_{rx}(t) = \frac{1}{4}[\cos(w_1 t - \phi) + \cos(-w_1 t - \phi) + \cos(2w_1 t - \phi) + \cos(-2w_1 t - \phi)] \tag{5.16}$$

Similarly, the output of the near-zero downconversion, where the receiver local oscillator Ω_d and the transmitter local oscillator Ω, are now offset by Θ, ($\Theta = \Omega - \Omega_d$) can be expressed as;

$$
\begin{aligned}
s_{rx}(t) &= \frac{1}{2}[\cos((\Omega+w_1)t)+\cos((\Omega-w_1)t)+\cos((\Omega+2w_1)t)+\cos((\Omega-2w_1)t)]\cos(\Omega_d t+\phi) \\
&= \frac{1}{4}[\cos((\Omega+\Omega_d)t+w_1 t+\phi)+\cos((\Omega-\Omega_d)t+w_1 t-\phi)+ \\
&\cos((\Omega+\Omega_d)t-w_1 t+\phi)+\cos((\Omega-\Omega_d)t-w_1 t-\phi) \\
&+\cos((\Omega+\Omega_d)t+2w_1 t+\phi)+\cos((\Omega-\Omega_d)t+2w_1 t-\phi)+ \\
&\cos((\Omega+\Omega_d)t-2w_1 t+\phi)+\cos((\Omega-\Omega_d)t-2w_1 t-\phi)]
\end{aligned}
\tag{5.17}
$$

The lowpass equivalent of the above signal can be written as

$$
\begin{aligned}
s_{rx}(t) = \frac{1}{4}[&\cos((\Omega_c-\Omega_d)t+w_1 t-\phi)+\cos((\Omega_c-\Omega_d)t-w_1 t-\phi) \\
&+\cos((\Omega_c-\Omega_d)t+2w_1 t-\phi)+\cos((\Omega_c-\Omega_d)t-2w_1 t-\phi)]
\end{aligned}
\tag{5.18}
$$

For $\Theta = (\Omega - \Omega_d)$, the low pass equivalent can be expressed as

$$
\begin{aligned}
s_{rx}(t) = \frac{1}{4}[&\cos(\Theta t+w_1 t-\phi)+\cos(\Theta t-w_1 t-\phi) \\
&+\cos(\Theta t+2w_1 t-\phi)+\cos(\Theta t-2w_1 t-\phi)]
\end{aligned}
\tag{5.19}
$$

It can be observed from the above equation that the two downconverted components, (Θ+w_1) and (Θ-w_1) do not overlap with each other. Thus the near zero downconversion reduces the errors in the phase difference of a multicarrier signal.

Lessons Learnt

Direct Downconversion Using DSB: For a positioning system that transmits a DSB multicarrier signal, and implements direct downconversion receiver architecture, phase distortion arises due to asymmetry in the wireless channel and the RF front end. This results in range estimation errors. Thus, for positioning systems that transmit a DSB multicarrier signal, a direct downconversion system cannot be implemented.

Near-Zero Downconversion Using DSB: As shown in the previous section, the phase distortions due to the wireless channel and RF front end asymmetry are eliminated by implementing near-zero downconversion radio architecture. Thus, for positioning systems that transmit a DSB multicarrier signal, a near-zero downconversion system has to be implemented.

Direct Downconversion Using SSB: Another possible option is to implement SSB transmitter architecture. For an SSB multicarrier signal, the problem of phase distortion between subcarriers, when using a DSB signal, due to overlap of asymmetrical LSB and the USB is eliminated. Thus, for positioning systems that transmit a SSB multicarrier signal, a direct downconversion system can be implemented.

Conclusion

In this chapter we discussed outdoor ranging test results using a single transmitter and single receiver. The results of these tests were inconsistent and further analysis of the ranging system was done to find out the source of the range estimation errors. The range estimation errors were primarily due to incorrect downconversion at the receiver when transmitting a DSB multicarrier signal.

The two solutions proposed to overcome this issue were, a) to use near-zero downconversion when transmitting a DSB multicarrier signal or b) to implement direct downconversion when transmitting an SSB multicarrier signal. Further tests were then performed after implementing near-zero downconversion at the receiver when transmitting DSB multicarrier signal, as minimum software and hardware changes were required. The indoor and outdoor test results using this near-zero downconversion system are discussed in the next chapter.

References

[1] R. J. Duckworth, “TOA Experiments, 03/10/05”, *WPI Internal Memorandum*, March 2005

[2] R. J. Duckworth, “TOA Experiments, 03/17/05”, *WPI Internal Memorandum*, March 2005

[3] R. J. Duckworth, “TOA Experiments, 03/25/05”, *WPI Internal Memorandum*, March 2005

[4] R. J. Duckworth, “TOA Experiments, 04/11/05”, *WPI Internal Memorandum*, April 2005

[5] R. J. Duckworth, “TOA Experiments, 05/23/05”, *WPI Internal Memorandum*, May 2005

[6] R. J. Duckworth, “TOA Experiments, 05/25/05”, *WPI Internal Memorandum*, May 2005

[7] R. J. Duckworth, “TOA Experiments, 05/27/05”, *WPI Internal Memorandum*, May 2005

[8] R. J. Duckworth, “TOA Experiments, 06/10/05”, *WPI Internal Memorandum*, June 2005

[9] J. Coyne, “Phase Analysis Testing Results, 06/24/05”, *WPI Internal Memorandum*, June 2005

[10] H. K. Parikh, “Progress Report, 07/05/05”, *WPI Internal Memorandum*, July 2005

[11] H. K. Parikh, “Progress Report, 07/06/05”, *WPI Internal Memorandum*, July 2005

Chapter 6 : Ranging & Positioning Using Near-Zero Downconversion

Introduction

As discussed in the previous chapter, the ranging system needs to implement near-zero downconversion when using a DSB multicarrier transmitted signal. The indoor and outdoor tests discussed in this chapter use this near-zero downconversion approach.

To implement near-zero downconversion, the transmitter and receiver LO frequencies no longer identical. This shift will result in the upper and lower sidebands of the DSB signal being spread apart, eliminating the overlap of the sidebands in the downconverted signal. For the subsequent ranging tests, the transmitter LO frequency was kept at 440MHz, but the receiver LO frequency is

offset by 17.09MHz to 422.91MHz. This offset frequency was chosen so that, after downconversion at the receiver, the LSB will occupy exactly the same 12.2MHz frequency span, from 2.4MHz to 14.6MHz, used in earlier tests. This choice minimized the required modifications to the ranging algorithms.

The RF transmitter and receiver PCBs used are the same as those used during previous tests. The basic hardware setup is slightly different from what was discussed in the previous tests and is shown in Figure 6.1. In these new tests, the local oscillators for the RF transmitter and receiver PCBs are generated using two independent signal generators. The sampling clocks for the DAC and the ADC are derived from the same signal generator as was the case in previous tests. These tests do not implement any averaging or spatial diversity at the receiver since we are interested in the improvement due solely to the change to near-zero downconversion.

Outdoor ranging test results are presented first, followed by indoor ranging test results. Since higher bandwidth, in theory results in better ranging/positioning accuracy, the RF system is then upgraded from 12MHz to 60MHz and also is upgraded form a single transmitter-single receiver ranging system to single transmitter-multiple receiver positioning system. NLOS indoor positioning test results are then discussed and the chapter concludes by presenting the limitations of the RF system, improvements to which are desired.

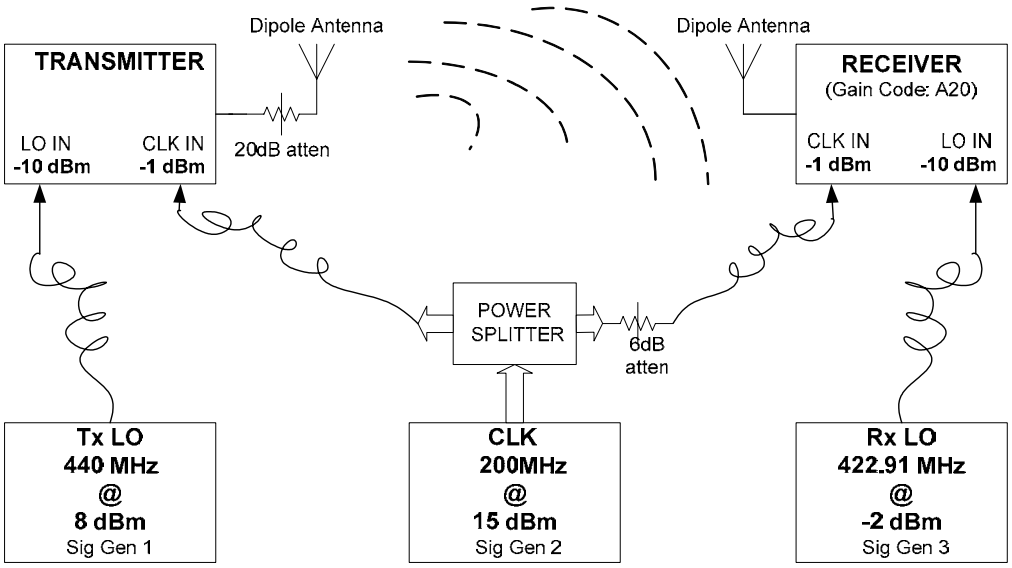

Figure 6.1 Range Estimation Wireless Test Setup

Outdoor Ranging Test Using Near-Zero Downconversion

This section describes the range estimation test setup and the results of the outdoor wireless tests using near-zero downconversion at the receiver. The receiver PCB and dipole antenna are placed on the right cart shown in Figure 6.2 and are kept fixed at the same location as in the previous tests. The transmitter PCB and the transmitter dipole antenna are placed on the left cart shown in Figure 6.2 and are moved away from the receiver starting at a distance of 4 meters and moving to a range of 30 meters. The test setup details are:

- Setup: Single Transmitter – Single Receiver
- Antenna Type: Dipole Antenna
- Transmitter: DSB Transmission
- Receiver: Near-Zero Downconversion Receiver
- Downconverted Baseband Signal Span: 12MHz
- Tx-Rx Sampling Clock: Synchronized
- Sampling Clock: 200MHz
- Tx-Rx Carrier Frequency: Un Synchronized
- Tx Carrier Frequency: 440MHz
- Rx Carrier Frequency: 422.91MHz
- Averaging: No Symbol Averaging
- Spatial Diversity: No Antenna Diversity

Figure 6.2 Outdoor Ranging Test Setup

The received signal was downloaded into a laptop where the range estimation algorithms are implemented and measurement data collected for five repeated runs were post processed. The range estimation results for all five runs are shown in Figure 6.3. The range estimation errors for each of the five runs are shown in Figure 6.4. It can be seen in the figure that when using near-zero downconversion the errors are consistently accurate to within 0.5m.

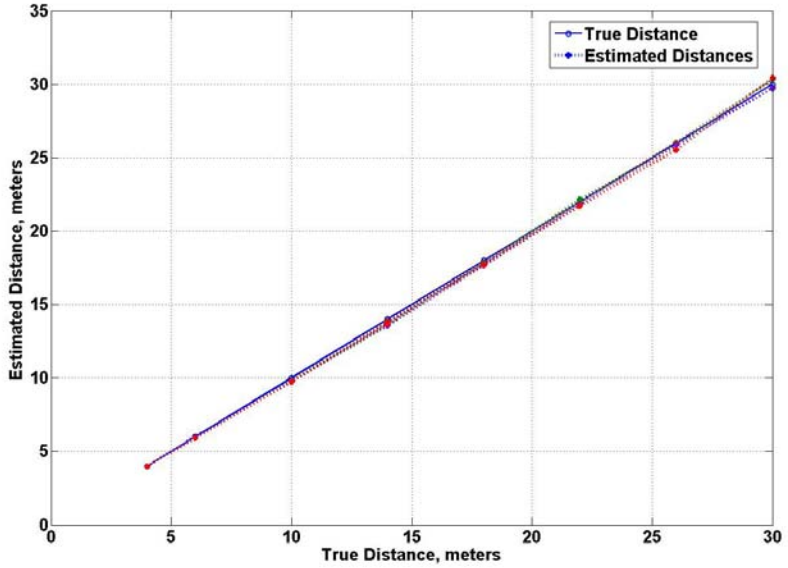

Figure 6.3 Outdoor Ranging Results for Five Repeated Runs

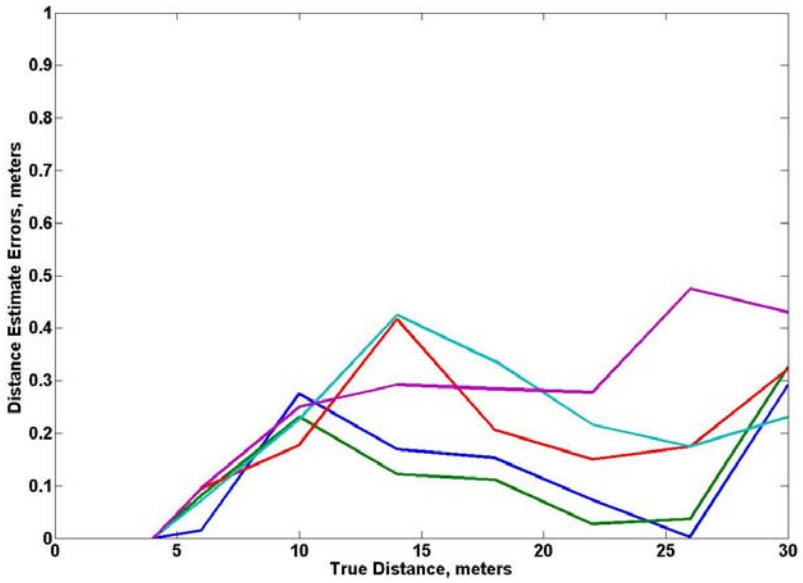

Figure 6.4 Outdoor Ranging Errors for Five Repeated Runs

Indoor Ranging Test Using Near-Zero Downconversion

Keeping the same test set up as that shown in Figure 6.5 which was used for outdoor tests, indoor wireless tests were performed in the same Atwater Kent 3rd floor corridor that was used in indoor tests discussed in previous chapters. As shown in Figure 6.5, the receiver is kept fixed and the transmitter is moved along the dotted line away from the receiver starting from 4m away and moving to a distance of 30m similar to the outdoor tests described earlier in this section.

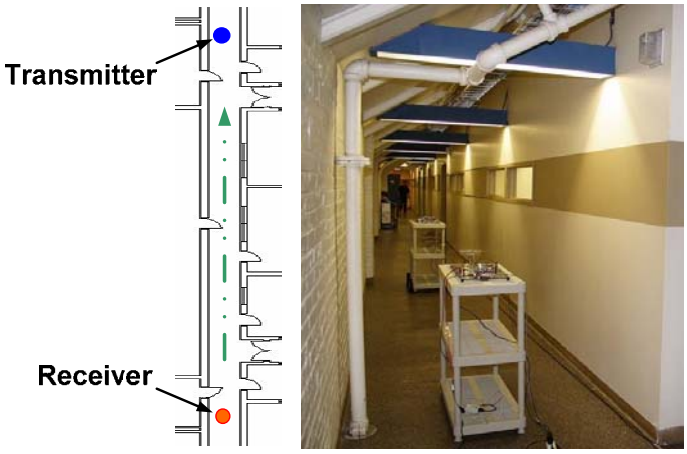

Figure 6.5 Indoor Ranging Test Setup

Similar to the outdoor tests, five tests were conducted for repeatability and the range estimation results for all five runs are shown in Figure 6.6. The range estimation errors for all five runs are shown in Figure 6.7 and it can be seen that they are all within 1m accuracy, even in presence of multipath indoors. The mean

and variance of the outdoor and the indoor range estimation results is shown in Table 6.1 and the error for these mean range estimates is shown in Table 6.2.

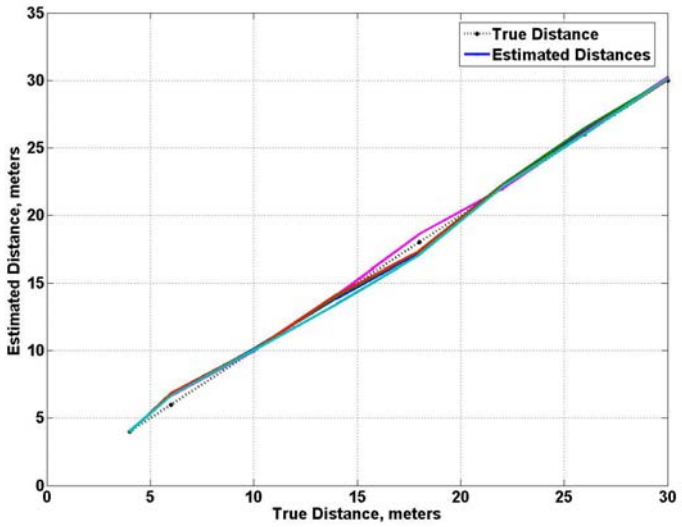

Figure 6.6 Indoor Ranging Results for Five Repeated Runs

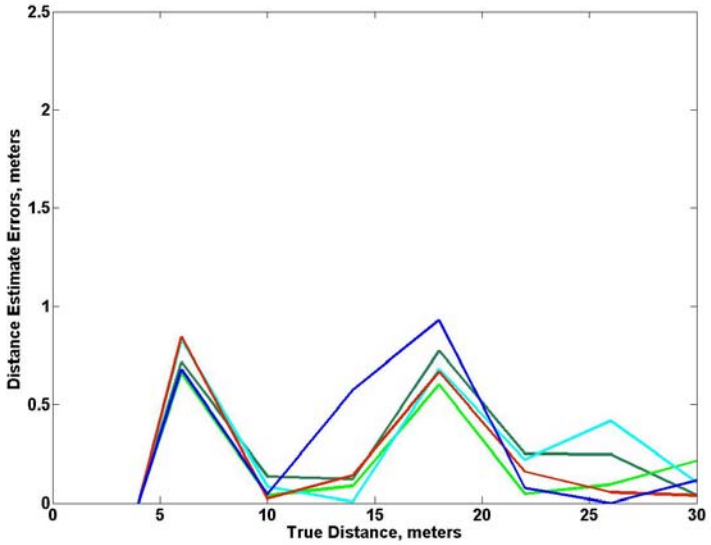

Figure 6.7 Indoor Ranging Errors for Five Repeated Runs

Table 6.1 Mean and Variance of Indoor and Outdoor Range Estimates

	Outdoor Results (meters)		Indoor Results (meters)	
True Range (meters)	**Mean**	**Variance**	**Mean**	**Variance**
4	4.00	0.000	4.00	0.000
6	5.93	0.002	6.74	0.007
10	9.76	0.001	10.04	0.004
14	13.71	0.019	13.90	0.082
18	17.78	0.008	17.50	0.384
22	21.91	0.028	22.13	0.014
26	25.84	0.041	26.16	0.028
30	30.11	0.117	30.10	0.005

Table 6.2 Errors for Indoor and Outdoor Mean Range Estimates

	Outdoor Results (meters)	Indoor Results (meters)
True Range (meters)	**Error**	**Error**
4	0	0
6	0.07	0.74
10	0.24	0.04
14	0.29	0.10
18	0.22	0.50
22	0.09	0.13
26	0.16	0.16
30	0.11	0.10

The jump in error plots shown in Figure 6.7 at the 6m and 18m ranges is due to the geometry of the horizontal polarized dipole antennas with respect to the ground and happens to be the distances which appear to be most affected by multipath for the prototype setup. Increasing BW, spatial diversity, and polarization diversity are some of the techniques that may reduce the jumps seen

in Figure 6.7, but even without these improvements the accuracy is under 1m and well within 3m.

Upgrade to 60MHz System

Theory dictates that the higher the bandwidth, the less the positioning error. Now, with the receiver operating using near-zero downconversion, the baseband signal consisting of 51 sinusoids was again changed to occupy a DC-30MHz bandwidth with the sinusoids spanning from 2.4MHz to 24MHz. The transmitter LO is set to 440MHz as before and thus the upconverted signal at the RF front end output now spans 60MHz (410MHz-470MHz) centered at 440MHz.

The RF transmitter frequency response is shown in Figure 6.8 and the upconverted DSB transmitted multicarrier signal centered at 440MHz is shown in Figure 6.9. The external BPF that is used in the transmitter RF front end has a 3dB BW of 50MHz (415MHz-465MHz) centered at 440MHz and the LPF used has a 3dB cutoff of 60MHz. The roll off seen in Figure 6.9 at both the ends of the spectrum is mainly due to the sharp roll off characteristics of the tubular BPF, with some contribution from the mixer and the power amplifier frequency response as well.

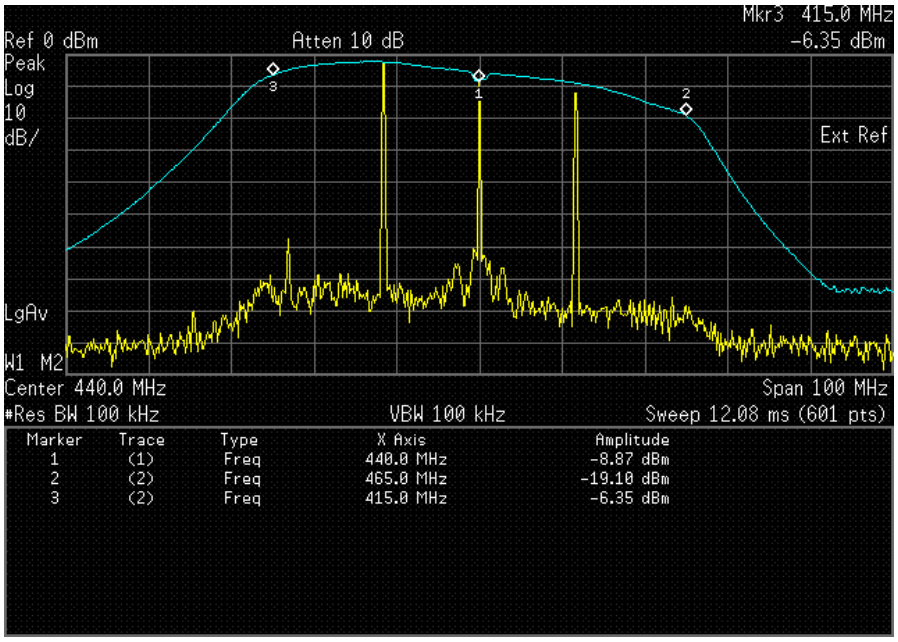

Figure 6.8 RF Transmitter Frequency Response

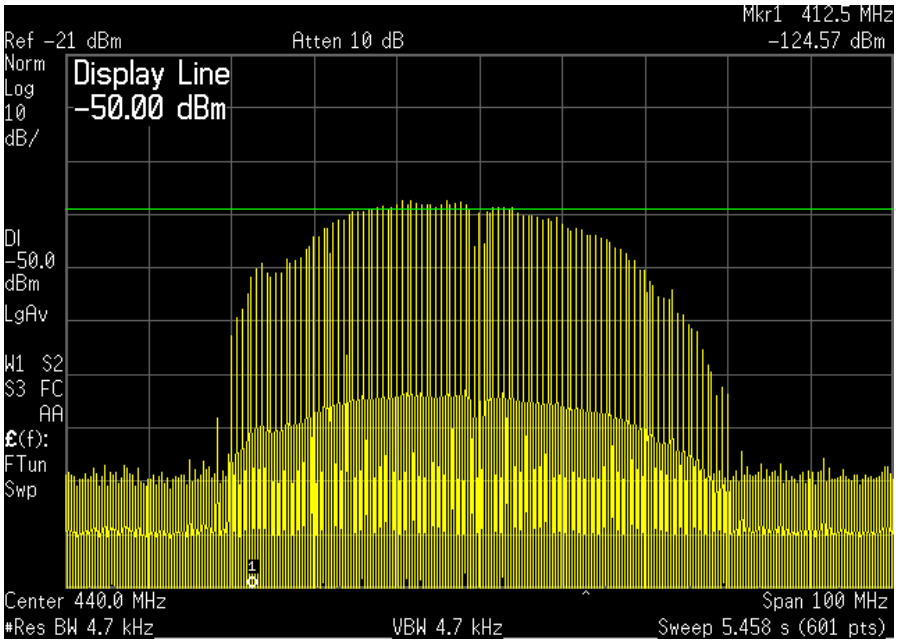

Figure 6.9 60MHz DSB Transmitter Output Spectrum Centered at 440MHz

The receiver LO is offset from the transmitter LO by 32MHz and is set at 408MHz. Thus, the near-zero downconverted multicarrier signal preserves both of the side bands and provides a 60MHz wide signal occupying the the spectrum from 2MHz to 62MHz. The transmitter output shown in Figure 6.9 is connected to the receiver input using a cable with appropriate attenuation and the downconverted receiver output is shown in Figure 6.10.

Again the roll off seen at the downconverted receiver output is mainly due to the tubular BPF at the receiver RF front end along with the non-flat frequency response of the mixer, LNA and VGA. The setup for the positioning system using multiple receivers is discussed in the next section.

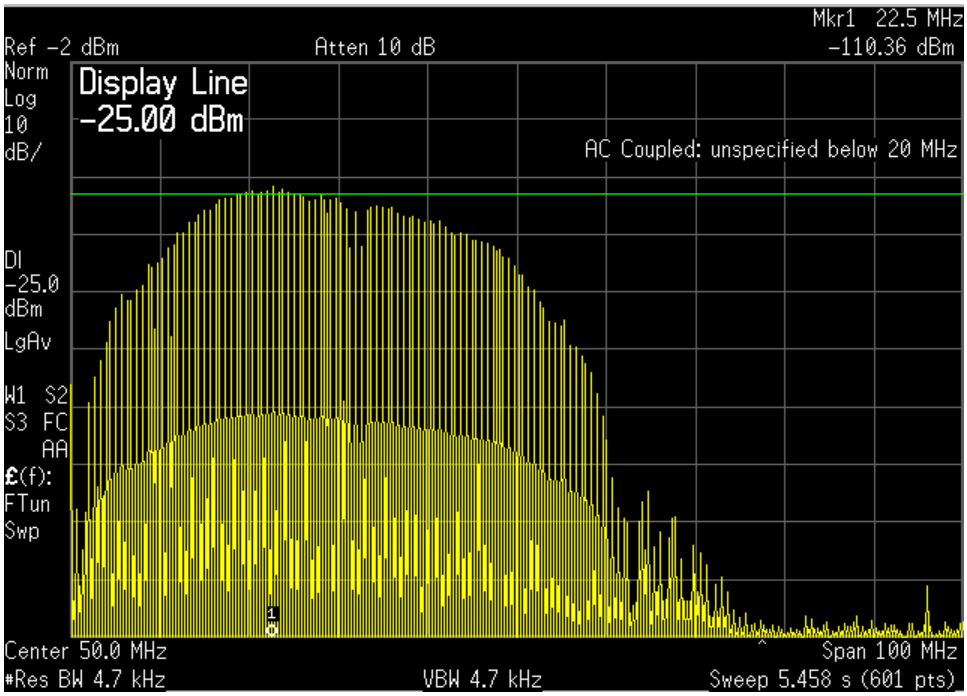

Figure 6.10 Receiver Near-Zero Downconversion Output Spectrum

Upgrade from Ranging System to Positioning System

After successful indoor ranging tests using a single transmitter and receiver, the system now needs to be upgraded from a ranging system to a positioning system that uses multiple receivers. The high level overview of the system setup using single transmitter and multiple receivers is shown in Figure 6.11.

This positioning system consists of a standalone transmitter consisting of both RF front end and digital back end, RF Receiver front end and the base station where the digital back end and signal processing algorithms are housed. The base station consists of ADCs for all the receivers so that they all are synchronized and are using a common sampling clock to avoid errors due to ADC sampling clock drifts.

The transmitter shown in Figure 6.11 consists of a PLL PCB, a Controller PCB, a digital back end and an RF front end. The Controller PCB is used to program the PLL PCB to set the required LO frequency at the transmitter. The baseband signal is generated by the digital back end which provides baseband input to the RF front end PCB. The RF transmitter front end upconverts this multicarrier wideband (MC-WB) signal and provides an output to the antenna which now spans from 410MHz to 470MHz. The dipole antenna used in previous tests is externally connected to the RF transmitter front end.

As shown in Figure 6.11, the receiver consists of an RF receiver front end PCB, PLL PCB, Antenna Switch and Controller PCB. This RF receiver is packaged into an enclosure, as shown in Figure 6.12. The antenna switch is a single pole four throw (SP4T) switch which is used to take advantage of spatial diversity. This switch has four inputs, allowing the system to multiplex up to four antennas. These multiple antennas can be switched continuously under the control of the Controller PCB. As each antenna is selected, the multicarrier signal received at that antenna is downconverted, sampled and fed to the algorithms for calculating a position estimate.

An external PLL PCB is used to provide the required LO at the receiver which is also programmed by the Controller PCB. In addition to the antenna switch and the PLL PCB, the Controller PCB also interfaces with the digital RF gain control on the receiver RF front end PCB.

The receiver implements near-zero downconversion and this downconverted signal at the output of RF front end PCB is then fed to the base station using a cable, referred to as the baseband cable. The downconverted outputs from all five receivers are thus fed to the base station where all the ADCs are housed. Synchronized sampling clocks at the base station are implemented to avoid errors in the positioning accuracy due to sampling clock drifts between the receivers. The digitized MC-WB signal is then transferred to a PC for further processing. The test setup details are:

- Setup: Single Transmitter – Multiple (five) Receivers
- Antenna Type: Dipole Antenna
- Transmitter: DSB Transmission
- Receiver: Near-Zero Down Conversion Receiver
- Downconverted Baseband Signal Span: 60MHz
- Tx-Rx Sampling Clock: Synchronized
- Sampling Clock: 200MHz
- Tx-Rx Carrier Frequency: Un Synchronized
- Tx Carrier Frequency: 440MHz
- Rx Carrier Frequency: 408MHz
- Averaging: 64 symbols
- Spatial Diversity: Supports up to four antennas / receiver

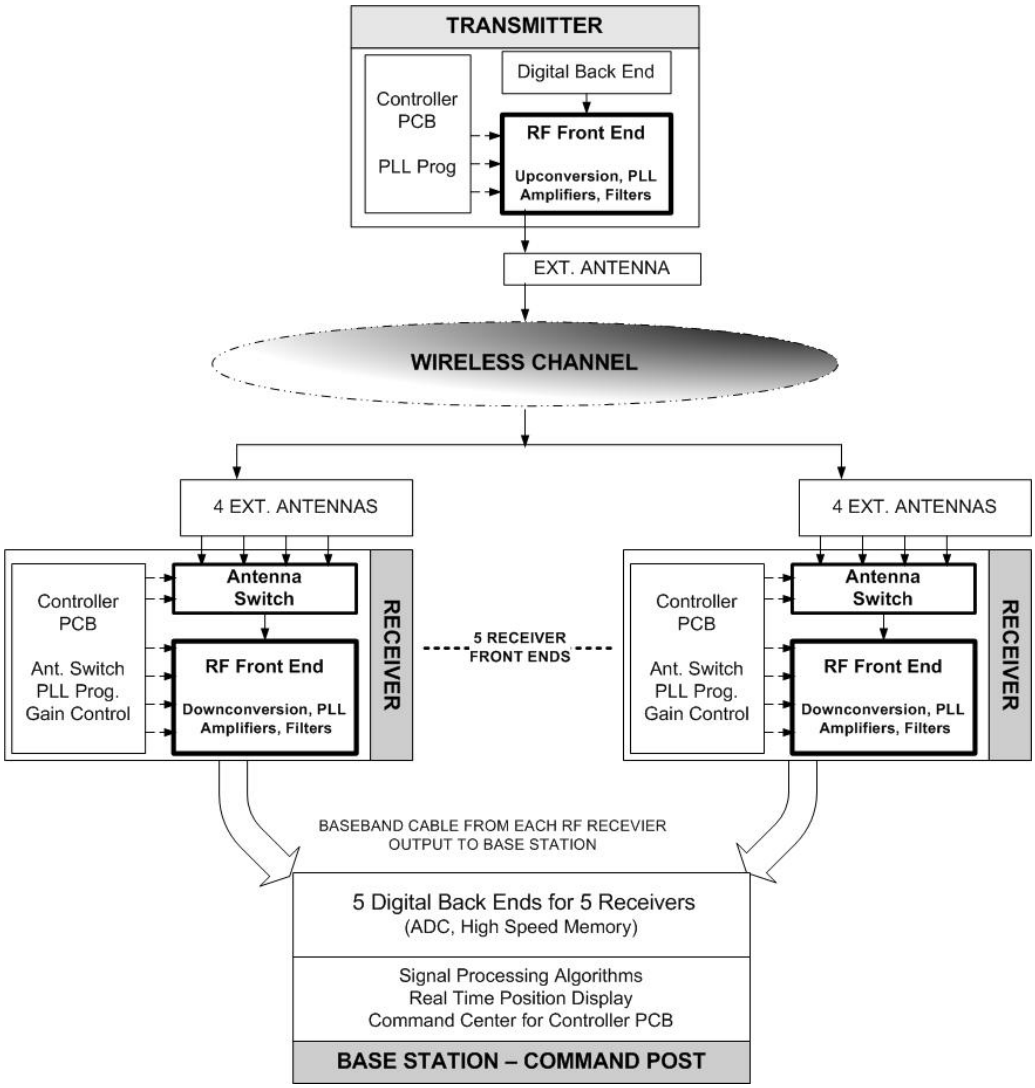

Figure 6.11 Position Estimation Wireless Test Setup

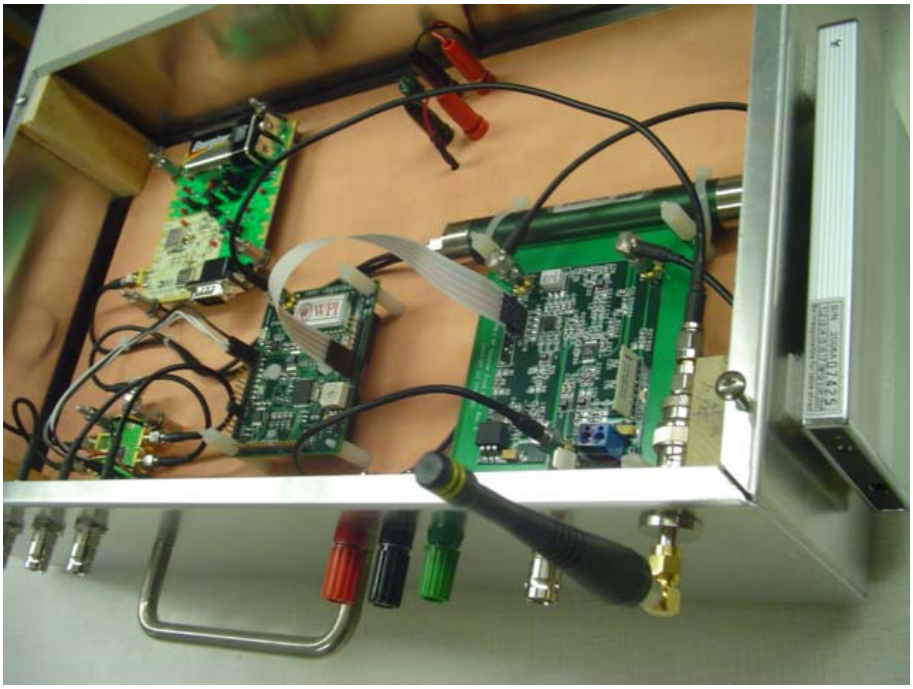

Figure 6.12 Receiver Enclosure

Positioning System Test Results

The positioning tests were performed using the setup discussed above using a single transmitter and multiple receivers. These tests were performed at three different indoor locations and the individual test setups and results are discussed in this section. The three test locations are WPI's Kaven Hall, WPI's Religious Center and WPI's Atwater Kent East Wing.

The Kaven Hall indoor test pictures are shown in Figure 6.13 where the figure on the right shows the antennas mounted on plastic stands outside of Kaven Hall. The picture on the left shows the transmitter inside Kaven Hall, which was moved to several locations to capture received signal at each of the locations.

Similarly the pictures for Religious Center and AK East Wing test setup are shown in Figure 6.14 and Figure 6.15. For all three test venues the antennas are setup outside the building and are looking indoors which is similar to the situation of fire trucks arriving at a fire scene, being parked outside the building and looking in to locate and track the firefighters inside the building.

Figure 6.13 Kaven Hall Indoor Test Setup

Figure 6.14 Religious Center Indoor Test Setup

Figure 6.15 AK East Wing Indoor Test Setup

The error vectors [1] for the three tests are shown in Figure 6.16, Figure 6.17, and Figure 6.18. The thick outline is the wall of the test venue and the breaks between them are the windows. The circles outside the wall are the antenna positions. 13 antennas are used to cover three sides of the Kaven Hall as shown in Figure 6.16, 16 antennas are used to cover all four sides of the Religious Center as shown in Figure 6.17 and 16 antennas are used to cover three sides of the AK East Wing as shown in Figure 6.18. The squares inside the wall are the true transmitter positions and the arrows are the error vectors. The length of the error vector signifies the error for that transmitter position and the end of the red arrow signifies the location of the estimated transmitter position.

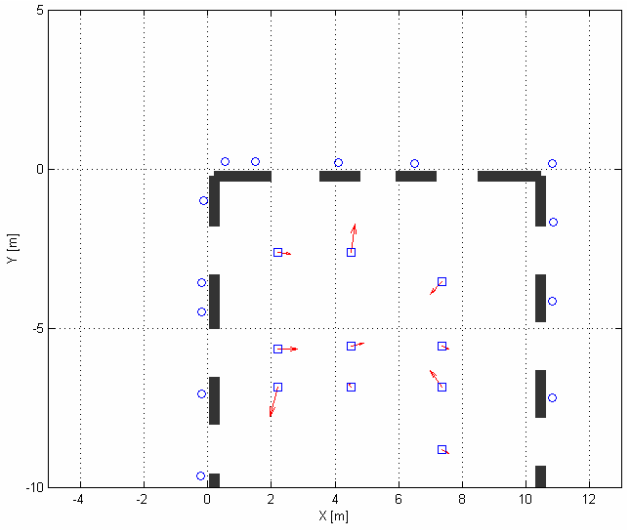

Figure 6.16 Kaven Hall Error Vector Plot

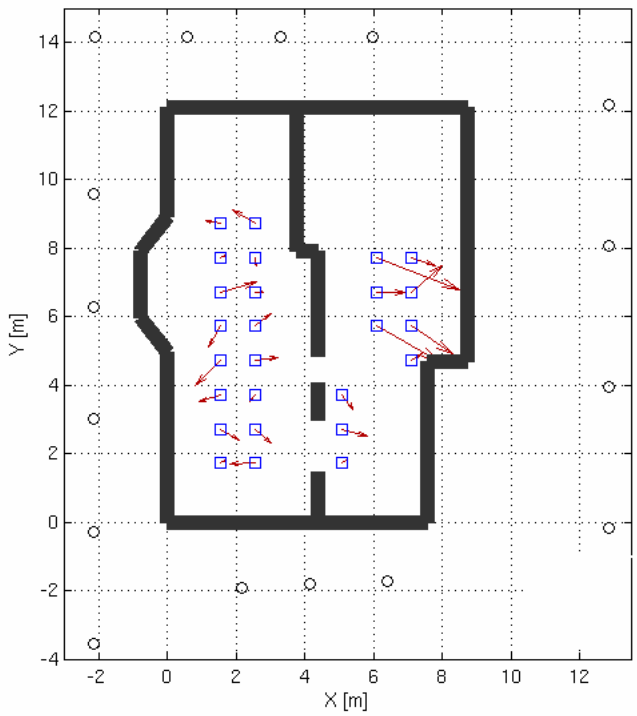

Figure 6.17 Religious Center Error Vector Plot

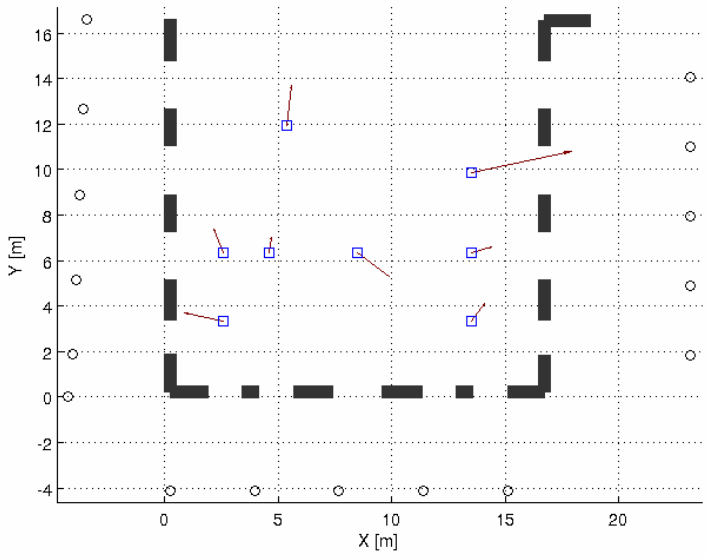

Figure 6.18 AK East Wing Error Vector Plot

Table 6.3 summarizes the results from Figure 6.16, Figure 6.17, and Figure 6.18. It can be seen that the mean error for all three test venues is less than 3m. It can also be seen in Figure 6.16, Figure 6.17, and Figure 6.18 that at some transmitter locations the error vector is greater than 3m which, at least in part, is due to the bad geometry of the receiving antennas with respect to that particular transmitter position. Overall consistent results were achieved indoors and increasing the multicarrier signal span is desired to further improve the position estimation accuracy.

Table 6.3 Summary of 60MHz Indoor Positioning Results

	Min. Error (m)	**Max. Error (m)**	**Mean Error (m)**
Kaven Hall	0.175	0.946	0.5
Religious Center	0.144	2.59	0.76
AK East Wing	0.66	4.5	1.68

These results are consistent with some indoor positioning prototypes. For example, implementations based on WiPS [2] and DOPLPHIN [3] also show indoor positioning accuracies of less than 1m. However, these systems are indoor-to-indoor positioning systems and are based on the presence of a pre-existing infrastructure. Such systems are suitable to locate and track indoor objects and inventory but are not suitable for a fire fighter specific application.

This is the first example of an outdoor-to-indoor positioning system which has achieved this level of performance that the author is aware of.

Lessons Learnt

Limitations of RF transmitter and receiver: As shown in Figure 6.9 and Figure 6.10, the frequency spectrum at the output of the transmitter and the receiver is not flat and high SNR degradation is observed at the ends of the spectrum. One of the major reasons for such an inefficient frequency response is due to the fact that the RF hardware is designed for multicarrier signal spanning a maximum of 50MHz, but the signal used for the positioning tests discussed in this chapter is a multicarrier signal spanning 60MHz.

Better flatness is desired to improve the SNR of the RF system. Also the transmitter and receiver RF enclosures use an external PLL PCB and an external tubular BPF having a 3dB BW of 50MHz. An integrated RF PCB which has the PLL PCB and the PBF onboard is desired. An improved RF shielding that not only isolates the RF and digital sections but also the RF amplifier, filter and mixer from each other is desired to further improve the isolation between the RF sections.

Moreover, the maximum transmitter output power for the phase 3 RF PCBs is -20dBm/SC. The FCC permission allows transmission at -10dBm/SC and higher transmitter output power is desired to increase the region of operation. The receiver VGA chip has limitations to operate only in the low gain mode as operating in high gain mode leads to increased noise floor, which results in SNR

degradation. A better VGA in the receiver RF chain is desired. The receiver enclosure shown in Figure 6.12 has an external antenna switch PCB and an integrated onboard antenna switch desired.

Furthermore wider bandwidth RF system is desired to improve the positioning accuracy. A 148MHz band centered at 625MHz was approved by FCC and thus it was decided to redesign the RF system which will have 148MHz bandwidth centered at 625MHz. This RF system redesign is referred to as Phase 4 RF prototype which also eliminates the above mentioned limitations.

Conclusion

In this chapter we discussed an indoor positioning test setup and results obtained using a single transmitter and multiple receivers. These tests were performed using the near-zero downconversion technique such that multicarrier signal spanning 60MHz was available for position estimation. This validated the near-zero downconversion idea and the observed positioning results were consistent with mean error of better than 3m.

It is believed that these results can be further improved by increasing the system bandwidth so that a multicarrier signal spanning much greater than 60MHz can be made available for position estimation. The limitations of the RF transmitter and receiver hardware were discussed and the RF hardware redesign and its specifications that eliminate these limitations will be discussed in detail in next chapter.

References

[1] V. Amendolare, B. Woodacre, *WPI Internal Memorandum*, 2006

[2] T. Kitasuka, K. Hisazumi, T..Nakanishi, "WiPS: location and motion sensing technique of IEEE 802.11 devices", *IEEE Proc*. July 2005

[3] Y. Fukuju, M. Minami, H. Morikawa, T. Aoyama, "DOLPHIN: an autonomous indoor positioning system in ubiquitous computing environment", *IEEE Proc*. May 2003

Chapter 7 : Optimized 148MHz Wideband RF System Design

RF Redesign

It was shown in Chapter 5 that range estimation using direct downconversion when a DSB multicarrier signal is transmitted results in errors due to the overlap of the asymmetrical LSB and USB which results due to multipath in the channel. This issue was resolved by implementing a near-zero down conversion architecture that uses a multicarrier signal spanning 60MHz. Limitations in the 60MHz RF system were identified and the desired

improvements were discussed in Chapter 6. These desired improvements led to the redesign of the RF hardware which is discussed in this chapter.

This RF hardware has been designed such that it can be mass produced with consistent performance and meets the required bandwidth, spurs, and output power. The detailed design document which includes the schematics and PCB layout drawing is provided in Appendix A and Appendix B.

For the redesign there are two options, the first involves retaining the DSB multicarrier signal, performing near-zero downconversion at the receiver. This is similar to the 60MHz system, but will address the shortcomings in the 60MHz system and improve it keeping the same architecture. The advantage of implementing such a DSB transmitter is that the required baseband signal is half of the DSB bandwidth which relaxes the sampling rate requirements.

The second option involves redesigning the RF hardware to transmit an SSB multicarrier signal, and performing direct downcoversion at the receiver. This will involve addressing the shortcomings of the 60MHz system, and improves it, while changing the RF architecture as well. The primary disadvantage of an SSB transmitter is that now the sampling rate requirements are doubled compared to a DSB transmitter.

However, although the DSB architecture is simpler, and easier to implement, it results in losing the spectral flexibility that is desired to coexist with other services using the same spectrum. Due to the symmetric nature of the DSB

signal, the system designer will lose the flexibility of inserting and nulling the subcarriers as needed, since nulling one carrier in one sideband results in nulling the associated carrier in the other sideband as well. Thus, in spite of increased sampling rate requirements, SSB radio architecture is chosen for the redesign since it will result in maximum spectral flexibility.

Since wider bandwidth is desired, a temporary experimental license was granted by the FCC to WPI to transmit a maximum of 10dBm total power in the 550MHz-698MHz band, thus providing 148MHz of bandwidth. Since this bandwidth was not available in the vicinity of 440MHz, this redesign will also require changing to a new center frequency.

Since we are using 51 subcarriers a 10dBm total power means that each subcarrier must be at or below -10dBm/SC to ensure FCC compliance. Within the 550MHz to 698MHz transmission band, the 12MHz band from 608MHz to 620MHz is forbidden by the FCC temporary license granted to WPI.

Figure 7.1 shows the multicarrier spectrum starting from 550MHz (marker 1) and ending on 698MHz (marker 4). The 12MHz band from 608MHz (marker 2) to 620MHz (marker 3) is the forbidden band. The subcarriers in this forbidden band are nulled, ensuring FCC compliance (there was no requirement on spurious emissions, but as a design goal we wished to keep these emissions 60dB below the subcarrier levels).

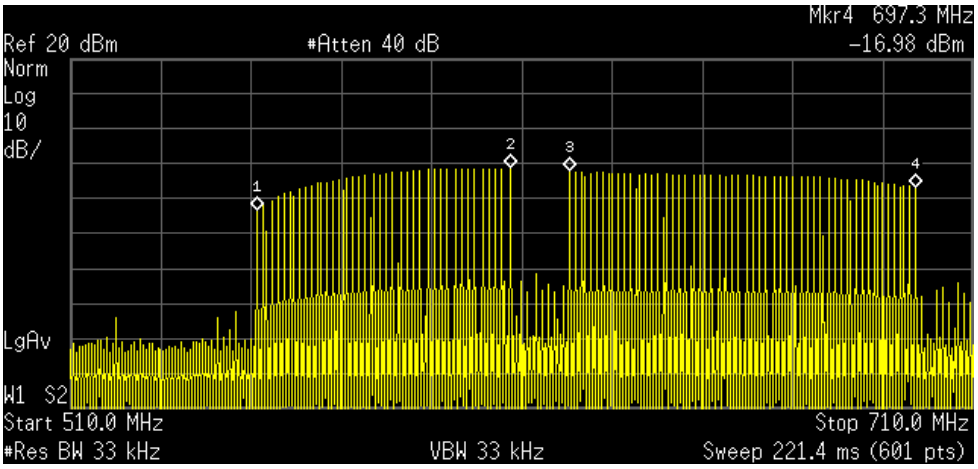

Figure 7.1 Example of Spectrum with Nulling the Subcarriers

RF Transmitter Architecture

The SSB transmitter is designed for a multicarrier signal consisting of 51 subcarriers with a power level of -10dBm/SC spanning from 550MHz to 698MHz. While the transmitter is capable of transmitting across the entire band, it is important that the baseband signal applied to the transmitter has no subcarriers placed in the forbidden band of 608MHz to 620MHz. The SSB implementation is done using the filtering method which filters out one of the two sidebands and retains the other. The frequency separation between the two sidebands must be wide enough to make the filtering method practical to use, but cannot be so much that it increases the sampling rate requirements excessively.

Thus, for the redesign it was decided to shift the baseband signal such that it spans from 30MHz to 178MHz as shown in Figure 5.2. An LO of 520MHz is used for upconversion which will result in the LSB spanning from 342MHz to 490MHz and the USB spanning from 550MHz to 698MHz as shown in Figure 5.2. This provides a 60MHz gap between the two sidebands which is good for completely filtering out one of the sidebands, which in our case is the LSB. Thus the transmitted spectrum is the USB from 550MHz to 698MHz.

Therefore, the required passband for the BPF is from 550MHz to 698MHz and the BPF roll off should be steep enough to filter out the LSB as well as any LO leakage. The LPF frequency cutoff is set to 178MHz and the LPF roll

off should be steep enough to filter out the alias at the DAC output. The sampling rate has to be greater than twice the maximum baseband frequency of 178MHz and both the DAC and ADC are set to a 440MHz sampling rate, which makes the LPF design practical.

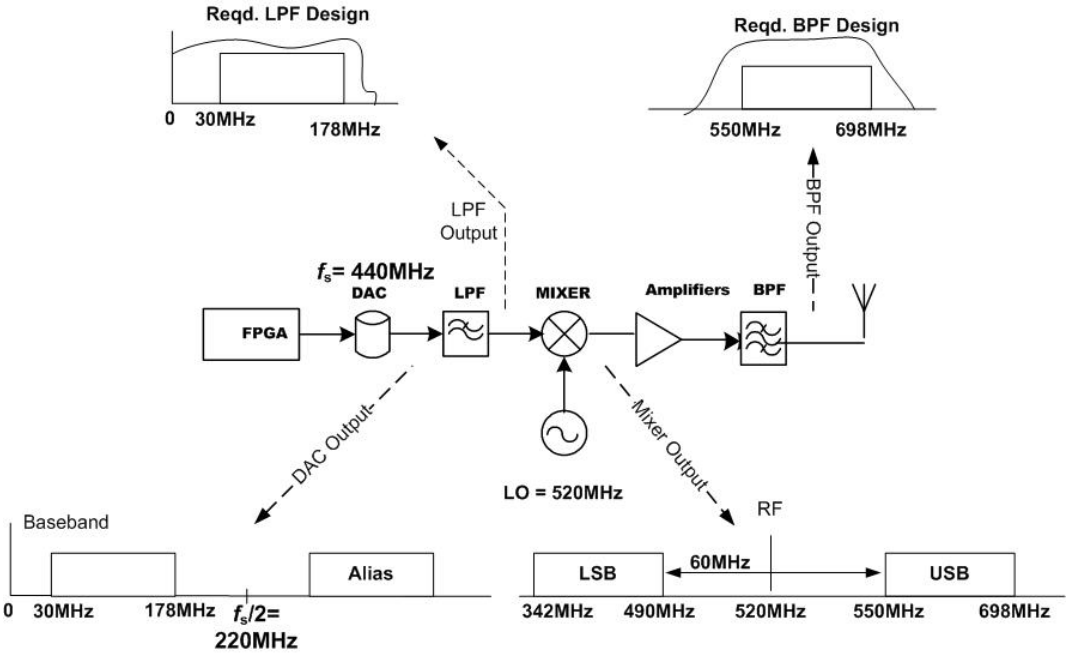

Figure 7.2 Baseband and RF Spectrum Occupancy for SSB Architecture

The DAC baseband output is set anywhere between -45dBm/SC and -50dBm/SC. For the RF transmitter to output a power level of -10dBm/SC the total system gain must be approximately 40dB. The proposed transmitter RF chain power budget analysis is shown in Figure 7.3. The attenuators between the RF components are important and are inserted to aid in maintaining stability by keeping the load impedance of each stage as real as possible.

The RF front end will be designed with three gain blocks to provide the required total gain of 40dB (for transmitter output power of -10dBm/SC). The three gain blocks in the RF chain are the micro-x ceramic packages. These amplifiers are wideband, operate from DC to 6MHz, provide a gain of about 23dB and have high *IIP3* of 10dBm.

An extra final power amplifier is included for future expansion which will allow increasing the total gain to 50dB (for transmitter output power of 0dBm/SC). This power amplifier will not be populated or used for the tests that are discussed in this and in the following chapters since WPI is not currently licensed to operate at this power level. An upconverting mixer used is a wideband mixer which can operate from DC to 1GHz input frequencies and the RF and LO are specified from 40MHz to 2.5GHz. The mixer is a passive mixer which requires an LO of 10dBm and has a conversion loss of 6dB. The *IIP3* is 22dB and the LO to RF isolation is typically 40dB. The required 10dBm LO at 520MHz will be generated from an onboard PLL eliminating the need for an external PLL PCB or external signal generator.

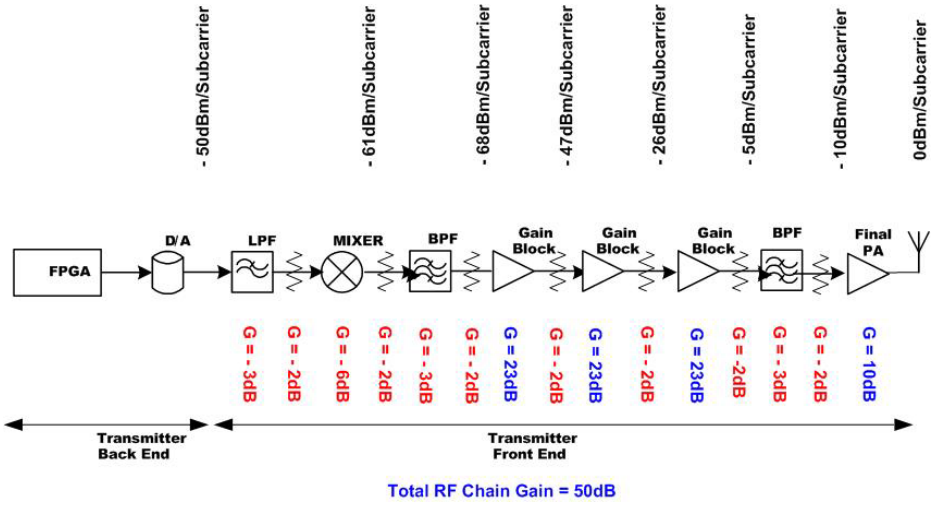

Figure 7.3 Transmitter RF Power Budget Analysis

Now the BPF and LPF specifications and the type of implementation need to be identified. Just due to the multiple amplification stages, the LO leakage at the antenna output will be 22dBm and both the sidebands will be at -10dBm/SC power level, as shown in Figure 7.4. Both the LSB and the LO leakage are spurious emissions and implementing two BPFs eases the BPF design.

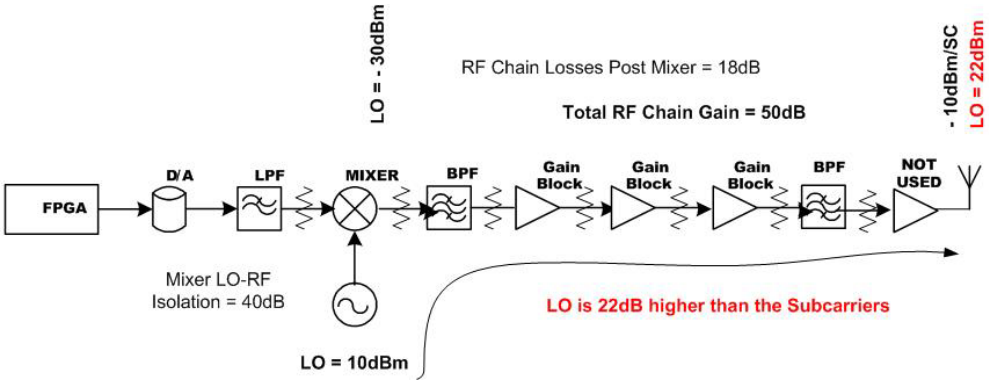

Figure 7.4 Spurious Emissions at Antenna Output

In the case of an unmodulated multicarrier type signal the FCC spurious emission requirements are not clearly defined. A review of the FCC Part 15 regulations, however, reveals that in most cases any unintentional emissions should be 60dBc (60dB below the intentional emission). In our case this means that for a -10dBm/SC multicarrier signal, the LO and the LSB are the unintentional emissions, and need to be below -70dBm.

The target spectral mask is shown in Figure 6.2 which shows the LSB, the USB and the LO spectrum occupancy. The LSB and the USB are separated by 60MHz for practical BPF implementation. It can be seen that the LO needs to be attenuated by 92dB and the LSB needs to be attenuated by 60dB to bring them under the spectral mask. The antenna frequency response characteristics can provide approximately 10dB of attenuation to out of band signal components. Thus it is desired that the BPF design be capable of attenuating the LO by at least 82dB and the LSB by at least 50dB.

Implementing the BPF in two parts simplifies the filter design by reducing the requirements on each filter. Taking this approach, it is desired that each of the two BPFs have a passband from 550MHz to 698MHz and provide 41dB attenuation at the 520MHz LO frequency, which is 30MHz lower than 550MHz. Thus, the two cascaded BPFs will have an effective attenuation of 82dB and the 10dB attenuation due to antenna frequency response will result in total LO attenuation of 92dB.

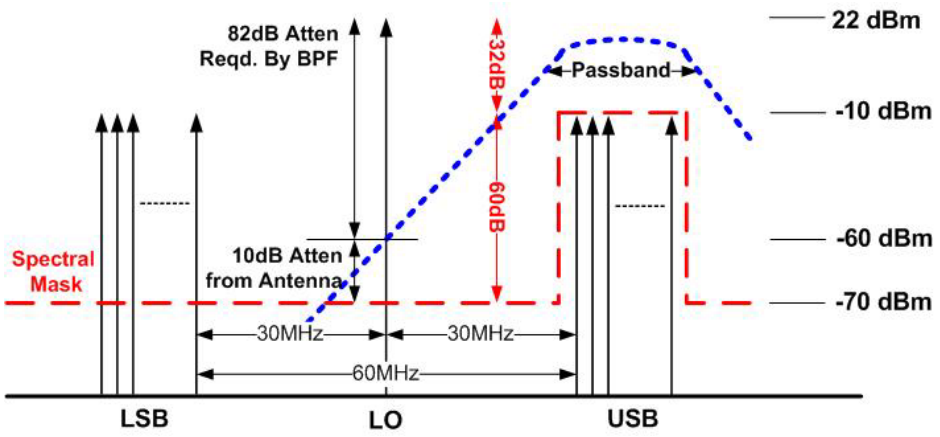

Figure 7.5 Spectral Mask

Since there are no spurious emissions in the spectrum higher than 698MHz, the roll off for the BPF on the high side of the spectrum need not be as sharp as that required for the lower side of the spectrum. This allows using different filter characteristics for the high and low pass sections of the filter, again allowing flexibility in design.

Now that the BPF design specifications are known, the next step is to choose the best BPF implementation. Since the transmitter needs to be low cost, the custom made expensive filter modules cannot be used, and thus an LC filter implementation was chosen for implementing the BPF. The BPF design is cascade of a 7-section LC Elliptical HPF with 3dB cutoff at 550MHz and a 7-section LC Chebychev LPF with 3dB cutoff at 698MHz.

The cascaded BPF was simulated in ADS as shown in Figure 7.6. During simulation, it was noted that the frequency response of the filter was very

sensitive not only to component values, but also to the PC board capacitance. Even minute changes in capacitance of 0.1pF could lead to significant a change in the BPF frequency response. It is important that after the PCB is fabricated the frequency response be very close to the desired frequency response. Thus during the simulations, the practical design aspects were considered and the simulations also included the footprints of the board layout as shown in Figure 7.6. The simulated BPF frequency response is as shown in Figure 7.7. It can be seen that the expected frequency response is within 1dB flatness from 566MHz to 679MHz and is within 3dB across the 550MHz to 700MHz band.

To increase the accuracy of the simulation, the exact S parameter files provided by the manufacturers for the anticipated L and C component values were imported into the ADS simulations to make the simulations as realistic as possible. As a result of these simulations, it was also recognized that the FR4 epoxy PC board material used in the 440MHz prototypes would not be sufficiently uniform in capacitance to result in acceptable filter performance. Therefore, there was an additional requirement that the board material be ROGERS 4003 which is much more uniform in capacitance and will also result in consistent performance among all the RF PCBs.

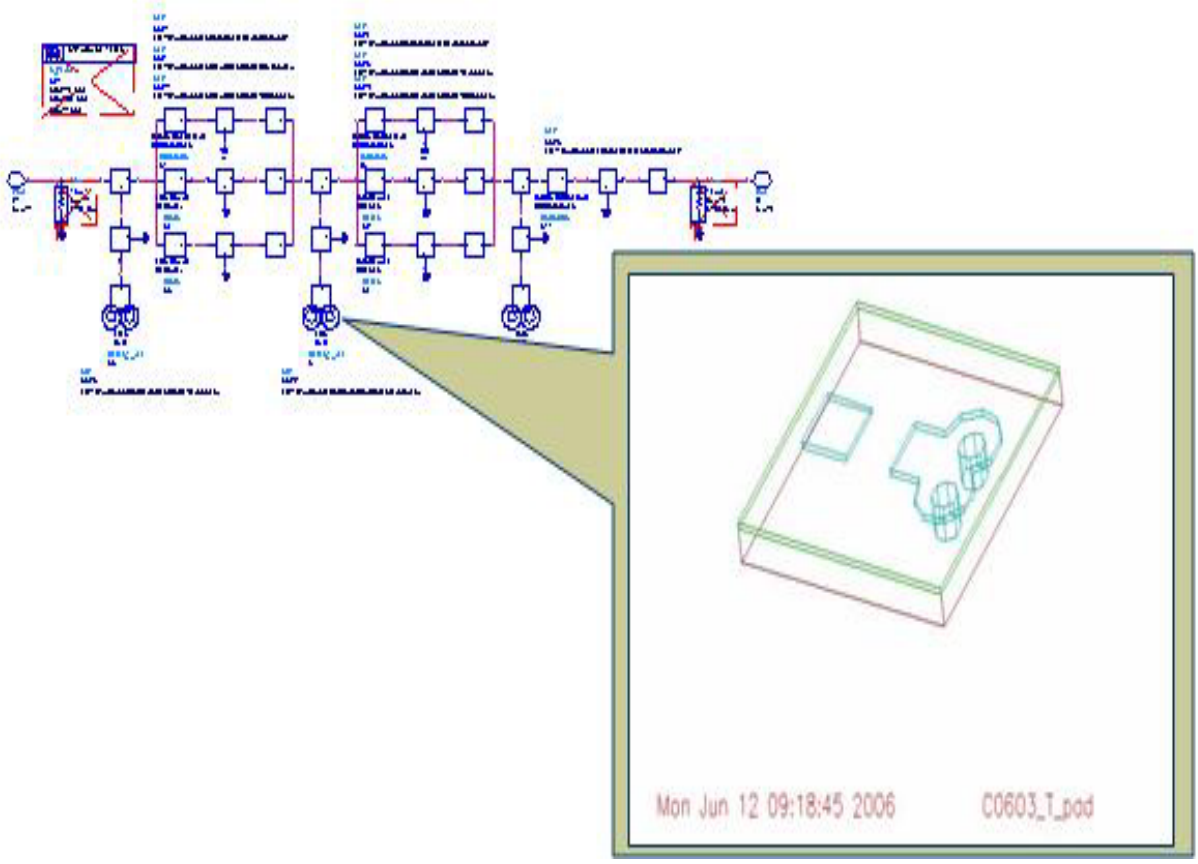

Figure 7.6 PCB Layout Effects for BPF Simulation in ADS

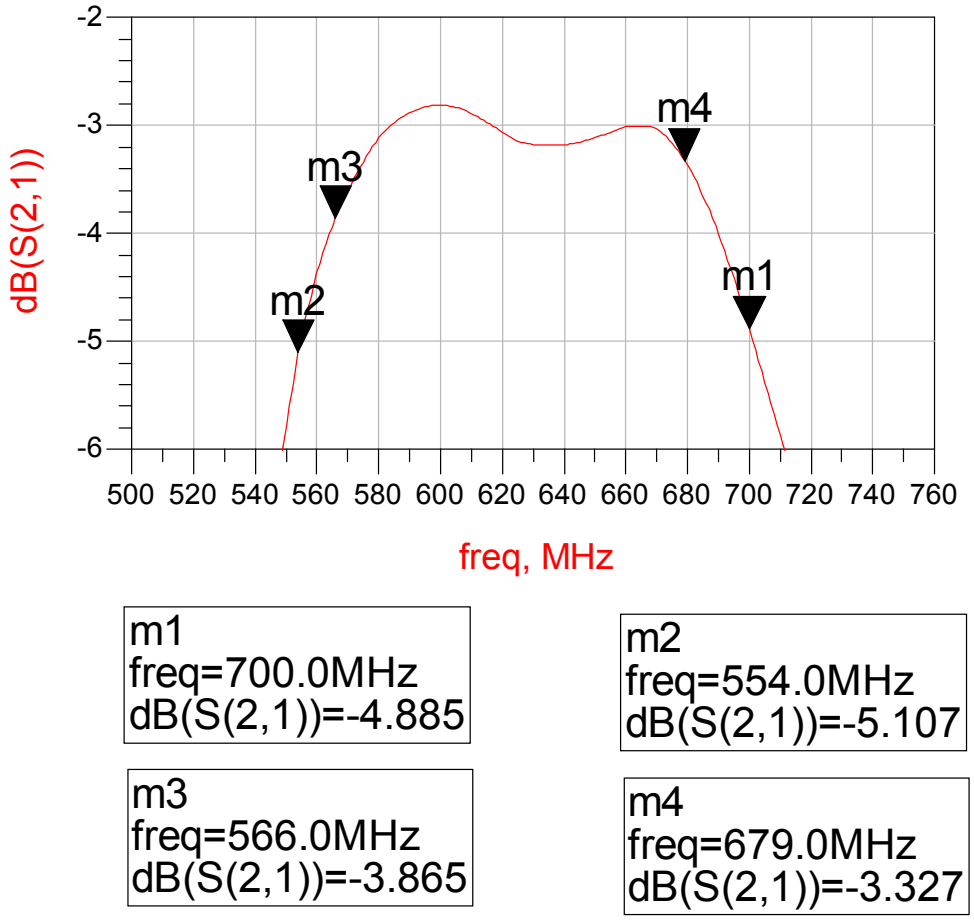

Figure 7.7 ADS Simulated BPF Frequency Response

RF Transmitter PCB Performance

The detailed design of the 550MHz transmitter that includes the schematics and the PCB layout is provided in Appendix A. In this section measurements which show critical performance parameters are discussed.

Figure 7.8 shows the baseband DAC multicarrier output which drives the transmitter baseband input. The multicarrier baseband signal input level is approximately -49dBm/SC with rolloff of approximately 3dB across 30MHz to 180MHz.

The inset shown in Figure 7.8 shows the close up of spectrum with the y-axis zoomed to the scale of 0.5dB/div and the x-axis zoomed to the scale of DC to 200MHz. The inset shows the roll off in the spectrum due to the DAC which is approximately 3dB from 30MHz to 178MHz, as indicated by the markers.

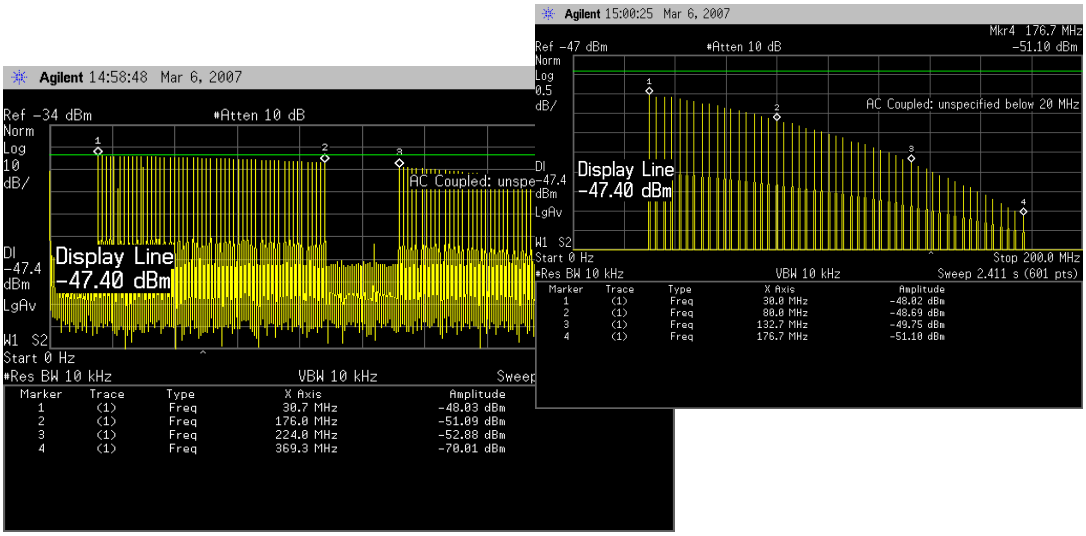

Figure 7.8 Transmitter Baseband Input

The LPF in the transmitter must be sharp enough to filter out the DAC alias. The achieved 7-section LC elliptical LPF frequency response is shown in Figure 7.9 and has approximately 40dB attenuation at the alias frequency which effectively eliminates the DAC alias. The achieved BPF (cascaded LPF-HPF) frequency response is shown in Figure 7.10. Each BPF provides approximately 38dB LO attenuation, thus providing a total of 76dB LO attenuation, close to the desired attenuation of 82dB.

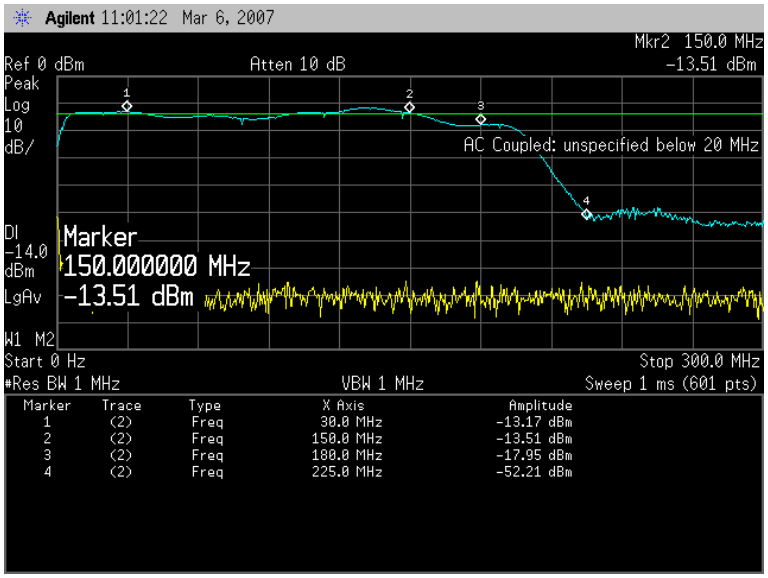

Figure 7.9 LPF Frequency Response

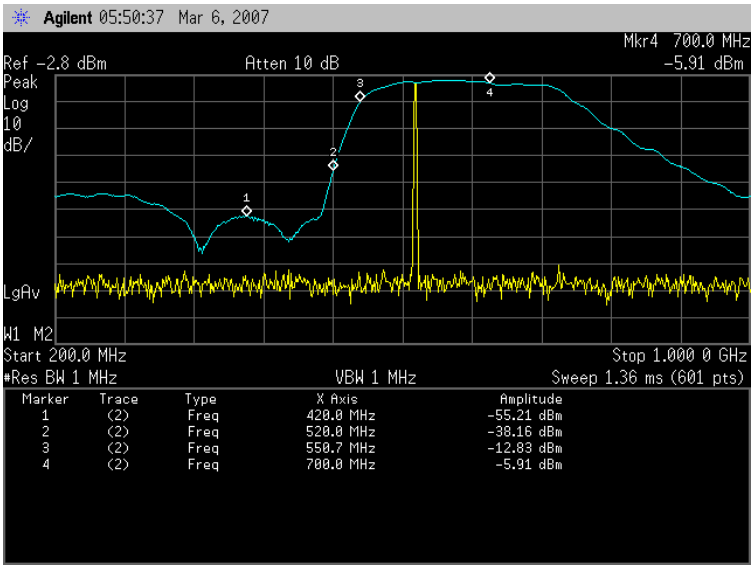

Figure 7.10 BPF Frequency Response

Figure 7.11 shows the required 11dBm LO mixer input of 520MHz, generated from the onboard PLL implementation. Figure 7.12 shows that the phase noise of the LO is -99dBc/Hz at 100Hz.

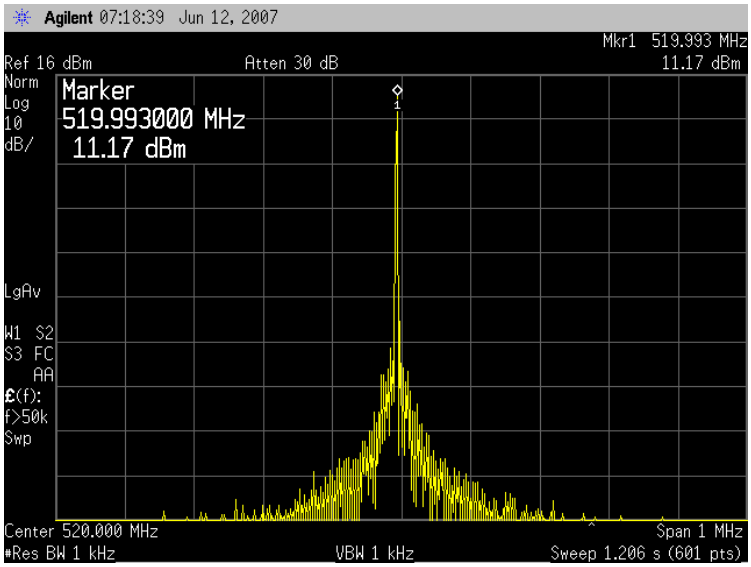

Figure 7.11 LO Mixer Input

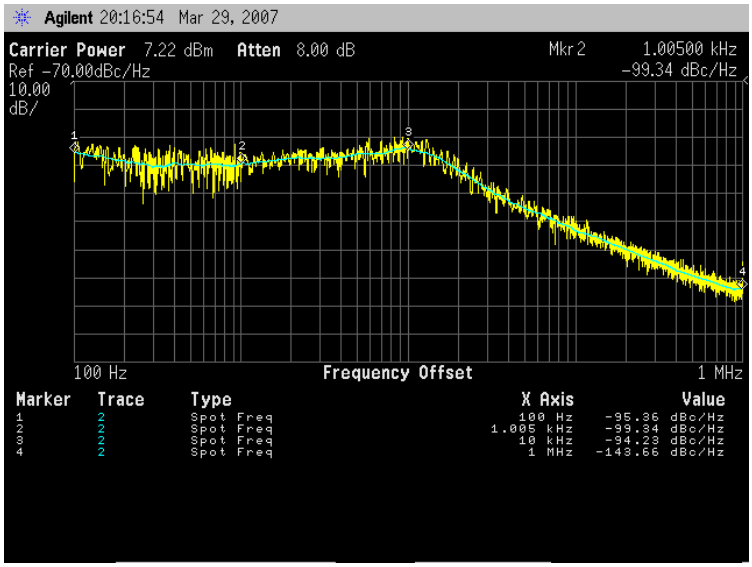

Figure 7.12 LO Mixer Input Phase Noise

Figure 7.13 shows the SSB transmitter output to the antenna and it can be seen that the LSB is completely eliminated and the LO at the output to the antenna is at -50.41dB which is acceptable, given that additional LO attenuation is provided by

the characteristics of the antenna. Ideally the LO level at the transmitter output would be below -60dBm so that the spurious emission goal would be satisfied regardless of the antenna used. For this reason, and the designed PCB has a provision to add a notch filter to further attenuate the LO if needed. The notch frequency response will slightly degrade the passband around the 550MHz edge so care in tuning must be taken if this notch filter is added.

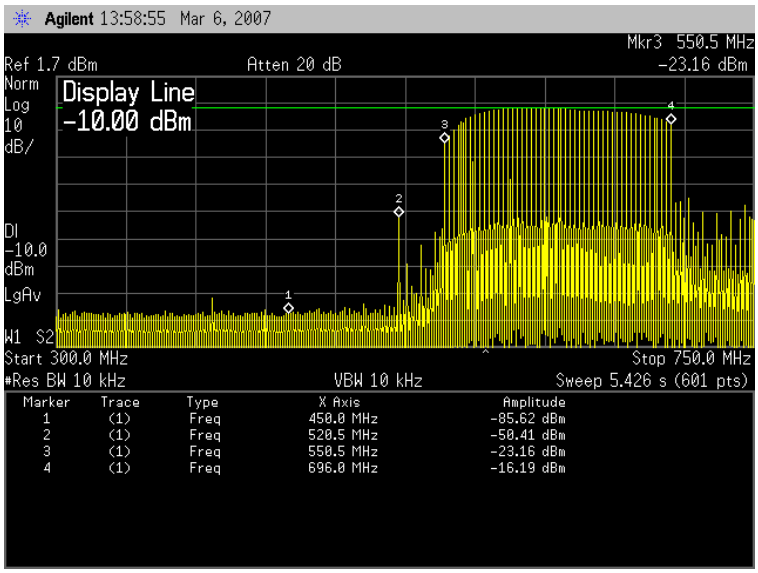

Figure 7.13 SSB Transmitter Output

The zoomed-in spectrum between the two subcarriers shown in Figure 7.14 shows the spectral purity and the spurs are approximately -65dBc (approximately at -75dBm) and the SNR at the antenna out is 70dB. Note that the spurs of -75dBm are consistent with what was predicted by the ADS simulations of Chapter 4, thus validating the RF design approach using two tone tests to characterize an RF system that uses orthogonal unmodulated multicarrier signals.

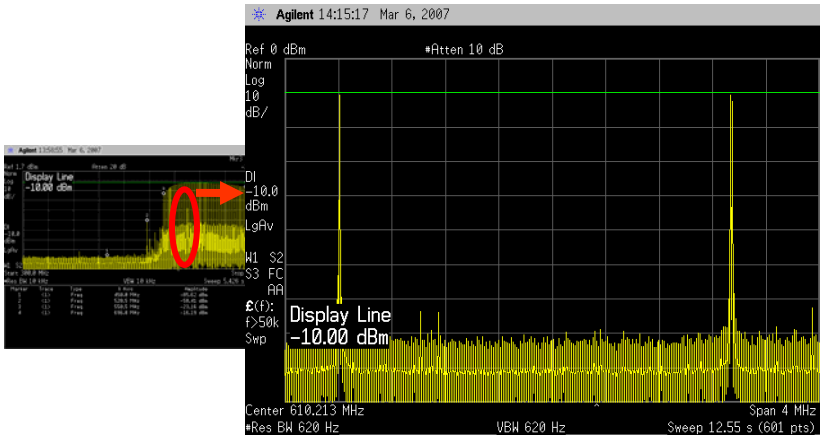

Figure 7.14 SSB Transmitter Output Spectral Purity

Figure 7.15 shows the magnitude flatness at the antenna output and it can be seen that from 570MHz to 670MHz the flatness is +/- 1dB and the roll off in the other sections of the band is due to the BPF and LPF frequency response that needs to be maintained for LSB, LO, and DAC Alias rejection. Figure 7.16 shows the complete transmitter which has a provision for shielding and isolating each of the RF blocks on the PCB.

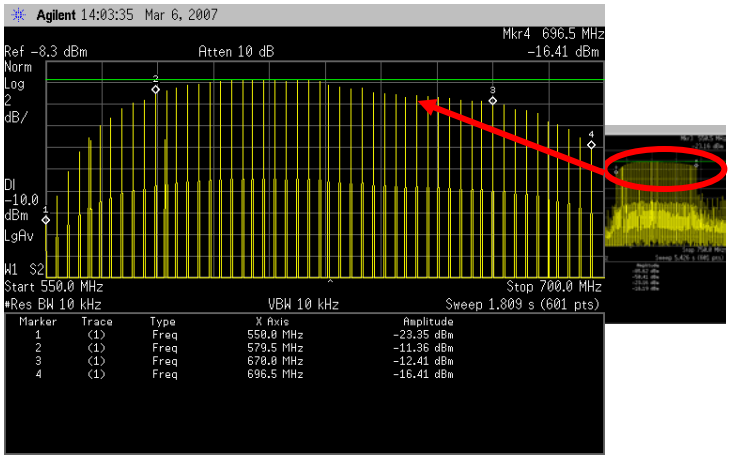

Figure 7.15 SSB Transmitter Output Magnitude Flatness

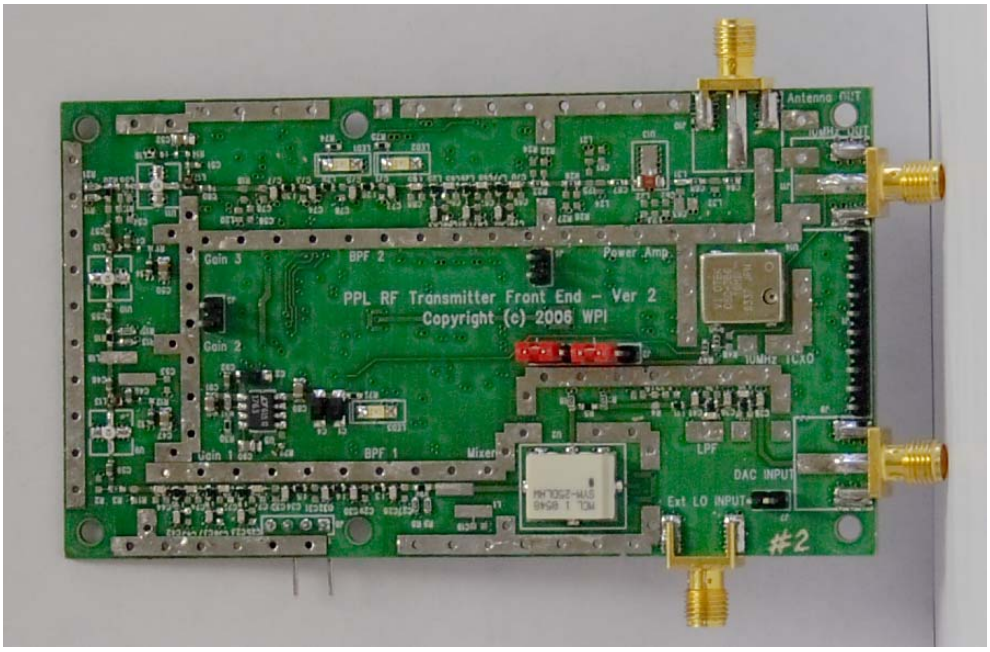

Figure 7.16 Un-Shielded Transmitter

RF Receiver Architecture

From the free space path loss equation, it is known that the receiving antenna will see power levels lower than -50dBm/SC when the transmitter is at a distance greater than 5m from the receiver. Thus, the receiver *IIP3* for the redesign will be set higher than -50dBm and is set to -20dBm. A receiver *NF* of 4.5dB or better is desired, which is low enough so as not to degrade the receiver sensitivity, while still keeping the desired *NF* value realistic and achievable.

The minimum SNR required is set to 0dB as the software provides processing gain of approximately 30dB using signal processing techniques like bandwidth extrapolation, symbol averaging and so on (the specific signal processing approaches are outside the scope of this thesis). The receiver sensitivity which is bandwidth dependent will deteriorate slightly for the 148MHz RF system as compared to the earlier 60MHz RF system. The desired receiver sensitivity based on the minimum required SNR (0dB), *NF* (4.5dB) and the BW (148MHz), is now -87dBm. Assuming an *IIP3* of -20dBm the desired SFDR is now 44dB. The total desired gain in the receiver RF chain is set to 55dB.

The receiver architecture implemented is a direct downconversion type which downconverts the received SSB signal spanning from 550MHz to 698MHz, back to a baseband of 30MHz to 178MHz (the 30MHz offset in the

baseband is due to the need to separate the sidebands in the baseband signal generated at the transmitter). The implemented RF receiver consists of an antenna switch, RF amplifiers, PLL, mixer, and Filters. The gain budget for the receiver is shown in Figure 7.17.

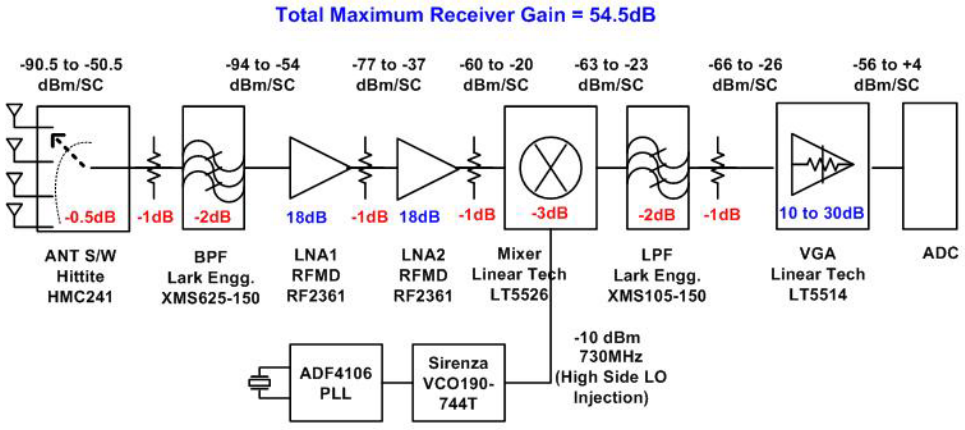

Figure 7.17 Receiver RF Gain Budget

The antenna switch is a SP4T switch which continuously switches between the four inputs to which four receiver antennas are connected. As in the earlier prototype, this switch is provided to implement spatial diversity at the receiver. Since the antenna switch is the first component in the receiver chain, its *NF* is very crucial for the cascaded *NF* of the receiver. Hence the switch chosen has a very low *NF* of 0.5dB and a very high *IIP3* of 44dBm.

The BPF is a custom made 8-section LC filter, with maximum insertion loss of -2dB within the 550MHz to 698MHz band and the 30dB bandwidth for the BPF is 520MHz to 730MHz. The LNA chosen has a gain of

18dB, low noise figure of 1.6dB, and has *IIP3* of 5.5dBm. Two LNAs are used in cascade to boost the received signal power level and bring it to the appropriate level before mixing it with the 730MHz LO signal.

Notice that high side LO injection is implemented at the receiver. This is because after evaluation of the chip, it was found that the LO-IF and the LO-RF leakage performance was better for high side LO injection as compared to that for low side LO injection.

The LPF following the mixer is a custom made 6-section LC filter with a maximum insertion loss of -2dB in its passband. The variable gain amplifier (VGA) used following the LPF has a gain variation range from 10dB to 30dB. The signal levels at the input of the VGA are high due to previous amplification states, thus the VGA *IIP3* needs to be high and is 37dBm. The attenuators inserted between the RF stages are important for stability and the ferrite beads added at the digital interface of the receiver RF PCB helps minimize the RF noise on the digital lines.

Receiver PCB Performance

The detailed design of the 550MHz transmitter that includes the schematics and the PCB layout is provided in Appendix B. The receiver RF front end shown in above figure was tested and the achieved receiver system parameters are shown in Table 7.1. Note that the achieved system parameters are consistent with the expected performance which again validates the two tone RF design approach for orthogonal unmodulated multicarrier signals.

Table 7.1 RF Front End System Parameters

System Parameter	**Expected After Component Selection**	**Achieved**
System G (dB)	54.5	50
System *NF* (dB)	4.1	4.5
System *IIP3* (dBm)	-16.8	-19
Rx. Sensitivity (dBm)	-87.7	-87
Rx. SFDR (dB)	47.3	45.3

The receiver RF PCB was tuned to provide the flatness of +/-1dB across the 148MHz bandwidth and the receiver frequency response is as shown in Figure 7.18. The receiver downconverted output when the transmitter output was

cabled directly to the receiver input is shown in Figure 7.19. The roll off at the ends of the receiver output is due to the roll off in the transmitter frequency response which is discussed in previously in this chapter. The receiver RF PCB is shown in Figure 7.20.

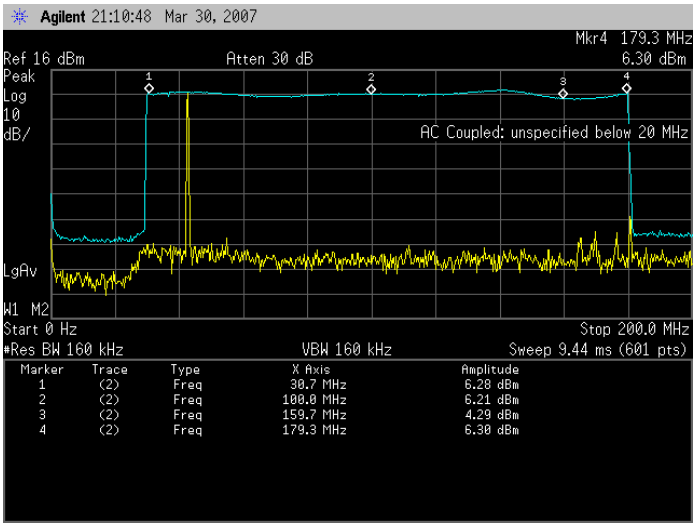

Figure 7.18 Receiver PCB Frequency Response

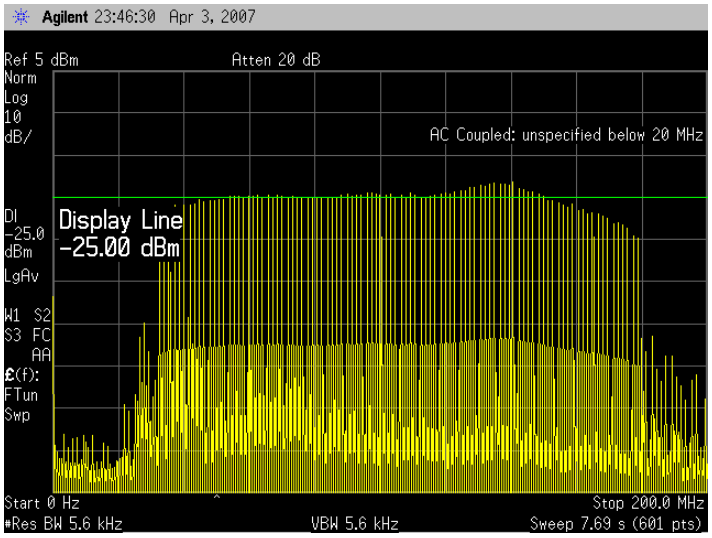

Figure 7.19 Downconverted Receiver Output

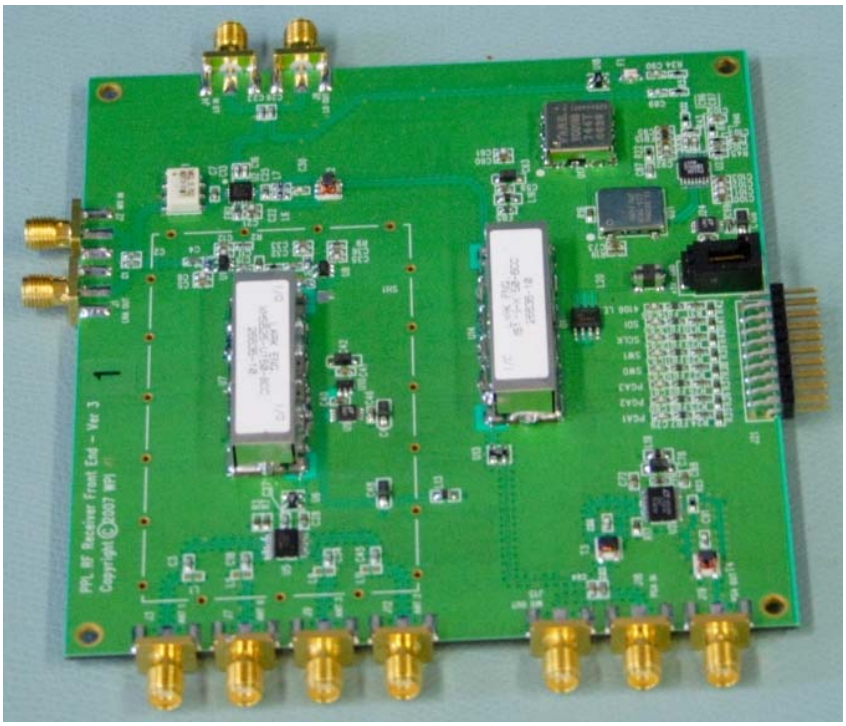

Figure 7.20 Receiver PCB

Conclusion

The limitations of the RF hardware of the 60MHz RF DSB system were eliminated in the new 148MHz RF SSB design. The 148MHz bandwidth RF system operates at center frequency 625MHz, thus the fractional bandwidth is 24%, and thus this new RF system classifies as a Carrier Based UWB as per the UWB definition (fractional BW > 20%). Such a Carrier Based UWB or MC-UWB system is also capable of modifying the spectrum to make the system compatible with existing systems. This new 148MHz UWB system will be used for further bench and field testing replacing the 60MHz WB system and these tests are discussed in next chapter.

Chapter 8 : Tests Using 148MHz RF System

Introduction

As discussed in the previous chapter, the RF system was redesigned from a 60MHz WB system to a 148MHz UWB system. The bench tests and the indoor tests discussed in this chapter use this redesigned RF system consisting of an SSB transmitter and a direct downconversion receiver.

The LOs for the transmitter and the receiver RF PCBs are now generated independently using their respective onboard PLLs. The transmitter LO frequency is set to 520MHz and the receiver uses high side LO injection and

is set to 730MHz. The transmitted signal spans from 550MHz to 698MHz and the downconverted signal spans from 30MHz to 178MHz.

The hardware setup for the tests discussed in this chapter is shown in Figure 8.1. The transmitted multicarrier signal is received, digitized and transferred to the base station. For receiver sampling clock synchronization, the receiver digital back end is incorporated with the base station. The 440MHz receiver sampling clocks for all five receivers are derived from one signal generator similar to the indoor and outdoor tests discussed in Chapter 6. The test setup details for the redesigned 148MHz RF system are:

- Setup: Single Transmitter – Multiple (five) Receivers
- Antenna Type: Dipole Antenna
- Transmitter: SSB Transmission
- Receiver: Direct Down Conversion Receiver
- Downconverted Baseband Signal Span: 148MHz
- Tx-Rx Sampling Clock: Synchronized
- Sampling Clock: 440MHz
- Tx-Rx Carrier Frequency: Un Synchronized
- Tx Carrier Frequency: 520MHz
- Rx Carrier Frequency: 730MHz
- Averaging: 64 symbols
- Spatial Diversity: Supports up to four antennas / receiver

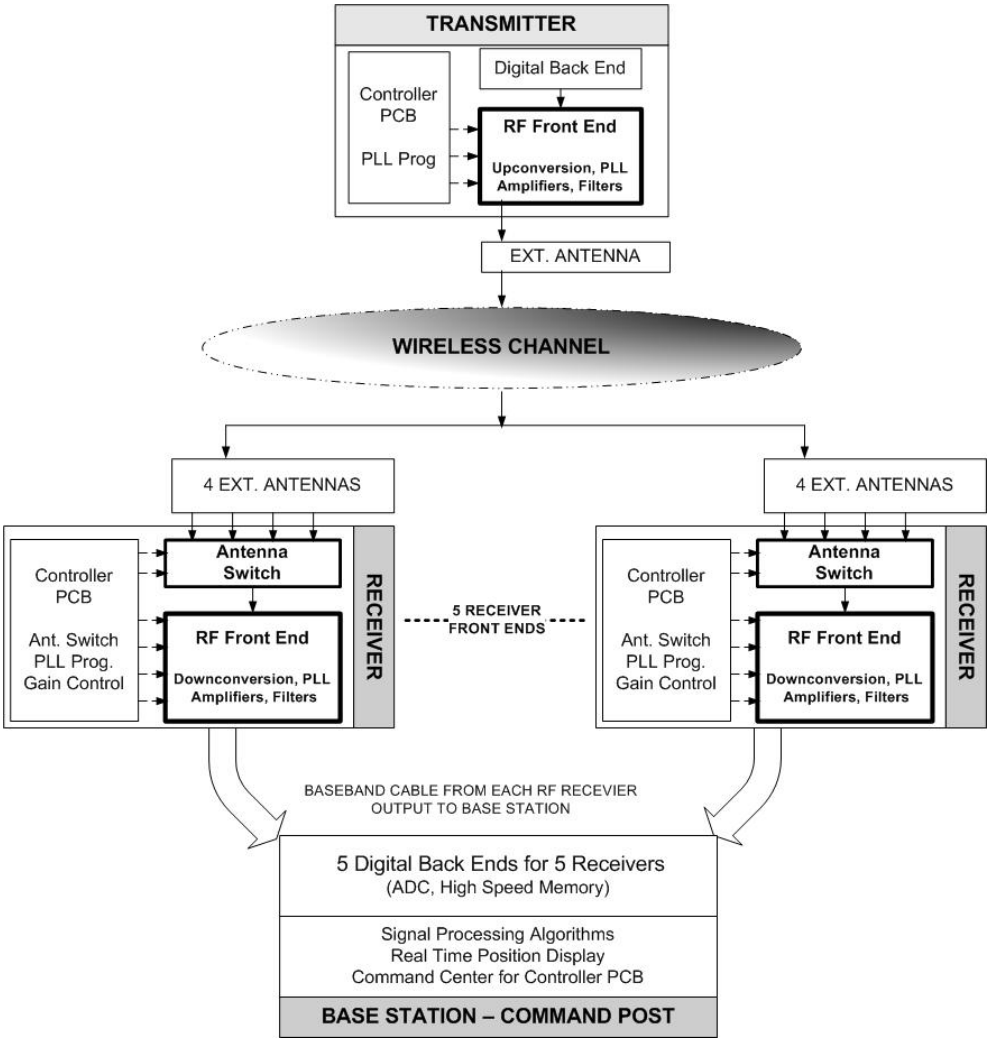

Figure 8.1 Position Estimation Wireless Test Setup

The receiver front end consists of two modules, the RF front end PCB (with onboard BPF, PLL, and Antenna Switch) and the Controller PCB. The antenna switch was discussed in Chapter 6 and is used to take advantage of spatial diversity. Each receiver front end has four inputs to switch up to four external antennas. The multiple dipole antennas are switched continuously using the

Controller PCB and the multicarrier signal at each antenna port is downconverted, sampled and fed to a post processor for calculating a position estimate. The Controller PCB interfaces with the digital interface on the receiver RF front end PCB to program the RF gain, PLL chip and to control antenna switching. Similarly, the transmitter RF front end consists of onboard filters, amplifiers, and PLL and the Controller PCB is used to program the PLL with the required transmitter LO.

Performance Comparison of 60MHz vs. 148MHz RF System

This section discusses the test setup and results for a performance comparison of the 60MHz and 148MHz RF systems. The test setup for the cable tests is similar to that shown in Figure 8.1, except that the wireless channel is eliminated. The transmitter output is directly cabled to the inputs of five receivers (only one antenna port is used per receiver) using appropriate power splitters and attenuation, thus providing a multipath free test setup.

The performance metric for this test is the improvement or degradation of the position estimate between the 60MHz non-optimized RF system and the 148MHz optimized RF system. Since the test is performed in a cabled environment, the only noise contribution is from the cable.

A positioning accuracy threshold of 0.1m is used for comparing each different system, meaning that in each test, the signal strength continues to be reduced as long as the positioning accuracy remains below 0.1m. The tests were broken down into five steps as shown below. The algorithms used in the tests discussed below are exactly the same for all test setups, and thus in this multipath free environment the improvement or degradation in the performance metric is purely due to differences in the RF transmitter and receiver characteristics.

1) Test 1: Observe position estimate using 60MHz non-optimized transmitter and 60MHz non-optimized receiver (receiver gain = 25dB), operating in the 410MHz to 470MHz band.
2) Test 2: Observe position estimate using a 60MHz optimized transmitter (this is the same transmitter design discussed in chapter 7, tuned to operate in the 410MHz to 470MHz band) and a 60MHz non-optimized receiver (receiver gain = 25dB), operating in the 410MHz to 470MHz band.
3) Test 3: Observe position estimate using a 60MHz optimized transmitter and 60MHz optimized receiver (receiver gain = 25dB), operating in the 550MHz to 698MHz band.
4) Test 4: Observe position estimate using a 148MHz optimized transmitter and a 148MHz optimized receiver (receiver gain = 25dB), operating in the 550MHz to 698MHz band.
5) Test 5: Observe position estimate using a 148MHz optimized transmitter and a 148MHz optimized receiver (receiver gain = 45dB), operating in the 550MHz to 698MHz band.

The non-optimized transmitter output spectrum (left spectrum) for the 410MHz to 470MHz band and the corresponding non-optimized receiver downconverted output spectrum (right spectrum) is shown in Figure 8.2. The spectrums shown in Figure 8.2 correspond to Test 1 and the roll-off seen is due to the non-flat mixer characteristics and filters used in the RF front ends. Better

flatness is desired for improving the SNR across the band which is achieved in the optimized RF design.

The optimized transmitter output spectrum (left spectrum) for the 410MHz to 470MHz band and the corresponding non-optimized receiver downconverted output spectrum (right spectrum) is shown in Figure 8.3. The spectrums shown in Figure 8.3 correspond to Test 2. As shown in the figure, the spectral flatness is improved significantly over that shown in Figure 8.2.

The optimized transmitter output spectrum (left spectrum) for the 550MHz to 698MHz band and the corresponding optimized receiver downconverted output spectrum (right spectrum) is shown in Figure 8.4. The spectrums shown in Figure 8.4 correspond to Test 4 and it can be seen that the spectrum is optimized for flatness and spectral purity over 148MHz. There is roll-off seen at the band edges which is mainly due to the BPF characteristics.

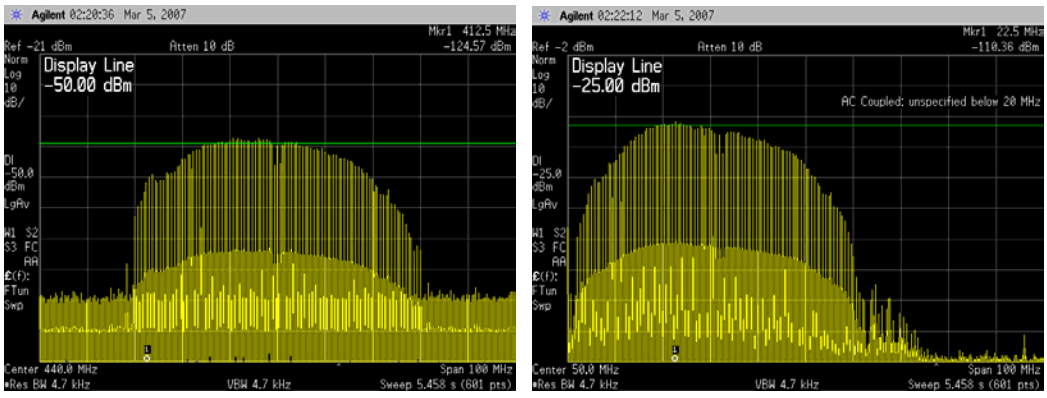

Figure 8.2 Transmitter Output (Left Spectrum) & Receiver Downconverted Output (Right Spectrum) for Test 1

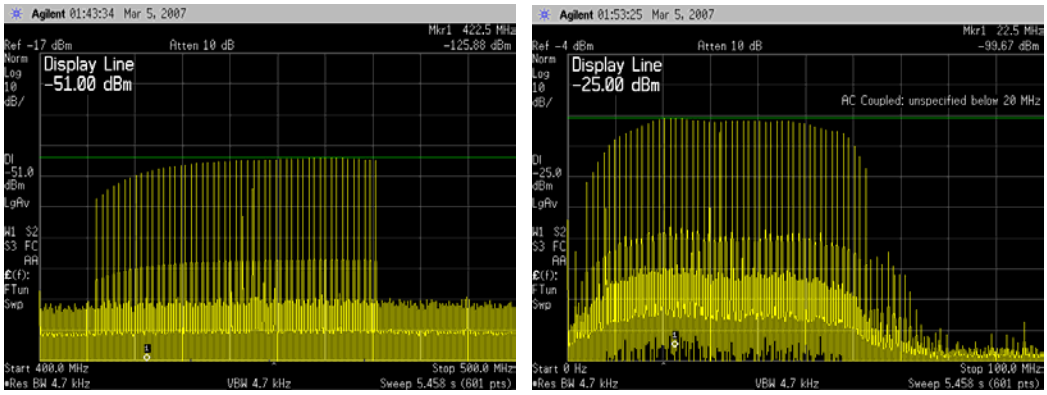

Figure 8.3 Transmitter Output (Left Spectrum) & Receiver Downconverted Output (Right Spectrum) for Test 2

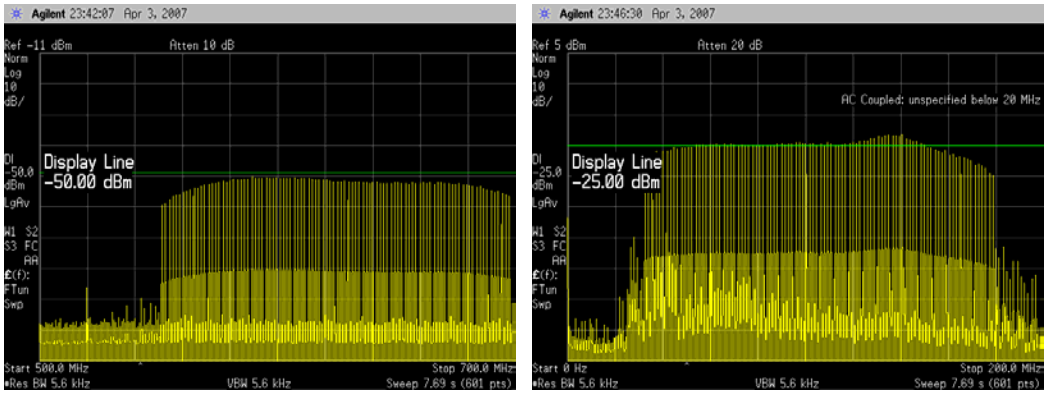

Figure 8.4 Transmitter Output (Left Spectrum) & Receiver Downconverted Output (Right Spectrum) for Test 4

During the five tests mentioned earlier, the receiver input power level was reduced from -50dBm/SC to -125dBm/SC by adding attenuators. The position estimation errors (those below the selected threshold of 0.1m) for all five test setups for various receiver input power levels are shown in Table 8.1.

Table 8.1 RF Performance Comparison

Rx IN (dBm/SC)	Test 1	Test 2	Test 3	Test 4	Test 5
-50	0.001	0.000	0.000	0.000	
-60	0.005	0.002	0.002	0.001	
-65	0.008	0.005	0.004	0.002	
-75	0.0082	0.018	0.012	0.006	
-85	> 0.1	0.069	0.046	0.017	
-90		> 0.1	0.075	0.030	
-95			> 0.1	0.052	0.008
-100				0.079	0.010
-105				> 0.1	0.020
-110					0.040
-115					0.070
-120					0.090
-125					> 0.1

The Test 1 results show the position estimation errors for the original 60MHz, non-optimized, RF hardware which is used as a baseline for comparison with results from Tests 2 to 5. Notice that for Test 1 the errors are greater than 0.1m, when the receiver input power falls to -85dBm/SC. In comparison, Test 2 shows the improvement in positioning accuracy due to optimizing the 60MHz transmitter. These improvements resulted in maintaining positioning accuracy when the receiver input power levels are as low as -90dBm/SC. Test 3 shows the results for both transmitter and receiver

optimizations. In this case, the effective noise floor for the optimized 60MHz system is -96dBm.

Test 4 shows the improvement in positioning estimate for the 148MHz optimized system. Comparing the results of Test 3 and Test 4 provides an indication of the improvement in positioning accuracy due to increasing the multicarrier span from 60MHz to 148MHz (note that there are changes in center frequency as well, but these should not effect the positioning accuracy for cable tests). Thus for a given level of signal, Table 8.1 shows that the 148MHz system (Test 4 results) is approximately 2 to 2.5 times as accurate as the 60MHz system (Test 3 results), in controlled environments. The theory would dictate that the 148MHz signal has 2.47 times the bandwidth, and therefore should have 2.47 times the accuracy of a 60MHz signal. Thus, the performance of the 148MHz system in controlled environments tracks the theory almost perfectly.

Comparing the results from Test 4 and Test 5 shows the further improvement in positioning estimate achieved due to increases in the receiver gain. By using the VGA to increase receiver gain, only when the receiver input power levels are lower than -125dBm/SC do the errors become greater than 0.1m. Thus, the optimized RF hardware makes it possible to detect extremely weak multicarrier signals. Comparing the results from Test 1 and Test 4 shows that using the optimized RF design with improved spectral purity results in a position estimation improvement of at least four times.

Indoor Field Tests Using 148MHz RF System

Chapter 6 discussed indoor positioning tests and the results obtained using the 60MHz RF system. Similarly, indoor tests were performed using the 148MHz system at the same locations and these results are discussed in this section. The three locations are WPI's Kaven Hall, WPI's Religious Center and WPI's Atwater Kent East Wing. The algorithm, the test setup and the transmitter and the receiver locations for this 148MHz RF system at all three locations are exactly the same as those used in the 60MHz RF system. Similar to the tests using the 60MHz system, the indoor transmitter was moved to several locations to capture received signals at each transmitter location.

The transmitted SSB signal is the left spectrum in Figure 8.5. Note that the gap from 608MHz to 620MHz is the restricted band as per the FCC permissions granted to WPI and is accomplished by simply not including those carriers in the generated signal. Thus, accounting for the forbidden region, the expected improvement due to increase in the multicarrier span would be approximately 2.2 times (the effective bandwidth now is 136MHz) of what was observed in 60MHz system. The corresponding receiver downconverted signal spectrum is shown in the right spectrum in Figure 8.5.

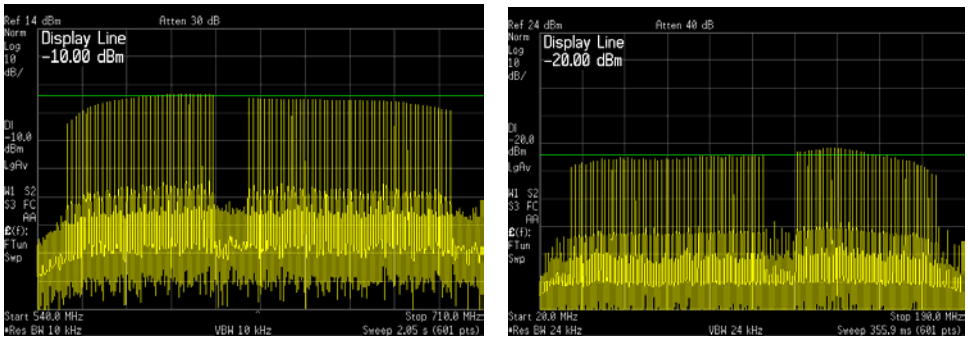

Figure 8.5 Transmitted and Received 148MHz spectrums

The error vector magnitude plots [1] for the three tests are shown in Figure 8.6, Figure 8.7, and Figure 8.8. The thick outline is the wall of the test venue and the breaks between walls are the windows. The circles outside the walls are the antenna positions. 13 antennas are used to cover three sides of Kaven Hall as shown in Figure 8.6, 16 antennas are used to cover all four sides of the Religious Center as shown in Figure 8.7 and 16 antennas are used to cover three sides of the AK East Wing as shown in Figure 8.8. The squares inside the wall are the true transmitter positions and the arrows are the error vectors. The length of the error vector signifies the error for that transmitter position and the end of the red arrow signifies the transmitter position estimate.

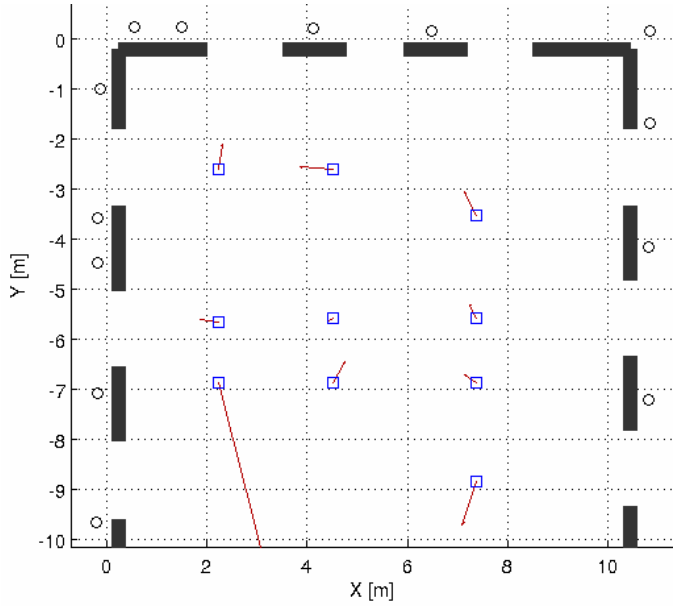

Figure 8.6 Kaven Hall Error Vector Plot

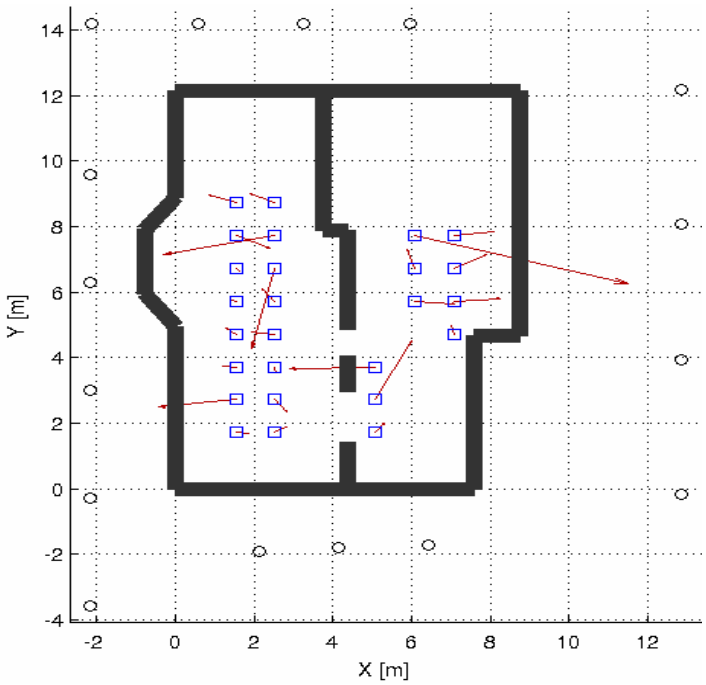

Figure 8.7 Religious Center Error Vector Plot

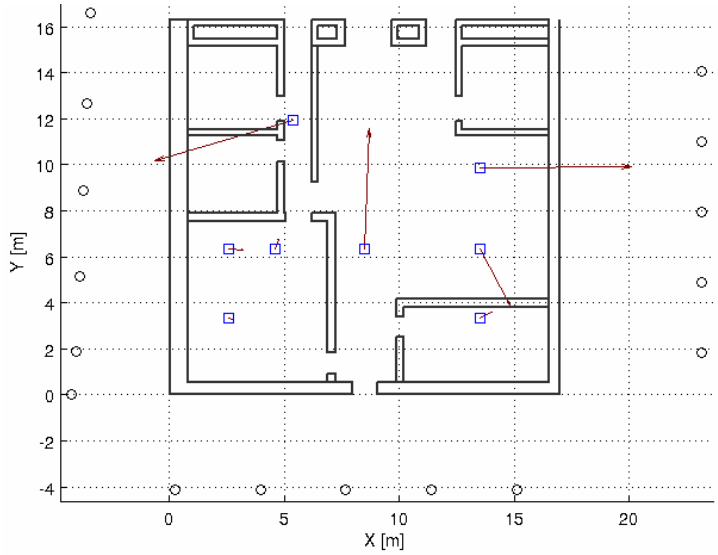

Figure 8.8 AK East Wing Error Vector Plot

Table 8.2 summarizes the results from Figure 8.6-Figure 8.8. It can be seen that the mean error for all the three test venues is less than 3m. It can also be seen in Figure 8.6-Figure 8.8 that at some transmitter locations the error vector is greater than 3m which, at least in part, is likely due to the bad geometry of the receiving antennas with respect to that particular transmitter position. Overall, consistent results were achieved indoors.

Table 8.2 Summary of 148MHz Indoor Positioning Results

	Min. Error (m)	**Max. Error (m)**	**Mean Error (m)**
Kaven Hall	0.14	3.7	0.79
Religious Center	0.13	5.62	1.09
AK East Wing	0.22	6.6	2.84

Wideband radio propagation modeling is discussed in [2], which presents the statistical behavior a channel using a 200MHz wideband signal and the expected error distribution for indoor positioning. The experimental setup in [2] is similar to the environments under which the above discussed tests were conducted. The experiments discussed in [2] show that the probability of the observed error being less than 10m is approximately 80% and that of observed error being almost/close to 0m is approximately 55%. In that study, the errors were mainly attributed to the Nondominant Direct Path (NDDP) conditions.

Statistical analysis of the test results shown in Table 6.3 is one of the future tasks identified in this thesis, but the above error values were consistent and repeatable and hence can be compared with the results predicted in [2]. From Table 6.3 all of the observed errors were less than 10m, indicating that the probability of obtaining this level of error is likely to be at least as high as that predicted in [2]. Similarly, the measured data points suggest that the observed error being close to 0m is approximately 30%, slightly lower than that predicted in [2].

While care should be taken in interpreting these results, since the locations of the transmit and receive antennas are not identical in both cases and since more measurements would be needed to produce a more comprehensive statistical analysis, some comments about the relatively better performance of the 148MHz system can be made. The improved accuracy of the 148MHz system

versus the 200 MHz system described in [2] appears to be due to two main reasons.

The first reason is the implementation of multicarrier-based advanced signal processing algorithms [3]. The second reason is the improved and optimized RF receiver, design as shown in Table 8.1 that reduces the NDDP by significantly improving receiver sensitivity. Table 8.1 showed that the theoretical receiver sensitivity due to hardware and software processing gain is approximately -120dBm, which lowers the probability of errors by reducing the NDDP errors. In general the results shown in Table 8.2 are within what is predicted in [2] which gives further confidence that the system performance is near optimum.

Lessons Learnt

Optimized RF Design: The results of Test 5 show that direct path signals that are very weak up to -120dBm, can be amplified without losing the signal integrity, thus improving the detection of weak direct path signals which leads to minimizing errors in position estimation. These results show that the optimized 148MHz RF design can improve the overall capability of detecting weak signals and can improve the positioning results by more than four times.

Narrowband Interference: The results for the indoor tests using the 60MHz (410MHz to 470MHz) RF system were discussed in Chapter 6 and those using the 148MHz (550MHz to 698MHz) RF system were discussed in this chapter. In theory, for the same test environment, the positioning accuracy should improve by increasing the bandwidth. This suggests that there are some fundamental limitations beyond which the positioning accuracies cannot be improved, even with increases in bandwidth.

Increasing the multicarrier span from 60MHz to 148MHz; one would expect the position estimates to improve by a factor of approximately 2.2. However, comparing results from Table 6.3 with results in Table 8.2, this performance improvement by factor of 2.2 is not observed. In fact the performance got worse as the average error for 148MHz RF system was always greater than that for 60MHz RF system for the same test venue.

One of the reasons for this could be a reduction in effective bandwidth due to in band TV channel interference. A TV station happens to operate close to 550MHz and this signal is picked up by the receiver and amplified as shown in Figure 8.9.

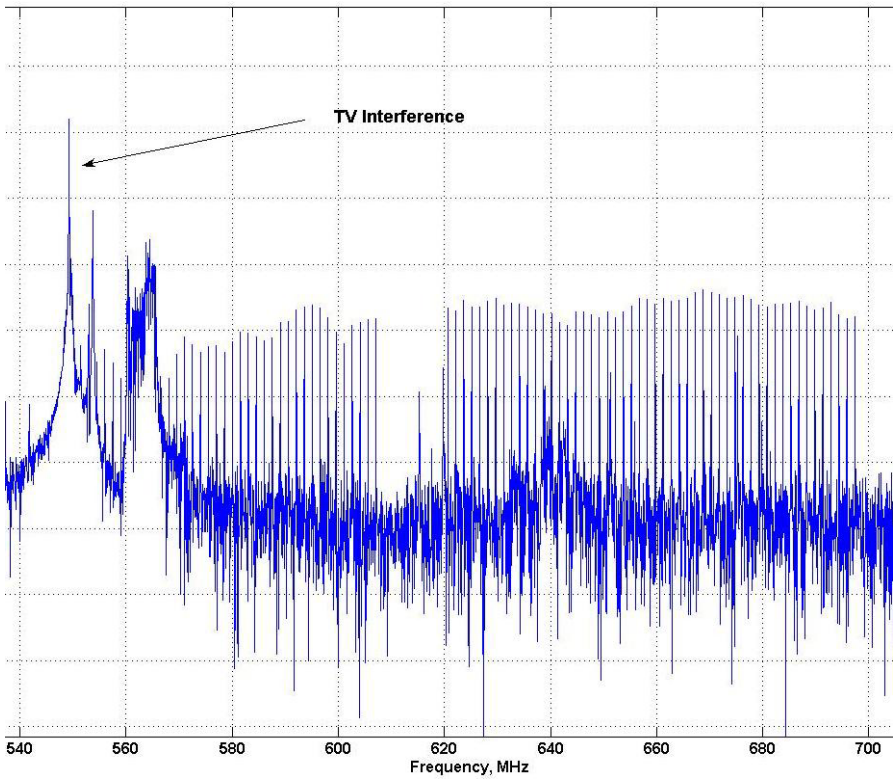

Figure 8.9 Received TV Interference Signal

A second possible reason for the deteriorated performance could be due to worse indoor propagation characteristics in the 625MHz band as compared to those in the 440MHz band, resulting in greater multipath. Finally, the dielectric properties

of the building materials could be adding greater delay in the 625MHz band as compared to that in 440MHz band, resulting in higher position estimation errors.

Conclusion

In this chapter we discussed indoor positioning test setup and results using optimized 148MHz RF transmitter and receivers. These tests were performed using SSB transmission and direct downconversion reception. The optimized RF design demonstrated improvement in the position estimates for tests performed in a multipath free environment. The indoor field test results were consistent with mean error of better than 3m. The performance improvement expected due to wider bandwidth was not observed and a few possible reasons for this were discussed which needs to be further investigated as discussed in the next chapter.

References

[1] V. Amendolare, B. Woodacre, *WPI Internal Memorandum*, 2007

[2] K. Pahlavan, P. Krishnamurthy, A. Beneat, "Wideband Radio Propagation Modeling for Indoor Geolocation Applications", *IEEE Communications Magazine,* Volume 36, April 1998

[3] D. Cyganski, J. A. Orr and W. R. Michalson, "A Multi-Carrier Technique for Precision Geolocation for Indoor/Multipath Environments", *Institute of Navigation Proc. GPS/GNSS*, Portland, OR, September 9-12 2003

Chapter 9 : Conclusion

RF System Evolution

The need for developing an indoor positioning system for fire fighters is well known and is becoming more and more important. WPI was granted financial support with a goal to design and develop an indoor precise positioning system which can track and locate fire fighters inside a building to a precision of 3m-6m. The PPL team at WPI has been working on developing such a system for more than four years and has successfully demonstrated such a prototype system. The technical aspects of the PPL project were divided into four fields as shown in Figure 9.1.

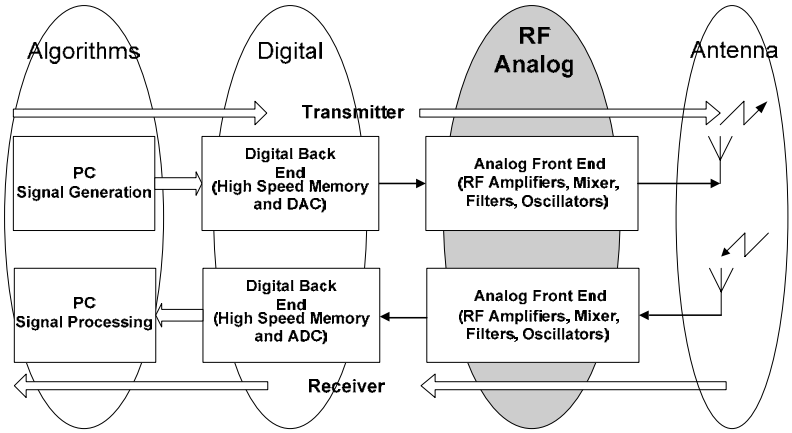

Figure 9.1 Position Estimation Wireless Test Setup

The RF prototype evolved over a few years from one consisting of extensive test and measurement equipment as discussed in Chapter 3 to a field deployable optimum RF design as discussed in Chapter 7. The Phase 1 RF transmitter-receiver shown in Figure 9.2 and the Phase 4 RF transmitter-receiver shown in Figure 9.3 shows the evolution that the RF system has undergone. An overview of the RF system evolution summary is shown in Table 9.1.

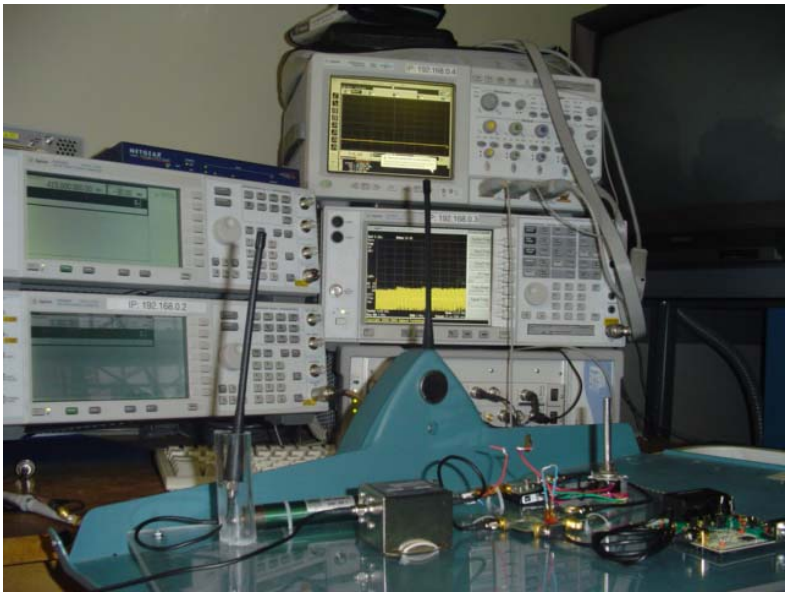

Figure 9.2 Phase 1 Transmitter-Receiver Setup

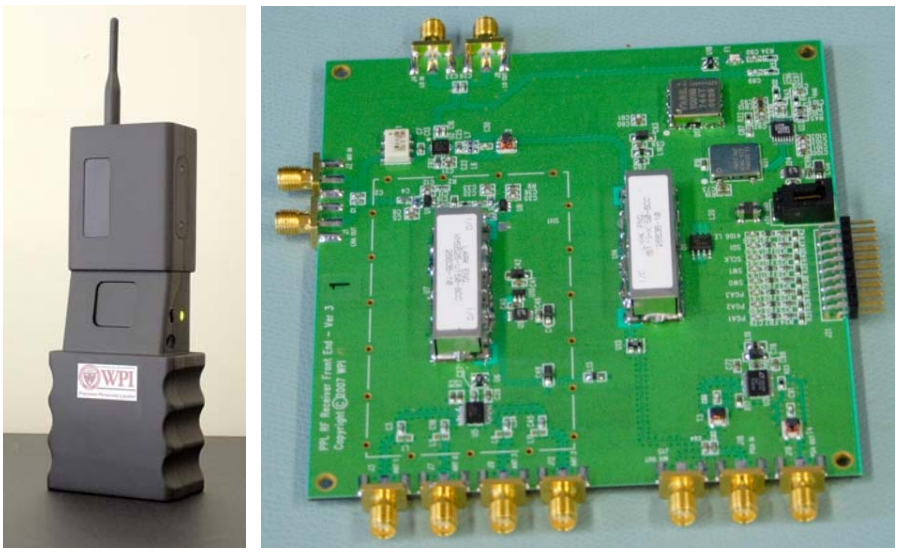

Figure 9.3 Phase 4 Transmitter-Receiver Setup

Table 9.1 RF System Evolution Summary

	RF Prototype	**System Test Setup**
Phase 1	Transmitter: PC and Vector Signal Generator (VSG) Receiver: Eval PCBs, PC, VSG, and Oscilloscope	Wireless 1 Tx 1 Rx 5-10 meters testing range
Phase 2	Transmitter: Eval PCBs for digital and analog modules Receiver: Eval PCBs for digital and analog modules	Wireless 1 Tx 1 Rx 5-10 meters testing range
Phase 3	Transmitter: Custom RF PCB design Receiver: Custom RF PCB design	Wireless 1 Tx Multiple Rx 30-40 meters testing range
Phase 4	Transmitter: Custom Optimized RF PCB design Receiver: Custom Optimized RF PCB design	Wireless 1 Tx Multiple Rx 50-60 meters testing range

As discussed in the previous chapter, increasing bandwidth by a factor of 2.2, did not lead to any improvement in positioning accuracy. Thus, there is need to further analyze the breakdown of errors from all known error sources, with the ultimate goal of minimizing the positioning error.

An error budget for a multicarrier based positioning system is proposed in Table 9.2 [1], which lists the error sources and their contribution during field tests.

Table 9.2 Optimized Realistic Error Budget

Error Sources	**Error Contribution (meters)**	**Design Constraints / Comments**
Sampling CLK Shift	0.003	< 10 ppm: Sampling CLK frequency error
Sampling CLK Drift	0.003	< 10 ppm: Sampling CLK frequency error
Local Oscillator Shift	0.010	< 2.5 ppm: Local oscillator frequency error
Local Oscillator Drift	0.010	< 2.5 ppm: Local oscillator frequency error
Receiver Geometry	0.30	Optimum receiver geometry very Important
Antenna Type	0.30	Need to use directional antennas at Receivers
Software Processing	0.10	Optimum selection of the useful spectrum
Path Loss / Shadow Fading	0.10	AGC implementation at the transmitter and receiver
External Interference	0.30	Optimum selection of the useful spectrum
NLOS	0.50	Better geometry, antenna, transmit power required
Multipath	0.50	Need for channel models specific to indoor positioning
Building dielectric Properties	0.50	Need to characterize delays induced by various building materials
Total System Error:	**2.626 meters**	

Any discrepancy in the transmitter and receiver sampling clocks results in degrading the positioning estimate. Using a sampling clock crystal of 10ppm or better minimized this error to less than 0.003m. Similarly, local oscillator frequency shift and drift results in error and using a crystal that was 2.5ppm or better, resulted in contributing less than 0.003m error. Receiver geometry and dilution of precision (DOP) plays an important role in minimizing errors in TDOA based systems and should be optimized.

The presence of receivers on only three sides of the building and not all four sides contributes to errors up to 0.3m. The antenna polarization, radiation pattern and antenna type also affects the position estimate to up to 0.3m. Directional antennas are desirable at the receivers, which along with optimum receiver geometry will result in less error. High range of variable gain control implementation both at the transmitter and at the receiver could be useful in combating severe path loss and shadow fading in NLOS indoor conditions provided signal integrity is maintained.

Narrowband interference from in-band TV stations can add 0.3m error in the position estimate. Signal processing algorithms that could optimally select only useful spectrum eliminating the narrowband interference portion of the spectrum can help reduce this error. It is well known that multipath and NLOS are the two major contributors for indoor positioning with each adding error of 0.5m or more.

In addition to the above mentioned error sources, there is one error source that is less well known and can result in adding errors of 0.5m or more. This source of error is due to building material dielectric properties and needs to be accounted in the error analysis [1]. The building material dielectric properties result in adding delay to the transmitted signal and the RF wave inside the material is going to be slower than the propagation of the RF wave in free space. Some basic analysis on the expected errors due to building material dielectric

properties is discussed in next section. Overall it can be seen from Table 9.2 that the major error sources are NLOS, multipath and building material dielectric properties.

The optimized error budget shown in Table 9.2 is an approximate practical and realistic lower bound, based on extensive bench and field tests. The error contributions due to clock and oscillator drifts and shifts can be made negligible as they are in control of the system designer. The bigger error contributions of the receiver geometry and external interference can be minimized but cannot be made negligible as they are often not in control of the system designer. The major sources of errors like NLOS, multipath and dielectric properties not in the control of the system designer and are among the biggest contributors to the indoor position error.

Effect of Building Materials

Some basic study on effect of building materials dielectric properties on position estimation is presented in this section. The materials used in the construction of a building do have an effect on the positioning estimation accuracy inside that building. The most common building materials are concrete, bricks and wood. All of these materials have different dielectric constants, meaning that the propagation of the RF wave inside the material is going to be slower than the propagation of the RF wave in free space. This results in a position estimation error which will be dependent on the dielectric material of the building.

Consider an NLOS, multipath free example of positioning inside a brick building as shown in Figure 9.4. The four receivers, as shown in the figure, are outside the building and are equidistant from the transmitter located inside the building. The three sides of the building consist of brick walls and one side consists of a wooden wall. The transmitter inside the building transmits a signal which penetrates through the brick and wooden wall and is received by the four receivers outside. Similarly, Figure 9.5 shows an example of indoor positioning that has additional inner wooden walls on the three sides and Figure 9.6 shows an example that has additional inner brick walls on the three sides.

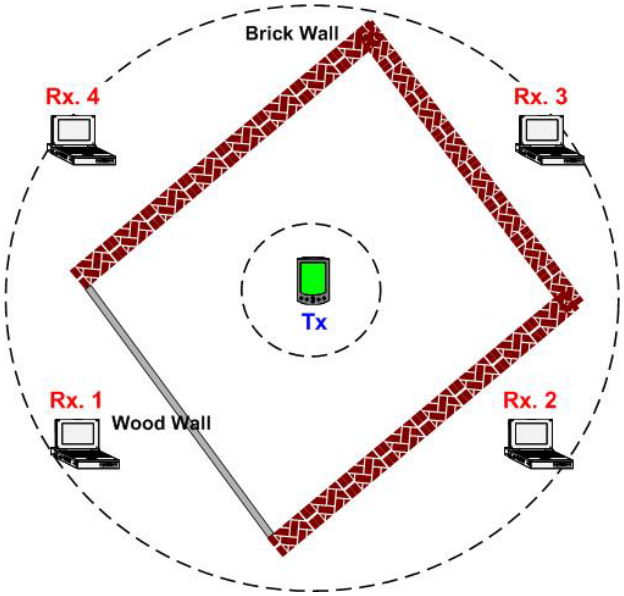

Figure 9.4 Indoor Positioning Case 1

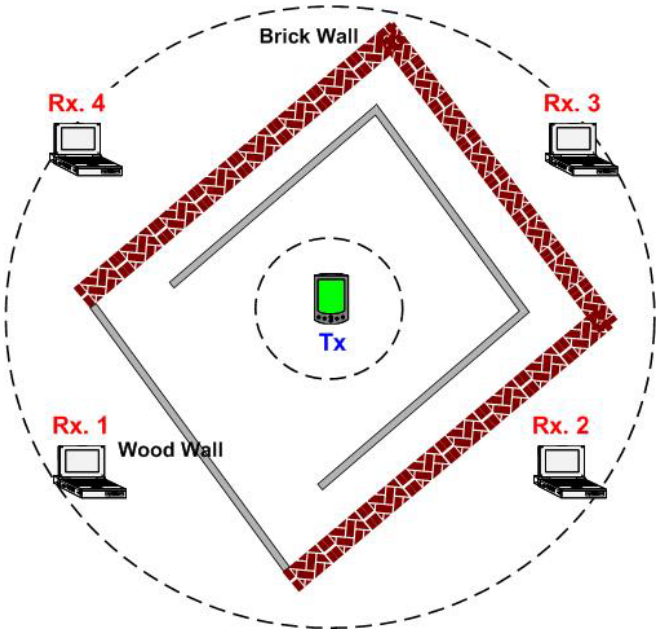

Figure 9.5 Indoor Positioning Case 2

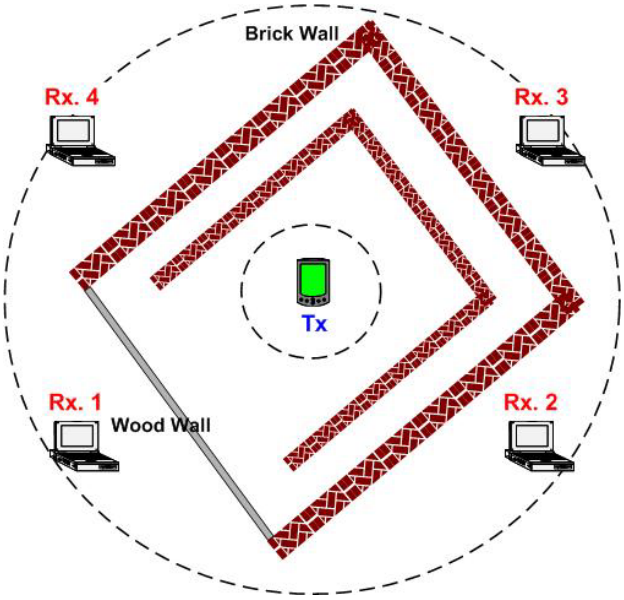

Figure 9.6 Indoor Positioning Case 3

Basic position estimation simulations [2] were performed for the three NLOS, multipath free cases depicted in Figure 9.4-Figure 9.6. The simulations do not consider the errors due to SNR degradation or due to multipath. The simulation results of position estimation errors for the above three cases are shown in Table 9.3. The case 1 results in positioning error of 0.412m. Case 2 results in increase in the positioning error just by adding one wooden wall and the error now becomes 0.483m. For case 3, simulates two brick walls which further increase the positioning error to 0.923m. The errors shown in this table are purely due to the difference in RF propagation speeds inside the brick wall and wooded wall due to their different relative dielectric constants. In the

simulations, the dielectric constant for brick wall was set to 4.5 and that for the wooden wall was set to 3.

Table 9.3 Position Estimation Errors Due to Building Materials

	Positioning Error
Case 1 - Figure 9.4	0.412m
Case 2 - Figure 9.5	0.483m
Case 3 - Figure 9.6	0.923m

From the errors it is clear that in addition to the well known error sources multipath and NLOS, the dielectric properties of the building materials add to the positioning error. To the best of author's knowledge no indoor positioning papers recognize and address this issue, which could very well be a fundamental limitation in indoor positioning system performance.

Existing indoor propagation models provide delay spread values, a part of which may be due to the building material dielectric properties. But for indoor positioning applications, the breakdown of this delay is required to understand how much of the total delay is caused due to multipath spread and how much of it is caused due to the building material. This breakdown of the observed delay is not at all important for indoor communication systems but takes significance when dealing with indoor positioning systems and is often forgotten or ignored while analyzing the positioning errors.

The indoor environment typically has more than two walls and just this could lead to indoor positioning errors of more than 2m-3m, depending on number of walls, the dielectric constant of the wall material, frequency and weather. The dielectric constants of the building materials are frequency dependent and also weather dependent and could vary significantly. For example depending on the type of wood, its dielectric will vary from 2 to 5 and depending on the frequency the dielectric for concrete varies from 26 to 10 over 50MHz to 1GHz [3].

Figure 9.7 shows the delay for various wall thicknesses due to different dielectric constants that will depend on the building material. The frequency dependent and weather dependent dielectric constant curves for commonly used building materials are unavailable. There is a need to perform tests that will result in such data which can then be used to calibrate the system thus minimizing the errors on indoor position estimates due to building dielectric material properties. Thus, this not so well known source of error needs to be considered in designing an indoor positioning system if accuracies of less than 3m are desired.

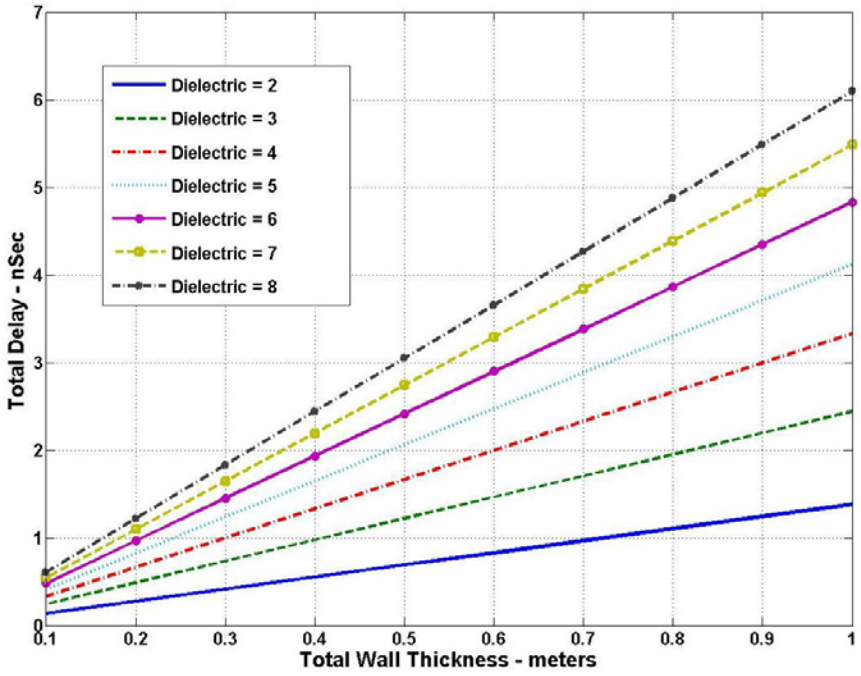

Figure 9.7 Signal Delay vs. Wall Thickness for Various Dielectric Constants

Thesis Summary

The thesis provided detailed insights to the following topics that were not previously available in the literature.

The simulations comparing the IR-UWB and MC-UWB based indoor positioning systems led to an important revelation that a multicarrier based positioning system is preferred over impulse radio based positioning systems. This is in contrast to the commonly seen literature that strongly associates precise positioning with IR-UWB.

To validate the above simulations, it was necessary to develop a field deployable MC-UWB based RF prototype. To simplify the RF design and development this thesis proposed to implement unmodulated and non orthogonal multicarrier signal structure. This also makes it possible to use simpler narrowband design techniques for RF evaluation. ADS simulations in conjunction with experimental results provided justification for using narrowband techniques to design a wide band system. The thesis also presented initial RF design parameters followed by successful cable tests that confirmed the theory of using multicarrier signals for positioning which was an important first step to develop the system further.

Further evaluation and testing provided insight to non-intuitive systemic issues resulting from direct down conversion type receiver architecture

when transmitting a Double Side Band (DSB). The thesis proposed using Single Side Band (SSB) radio architecture when using multicarrier signal. Such an optimized 24% fractional bandwidth MC-UWB RF system was designed that under controlled cable testing shows improvement in positioning accuracy by approximately four times over the non optimized RF design.

Finally the extensive experimental results using the optimized RF system lead to a realistic Total System Error (TSE) for multicarrier positioning systems. This TSE led to identification of an important error source resulting due to building dielectric materials, which to the best of author's knowledge has been forgotten and ignored by all other existing literature on positioning systems. This building dielectric material effect on positioning accuracy could be an important limitation in improving positioning accuracy to within 1m, and is topic for future research.

References

[1] H. K. Parikh, W. R. Michalson, "RF Based Indoor Positioning System and Its Error Sources", To Appear: *IEEE Proc. International Conference on Acoustics Speech and Signal Processing*, Las Vegas, NV, March 30-April 4 2008

[2] B. Friedlander, "A Passive Localization Algorithm and Its Accuracy Analysis", *IEEE Journal of Oceanic Engineering*, Vol. OE-12, No 1, pp. 234-245, January 1987

[3] R. Antoine, "Dielectric Permittivity of concrete between 50MHz and 1GHz and GPR measurements for building materials evaluation", *Journal of Applied Geophysics*, Vol. 40, pp. 89-94, 1998

Appendix A: Transmitter RF Design

Schematics

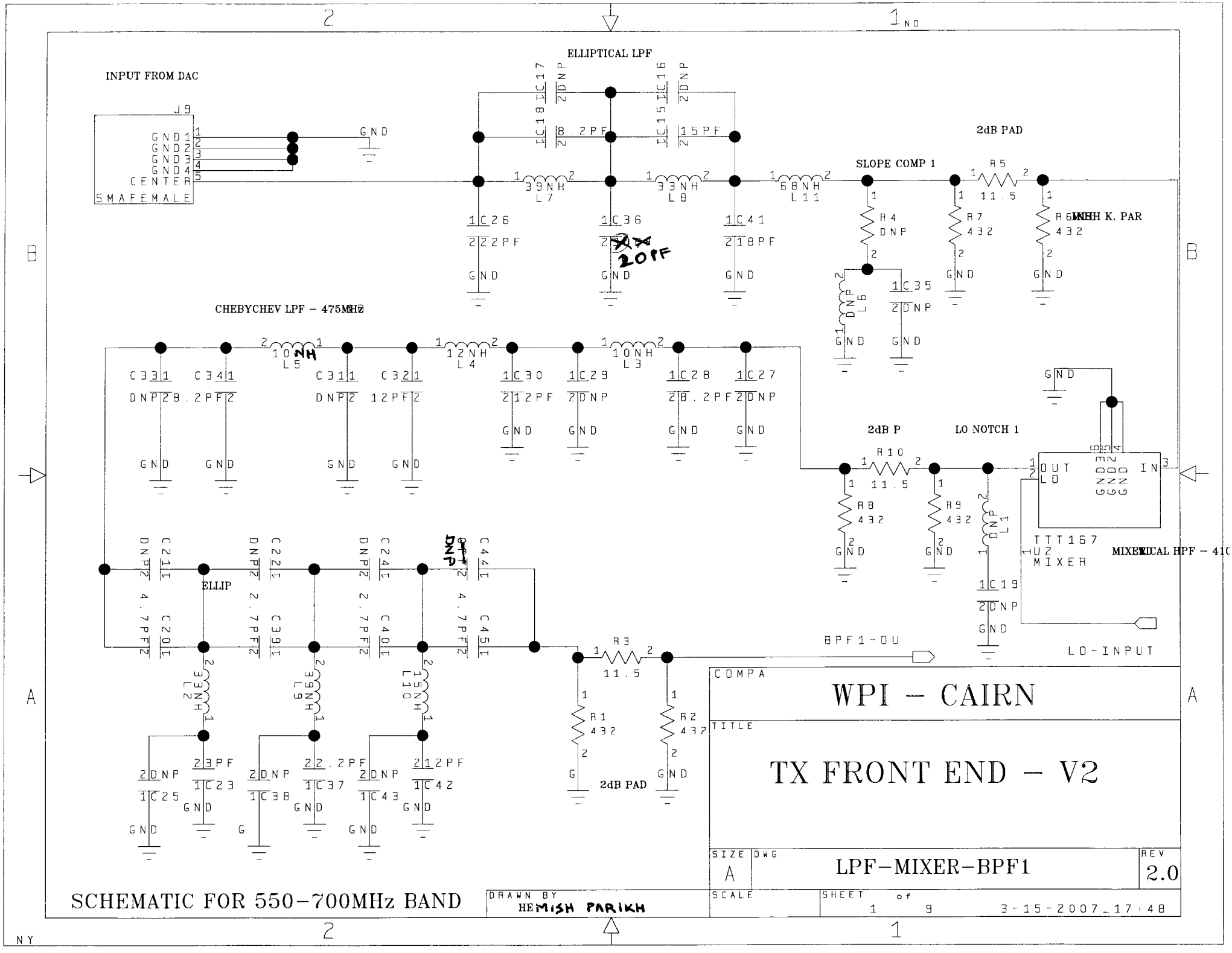
INPUT FROM DAC
J9
GND1
GND2
GND3
GND4
CENTER
SMAFEMALE
GND
ELLIPTICAL LPF
IC18 IC17 2DNP
IC15 IC16 2DNP
2B.2PF
15PF
39NH L7
33NH L8
68NH L11
1C26 22PF
1C36 20PF
1C41 18PF
2dB PAD
SLOPE COMP 1
R5 11.5
R4 DNP
R7 432
R6 432
1C35 2DNP
L6 DNP
CHEBYCHEV LPF – 475MHz
10NH L5
12NH L4
10NH L3
C331 DNP2 8.2PF2
C341
C311 DNP2 12PF2
C321
1C30 12PF
1C29 2DNP
1C28 8.2PF
1C27 2DNP
2dB P
LO NOTCH 1
R10 11.5
R8 432
R9 432
L1 DNP
1C19 2DNP
TTT167
U2
MIXER
GND2
GND3
DOUT
LO
IN
C211 DNP2 4.7PF2
C201
C221 DNP2 2.7PF2
C231
C241 DNP2 2.7PF2
C251
C441 4.7PF2
C451
ELLIP
L12 3NH
L9 3NH
L10 15NH
1C25 2DNP
1C23 3PF
1C38 2DNP
1C37 2.2PF
1C43 2DNP
1C42 12PF
R3 11.5
R1 432
R2 432
2dB PAD
BPF1-OU
LO-INPUT
COMPA
WPI – CAIRN
TITLE
TX FRONT END – V2
SIZE A
DWG
LPF–MIXER–BPF1
REV 2.0
DRAWN BY HEMISH PARIKH
SCALE
SHEET 1 of 9
3-15-2007_17:48
SCHEMATIC FOR 550–700MHz BAND

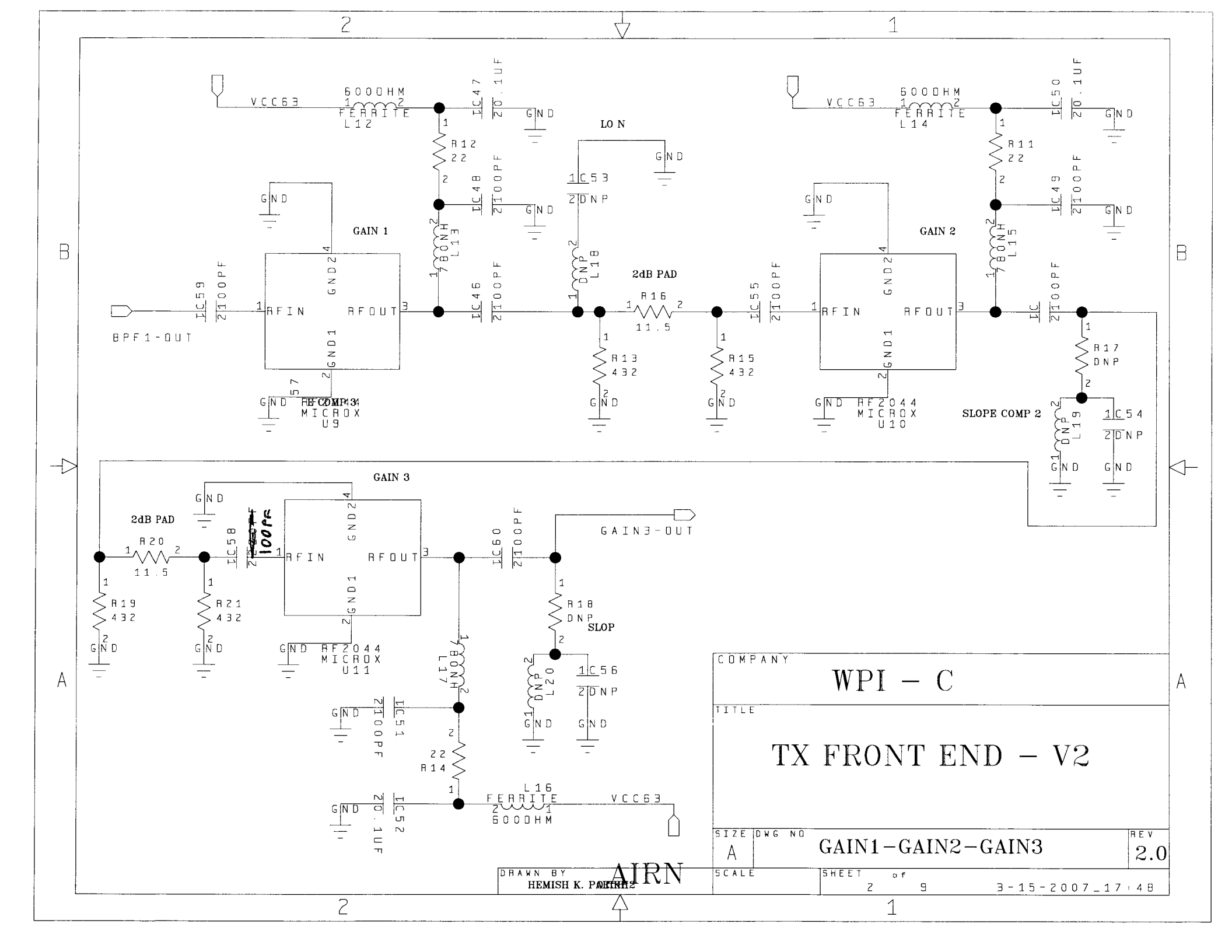
VCC63
600OHM FERRITE L12
IC47 20.1UF
GND
R12 22
IC48 2100PF
LO N
C53 DNP
L13 780NH
DNP L18
GAIN 1
2dB PAD
R16 11.5
IC59 2100PF
IC46 2100PF
IC55 2100PF
BPF1-OUT
RFIN
RFOUT
GND2
GND1
R13 432
R15 432
RF2044 MICROX U9
RF2044 MICROX U10
VCC63
600OHM FERRITE L14
IC50 20.1UF
R11 22
IC49 2100PF
L15 780NH
GAIN 2
IC 2100PF
R17 DNP
C54 DNP
L19 DNP
SLOPE COMP 2
GAIN 3
2dB PAD
R20 11.5
IC58 100PF
R19 432
R21 432
IC60 2100PF
GAIN3-OUT
R18 DNP
SLOP
L20 DNP
C56 DNP
L17 780NH
IC51 2100PF
22 R14
IC52 20.1UF
L16 FERRITE 600OHM
VCC63
COMPANY
WPI – C
TITLE
TX FRONT END – V2
SIZE A
DWG NO GAIN1–GAIN2–GAIN3
REV 2.0
DRAWN BY HEMISH K. PATEL
AIRN
SCALE
SHEET 2 of 9
3-15-2007_17:48

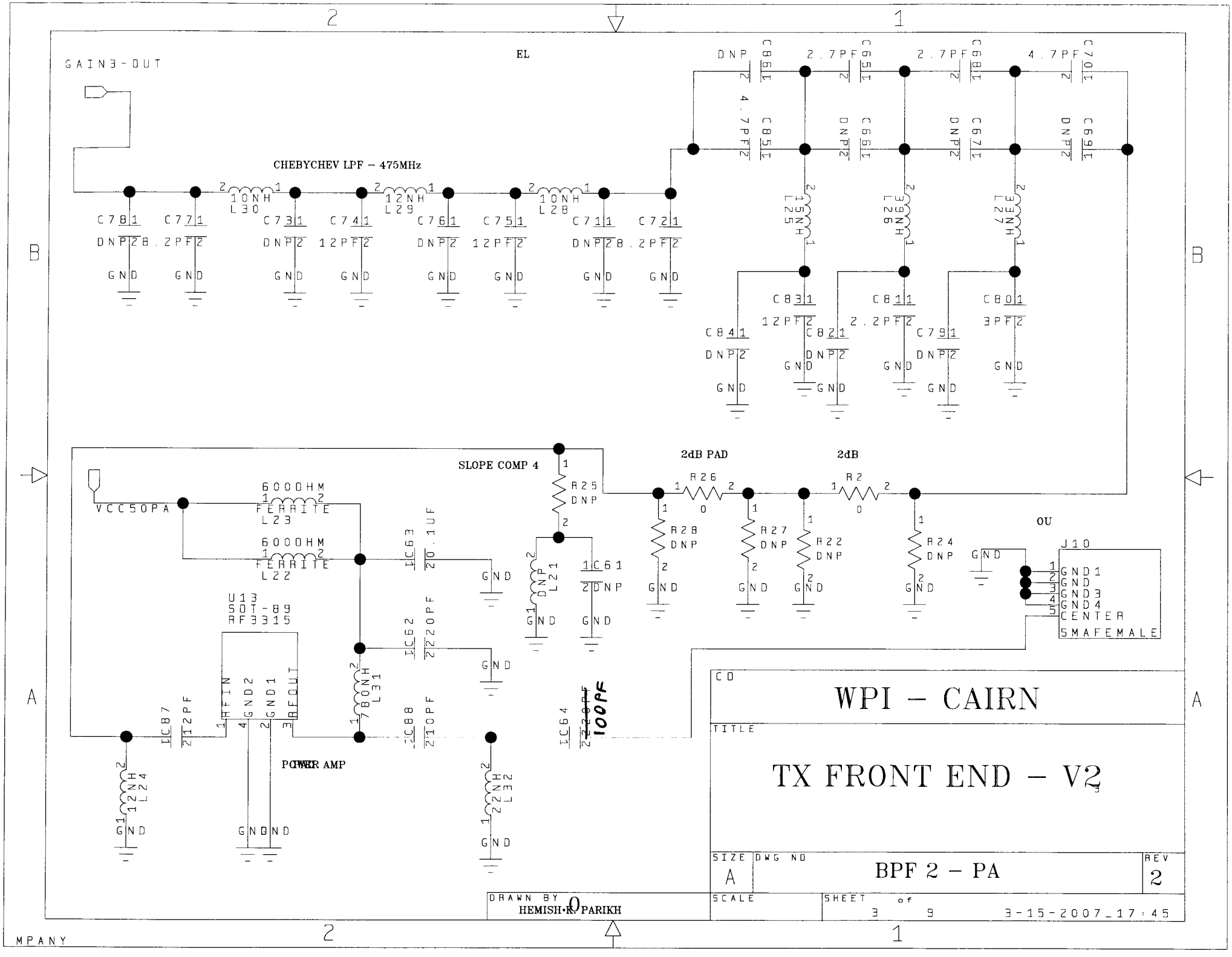
GAIN3-OUT
EL
CHEBYCHEV LPF – 475MHz
SLOPE COMP 4
2dB PAD
2dB
VCC5OPA
POWER AMP
WPI – CAIRN
TX FRONT END – V2
BPF 2 – PA
HEMISH K PARIKH
3-15-2007_17:45

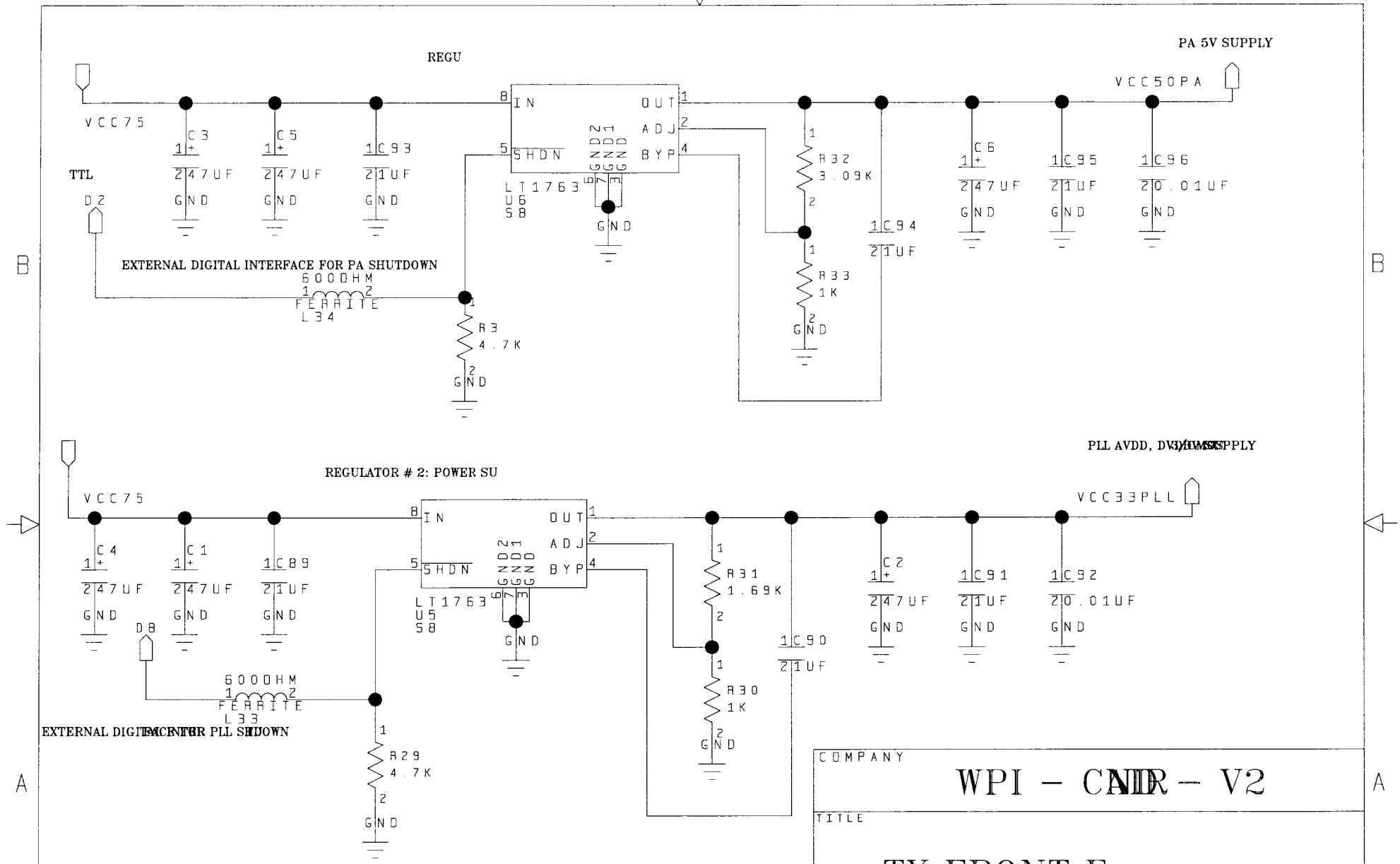
REGU
PA 5V SUPPLY
VCC75
C3
247UF
GND
C5
247UF
GND
C93
21UF
GND
TTL
D2
EXTERNAL DIGITAL INTERFACE FOR PA SHUTDOWN
600OHM
FERRITE
L34
R3
4.7K
GND
LT1763
U6
S8
IN
OUT
SHDN
ADJ
BYP
GND2
GND1
GND
R32
3.09K
R33
1K
C94
21UF
C6
247UF
C95
21UF
C96
20.01UF
VCC50PA
REGULATOR # 2: POWER SU
PLL AVDD, DV
SUPPLY
VCC75
C4
247UF
C1
247UF
C89
21UF
D8
600OHM
FERRITE
L33
R29
4.7K
LT1763
U5
S8
R31
1.69K
R30
1K
C90
21UF
C2
247UF
C91
21UF
C92
20.01UF
VCC33PLL
DNP R34, R29, R38 TO BYPASS SHTD MOD
WIRE J1.2, J1.3, J1.8 TO J
AND WIRE J1.2, J1.3, J1.8 to J2.1 or J3.3
COMPANY
WPI – CAMDR – V2
TITLE
TX FRONT E
SIZE
A
DWG NO
POWER 5V – PLL & PA
REV
2.0
DRAWN BY
HEMISH K. PARIKH
SCALE
SHEET
4 of 9
3-15-2007_17:12

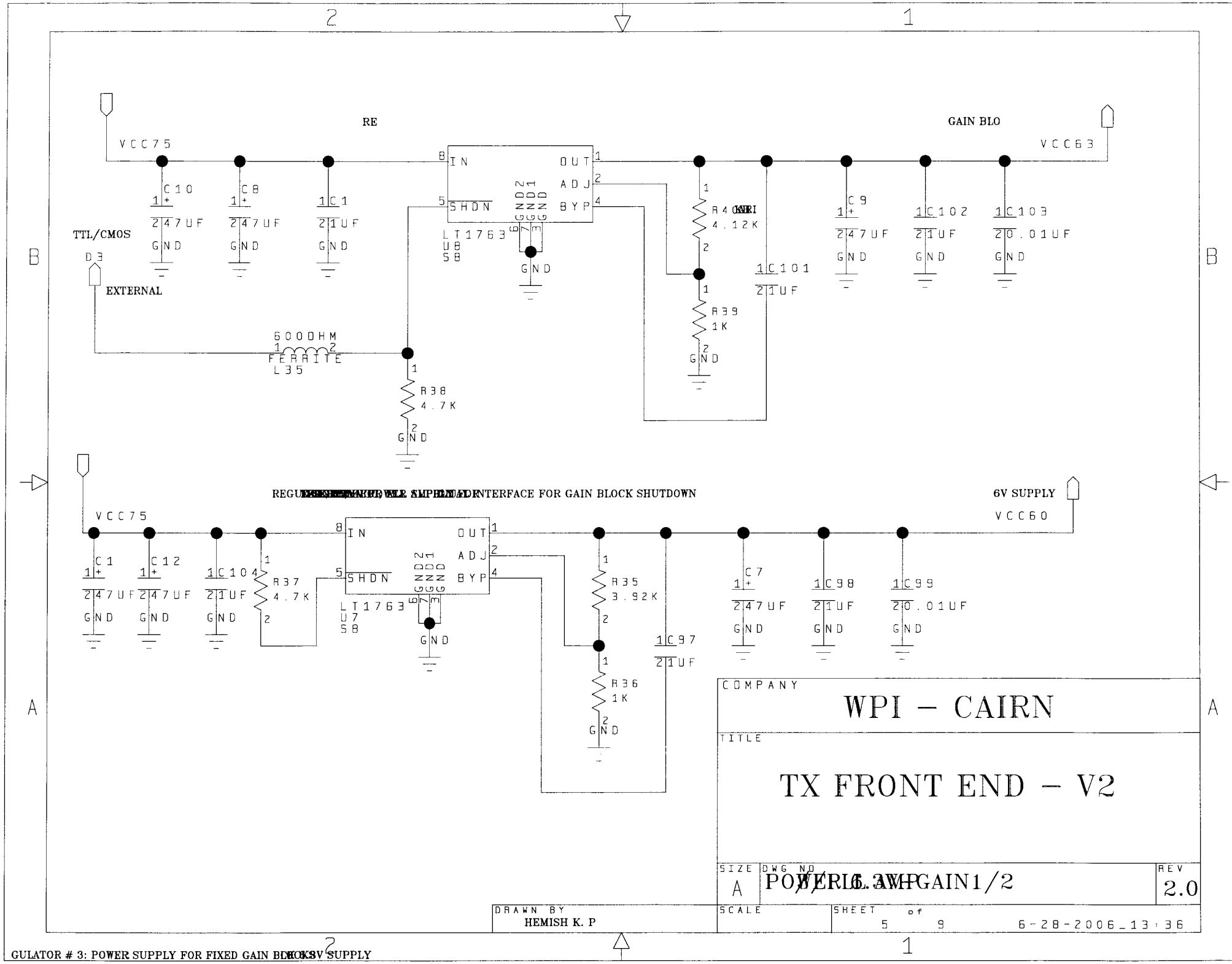
RE
GAIN BLO
VCC75
VCC63
C10
247UF
C8
247UF
C1
21UF
IN
OUT
ADJ
SHDN
BYP
GND2
GND1
GND
LT1763
U8
S8
R40
4.12K
C9
247UF
C102
21UF
C103
20.01UF
TTL/CMOS
D3
EXTERNAL
600OHM
FERRITE
L35
R38
4.7K
R39
1K
C101
21UF
REGU
INTERFACE FOR GAIN BLOCK SHUTDOWN
6V SUPPLY
VCC60
C1
247UF
C12
247UF
C104
21UF
R37
4.7K
LT1763
U7
S8
R35
3.92K
R36
1K
C97
21UF
C7
247UF
C98
21UF
C99
20.01UF
COMPANY
WPI – CAIRN
TITLE
TX FRONT END – V2
SIZE
A
DWG NO
POWER_3V_GAIN1/2
REV
2.0
DRAWN BY
HEMISH K. P
SCALE
SHEET
5 of 9
6-28-2006_13:36
GULATOR # 3: POWER SUPPLY FOR FIXED GAIN BLOCKS
6V SUPPLY

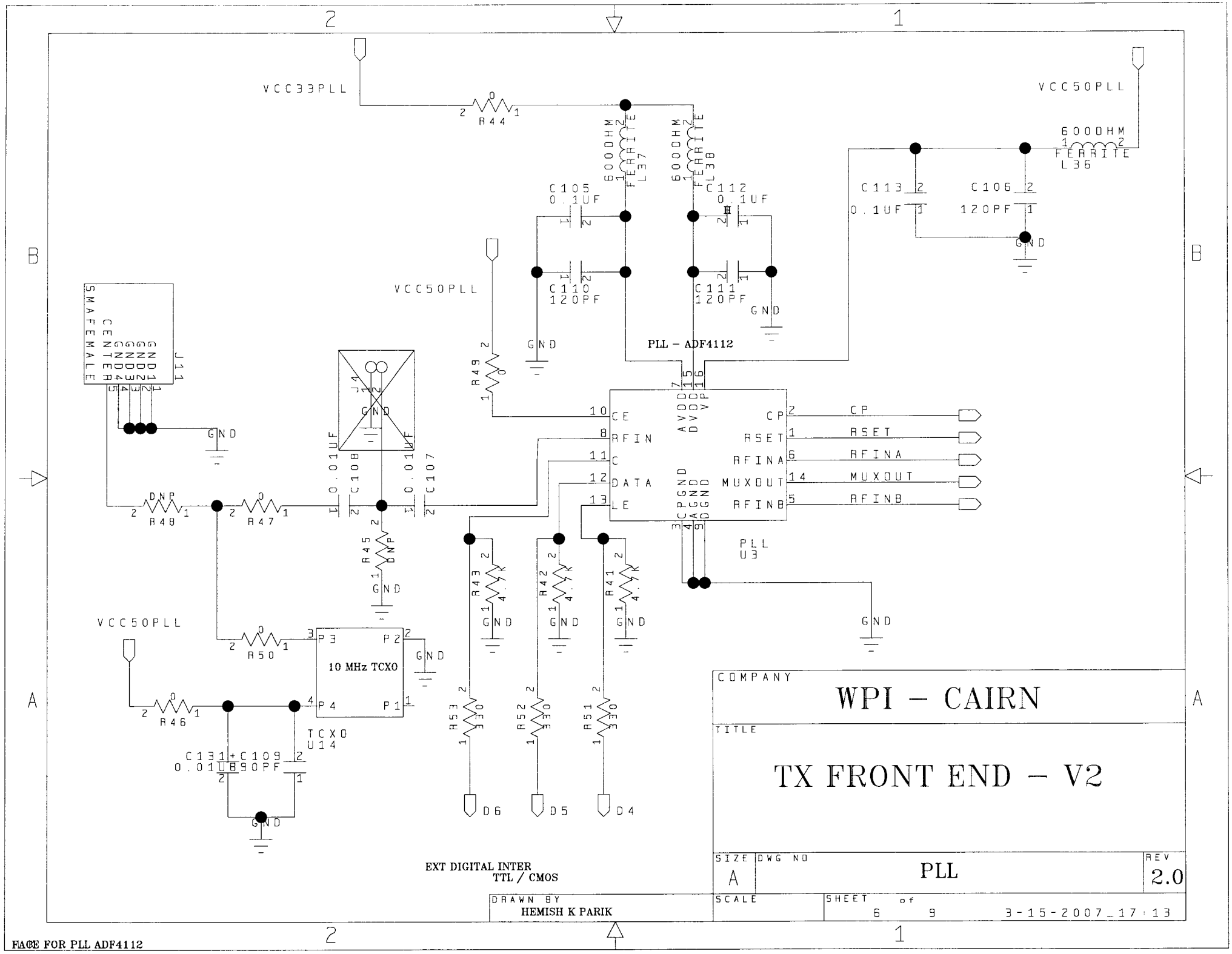
VCC33PLL
R44
0
600OHM FERRITE L37
600OHM FERRITE L38
VCC50PLL
600OHM FERRITE L36
C105 0.1UF
C112 0.1UF
C113 0.1UF
C106 120PF
C110 120PF
C111 120PF
GND
PLL – ADF4112
R49
SMAFEMALE CENTER GND1 GND2 GND3 GND4 J11
J4
0.01UF C108
0.01UF C107
DNP R48
R47
R45 DNP
CE
RFIN
C
DATA
LE
AVDD DVDD VP
CP
RSET
RFINA
MUXOUT
RFINB
AGND DGND CPGND
CP
RSET
RFINA
MUXOUT
RFINB
PLL U3
R43 4.7K
R42 4.7K
R41 4.7K
R50
10 MHz TCXO
P3 P2 P4 P1
R46
TCXO U14
C131+C109 0.01UF 50PF
R53 330
R52 330
R51 330
D6
D5
D4
EXT DIGITAL INTER
TTL / CMOS
COMPANY
WPI – CAIRN
TITLE
TX FRONT END – V2
SIZE A
DWG NO PLL
REV 2.0
DRAWN BY HEMISH K PARIK
SCALE
SHEET 6 of 9
3-15-2007_17:13
FACE FOR PLL ADF4112

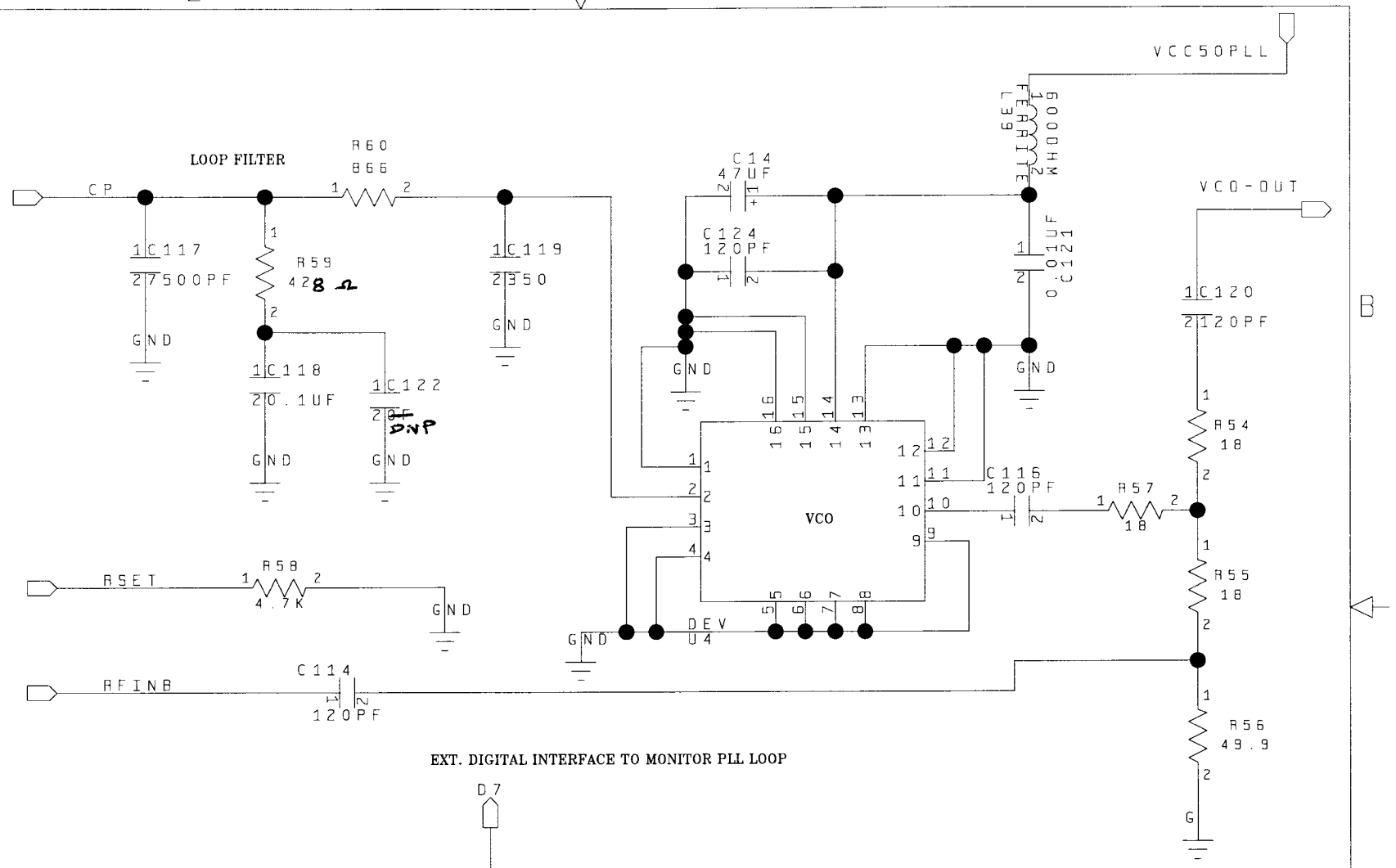

COMPANY: WPI – CAIRN			
TITLE: TX FRONT			
SIZE: A	DWG NO: PLL		REV: 2.0
DRAWN BY: HEMISH K PARIKH	SCALE:	SHEET: 7 of 9	3-15-2007_17:15

END – V2

ICE=VCO

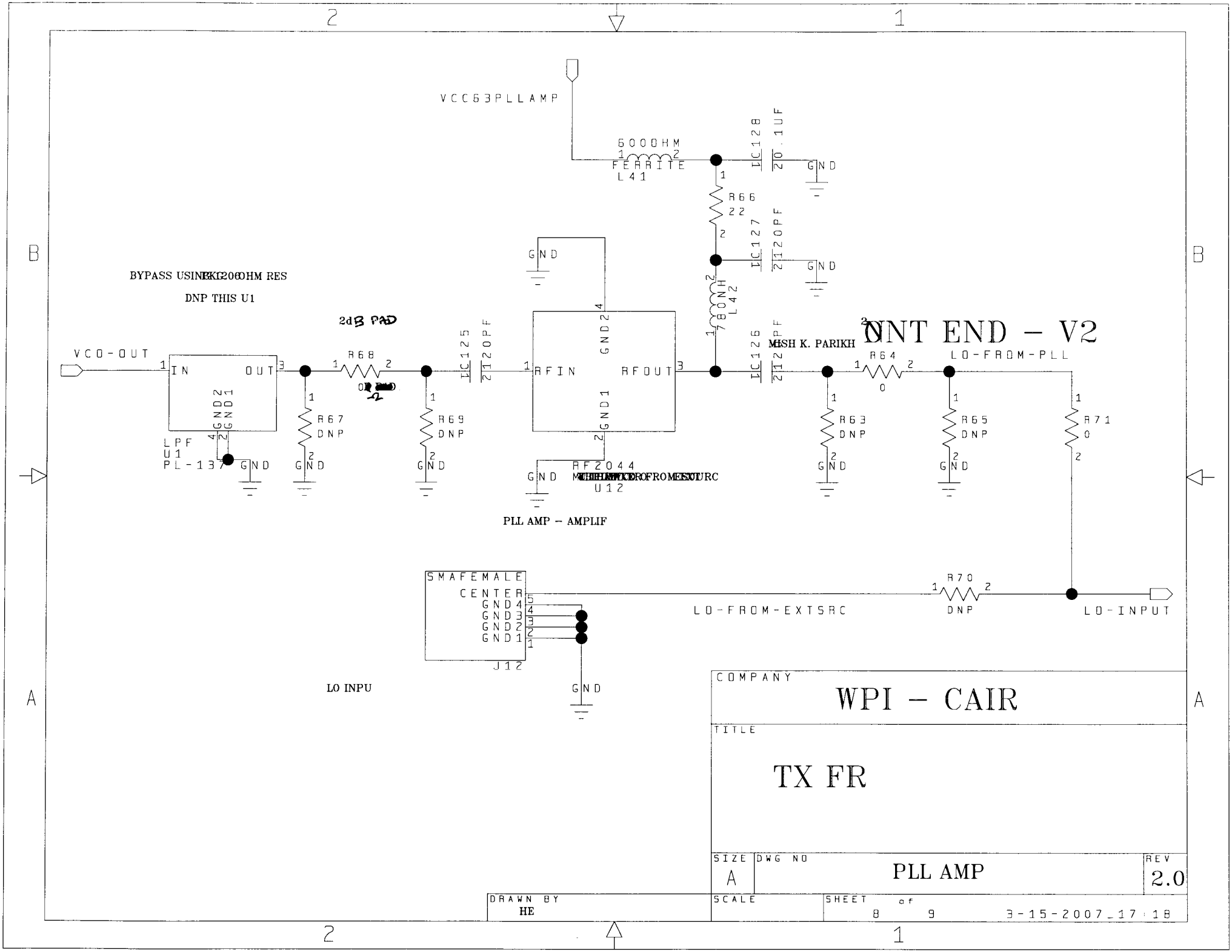
VCC63PLLAMP
600OHM
FERRITE
L41
C128
0.1UF
GND
R66
22
C127
120PF
780NH
L42
C126
120PF
BYPASS USING 2000HM RES
DNP THIS U1
2dB PAD
VCO-OUT
IN
OUT
GND2
GND1
LPF
U1
PL-137
R68
R67
DNP
R69
DNP
C125
120PF
RFIN
RFOUT
GND2
GND1
RF2044
U12
R64
0
LO-FROM-PLL
R63
DNP
R65
DNP
R71
0
SMAFEMALE
CENTER
GND4
GND3
GND2
GND1
J12
LO-FROM-EXTSRC
R70
DNP
LO-INPUT
PLL AMP – AMPLIF
LO INPU
MISH K. PARIKH
NT END – V2
COMPANY
WPI – CAIR
TITLE
TX FR
SIZE
A
DWG NO
PLL AMP
REV
2.0
DRAWN BY
HE
SCALE
SHEET
8 9
3-15-2007_17:18

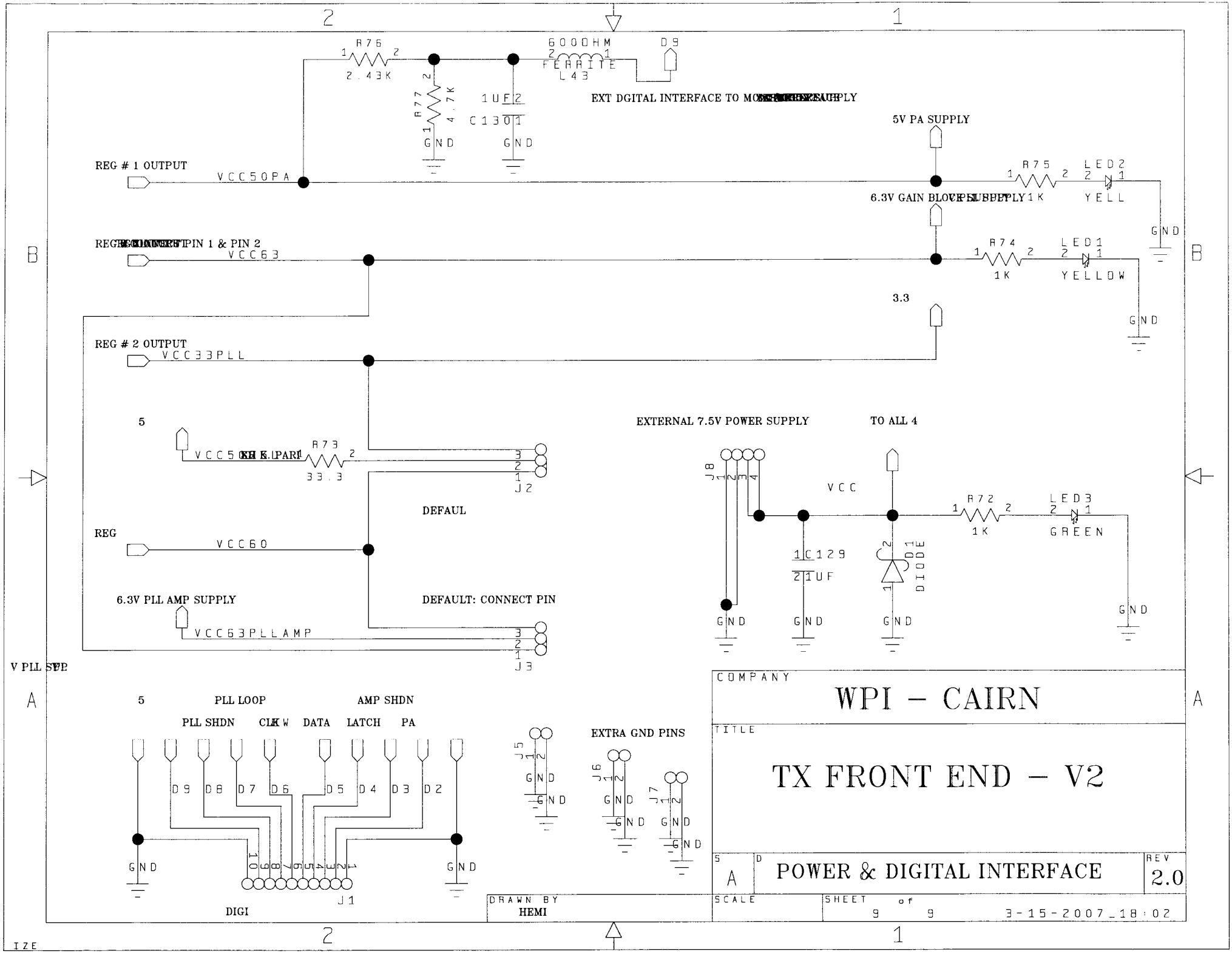
R76
2.43K
600OHM
FERRITE
L43
D9
R77
4.7K
GND
1UF
C1301
GND
EXT DGITAL INTERFACE TO MO
5V PA SUPPLY
REG # 1 OUTPUT
VCC50PA
R75
1K
LED2
YELL
6.3V GAIN BLO
GND
REG
PIN 1 & PIN 2
VCC63
R74
1K
LED1
YELLOW
GND
3.3
REG # 2 OUTPUT
VCC33PLL
GND
5
R73
33.3
J2
DEFAUL
EXTERNAL 7.5V POWER SUPPLY
TO ALL 4
J8
VCC
R72
1K
LED3
GREEN
1C129
21UF
D1
DIODE
GND
GND
GND
GND
REG
VCC60
6.3V PLL AMP SUPPLY
DEFAULT: CONNECT PIN
VCC63PLLAMP
J3
V PLL SUP
5
PLL LOOP
AMP SHDN
PLL SHDN
CLK
W
DATA
LATCH
PA
D9
D8
D7
D6
D5
D4
D3
D2
GND
GND
J1
DIGI
J5
GND
GND
EXTRA GND PINS
J6
GND
GND
J7
GND
GND
COMPANY
WPI – CAIRN
TITLE
TX FRONT END – V2
S
A
D
POWER & DIGITAL INTERFACE
REV
2.0
DRAWN BY
HEMI
SCALE
SHEET
of
9
9
3-15-2007_18:02
IZE

PCB Layout

transmitter_v3.pcb - Mon Sep 18 14:48:59 2006

FINAL

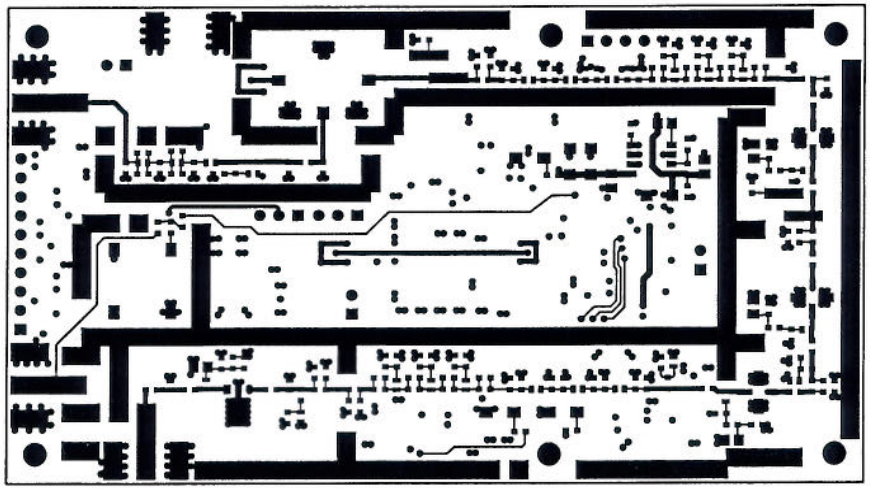

ARTTOP.pho – Mon Sep 18 14:48:53 2006

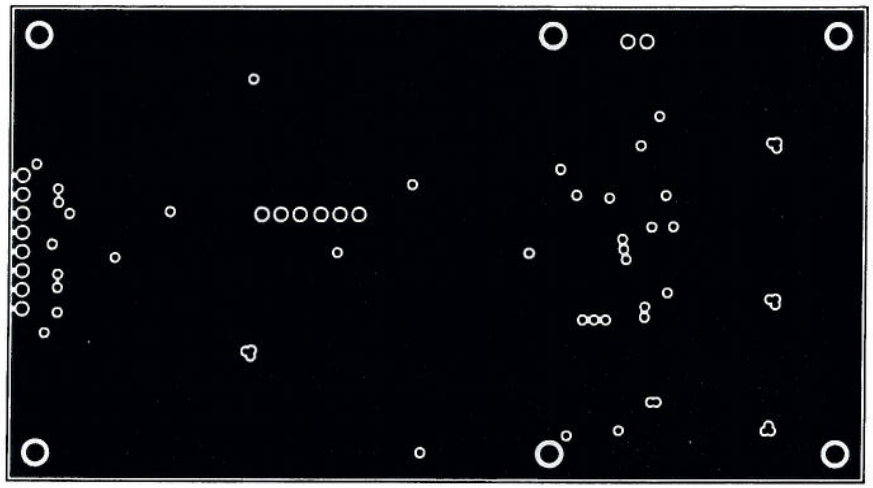

ARTL2.pho - Mon Sep 18 14:48:53 2006

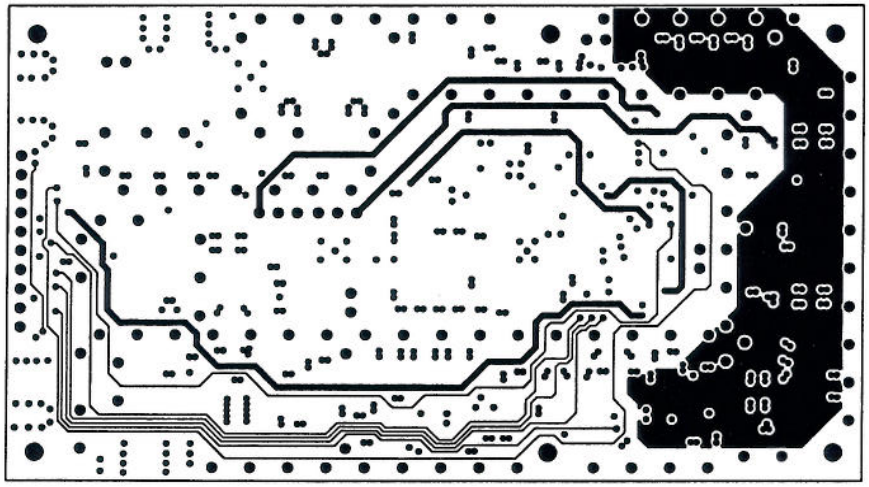

ARTL3.pho – Mon Sep 18 14:48:54 2006

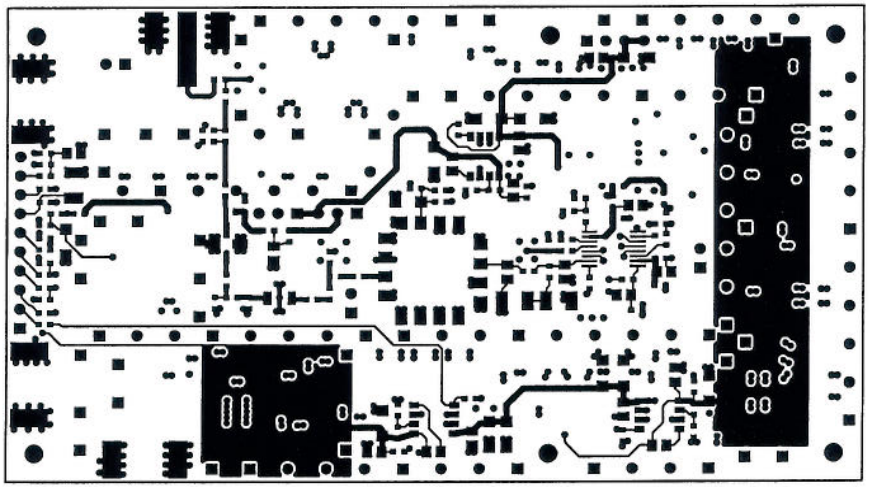

ARTBOT.pho – Mon Sep 18 14:48:53 2006

Appendix B: Receiver RF Design

Schematics

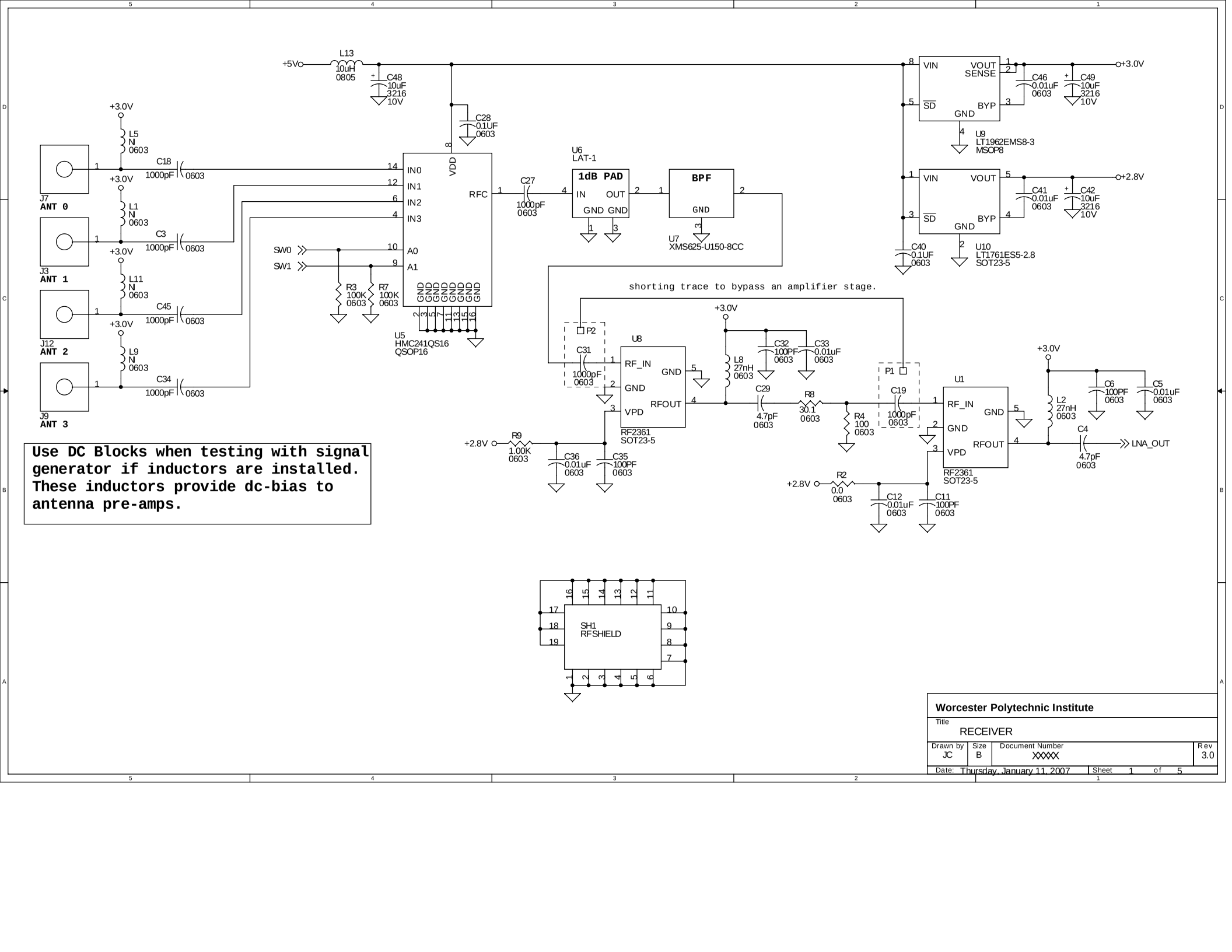

Use DC Blocks when testing with signal generator if inductors are installed. These inductors provide dc-bias to antenna pre-amps.

Worcester Polytechnic Institute			
Title: RECEIVER			
Drawn by: JC	Size: B	Document Number: XXXXX	Rev: 3.0
Date: Thursday, January 11, 2007	Sheet 1 of 5		

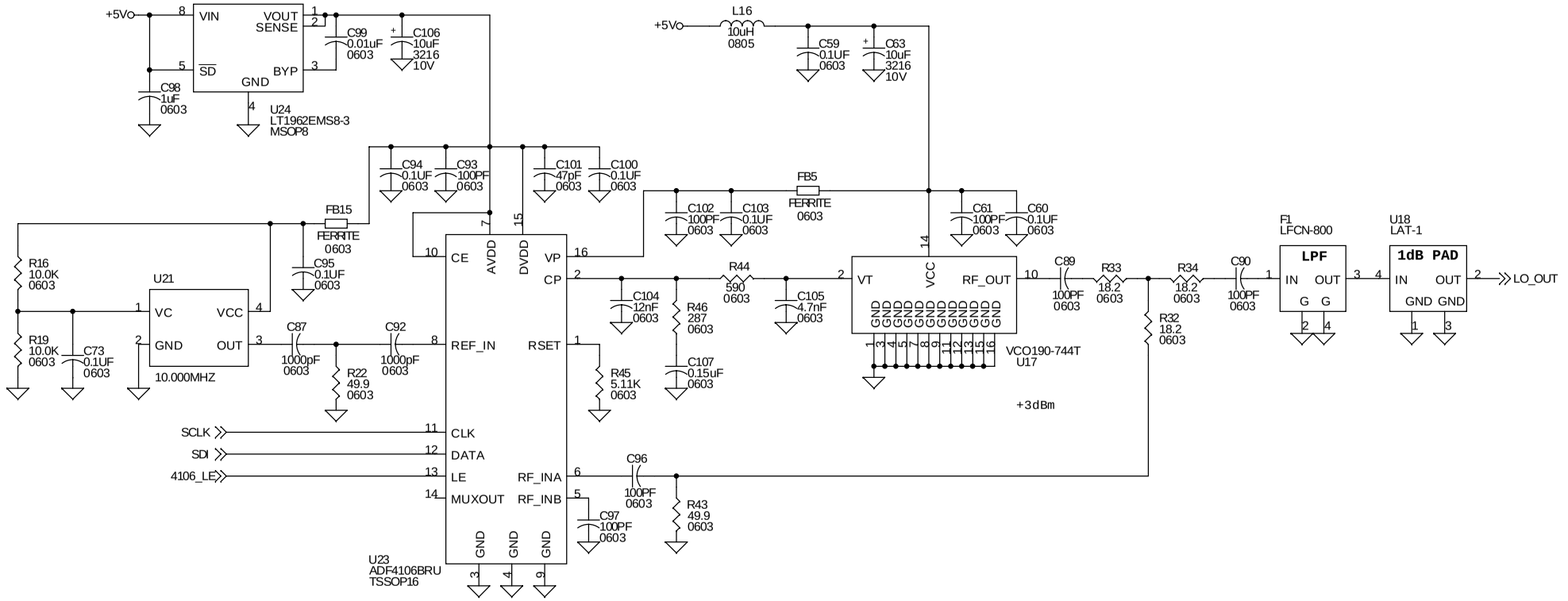

Worcester Polytechnic Institute			
Title: RECEIVER			
Drawn by: JC	Size: B	Document Number: XXXXX	Rev: 3.0
Date: Thursday, January 11, 2007	Sheet 2 of 5		

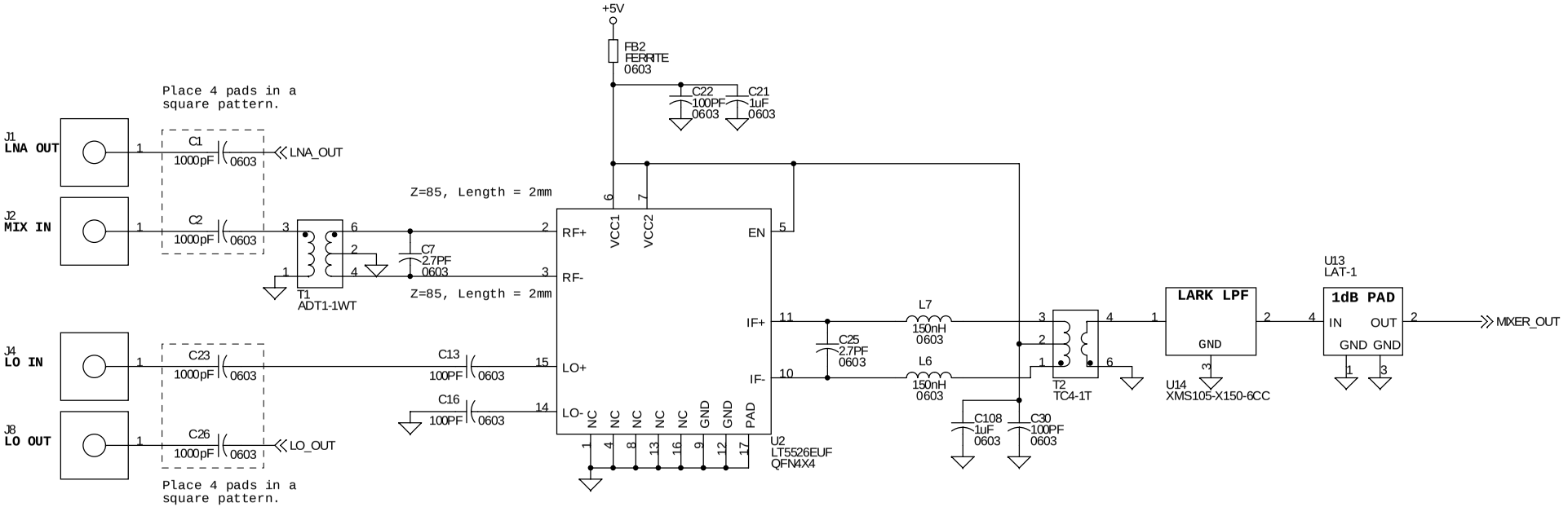

LO input level = -5dBm

Worcester Polytechnic Institute			
Title: RECEIVER			
Drawn by: JC	Size: B	Document Number: XXXXX	Rev: 3.0
Date: Thursday, January 11, 2007	Sheet 3 of 5		

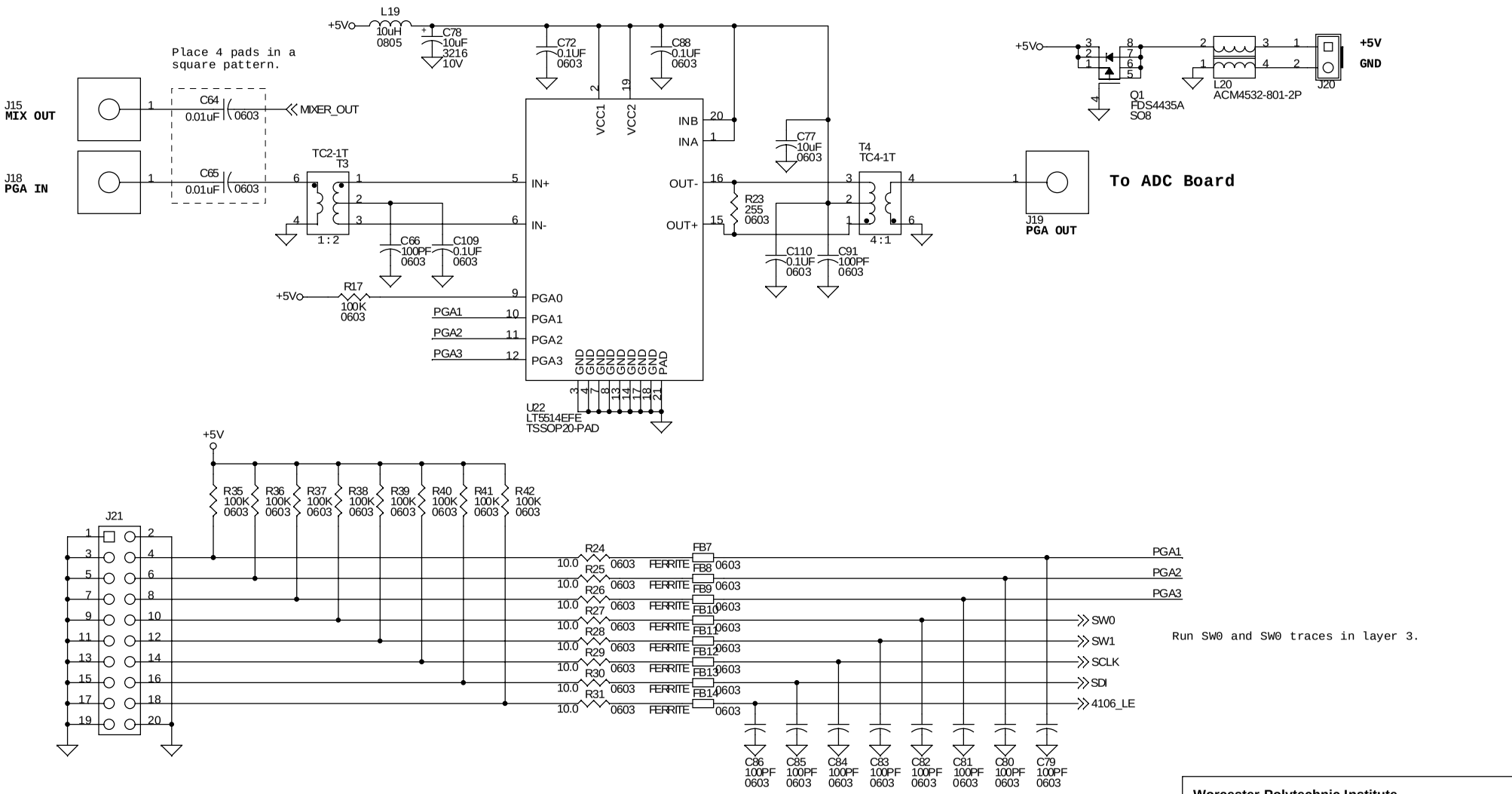

Worcester Polytechnic Institute			
Title: RECEIVER			
Drawn by: JC	Size: B	Document Number: XXXXX	Rev: 3.0
Date: Thursday, January 11, 2007	Sheet 4 of 5		

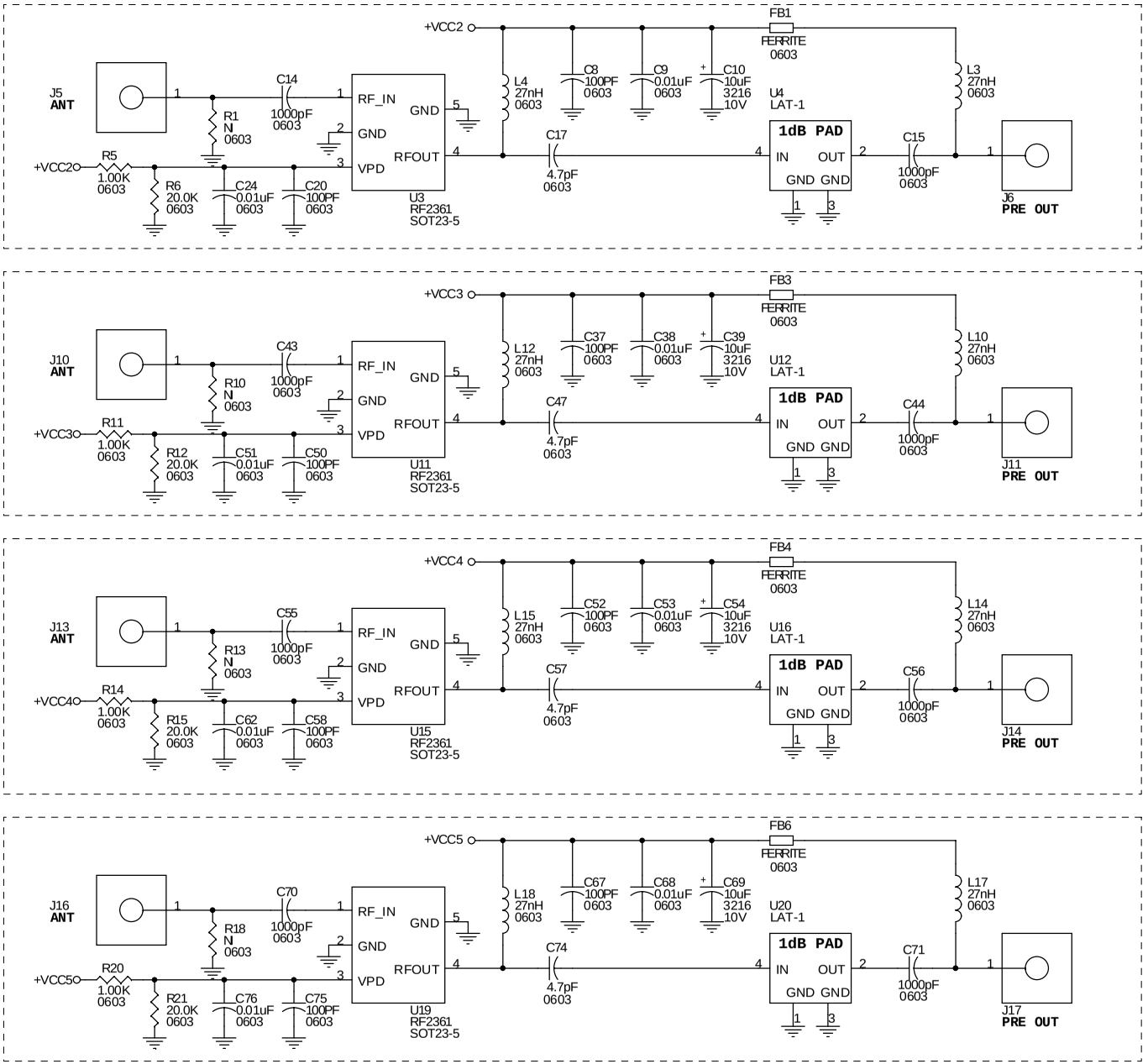

These 4 optional pre-amps can be used right at the antenna base before the coax cable. These 4 individual circuits should be placed on one side of the board with V-score lines.

The metal box for the antenna pre-amp is Pomona 2399.

Worcester Polytechnic Institute			
Title: RECEIVER			
Drawn by: JC	Size: B	Document Number: XXXXX	Rev: 3.0
Date: Thursday, January 11, 2007	Sheet 5 of 5		

PCB Layout

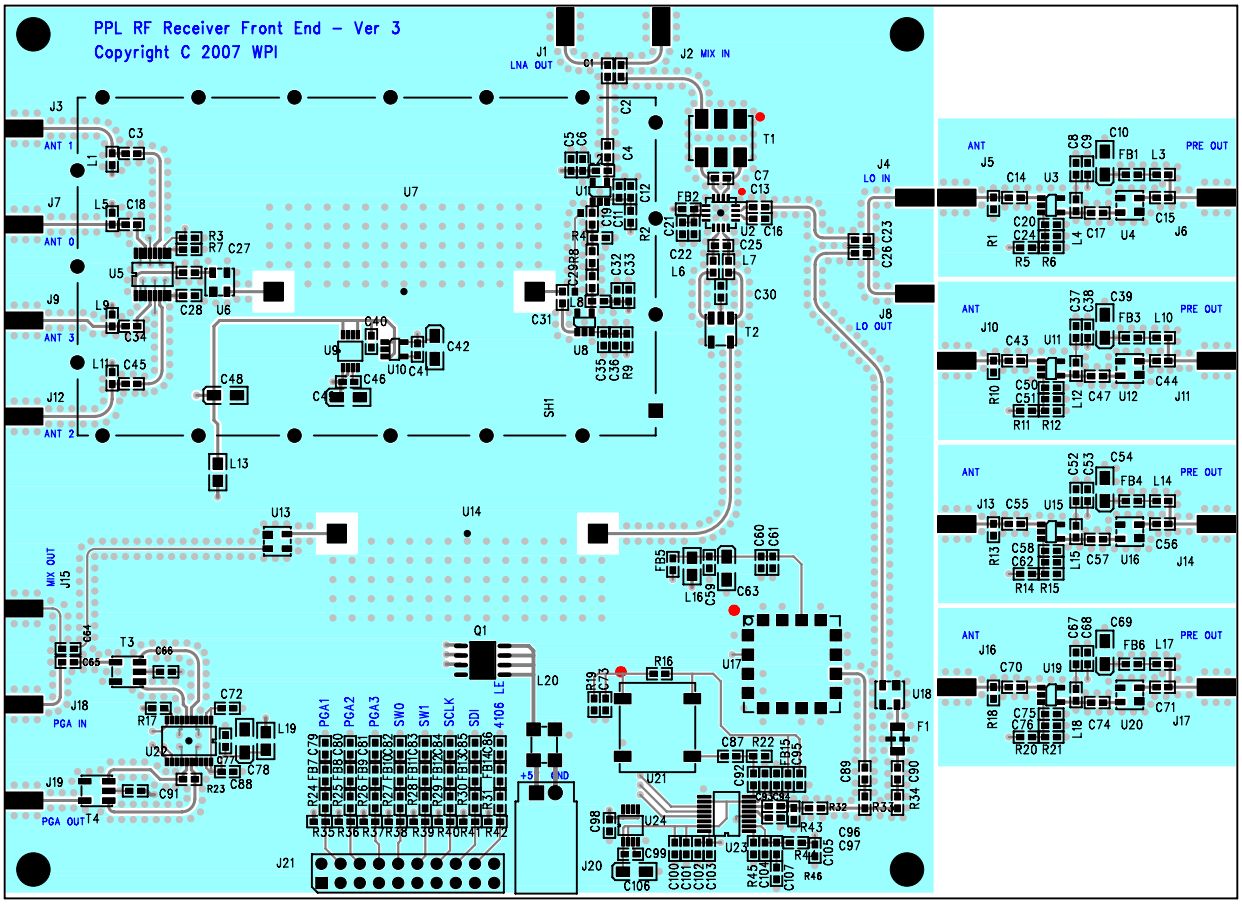

RECEIVER REV 3.pcb – Thu Jan 11 23:34:00 2007

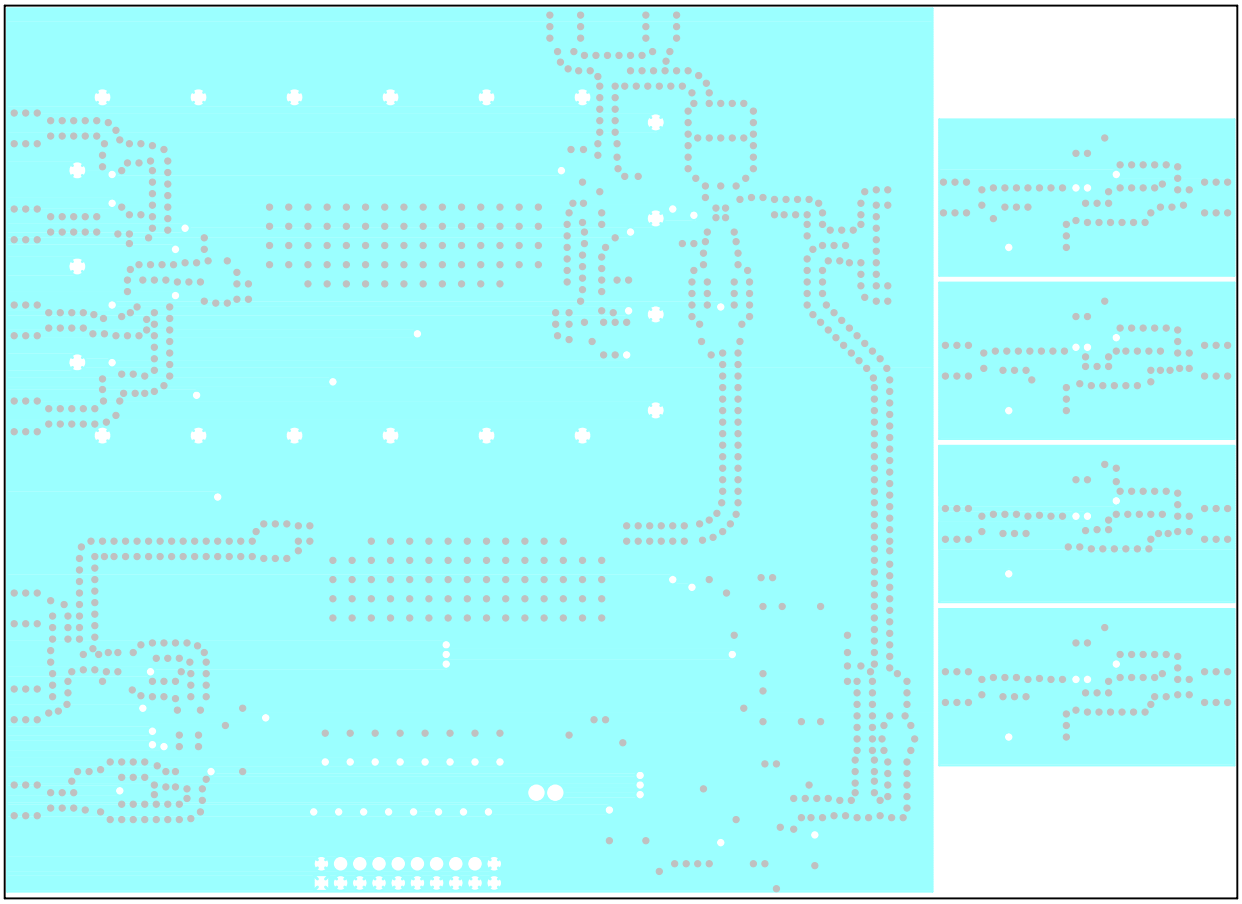

RECEIVER REV 3.pcb – Thu Jan 11 23:38:22 2007

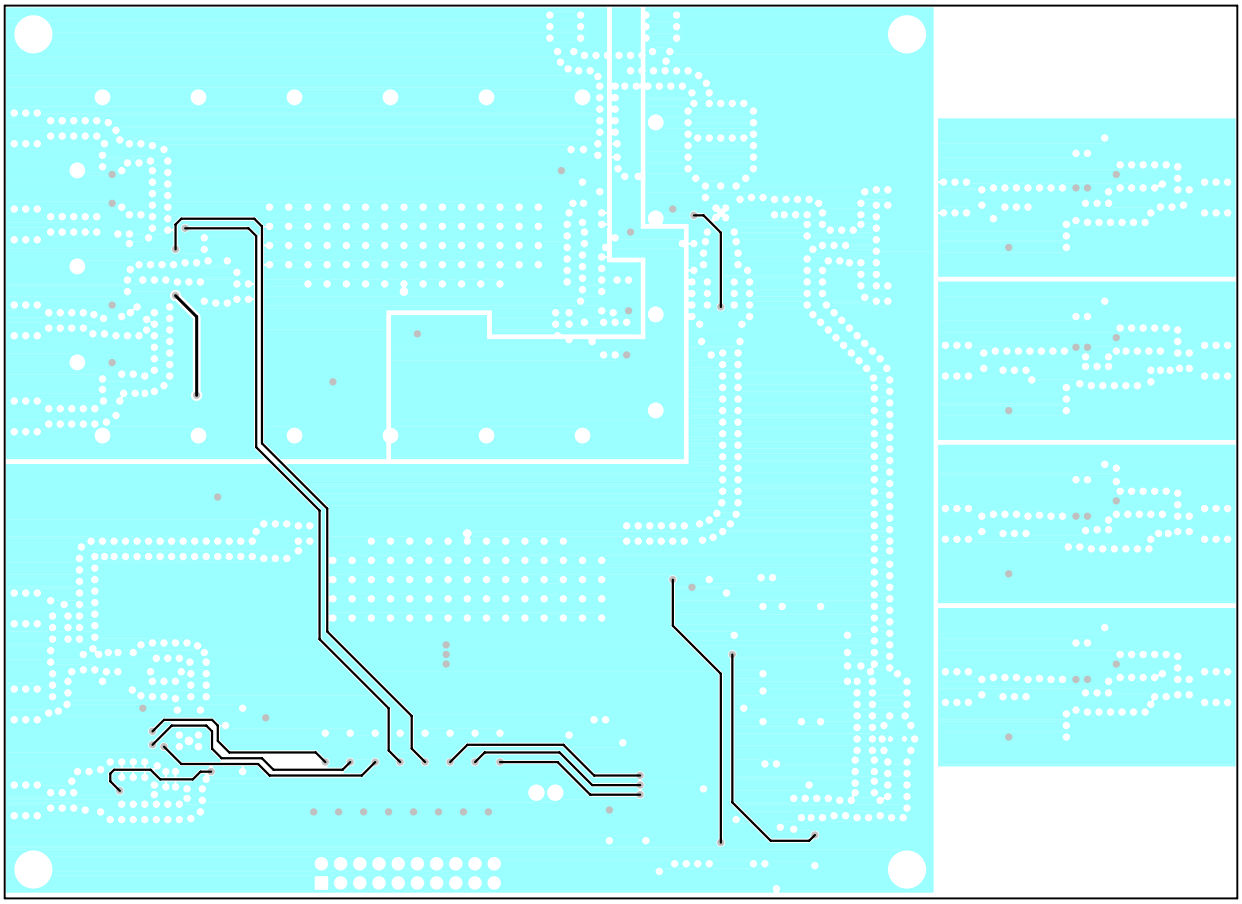

RECEIVER REV 3.pcb – Thu Jan 11 23:39:17 2007

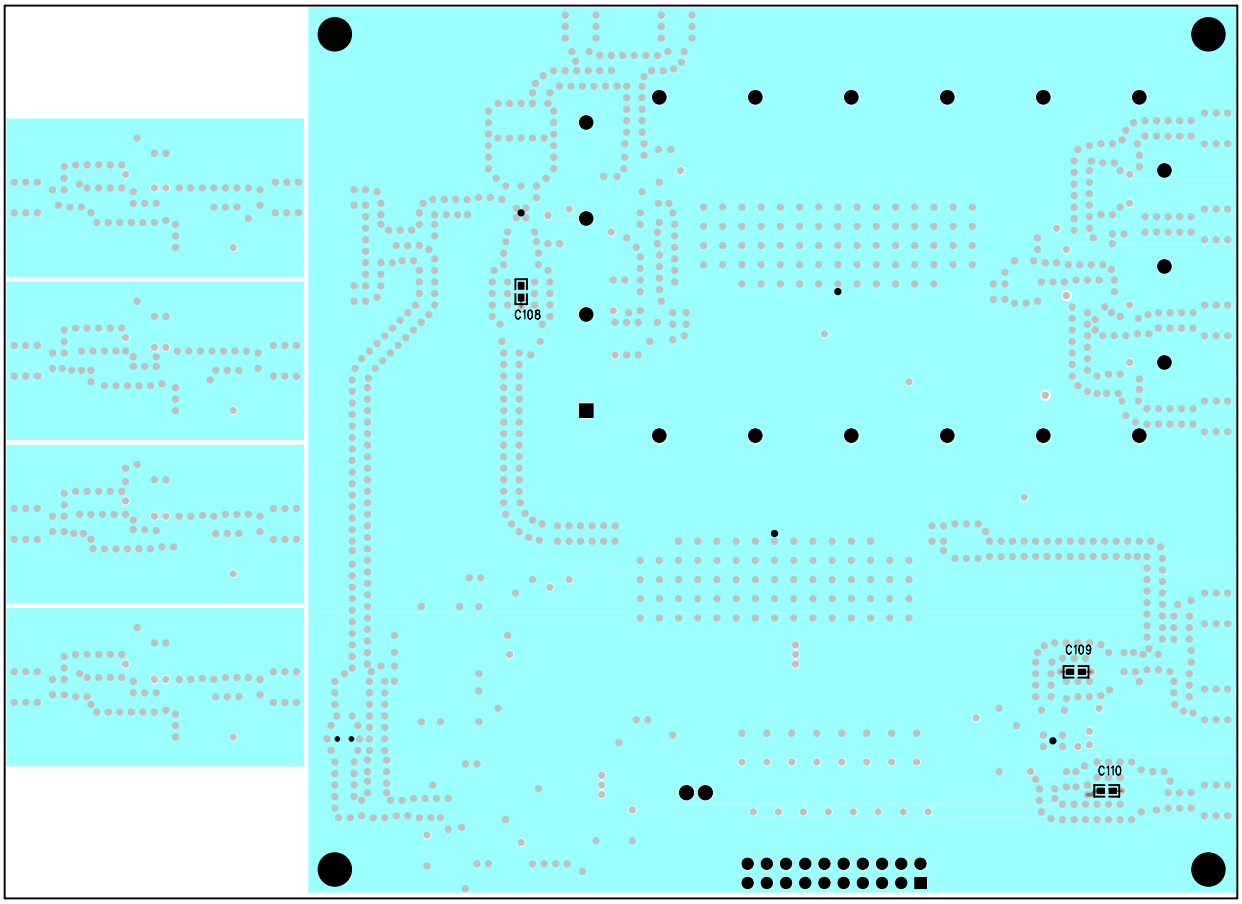
C108
C109
C110